

Distribution of Miocene deep-water reservoirs, and factors controlling their deposition and reservoir quality, southern Gulf of Mexico

by

Hilda Clarisa Gutierrez Paredes

A thesis submitted in partial fulfillment of the requirements for the degree of

Doctor of Philosophy

Department of Earth and Atmospheric Sciences
University of Alberta

© Hilda Clarisa Gutierrez Paredes, 2018

ABSTRACT

The factors controlling the distribution, geometry, and quality of the Miocene reservoirs, in an area located in the southern Gulf of Mexico (in the offshore part of the Tabasco State) were attained through detailed stratigraphic and facies analyses combined with seismic facies and 3D seismic-derived plan-view images. The depositional systems are dominantly represented by submarine fans (channel systems and frontal splays), lobes of debrites and mass-transport complexes. The main depositional processes were related to turbidity current; debris flows were of secondary importance, as was deposition from the fallout of suspended hemipelagic mud particles.

A sequence-stratigraphic analysis was performed to identify significant surfaces, systems tracts, and sequences for the Miocene succession. Five genetic sequences and eleven stratigraphic surfaces were correlated throughout the study area. The Miocene succession, from older to younger deposits, consists of: mass-transport deposits and turbidite deposits (lower Miocene); debrite deposits and turbidite deposits (middle Miocene); and debrite deposits and turbidite deposits (upper Miocene). These sedimentation cycles are delineated by regionally extensive maximum flooding surfaces within condensed sections of hemipelagic mudstone which represent starved basin floors. These maximum flooding surfaces are the key surfaces for the construction of the Miocene stratigraphic framework. The falling-stage system tracts form the bulk of the Miocene sequences. Individual sequence geometry and thickness were controlled by tectonics, halokinesis and large-scale sedimentation patterns. The Tortonian (upper Miocene) sequence includes sandy deposits, whereas the overlying Messinian sequence includes sandy facies at the base and muddy facies at the top; this trend reflects the change from slope to shelf settings.

The Miocene depositional elements were deposited in an irregular paleotopography strongly affected by regional and local tectonics. As a result, the recorded deformational events (contraction and extension) together with the halokinesis played an important role in the sedimentation of the area. Such interaction occurred in two ways; the structural elements modified the paleotopography of the basin creating accommodation space for clastic deposition and controlled the entry of sediments to the basin. During the Oligocene to early Miocene, the main depocenter was bounded by diapirs, salt sheets and structural highs formed by older salt anticlines; on the other hand, for the middle Miocene the depocenters were confined by the presence of shortened diapirs and salt sheets in the periphery and structural highs in the south of the study area. The formation of these depocenters provided the accommodation space for sediments deposition; as a result, during the early to middle Miocene, the deposits were confined to these depocenters forming ponded lobes. At the end of the middle Miocene, these depocenters were filled and channel-levee systems and frontal splay complexes predominated in an unconfined setting. During the late Miocene the depocenter's formation was controlled by an extensional event, which provided the accommodation space for sediment deposition in half grabens, frontal splays and channel-levee systems being the most important depositional elements. All these structural elements had significant implications for the architecture and internal organization of the turbidite systems.

Finally, establishing the link between the sequence stratigraphic framework, depositional facies, and diagenetic alterations was critical to determine the main factors controlling the reservoir quality of the Miocene sandstones. The Miocene deep-marine sandstones were attributed to the falling-stage and lowstand system tracts. The middle Miocene falling-stage systems tracts included medium- to very fine-grained, and structureless sandstones deposited in channels and

frontal splays, and muddy sandstones, and sandy debrites deposited in lobes. The lowstand system tracts consist of medium- to very fine-grained massive and normally graded sandstones deposited in frontal splay complexes. The upper Miocene falling-stage systems tract includes medium- to coarse-grained, structureless sandstones deposited in channel systems and frontal splays, as well as lobes of debrites composed of grain flows and hybrid-flow deposits. The lowstand systems tracts include fine-grained sandstones deposited in overbank deposits.

The results reveal that the depositional elements with the best reservoir quality are the frontal splays deposited during the falling-stage system tracts. The reservoir quality of the Miocene sandstones was controlled by a combination of depositional facies, sand composition and diagenetic factors (mainly compaction and calcite cementation). Sandstone texture controlled primarily by depositional facies appears to be more important in comparison to sandstone composition when determining reservoir quality; and compaction was more important than cementation to porosity destruction, which only stopped when complete calcite cementation occurred.

P R E F A C E

This thesis is an original work by Hilda Clarisa Gutierrez Paredes. Part of this thesis has been previously published; these publications were adapted as chapters as follows.

Chapter 2 of this thesis was published as Gutierrez Paredes H.C, Catuneanu O, and Hernández Romano U., “Miocene depositional environments and processes, and depositional elements in the southern Gulf of Mexico”. *Geological Journal*, 2017; 1-30.<https://doi.org/10.1002/gj.2948>. I was responsible for the data collection, analysis and interpretation, as well as the manuscript composition. Catuneanu O. was the supervisory author and was involved with concept formation and manuscript composition. Hernández Romano U. was the supervisory author and contributed to manuscript edits.

Chapter 3 was published as Gutierrez Paredes H.C, Catuneanu O, and Hernández Romano U., “Sequence stratigraphy of the Miocene section, southern Gulf of Mexico”. *Marine and Petroleum Geology*.201. 86.711-732. Our contributions were held as in Chapter 2.

Chapter 5 was published as Gutierrez Paredes H.C, Catuneanu O, and Hernández Romano U., “Controls on the quality of Miocene reservoirs, southern Gulf of Mexico”. *Journal of South American Earth Sciences*.2018.81.45-65. Our contribution was held as above.

*For my wonderful family who have shown me unconditional
love, support and encouragement throughout the years.*

ACKNOWLEDGEMENTS

The completion of this PhD would not have been possible without the constant support from various people. I wish to acknowledge the efforts of my supervisor Octavian Catuneanu, who has dedicated his time to ensure the completion of this work by not only proofreading it, but by teaching me how to improve it. As well as, I thank him for being interested in my research and taking me in as his student. Likewise, it is important to mention the support from my supervisor from PEMEX, Ulises Hernández Romano, since his guidance allowed me to attain my goals. As well as, I thank him for always keeping me focused to ensure the completion of my research.

I would like to offer my gratitude towards my supervisory council committee members Drs. Nick Harris, John Waldron, Karlis Muehlenbachs and Jaime Urrutia-Fucugauchi for their feedback and constructive criticism. They have taught me how to evaluate my own work in a more insightful way.

I also thank CONACYT and PEMEX for funding my research and for giving me the opportunity to contribute to the scientific world with my research. In specific to the authorities of PEMEX, Engineers Jose Antonio Escalera, Ignacio Pereznegrón, Marco Antonio Arreguín and Leonardo Aguilera. I greatly appreciate your support.

Furthermore, I would like to highlight the great support received from my co-worker and friend, Rolando Peterson. I am grateful for his insight and helpful contribution to this research.

TABLE OF CONTENTS

CHAPTER 1: INTRODUCCION

SCOPE.....	1
STUDY AREA.....	3
OBJECTIVES	3
DATA BASE AND METHODOLOGY.....	4
Data base	4
Seismic Data	4
Well Data	5
Methodology.....	5
Data compilation and database integration	5
Depositional environments, processes and depositional elements	6
Sequence Stratigraphy	6
Tectonic influence on the morphology, facies distribution and architecture of Miocene reservoirs.....	7
Quality of the reservoir rocks	7
STRUCTURE OF DISSERTATION	8
REFERENCES	10
FIGURES	11

CHAPTER 2: MIOCENE DEPOSITIONAL ENVIRONMENTS, PROCESSES, AND DEPOSITIONAL ELEMENTS IN THE SOUTHERN GULF OF MEXICO

INTRODUCTION	14
REGIONAL GEOLOGICAL SETTING	16
METHODOLOGY	18
PALEOBATHYMETRY	19
SEDIMENTARY FACIES AND DEPOSITIONAL PROCESSES	21
Nomeclatural considerations (Facies models)	21
Lithofacies description and depositional processes	22
Facies 1: Intraclast mudstone breccia	22
Facies 2: Intraclast mudstone conglomerate	23
Facies 3: Massive sandstone with floating pebbles or intraclasts.....	24
Facies 4: Structureless (massive) sandstone	25
Facies 5: Normally graded sandstone	26
Facies 6: Laminated sandstone	27
Facies 7: Muddy sandstone	28
Facies 8: Rippled, parallel and cross-laminated heterolithic units	28
Facies 9: Laminated siltstone and mudstone.....	29
Facies 10: Massive mudstone.....	30

Facies 11: Distorted heterolithic units.....	31
Facies 12: Mudstone clast breccia with sand injections.....	31
Facies 13: Heterolithic units of rippled and parallel laminated volcanic siltstone and fine-grained sandstone	32
FACIES ASSOCIATIONS (DEPOSITIONAL ELEMENTS)	33
Channel facies associations.....	33
Channel Fill.....	33
Channel Margin.....	34
Leveed-channel facies association.....	35
Frontal splay facies association.....	36
Proximal.....	36
Distal.....	36
Lobes of debrites and associated flows facies association	38
Debrites.....	38
SEISMIC DEPOSITIONAL ELEMENTS.....	40
Interpretation.....	40
Depositional elements.....	41
Mass-transport complexes (MTC).....	41
Lobes of debrites and associated flows.....	43
Submarine channels.....	44
Frontal splays.....	47

DISCUSSION	49
CONCLUSIONS	52
ACKNOWLEDGEMENTS.....	53
REFERENCES.....	53
FIGURES.....	66

CHAPTER 3: SEQUENCE STRATIGRAPHY OF THE MIOCENE SECTION, SOUTHERN GULF OF MEXICO

INTRODUCTION.....	89
GEOLOGICAL SETTING.....	92
METHODS AND DATA SETS.....	94
DEPOSITIONAL ENVIRONMENTS.....	96
CHRONOSTRATIGRAPHIC FRAMEWORK.....	100
SEQUENCE STRATIGRAPHIC FRAMEWORK	102
Nomenclatural considerations	102
Stratigraphic surfaces.....	103
Basal Surface of Forced Regression (BSFR).....	103
Correlative Conformities (CC).....	104
Maximum Flooding Surfaces with Condensed Sections (MFS/CS).....	105
Systems Tracts.....	107
Highstand Systems Tract (HST)	108
Falling-Stage Systems Tract (FSST)	108

Lowstand Systems Tract (LST) and Transgressive Systems	
Tract (TST).....	109
Sequences.....	110
Middle Oligocene (Rupelian) - Lower Miocene (Burdigalian)	
(27.1-18.3 MA.)	110
Lower Miocene (Burdigalian) 18.3-16.4 MA	111
Middle Miocene (Serravallian) 16.4-11.2 MA	113
Upper Miocene (Tortonian) 11.2-7.12 MA	115
Upper Miocene (Messinian) 7.12-5.32 MA	116
DISCUSSION	117
CONCLUSIONS	120
ACKNOWLEDGMENTS	122
REFERENCES	122
FIGURES	129

CHAPTER 4 TECTONIC INFLUENCE ON THE MORPHOLOGY AND DISTRIBUTION OF MIOCENE RESERVOIRS, SOUTHERN GULF OF MEXICO

INTRODUCTION	150
GEOLOGICAL SETTING	152
Regional Tectonic-sedimentary framework	152
Sequence stratigraphic framework.....	156
DATA AND METHODOLOGY	157

DEPOSITIONAL ELEMENTS AND THEIR SEISMIC

FACIES	158
Mass-transport complexes (MTC).....	158
Lobes of debrites and associated flows	159
Submarine channels	160
Frontal splays	161
AGES OF DEFORMATIONAL EVENTS	162
Deformational event D1 (Late Jurassic-Late Cretaceous)	162
Deformational event D2 Paleogene (Eocene-Oligocene)	163
Deformational event D3 Neogene (middle Miocene-late Miocene)	164
Deformational event D4 Neogene (Pliocene-Pleistocene)	164
TECTONO-SEDIMENTARY DEVELOPMENT.....	165
Sequence A Middle Oligocene-lower Miocene (27.1-18.3 Ma)	165
Sequence B lower Miocene (18.3-16.4 Ma)	167
Sequence C middle Miocene (16.4-11.2 Ma)	168
Sequence D upper Miocene (11.2-7.12 Ma)	169
Sequence E upper Miocene (7.12-5.32 Ma)	170
DISCUSSION	171
Structural controls on deposition	171
CONCLUSIONS	174
ACKNOWLEDGMENTS	174
REFERENCES	175
FIGURES	180

CHAPTER 5: CONTROLS ON THE QUALITY OF MIOCENE RESERVOIRS, SOUTHERN GULF OF MEXICO

INTRODUCTION	192
GEOLOGICAL SETTING	194
Tectonic framework	195
Stratigraphic framework.....	195
METHODOLOGY	197
DEPOSITIONAL SYSTEMS AND FACIES	199
Channel Facies Associations	200
Frontal splay facies associations	201
Lobes of debrites and hybrid sediment gravity flows facies associations	202
DETRITAL COMPOSITION, CLASSIFICATION AND PROVENANCE.....	203
Sandstone Provenance	206
DIAGENETIC ALTERATIONS.....	207
Compaction	207
Cements	208
Alteration	209
Dissolution	209
Clay minerals	210
General diagenetic sequence	211

RESERVOIR QUALITY	217
Porosity	217
Permeability	218
DISCUSSION	219
Provenance Controls on Reservoir Quality	219
Sequence Stratigraphic Controls on Reservoir Quality	220
Facies Controls on Reservoir Quality	222
Diagenetic Controls on Reservoir Quality	223
CONCLUSIONS	226
ACKNOWLEDGEMENTS.....	227
REFERENCES	228
FIGURES	239

CHAPTER 6: FINAL REMARKS, CONCLUSIONS AND RECCOMENDATIONS

FINAL REMARKS.....	257
CONCLUSIONS	259
RECOMMENDATIONS	262
REFERENCES	264

LIST OF TABLES

CHAPTER 2

TABLE 2.1 87

TABLE 2.2 88

CHAPTER 3

TABLE 3.1 149

CHAPTER 5

TABLE 5.1 256

LIST OF FIGURES

CHAPTER 1

Figure 1.1	11
Figure 1.2	12
Figure 1.3	13

CHAPTER 2

Figure 2.1	66
Figure 2.2	67
Figure 2.3	68
Figure 2.4	69
Figure 2.5	70
Figure 2.6	70
Figure 2.7	71
Figure 2.8	72
Figure 2.9	73
Figure 2.10	74
Figure 2.11	75
Figure 2.12	76
Figure 2.13	77
Figure 2.14	78
Figure 2.15	79
Figure 2.16	80
Figure 2.17	81

Figure 2.18	82
Figure 2.19	82
Figure 2.20	83
Figure 2.21	84
Figure 2.22	85
Figure 2.23	86

CHAPTER 3

Figure 3.1	129
Figure 3.2	130
Figure 3.3	131
Figure 3.4	132
Figure 3.5	133
Figure 3.6	134
Figure 3.7	135
Figure 3.8	135
Figure 3.9	136
Figure 3.10	136
Figure 3.11	137
Figure 3.12	138
Figure 3.13	139
Figure 3.14	140
Figure 3.15	141
Figure 3.16	142

Figure 3.17	143
Figure 3.18	143
Figure 3.19	144
Figure 3.20	145
Figure 3.21	146
Figure 3.22	147
Figure 3.23	148

CHAPTER 4

Figure 4.1	180
Figure 4.2	181
Figure 4.3	182
Figure 4.4	183
Figure 4.5	184
Figure 4.6	186
Figure 4.7	186
Figure 4.8	187
Figure 4.9	188
Figure 4.10	189
Figure 4.11	190
Figure 4.12	191

CHAPTER 5

Figure 5.1	239
Figure 5.2	240

Figure 5.3	241
Figure 5.4	242
Figure 5.5	243
Figure 5.6	244
Figure 5.7	245
Figure 5.8	246
Figure 5.9	247
Figure 5.10	248
Figure 5.11	249
Figure 5.12	250
Figure 5.13	251
Figure 5.14	252
Figure 5.15	253
Figure 5.16	254
Figure 5.17	255
Figure 5.18	255
Figure 5.19	256

Chapter 1

Introduction

1. Scope

This research project dealt with the distribution and prediction of the sandstones deposited in deep-water settings including the quality of the reservoir sands in the Miocene successions. The identification of depositional processes through the analysis of facies was critical to determine the depositional elements and the variability of reservoir quality. An inherent difficulty in the interpretation of deep-water sequences was that facies changes respond to complex and varied controls. Once the sediment reached the shelf margin and beyond, the sedimentary delivery system and the receiving basin configuration were the primary factors that govern overall fan morphology and lithofacies distribution. Mutti and Normark (1991) emphasized the composition and volume of turbidity currents, as well as the basin type and configuration, as the primary factors controlling the geometry and facies patterns of turbidite systems. Prather (2003) showed that slope topography strongly affects the distribution, quality, and production performance of many deep-water reservoirs.

Johannessen and Steel (2005) mentioned that deep-water sands, generated largely by sediment gravity flows, accumulate in a range of slope and basin-floor environments. They can sometimes be seen in clear relationship with a delivery system from an adjacent shelf edge, and in such cases, the nature and linkage between the shallow water and deep-water areas can be determined by critical examination of the different segments (shelf, slope and basin floor) of the shelf margin system. Moreover, the determination of facies/processes of the sediment-delivery system at the shelf margin and the identification of significant channels at the shelf edge or on the uppermost

slope are important additional parameters. These indicators are critical signs of the presence/absence of deep-water sands farther downslope.

Previous studies performed in the study area mentioned the importance of the sediment supply and the influence of halokinesis in sedimentation. However, in this study, other important factors controlling the reservoirs distribution and their architecture have been discussed, such as the occurrence and style of deep-water deposition. The controls on deep-water sedimentation mentioned by Posamentier and Kolla (2003) are shown in the diagram of Fig. 1.1.

In addition, understanding the dominant controls over the spatial and temporal distribution of the depositional elements can improve the prediction of the reservoir and seal facies, which are important in the exploration for hydrocarbons.

To achieve a better understanding of the spatial relationships of the stratigraphic units and the internal architecture, a sequence-stratigraphic framework for the Miocene units was established. This method helped to understand the relationships among rock layers, their seismic expression and their depositional environments for a more accurate prediction of the reservoir rocks. It was also important to determine how spatial and stratigraphic variations in sand distribution impacted reservoir heterogeneity.

The impact of the tectonics in the sedimentation was also analyzed; we observed that the sea floor topography, controlled by tectonics and halokinesis, affected the distribution pattern of turbidite deposits; also, that the paleotopography was focusing the flows and sediment transport pathways by impeding sediment transport to the basin through the development of structural barriers and the formation of the intra slope basins.

One disregarded aspect in the area was the diagenesis of the reservoir rocks. This process was crucial to comprehend the quality and heterogeneity of the reservoir rocks in the Miocene units, since they influence the porosity and permeability. Furthermore, linking the types and distribution of diagenetic processes to depositional facies and sequence stratigraphic framework of these clastic successions helped to predict the degree of diagenetic alterations controlling the quality of Miocene reservoir sands.

2. Study Area

The study area is located offshore in the southern portion of the Gulf of Mexico, in the coastal region of Tabasco State, in a present-day continental platform setting, where water depths range from 0-100 m.

According to Guzman, and Marquez-Dominguez, (2001) the study area belongs to the Province Cuencas del Sureste, which has been the most prospective petroleum province in Mexico. (Fig. 1.2).

3. Objectives

The main objective of this research was to determine the distribution and quality of the Miocene deep-water reservoirs in an area located in the southern Gulf of Mexico. To achieve the main purpose of this research, four primary objectives were set:

1. - Use an integrated data set of 3D seismic, wireline logs, cores and biostratigraphy to determine the main paleo-depositional environments, depositional processes, main lithofacies, facies associations and depositional elements of the Miocene units.

2. - Develop a sequence-stratigraphic framework of the Miocene units and define the overriding controls on the architectural stratigraphy of these deep- water sequences.
3. - Determine the tectonic influence on the morphology, facies distribution and architecture of the Miocene reservoirs.
4. - Identify the main factors affecting the quality of the Miocene sandstone reservoir

4. Database and Methodology

4.1 Database

The data used in this study comprise seismic and well information.

4.1.1 Seismic Data

The 3D seismic survey was integrated by merging 2 seismic surveys in their pre-stack time migration (PSTM) versions with and without filtering and gain. The SEG polarity convention in this seismic survey is the American (positive for the peak and negative for the trough). The quality of the seismic information is fair to good in the areas not affected by allochthonous salt bodies and fair in the areas affected by them. The characteristics of the complete 3D seismic survey merge are listed below.

Surface: 1,600 Km²

Bin size: 25 x 25

Fold: 60

Maximum Offset: 6150 m

Record Length: 5000 ms

This survey was processed close to the zero phase.

4.1.2 Well Data

The well data come from 12 wells, including conventional logs, such as: gamma ray, resistivity, spontaneous potential, density, neutron porosity, p-wave sonic, caliper, and mud logs. Additionally, the well data included special logs, such as: spectral gamma ray, survey logs and vertical seismic profiles. In reference to the core samples, this project was provided with 13 core recovered from the upper and middle Miocene. The information from these cores includes lab analysis data such as porosity, and vertical and horizontal permeability. For this project 150 thin sections were available for petrographic studies, as well as 100 images from scanning electronic microscopy (SEM). In addition, the well cuttings of the 12 wells were available. Finally, the paleontological data of these wells were also provided and included high-resolution biostratigraphy and paleontological data (only planktonic foraminifera).

4.2 Methodology

The methods applied in this research were diverse and a multidisciplinary approach was performed to obtain meaningful results. Fig. 1.3 shows the workflow used in this project, described as follows.

4.2.1 Data compilation and database integration

The first step in this work was to request the information from the Mexican oil company (PEMEX). Once granted, the data were analyzed, validated and integrated into databases. The first database comprised the electronic information collected from 12 wells. The second database incorporated all of the previous studies of regional geology, stratigraphy, sedimentology, tectonics and structural geology performed in the study area. This database also included a literature review of all of the fields related to the project topics to construct a theoretical

framework of each stage. The third database consisted of a seismic project in the Petrel[®] interpretation system platform, where the seismic surveys, well logs and core data were loaded.

4.2.2 Depositional environments, processes and depositional elements

The interpretation of the paleodepositional environments was done through paleobathymetric analysis combined with lithofacies description, depositional processes identification and definition of the main depositional elements by using the integration and interpretation of multiple data sets (biostratigraphy, cores, well logs, and seismic). The main sedimentary facies and depositional processes were interpreted from cores, and these interpretations were combined with the facies associations (from cores and well logs interpretation) and 3D seismic's geomorphology. The method involved the study of the basin geomorphology and depositional systems using 3D seismic-derived plan-view images (Posamentier, Davies, Wood et al., 2007), and allowed an accurate understanding of lithologic patterns and an enhanced prediction of the distribution of reservoir, as well as seal facies; in this stage, interval attribute maps and horizon attribute maps were generated.

4.2.3 Sequence Stratigraphy

To develop the sequence stratigraphic framework of the Miocene succession a multidisciplinary approach was undertaken and diverse data sets (3D seismic data, core data, well logs and high-resolution biostratigraphic data) were integrated. The chronostratigraphic framework was built using biostratigraphic information (biozones). Later, as recommended by Catuneanu et al. (2009), a model-independent framework was applied in this study, with the identification of all the genetic units and bounding surfaces present in the Miocene successions. Following this, the well logs were interpreted to identify the stacking patterns and the

stratigraphic surfaces, such as: correlative conformities, maximum flooding surfaces, and basal surfaces of forced regression. Afterwards, the key surfaces were tied to seismic data for seismic stratigraphic correlation, establishing the preliminary framework to interpret the seismic sequences employed later to spatially delineate the stratigraphic cycles.

4.2.4 Tectonic influence on the morphology, facies distribution and architecture of Miocene reservoirs.

To understand the role of the tectonics in the distribution of the depositional facies and the sediment pathways the following methods were employed: 1) Analysis of the structural deformational systems based on previous studies from this area. 2) Description of the seismic facies on the basis of reflection character (amplitude, continuity, geometry and seismic pattern) in cross-section and plan-view geometry on seismic amplitude attribute maps. 3) Integration of the isochrons of the genetic sequences with TWT structure maps and cross-sectional geometry to determine structural style and evolution.

4.2.5 Quality of the reservoir rocks

To identify the main depositional and diagenetic factors affecting the porosity of the Miocene sandstone reservoirs in the study area, and to determine the general trends of reservoir quality factors reducing porosity, the following methods were employed: 1) Petrographic analysis of thin sections and counting points were performed to determine framework grain, cement composition, porosity types, and grain size. 2) SEM analyses of selected samples were used to determine the mineral composition, textural relationships and diagenetic products; as well as X-ray diffraction of selected samples to determine the mineral composition.

The porosity and permeability data from standard petrophysical nitrogen porosity and air permeability were used.

5. Structure of dissertation

This dissertation was written in paper format and was divided in four independent, yet complementary chapters following this introduction. A final chapter (Chapter 6) reviews the salient contributions of the four primary papers and provides suggestions for future research arising from these results. A brief description of each chapter is provided below.

Chapter 2, Miocene depositional environments, processes, and depositional elements in the southern Gulf of Mexico. A version of this chapter co-authored with Octavian Catuneanu and Ulises Hernández-Romano was published by Geological Journal. Gutierrez Paredes H.C, Catuneanu O, and Hernández Romano U., “Miocene depositional environments and processes, and depositional elements in the southern Gulf of Mexico”. Geological Journal, 2017; 1-30.<https://doi.org/10.1002/gj.2948>. This chapter investigates the main lithofacies, processes and the depositional elements occurred during the Miocene.

Chapter 3, Sequence Stratigraphy of the Miocene section, southern Gulf of Mexico. A version of this chapter co-authored with Octavian Catuneanu and Ulises Hernández-Romano was published by Marine and Petroleum Geology Journal. Gutierrez Paredes H.C, Catuneanu O, and Hernández Romano U., “Sequence stratigraphy of the Miocene section, southern Gulf of Mexico”. Marine and Petroleum Geology.201. 86.711-732. This chapter was focused on the interpretation of stratigraphic sequences. Sequence analysis was used to identify significant surfaces, systems tracts and sequences of the Miocene succession.

Chapter 4. Influence of tectonics in the morphology and facies distribution in Miocene reservoirs southern Gulf of Mexico. A version of this chapter co-authored with Rolando Peterson-Rodríguez, Octavian Catuneanu and Ulises Hernández-Romano was submitted to Journal of South American Earth Sciences. This chapter addresses how to evaluate the deformational events (especially the contractional event) that have controlled the distribution of sediments and the external geometry of their deposits by modifying the paleotopography of the basin, by creating accommodation space for clastic deposition and by controlled the sediment pathways.

Chapter 5. Controls on the quality of Miocene reservoirs southern Gulf of Mexico. A version of this chapter co-authored with Octavian Catuneanu and Ulises Hernández-Romano was published by Journal of South American Earth Sciences. Gutierrez Paredes H.C, Catuneanu O, and Hernández Romano U., “Controls on the quality of Miocene reservoirs, southern Gulf of Mexico”. Journal of South American Earth Sciences.2018.81.45-65. This chapter was focused on determining the main controls on the reservoir quality of the Miocene sandstones; as well as exploring the possible links between the sequence stratigraphic framework, depositional facies and diagenetic alterations.

References

- Catuneanu, O., Abreu, V., Bhattacharya, J.P., Blum, M. D., Dalrymple, R.W., Eriksson, P. G., et al., 2009.** Towards the standardization of sequence stratigraphy. *Earth-Science Reviews*, 92.
- Gutierrez Paredes H.C, Catuneanu O, and Hernández Romano U.,** Sequence stratigraphy of the Miocene section, southern Gulf of Mexico. *Marine and Petroleum Geology*.201. 86.711-732.
- Gutierrez Paredes H.C, Catuneanu O, and Hernández Romano U.,** “Miocene depositional environments and processes, and depositional elements in the southern Gulf of Mexico”. *Geological Journal*, 2017; 1-30.<https://doi.org/10.1002/gj.2948>.
- Catuneanu O, and Hernández Romano U.,** “Controls on the quality of Miocene reservoirs, southern Gulf of Mexico”. *Journal of South American Earth Sciences*.2018.81.45-65.
- Guzmán, A.E., and Marquez Domínguez, B., 2001.** The Gulf of Mexico Basin South of the Border: The petroleum Province of the twenty first century” in M.W. Downey, J.C. Threet and W.A. Morgan, (Eds). AAPG Tulsa.
- Mutti, E., and Normark, W.R., 1991.** An integrated approach to the study of turbidite systems: Seismic facies and sedimentary processes of submarine fans and turbidite systems: Springer-Verlag New York Inc., 75-105.
- Posamentier H., Davies R.J., Wood L., and Cartwright J.A., 2007.** Seismic geomorphology –An Overview. In *Geological Society London Special Publications*. DOI: 10.1144/GSL.SP.2007.277.01.01
- Posamentier, H.W., and Kolla V., 2003.** Seismic geomorphology and stratigraphy of depositional elements in deep-water settings. *Journal of Sedimentary Research*, 73,367-388.

Prather B.E., 2003. Controls on reservoir distribution, architecture and stratigraphic trapping in slope settings. *Marine and Petroleum Geology*. 20(6):529-545.

Figures

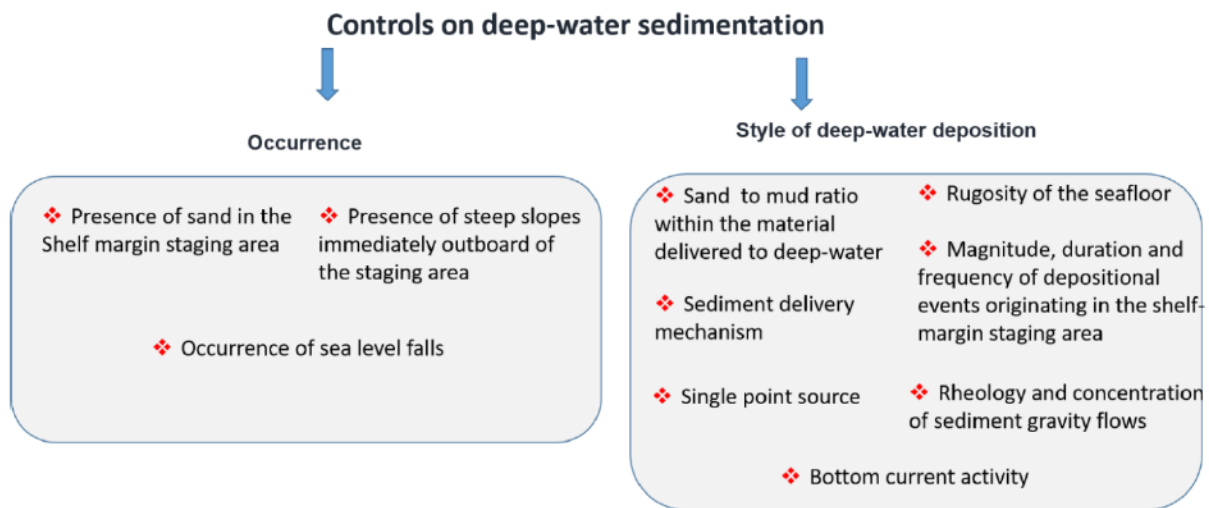


Figure 1.1 This diagram shows the main controls on deep-water sedimentation according to Posamentier and Kolla, (2003).

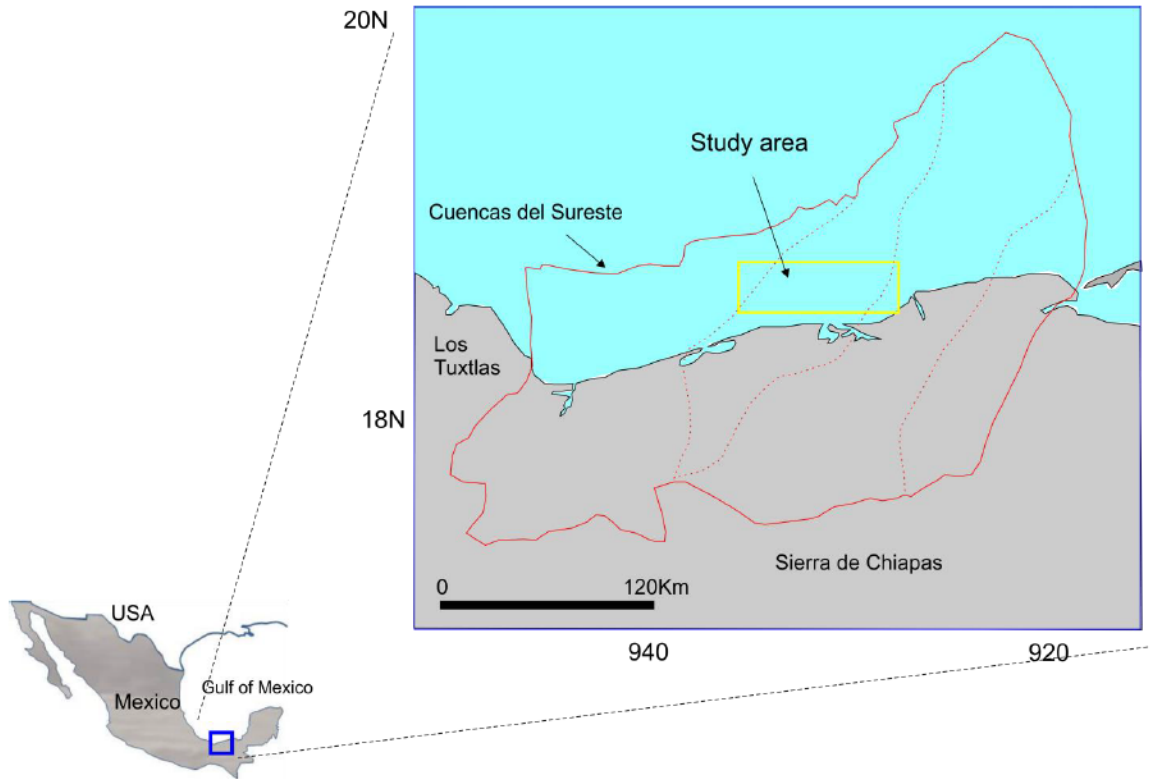


Figure 1.2. Location map for the study area in the southern Gulf of Mexico.

Data and Methodology

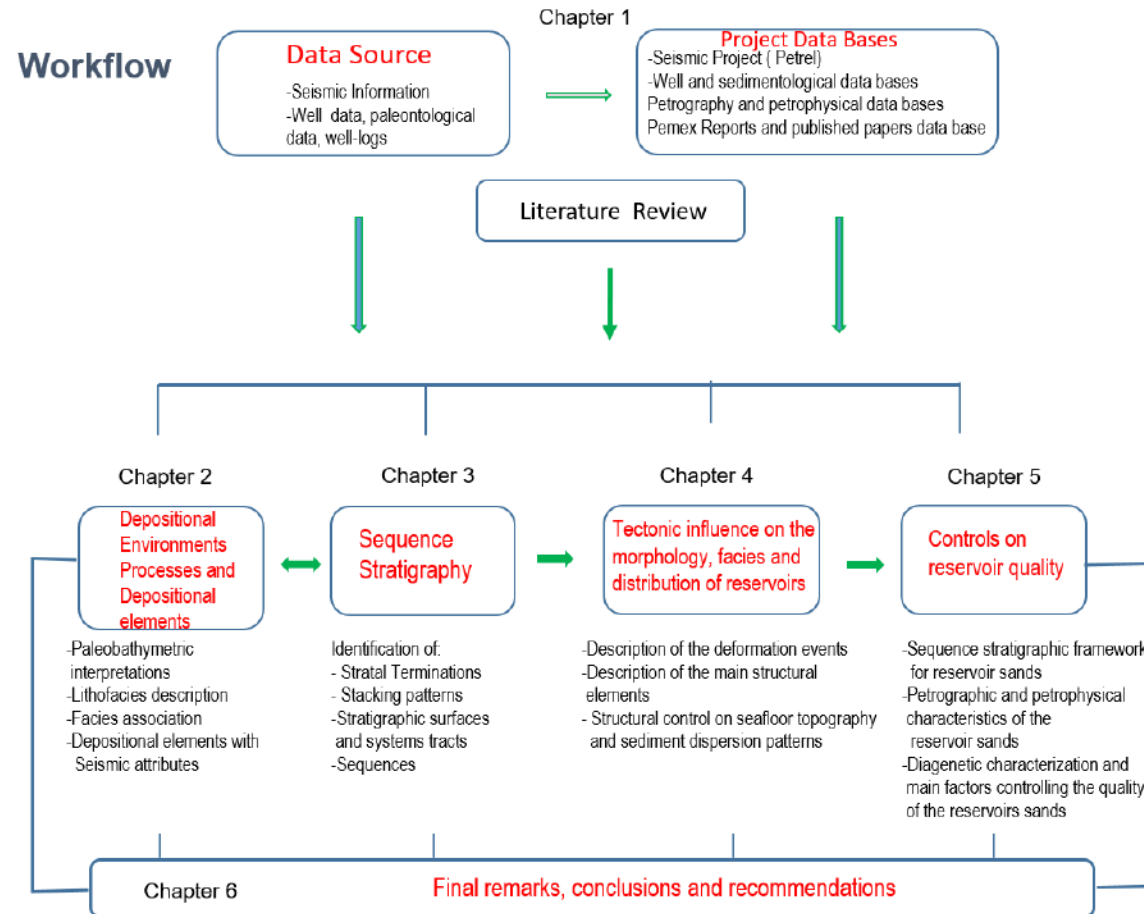


Figure 1.3 Workflow of the methods used in this project.

Chapter 2

Miocene depositional environments, processes, and depositional elements in the southern Gulf of Mexico

1. Introduction

Detailed stratigraphic and facies analyses were conducted and combined with seismic facies and 3D seismic-derived plan-view images to interpret the depositional environments, processes, and depositional elements during the Miocene for an area located in the southern Gulf of Mexico. The results showed that deposition during the Miocene mainly occurred in a slope setting, with bathymetric changes associated with highs and depocenters related to structural features. From the sedimentological interpretation, 13 sedimentary facies were identified. The abundant lithofacies were structureless (massive) sandstone and massive mudstone. Rippled, parallel and cross-laminated sandstone and siltstone were found in minor proportions. The main depositional processes were related to turbidity currents, including high-density and low-density currents; debris flows (mud flows and grain flows) were of secondary importance, as was deposition from fallout of suspended hemipelagic mud particles. The vertical and lateral distributions of facies revealed seven facies associations linked to depositional environments. These facies associations were the building blocks that were used to characterize the depositional elements recognized on seismic data. The main depositional elements identified were mass-transport complexes, submarine channels and, frontal splays. Finally, interpretations from different data sets enabled the conclusion that during the Miocene in this area submarine fans were deposited on an irregular

paleotopography, with topographic lows and highs mainly controlled by structural features.

Deep-water depositional systems are important targets for hydrocarbon exploration and production in areas such as the Gulf of Mexico, offshore Nigeria, offshore Angola and offshore Brazil, among others. However, the study of these deposits has been a difficult process due to their variability and complexity, as well as the difficulty of reconciling the features of modern and ancient systems. Moreover, exploration and development in deep-water settings is expensive and risky. Despite these difficulties, understanding the stratigraphic architecture, facies distribution and factors controlling these deposits is critical. In addition, an improvement in our understanding of the geometric and sedimentological features of turbidite systems, should improve predictions for the depositional models.

The Mexican petroleum company (PEMEX) performed several geological studies to identify the depositional systems present in this area. However, these studies did not consider the depositional processes responsible of the distribution of sediments despite their importance, or all types of sediment gravity flows present in the area. Similarly, facies descriptions and interpretations of facies associations were not conducted. The purpose of this chapter was to perform an integrated study using different data sets to determine the paleo-depositional environments during the Miocene and, most importantly, to identify the main processes responsible for the transport and deposition of sedimentary facies for an offshore area in the southern Gulf of Mexico. Thus, the aims of this work are threefold. The first goal is the interpretation of the paleobathymetric conditions, the second is the interpretation of the main sedimentary facies and depositional processes, and the last is the interpretation of facies associations in terms of depositional elements to help calibrate the depositional elements

identified using seismic data. To achieve these objectives, multiple data sets (biostratigraphy, cores, well-logs, and seismic) were integrated in order to define the paleobathymetric and sedimentological interpretations (main sedimentary facies, facies associations and depositional processes). These inputs were combined with the interpretation of depositional elements based on seismic facies and 3D seismic-derived plan-view images.

2. Regional Geological Setting

The study area is located offshore in the southern portion of the Gulf of Mexico in a present-day continental platform setting, where water depths range from 0 to 100 m. (Fig. 2.1).

In the Gulf of Mexico province, the tectonic setting has been dominated by the development of a passive margin (Barton and Buffler, 1994; Pindell, 1985; Ross and Scotese, 1998; Salvador, 1987, 1991) overprinted by Laramide orogenic effects which occurred in the southern part of the Gulf of Mexico from the Paleocene to middle Eocene (Escalera-Alcocer and Hernández-Romano, 2009; Pindell and Kennan, 2002) and Chortis Block migration along the Pacific margin starting in the Eocene to reach the present day position (Pindell and Kennan, 2009; Rogers, Mann and Emmet, 2007; Ross and Scotese, 1988). All of these regional tectonic events along with local tectonic events (salt tectonics) had a great impact on the deformational events that occurred in the southern Gulf of Mexico, as explained by Angeles-Aquino, et al. (1994); Cruz Mercado et al. (2009); Gómez-Cabrera and Jackson (2009); Prost and Aranda (2001); Robles-Nolasco et al. (2004); Salomón-Mora, et al. (2009). During the middle Miocene occurred the maximum deformation that folded and thrust the rocks in the southern Gulf of Mexico (Chiapanecan Orogeny, Sánchez-Montes de Oca, 1980). Following, this contractional event, an extensional gravitational event occurred, giving rise to the

development of collapsed blocks associated with listric fault systems, and salt withdrawal (Aquino-Lopez et al., 2004; Padilla y Sánchez, 2007) (Fig. 2.2).

Regarding the stratigraphy in this area, the pre-rift and syn-rift deposits are inferred from the neighboring onshore areas. According to Angeles-Aquino, et al. (1994) and Escalera-Alcocer and Hernández-Romano (2009), the basement rock could be similar to that found in the Sierra de Chiapas (Chiapas Massif) and the Yucatan Block, which are composed of granitic and metamorphic rocks; the ages of these rocks range from Late Silurian to Permian. The syn-rift deposits comprise red beds derived from erosion of basement rock and volcanic rocks deposited in grabens during the Late Triassic and Early Jurassic (Buffler and Sawyer, 1985; Salvador, 1987). At the southern margin of the Gulf of Mexico, the continental syn-rift deposits are represented by the Todos Santos Formation, which crops out in the Sierra de Chiapas and eastern Oaxaca. Thicker salt deposits of Callovian age overlie these rocks. Salvador, (1987 and 1991) mentioned that these deposits mark the end of the rift stage and are contemporaneous with the age of Louann Salt. Angeles-Aquino et al. (1994) suggested that the Callovian salt in Campeche Sound was mobilized during the Oligocene and that related deformation continued until the early Miocene. Overlying the autochthonous salt, drift-related deposits characterizing a marine transgression ranged from shallow to deep marine environments. Consequently, during the Oxfordian and Kimmeridgian, siliciclastic rocks were deposited along the littoral zones, carbonate rocks on the ramps and thin beds of shale and carbonates in open marine conditions. During the Tithonian, a maximum marine transgression occurred that triggered the deposition of the main source rocks in the whole area. From the Late Jurassic until the Late Cretaceous carbonate rocks were deposited in outer ramp and basinal settings.

During the Cenozoic, the sedimentation changed from carbonate to siliciclastic due to the onset of the Laramide orogeny. The resultant Laramide foreland basins were the sites of deltaic deposits, slope gravity-flow deposits, turbidites and slumps during the Paleogene. During the Neogene, the migration of the Chortis block engendered Neogene basins that were filled by massive siliciclastic influx. From the Paleogene to the late Miocene, the sedimentation occurred in deep-water depositional settings. From the end of the Neogene to recent time, the linked contractional and gravitational tectonic systems caused thick siliciclastic strata-filled listric growth-fault blocks, synclines and salt-controlled basins. At this time in the area, siliciclastic rocks were deposited in slope-shelf-deltaic depositional systems. Fig. 2.2 shows the regional stratigraphic chart for the area during the Mesozoic and Cenozoic; as well as the regional tectonic and deformation events that affected the study area.

3. Methodology

Interpretation of the depositional sedimentary environments was performed by the integration of multiple data sets (biostratigraphy, cores, well logs, and seismic profiles). Biostratigraphic data from 12 proprietary PEMEX exploration wells were integrated with well logs and seismic data and used to update the stratigraphic framework for the Miocene and to produce the paleobathymetric maps. Sedimentological interpretation (sedimentary facies, facies associations and depositional processes) was accomplished using 13 cores (each one of 9 m) and well-log motifs. Facies analyses were completed by defining the bed thickness, bedding style, sedimentary structures, grain size and general composition.

In this work, a 3D seismic survey was used, covering an area of 1600 km² with a bin spacing of 25 m and, a record length of 5 s two-way time (TWT), and the survey was processed

close to the zero phase. The seismic quality was good between 0 to 3000 ms, and the display polarity used the normal SEG (Society of Exploration Geophysics) convention. Red-green-blue (RGB) spectral decomposition and variance volumes were generated from 3D seismic data across the entire study area with the usage of Schlumberger's Petrel software. The variance volume was used to visualize geological features associated with abrupt lateral changes in seismic reflections such as depocenters and margins of submarine channels. RGB spectral decomposition volumes were used to visualize depositional elements. Horizon-based extractions from different seismic attributes were performed; however, the best images were provided by the root mean square (RMS) amplitude seismic attribute.

Finally, the interpretations from different data sets were combined to determine the depositional environments and depositional elements existing during the Miocene in the study area.

4. Paleobathymetry

Four paleobathymetric maps were constructed for the Miocene units using the benthic foraminifera assemblages; the paleobathymetric environments were interpreted based on the paleobathymetric profile proposed in unpublished works for the Mexican petroleum basins (PEMEX-IMP, 2000, Sánchez et al., 2002 and 2004) (Fig. 2.3). In the construction of these regional paleobathymetric maps, structural interpretations, and isochron maps were considered.

The resulting maps (Fig. 2.4) show the paleobathymetry existing in the area, which varies from outer neritic to lower bathyal, as well as exhibit the general basin-ward movement of the paleobathymetry through time, which reflects the overall progradation of the continental margin during the Miocene. These maps also exhibit bathymetric highs and lows that could be related to,

salt structures, salt withdrawal features, antiforms and faults. Corliss and Fois (1990); Loubere, Gary, and Lagoe (1993, cited in Villamil et al., 1998), mentioned that benthic foraminifera communities are mainly affected by sediment supply and consistency of physical and biogeochemical bottom conditions; however, other authors such as Villamil et al.(1998) and Fillon (2007) argued that areas with abrupt bathymetric variations are more susceptible to syndepositional tectonics (salt bodies and faults) and the topography of the slope is constantly changing in response to sedimentation; on the basis of this interpretation, the slope paleotopography was constantly changing in association with sedimentation and deformation in this area. As a result, for the early Miocene, the predominant paleobathymetry is middle bathyal, with the upper bathyal zone represented in areas with topographic highs and the lower bathyal zone represented in areas with topographic lows. For the middle Miocene, the prevalent paleobathymetry is upper bathyal, with areas of middle bathyal and lower bathyal zones in topographic lows; for the late Miocene, the advance of the outer neritic to the upper bathyal exhibits the sedimentary evolution of the basin. All the maps exhibit the coexistence of microfauna of different bathymetries; these mixtures are probably the result of benthic fauna transported by turbidity currents rather than contamination during their recovery, or changes in the sea level.

The fluctuations in the paleobathymetric conditions in Miocene maps (Fig. 2.4) illustrate the effects of tectonics and sedimentation on the paleobathymetry more than variations in sea level. These shifts should be not considered as traditional paleobathymetric models, which represent smooth and gently dipping topography from shelf to abyssal plain and oversimplified bathyal settings with paleobathymetric relief; for this reason, Villamil et al. (1998) recommended the use of three-dimensional models in basins with active salt tectonics such as the Gulf of

Mexico. According to their work, the advantages of 3D models are: a) 3D models consider lateral variations in sea-bottom topography and the consequences of salt features (sedimentation pathways and accumulation sites; b) 3D models emphasize the importance of sea bottom structure, differential sediment supply, and stratigraphy; and c) most important of all, these models incorporate modern views of the morphologic and environmental complexity of deep-water depositional systems.

5. Sedimentary facies and depositional processes

5.1 Nomenclatural considerations (Facies models)

Bouma (2000, 2004), Walker (1992) and Shanmugam (2006) stated that there is no unique model that cover the full spectrum of turbidity systems due to they depend on different parameters. Each deep marine depositional system is unique in detail with similarities in general. The misuse of the ancient sedimentary fan models might force the geology of a turbidite system into the wrong model and therefore may yield erroneous predictions. However, the use of analogues can work if deep water systems are compared carefully. For this reason, each deep water clastic system should have its own sedimentary model by taking into account all the controlling parameters such as tectonics, climate, sea level changes, processes and sedimentary characteristics (Bouma, 2004). Based on these considerations, the facies scheme proposed for the study area is an applicable adaptation of the main sedimentary schemes for systematizing the wide facies spectrum.

Process sedimentology was applied on 13 cores from the Miocene in order to establish a systematic facies scheme and the interpretation of the processes involved. The present facies analysis was achieved by defining bed thickness, bedding style, sedimentary structures, grain

size and general composition. In general, the facies scheme is organized from the coarsest to the finest and other facies that include conglomeratic facies, sandstone facies, fine grained facies, post-depositional facies and volcanoclastic facies.

Processes and products, as well as their mechanisms of deposition and types of settling behavior for the main sediment gravity flows identified in this study, are summarized in Fig. 2.5.

This section employs the facies scheme of Bouma (1962) in the description of the sedimentary facies resulting from turbidity currents and the classification scheme, proposed by Johansson and Stow (1995) in the case of sandstone beds with shale clasts that form as a result of debris flows and high-density turbidity current deposits. A summary of this classification scheme is shown in Fig. 2.6.

The nomenclature used in the facies description is similar to that was used by Sánchez-Hernández (2013) for an area in the SW Gulf of Mexico.

5.2 Lithofacies description and depositional processes

As a result of the interpretation of available cores (only from the middle and upper Miocene), 13 siliciclastic lithofacies were recognized. A summary of the lithofacies descriptions, main features and the depositional processes is shown in Table 2.1. Examples of each sedimentary facies are provided in Fig. 2.7.

Fig. 2.8 shows a summary of the sedimentary facies interpreted in this study, and their related processes, mechanisms for initiation and transport and post-depositional modifications.

5.2.1. Facies 1 Intraclast mudstone breccia

Description

This facies is composed of disorganized and very poorly sorted boulder-sized mudstone intraclasts, supported by fine sand and a muddy matrix. The average bed thickness is 15 cm. The upper and basal contacts are sharp, irregular and flat. The color of the clasts is mainly greenish-gray and dark. The clasts are angular to subangular and irregularly shaped. Some shale clasts are dispersed; others are in contact and occur throughout the sand bed. This facies is associated with massive sandstone. (Fig. 2.7A).

Interpretation

Debris flow. This facies corresponds to Type A1 in the classification scheme of Johansson and Stow (1995); according to their work, these deposits are formed by disruption and dislocation of shale beds because of the channel margin collapsing, where both disruption and dislocation are independent of any turbidity current flow within the channel.

5.2.2. Facies 2. Intraclast mudstone conglomerate

Description

This facies comprises disorganized and very poorly sorted boulder-sized mudstone intraclasts supported by fine sand and muddy matrix. The beds range in thickness from 20 cm to 1.30 m. The upper contact is sharp and irregular, and the basal contact is sharp, irregular and flat. The color of the clasts is mainly greenish-gray, and their sizes range from 0.2 to 20 cm. The clasts are subrounded, and some of them are oval-shaped. The shale clasts are dispersed, in other places, they are in contact, and they occur throughout the sand bed. This facies can be associated

with muddy sandstone and massive sandstone. Inverse grading occurs at the base of the deposit. (Fig. 2.7 B).

Interpretation

These deposits are interpreted as sandy debrites where the clasts are carried along by a debris flow. The shale intraclasts can be derived from erosion of the channel floor and walls, collapsing of the channel margin or free-fall of shale rocks from steep slopes. This facies corresponds to Type B1 in the classification scheme of Johansson et al. (1995).

5.2.3. Facies 3 Massive sandstone with floating pebbles or intraclasts

Description

This facies consists of structureless sandstone that is coarse to medium- grained, with scattered pebbles or intraclasts. The bed thickness varies from 10 to 50 cm. The upper and lower contacts are sharp, irregular and flat. The clasts range in size from granules to pebbles. The pebbles are brown and rounded, and they are mainly composed of quartz and lithic fragments. Pebble orientation is parallel and subparallel; these grains can be grouped along discrete horizons or isolated. The intraclasts are subangular and irregularly shaped; compositionally, the clasts may be claystone-mudstone, siltstone or fine-grained sandstone and are observed mainly in clusters. Both pebbles and intraclasts are located on the base and less frequently in mid-bed. Occasionally, flame structures, load casts and leaf fragments are present within this facies. (Fig. 2.7 C).

Interpretation

These deposits can be interpreted as derived from very high-density turbidity currents, where the sediment support mechanism hindered settling and turbulent flow occurred with clasts

deposited in the final stage (Kneller and Branney, 1995). Other possible mechanisms include erosion or ripping-up, during the passage of turbidity currents of previously deposited fine-grained sediment on the ocean floor, with the incorporation of the clasts into the basal portion of a sand-rich turbidity current (Mutti and Nilsen, 1981; Nielsen and Kerr, 1978). Finally, in the case of mid-bed shale clasts, these could settle through a flow and come to rest on a previously formed high-density inertia-flow layer, with pseudolaminar behaviour (Bagnold, 1954; Lowe, 1982).

These facies correspond to types B2 and B3 in their classification scheme of Johansson and Stow (1995).

5.2.4. Facies 4 Structureless (massive) sandstone

Description

This lithofacies is formed by gray and brown consolidated and unconsolidated sand without any recognizable bedding surfaces or other primary sedimentary structures. Grain size varies from medium to fine and grains are subangular to subrounded and poorly sorted. The grains can be supported by a sparse mud matrix or be poorly or well cemented with calcite. This facies is internally homogeneous and very thick-bedded (from 20 cm to 1.5 m). The basal contact is mainly planar, underlain by fine-grained facies and sometimes it is sharp with crude normal grading and weakly lamination. The upper contact is planar, overlain by fine grained laminated facies. Amalgamation surfaces are common, but sometimes are difficult to identify in the cores; however, they are revealed by load casts and by a slight upward decrease in grittiness determined by touch. This facies is abundant through all the cores examined. This facies corresponds to the Ta Bouma division. Examples of massive sands are shown in Fig. 2.7D and 2.9.

Interpretation

The origin of massive sands is highly debated and has been attributed to debris flows and high-density turbidity currents. In this study, this facies has been interpreted as a result of incremental deposition in a layer-by-layer-fashion from high-density turbidity currents, on the basis of the following criteria: a) The presence of amalgamation surfaces and occasional load casts; the presence of load casts is indicative of amalgamation and rapid deposition of sand (Duranti and Hurst, 2004); b) Massive sandstones deposited by high-density turbidity currents are poorly sorted (Amy, et al., 2005; Amy, et al., 2006; Talling, et al., 2012); and c) Laterally equivalent layers or those enclosed by planar-laminated intervals indicate that massive sandstone was also deposited by turbidity currents (Kneller and Branney, 1995, Posamentier and Walker, 2006, Sumner et al., 2012; Talling, et al., 2007; Talling et al., 2012).

5.2.5. Facies 5 Normally graded sandstone

Description

This facies is composed of brown and gray sand and sandstone, medium-grained at the base to fine-grained sand and siltstone at the top. The bed thickness varies from 10 cm to 1.30 m. The upper and lower contacts are mainly flat and occasionally sharp and irregular. The upper contact is usually overlain by another sandstone unit with similar characteristics to form an amalgamated package. The upper portion of the bed (siltstone) shows irregular lamination or tangential cross-lamination from sand bioturbation. The TaTb Bouma divisions are common in this facies Fig. 2.7 (E) shows examples of this lithofacies.

Interpretation

This facies is interpreted as a result of deposition from turbulent suspension, where the turbidity current velocity decreases systematically during deposition (Sanders, 1960), and the grading is a function of pseudoplastic behavior of a particle suspension.

5.2.6. Facies 6 Laminated sandstone

Description

This facies consist of medium to fine-grained sandstone. Bed thickness ranges from 13 cm to 1.30 m. The upper and basal contacts are sharp, irregular and flat. Frequently laminated sandstone is overlain and underlain by massive sandstone or shale and less frequently it underlain by debrites. The types of laminae comprise irregular to faint laminae, planar lamination, tangential lamination, and cross-lamination. In these intervals climbing ripples and laminae of organic matter can also be observed. This laminated sandstone facies corresponds to the Tb Bouma interval. Fig. 2.7F show examples of this sedimentary facies.

Interpretation

In the literature, it is mentioned that planar-laminated sand intervals can be formed by both low-density turbidity currents and high-density turbidity currents. Bannerjee (1977), Kuenen (1966), Hiscott (1994), Sumner, Amy, and Talling (2008), and Vrolijk and Southard (1997) mentioned that the majority of these intervals are most likely formed by traction carpets beneath high-density turbidity currents. Lowe (1982) mentioned that sandstones with planar and cross-lamination are related to deceleration by the passage of sediment from suspended to bed loads, and subsequent deposition by traction sedimentation is associated with low-density turbidity currents.

5.2.7. Facies 7 Muddy sandstone

Description

This lithofacies is formed by clay-rich sandstone and thin intercalations of silty sandstone. The sandstone is fine to medium-grained with a mud-rich sand matrix. This facies can be present in intervals of 10 to 25 cm where it is encased by massive sand or thicker, up to 6 m. The upper contact is flat, and the lower contact is sharp and erosional. This facies is most commonly homogeneous, ungraded and structureless; however, indistinct parallel lamination may occur. Floating mudstone chips are present at the base of this facies (Fig. 2.7G).

Interpretation

This facies is interpreted as a result of cohesive debris flows with a mud-rich sand matrix. The ungraded character suggests deposition by abrupt en masse freezing of the flow. These debrites have a low strength, that is sufficient to support sand but insufficient to support large clasts (Amy et al., 2006; Hampton, 1975; Sumner, Talling and Amy, 2009; Talling et al., 2012); also this type of debrite is thick and very extensive over distances of several tens of kilometers.

5.2.8. Facies 8 Rippled, parallel and cross-laminated heterolithic units

Description

This facies is represented by fine-grained sandstone and siltstone interbedded with mudstone of turbiditic or hemipelagic origin. This facies occurs in beds of 5 to 80 cm thick. The lower contact of this facies is planar and sharp; the upper contact may be gradational or abrupt with an associated mudstone cap. Common sedimentary structures are planar tabular bedding, tangential laminations, climbing ripples, trough cross-stratification and occasional hummocky

cross-stratification, and seldom lenticular and imbrication structures; this facies is sometimes disrupted by small burrows (*Skolithos*, *Thalassinoides*, *Zoophycos* and *Nereites*) or deformation structures (load casts, and flame structures). The Tc, Tde Bouma divisions are common in this facies. Fig. 2.7H shows examples of this lithofacies.

Interpretation

Based on numerous flume experiments, ripple cross-laminated sand intervals are deposited from dilute and turbulent suspensions accompanied by low rates of sediment fallout (Baas and Peakall, 2011; Talling et al., 2012). According to Lucchi and Valmori (1980), thin sandstone beds associated with siltstone/mudstone are probably deposited in a frontal position of the main feeder or an off-axis/fringe area, through the alternation of sediment suspension fallout and low to medium-density currents. The presence of current ripples and trough cross-stratification within the thin sandstones beds indicates tractional processes and bedload transport, during a low-density turbidity flow event (Talling et al., 2012).

5.2.9. Facies 9 Laminated siltstone and mudstone

Description

This facies comprises gray to greenish-gray, structureless to thin-bedded mudstone interbedded with siltstone and silty mudstone. These beds occur in units of 0.2 to 5 m thick. Silt-mud couplets, either as discrete beds or as interlaminated units, are common in this facies. The upper and lower contacts are sharp, irregular and planar. Common sedimentary structures are parallel, inclined and irregular lamination, lenticular features, load casts, and bioturbation (*Nereites ichnofacies*) (Fig. 2.7I). In the Bouma classification scheme, this facies corresponds to the Td and Te divisions.

Interpretation

The possible mechanisms to explain this facies are a relatively rapid deposition from low-concentration turbidity currents (when irregular and lenticular laminae are present) and deposition from suspension clouds of distal waning dilute turbidity flows (when parallel and inclined laminations and low-amplitude ripples are present), as well as relatively slow uniform deposition from low-concentration turbidity currents (when thin regular and parallel laminations are present).

5.2.10. Facies 10 Massive mudstone

Description

This lithofacies includes massive dark and gray-green mudstone with faint horizontal laminae, in which zones of bioturbational mottling may be developed. Bed thickness ranges from 2 to 9 m. This facies has sharp bases and gradational tops. The beds can be structureless or irregularly or finely laminated and they sometimes show varying degrees of bioturbation; *Nereites* ichnofacies is common. This facies is accompanied by pyrite nodules, coal laminae, planktonic foraminifera, shell material and other organic material, either bedded or chaotic. Examples are shown in the Fig. 2.7J.

Interpretation.

The common bioturbation and faint lamination suggest a hemipelagic origin formed by settling of sediment particles from the ocean in the time period between density flow events.

5.2.11. Facies 11 Distorted heterolithic units

Description

This facies frequently involves fine-grained sediments (sandstone, siltstone and mudstone) and includes convolute beds, slumps, and contorted packets. The bed thickness is usually thin, from 0.25 to 1 m. The upper and lower contacts are sharp and irregular. Ichnofossils are occasionally present; (Fig. 2.7K).

Interpretation

When the slumped beds are thin, within a low degree of disruption and with alternating contorted and un-contorted beds, it is probable that this has a local origin from the collapsing of unstable channel walls and overbank deposits. In addition, it is possible to have more disrupted beds associated within massive sandstone with floating intraclasts; this case corresponds to transformation flows from more distal slumps into muddy-debris flows.

5.2.12. Facies 12 Mudstone clast breccia with sand injections

Description

This facies comprises numerous angular mudstone clasts incorporated into a matrix of structureless sandstones, (Fig. 2.7L). The size of the mudstone clasts ranges from a few millimeters to several centimeters. Clasts are mainly angular, but can have other shapes; they also show a crude alignment. Bed thickness ranges from 10 to 80 cm. Breccia margins are dentate and discordant with the shale host. Adjacent mudstone clasts are linked together with thin mudstone connections named roof pendants. This facies is encased in laminated muddy sandstone.

Interpretation

This post-depositional sedimentary facies is formed by breaching of mudstone and injection of sand as a result of fluid overpressuring and resultant sand injection. Roof pendants, dentate margins, angularity and connections of the mudstone clasts are several of the hallmark features that Duranti and Hurst (2004) noted for the formation of this type of breccia. Several triggering mechanisms of sand injections are given in the literature, but according to Shanmugam (2012), the most commonly cited are sedimentary slumping, sedimentary depositional loading and seismicity-induced liquefaction.

5.2.13. Facies 13 Heterolithic units of rippled and parallel laminated volcanic siltstone and fine-grained sandstone

Description

This lithofacies consists of very fine-grained sand to silt-sized ash tuff and mudstone. Bed thickness range is from 13 cm to 3 m. Slumped and distorted beds are developed to different degrees in the upper part of this facies. Common sedimentary structures include laminae, cross-stratification, prograding ripples, tabular sigmoidal features, trough cross-lamination, and convolute structures and, less commonly, gutter casts and flame structures. The Tc, Td and Te Bouma divisions are common in this facies (Fig. 2.7M).

Interpretation

This facies is the result of volcanoclastic turbidite currents. These deposits were formed by secondary currents after the primary ash deposits were emplaced into submarine environments from pyroclastic fall. The upper part of the volcanoclastic turbidity is the turbulent transport system for the flow, whereas the viscous basal part is the depositional system.

According to Doronzo and Dellino (2013), the common sedimentary structures in these deposits are cross-laminae, planar and convolute laminae, and massive beds.

6. Facies Associations (Depositional elements)

The 13 lithofacies types previously described were grouped into seven general facies associations that were interpreted in terms of depositional systems. These spatially related facies were interpreted according to the depositional architectural element scheme of Mutti and Normak (1987, 1991), modified and expanded by Chapin, Davies, Gibson, and Pettingill (1994), Mahaffie. (1994), Richards, Bowman, and Reading (1998) and Elliot (1998), and summarized by Weimer and Slatt (2004). Here, we used the term frontal splay, instead of sheet sands, for the deposits at the termini of the channels, to avoid confusion in the description of the depositional elements mentioned later in this work.

These facies associations were also linked to depositional environments and were the building blocks to characterize the depositional elements recognized through the usage of seismic data. Table 2.2 summarizes the main facies association features recognized from cores and the interpretation of well-log signatures.

6.1 Channel Facies associations

6.1.1. Channel fill

This group of facies is characterized by the amalgamation of thick-bedded structureless sandstones (F4), normally graded sandstones (F5), and shale clast breccias (F1). Erosional bases for the sands beds are common, as well as amalgamation surfaces; which were identified in the studied cores, by subtle changes in color and grain size. Channel-axis deposits have high net-gross value; and these deposits correspond to the Bouma Ta division; on the other hand, channel-

off axis deposits comprise thin intercalations of massive sandstone with laminated sandstone, and correspond to the Tad Bouma divisions. The presence of erosional bases for the sandstones beds and shale intraclasts, the interbedding of debrites with turbidites and the abundance of chaotic-appearing features are several of the criteria mentioned by Weimer and Slatt (2004) to differentiate channel-fill sands from frontal splays (Fig. 2.10A).

This facies association was probably the result of repetitive and rapid deposition from high-density turbidity currents along a channel axis; this is inferred from the thick bedding (>3 m), the absence of fine-grained facies and the occurrence of amalgamation surfaces.

6.2.2. Channel margin

This group of facies is characterized by massive sandstone with mudstone intraclasts (F3), normally graded sandstones (F5), rippled, parallel and cross-laminated sandstone and siltstone (F8), laminated siltstone and mudstone (F9) and distorted heterolithic units (F11). Grain size and bed thickness are more variable due to the heterolithic composition; because of this characteristic, the sand net to gross ratio decreases. In this facies association, the Bouma Te, Td, Tc and Ta divisions are frequent.

These deposits occur in the lateral transition from channel off-axis to the channel margins, when the flow turbulence is not high enough to remove the fine-grained deposits. Instead, less erosion is inferred from the channel axis to the margin. The presence of distorted heterolithic units supports the interpretation of the collapse of channel walls.

Channel fill deposits in well logs commonly exhibit a boxcar log motif (cylindrical/box shape), and channel margin deposits show a fining-upward pattern. An example of the

interpretation of well log patterns and cores is shown in Fig. 2.11; this example comes from well A and the channel facies association is observed in core 2.

6.2 Leveed-channel facies association

This facies association comprises massive sandstone for the channel fill, with intercalations of thinly bedded sandstones, siltstones and shales for the levee deposits. Such association is represented by facies F4, F5, F6, F8, and F10; Facies F3 and F11 could be present, as a result of slumping and debris flow. The levee sub-environment is suggested by the deposition of siltstones with climbing ripples and parallel laminations, as well as the presence of beds with rip-up mudstone clasts and distorted heterolithic units (Posamentier and Walker, 2006). This facies association include Bouma Tb, and Tcde divisions. Bioturbation (*Zoophycos* and *Nereites ichnofacies*) is another characteristic of this facies association. Ratty log-motif is common, and thin upward in association with a channel. Examples of this facies association are shown in Fig. 2.10B and Fig. 2.11 core 3.

This group of facies were deposited along the margins of the channels where low-density turbidity currents formed overbank deposits. Minor erosion occurs in the proximal levee, as a result of an occasional increment in sediment concentration, turbulence and the angle of the slope. According to Talling et al. (2012) thin turbidite sand layers are common on channel – levees where levee deposits show evidence of dilute flow in the form of Tc, Td and Tb intervals if they are formed by bedwaves.

Leveed channels are frequently associated with other architectural elements, such as basal debris flows, frontal splays dissected and overlain by distributary channels, and hemipelagites.

6.3 Frontal Splay facies association

6.3.1. Proximal

This facies association comprises massive consolidated and unconsolidated sand (F4) and laminated sandstone (F6) and, in minor proportions massive sandstone with scarce floating pebbles at the base or shale intraclasts (F3) and laminated siltstone and mudstone (F9). This facies group frequently shows several flows that are amalgamated in an ordered stacking pattern. The amalgamation surfaces are marked by floating pebbles or very thin siltstone partings. The net-gross ratio is high. The Bouma Ta division predominates in amalgamated sands beds Fig. 2.12A. This facies association has coarsening to thickening-upward patterns. Some criteria that are diagnostic to frontal splays in cores are listed by Slatt , Jordan, and Davis (1994); Slatt, Stone, and Weimer (2000); and Witton-Barnes, Hurley, and Slatt. (2000) and include the following : a) high proportion of the Bouma Ta division; b) absence of the Bouma Tc division; c) lack of erosive bases; d) scarce or no shale clasts within the sand beds; e) few slumps or debrites; and f) somewhat ordered stacking patterns.

This facies association is mainly the result of high-density turbidity currents, and generally occurs in a more proximal environmental setting (Weimer and Slatt, 2004).

6.3.2. Distal

This facies association comprises fine-grained sandstone (F4), with beds of 14 cm thickness, intercalated with laminated siltstone and mudstone (F9), with beds of 7 cm; in minor proportions there is massive sandstone with floating pebbles (F3). The top and bottom contacts are planar. Sedimentary structures include load casts, planar features, and tabular sigmoidal and ripple laminations; some lenses of fine-grained sandstones and concretions of silt are also

observed. Fig. 2.12(B) shows an example of a distal frontal splay. The Ta and Td Bouma divisions are frequently present. Boxcar and coarsening-upward log-motifs are common; bow patterns are present when frontal splays are related to the waning or abandonment of a submarine fan (Fig. 2.11, core 1). Johnson, et al. (2001) provide several general characteristics of frontal splays, including the following: a) They have a tabular geometry with planar upper and lower surfaces; b) They are interbedded with siltstone and mudstone; c) They are thinner; d) They are dominated by ripple-laminated Tc beds; e) Layered sands are interbedded sand and mud packages, and f) They are common between channels in the mid-to upper fan and in more distal parts or lateral part of the fan (Weimer and Slatt, 2004). This facies association is the result of low-density turbidity currents.

Other examples of layered sands in more distal fans include ash tuff with very fine sand, and silt sizes (F13) and mudstone (F10). This association in some instances accompanied in minor proportions by distorted heterolithic units (F11). Siliceous cement is also present in these sandstones. This facies shows compensation cycles and may contain the complete set of Bouma divisions. An example of this type is illustrated in Fig. 2.11, Core 4.

The presence of ash tuff in some of these beds implies that these deposits resulted from explosive siliceous volcanic eruptions emplaced into deep-water settings. Flow transformations may have taken place from granular sediment density currents that evolved into turbidity currents basinward.

6.4 Lobes of debrites and associated flows facies association

6.4.1. Debrites

This facies association is mainly represented by muddy sandstone (F7), and is associated with thin intervals of facies F8, F9 and F11. Faults and fractures are abundant in the top and contortions related to faults at the base. The muddy sandstone is the result of cohesive debris flows, and the thin intervals are related with distal turbidites with Bouma T_{cde} divisions. Coarsening and box-shaped log patterns are common. Fig. 2.13 (well K and well G Core 2, illustrated examples of this type of lobes.

Other type of lobes is formed by hybrid sediment gravity flow deposits, in this case the facies association includes intraclast mudstone breccia (F1), intraclast mudstone conglomerate (F2) associated with structureless sandstone (F4), laminated sandstone (F6), laminated siltstone and mudstone (F9) and heterolithic units with sand injections (F12). The Ta, Tb and Te Bouma divisions are common in the upper part of the deposit, and the Bouma Ta division is common in the lower part. Coarsening-upward with serrate character and boxcar log patterns are observed in this group (Fig. 2.14).

Many studies have documented that both fluid turbulence and matrix strength can act simultaneously within the same flow; as a result, turbidity currents and debris flows are often genetically related. Additionally, different terms have been used to describe the deposits of such flows (Haughton, et al., 2003; Lowe et al., 2003; Pyles and Jennette, 2009; Talling, et al., 2004). These hybrid sediment gravity flows are named in the literature as “slurry flows” (Lowe and Guy, 2000), “co-genetic turbidite debrite” (Talling et al., 2004), “sandy debris flows” (Shanmugam, 1996), “concentrated density flows” (Mulder and Alexander, 2001) or

“hyperconcentrated flows” (Dasgupta, 2003). The deposits resulting from this type of flows have been named “hybrid sediment gravity flow deposits” (Haughton, et al., 2009), “linked debrite-turbidite beds” (Haughton et al., 2003) and “densites” (Gani, 2004). Moreover, Haughton et al. (2009) proposed a complete hybrid deposit composed of 5 divisions as follows: a) a lower structureless sandstone (high-density current); b) banded sandstone (transitional flow); c) clast-rich muddy sandstone (debris flow); d) laminated sandstone (low-density turbidity current); and e) mudstone cap (suspension fallout).

Different models have been proposed to explain the origin of these deposits. According to Sohn et al. (2000) the transformation from debris flow to turbidity current was based on the initial flow condition of hydroplaning and non-hydroplaning debris flow. Pickering and Corregidor (2005) mentioned that linked debrite-turbidites deposits are the products of flow transformations that resulted from multiphase granular flows. For Felix and Peakall (2006), this transformation was a combination of the erosion of material from the dense mass, the breaking apart of the dense underflow, the breaking of internal waves and turbulent mixing. Finally, Talling et al. (2004) mentioned that the transformation from debris flow to turbidite and the reverse was due to mixing and dilution, seafloor erosion, flow deceleration and deceleration of low-coherency debris flow.

7. Seismic Depositional Elements

7.1 Interpretation

Deep-water depositional elements were imaged and interpreted through the analyses of time slices, horizon slices and interval attributes, using a 3D seismic survey that comprises the merger of different seismic volumes in their post-stacked time migration versions. The morphology of deep-water systems was imaged in 3D seismic data by extraction of volume-based attributes, such as variance and spectral decomposition, to detect the morphology of the channels, especially at lower frequencies. Seismic attributes based on the interpreted horizons and horizon slices were utilized: sweetness, mean amplitude, maximum negative amplitude and root-mean-square (RMS) amplitude. However, the RMS attribute gave the best response to characterize this deep-water system. The interpretation of depositional elements considered the interactions between seismic sections in plan views. The examples shown in this study were between 2000 and 4500 m, and some of them were not well imaged on plan-view seismic attribute maps; however, some examples were calibrated with well information (well-logs and cores).

In this work the physical properties of the shales, sands and sandstones of calibrated examples from wells were also considered; and in this area, we knew that high amplitudes are related to sand and sandstones and low amplitudes to shales.

For the purpose of this study, the concept of depositional elements proposed by Mutti and Normark (1991) and modified by Posamentier (2003) was used.

7.2. Depositional elements

The depositional elements described below formed the building blocks of the Miocene deep-water depositional systems. Each element has some diagnostic seismic facies defined by external geometries and internal facies, and in some cases characteristic upper and lower surfaces. Their diagnostic properties are presented together along with the interpretation of the sedimentary facies, as well as their formative processes. Moreover, the analysis of depositional elements integrated stratigraphic, geomorphologic and facies observations on the basis of seismic, core and borehole data. The integration of facies descriptions and process sedimentology leads to the identification of larger-scale depositional or architectural elements, and their linkage with depositional systems. Depositional elements are on the order of ten to a few tens of meters in thickness and may extend laterally for tens to hundreds of meters.

A summary of the main depositional elements and their linkage with facies association and well-log patterns is shown in Fig. 2.15.

7.2.1 *Mass-transport complexes (MTC)*

A clear definition of mass-transport complexes (MTCs) remains under debate. Weimer (1989) used this term with a sequence stratigraphic connotation and included features that occur at the base of depositional sequences and are overlain and /or overlapped by channel and levee sediments. Moscardelli (2006) defined MTCs as “all kinds of sediment gravity flows” except for turbidity currents and proposed a classification based on seismic facies. Pickering and Corregidor (2005) used a general term to embrace a wide range of deposits due to individual flow events that could not always be identified. Thus, they included chaotic deposits in MTCs, usually with viscoplastic deformation and bedding disruption; which represent a wide range of

processes, including slides, slumps, debris flow, and turbidity currents. Seismic facies with chaotic to hummocky reflections have been interpreted as mud-rich deposits derived from gravity-driven mass-wasting processes, including debris flows, and slumps (Gee and Gawthorpe, 2006; Posamentier and Kolla, 2003).

In this study we use the term mass transport complexes on the basis on seismic facies that vary from thrust, to rotated and contoured blocks, slide blocks, chaotic and hummocky reflections, with poor to fair continuity and variable amplitude as a result of all kind of sediment gravity flows; according to this usage there are two types of MTCs recognized in this area.

Type I MTCs. This deposit type ranges in thickness from 440 to 540 meters, and mainly comprises extra-basinal carbonate platform deposits. The erosive nature of these MTCs can be clearly observed in seismic profiles. Detailed correlation and mapping show that the base is strongly diachronous (dated with paleontological data from the middle Oligocene to the lower Miocene); the upper surface is mounded and irregular, which indicates the bathymetry after the time of erosion. On seismic data, this element is recognized by its variable amplitude, with low-amplitude internally chaotic and high-amplitude contorted seismic facies. In map view, it has a lobate shape that reflects the relative confinement of the basin. The irregular upper surfaces of MTCs created local ponded accommodation, with the depressions upon which thin packets of heterolithic sediments infilling the residual topography (Fig. 2.15). Examples of this unit from wells show extra-formational clasts to cobble/boulder size of carbonate material (mudstone-wackestone) supported by a muddy matrix and fragments of corals and shells, with varying degrees of visco-plastic deformation. This unit also includes heterolithic sediments. This type of MTC probably represents the early phases of fan development when the upper slope and outer

shelf to the littoral zone collapsed and was redeposited in deep-water by sediment slides, slumps and debris flows (Pickering and Corregidor, 2005).

Type II MTCs. This type is mainly recognized in the lower Miocene. It is thinner in comparison with the previous one, and it has a variable thickness of up to 60 ms TWT. Its composition can be quite variable and depends on the nature of the sediment that failed, but in many cases consists of muddy sediment. Information from wells includes mud-rich deposits. The base and the top of this unit are planar with little apparent erosion and pinch out laterally. In seismic cross-sections, this element is identified by discontinuous reflections of medium to low amplitude; externally, it is mounded, and internally, it has contoured and hummocky facies, with small thrust faults and compressional structures. This deposit is overlain by two continuous parallel reflections of high amplitude that correspond to a condensed interval of pelagic deposits. On an RMS amplitude extraction map, a mottled appearance is observed; this seismic facies is characteristic of these deposits. This element is observed on the east of the area on the flanks of a salt body in topographic lows, so probably this deposit was formed as a result from mass wasting along oversteepened salt flanks. Seismic facies with similar characteristics have been interpreted as mud-rich deposits, derived from gravity-driven processes related with salt tectonics (Figs. 2.15 and 2.16).

7.2.2 Lobes of debrites and associated flows.

This type of lobe was recognized in the middle and upper Miocene units. They have a variable thickness, than not more of 100 ms TWT thick; their composition can be quite variable and depends on the nature of the sediment that failed, but in many cases consists of heterolithic sediments that tend to contain the greatest portion of sand-grade sediment. In cross-sections, this type of lobes is typically encased by two reflections of medium to high amplitude that pinch out

laterally; these surfaces with steepedges can give the appearance of mounding. In general, their basal surfaces are grooved, and in plan view, these grooves have long and linear features. Internally, these lobes have chaotic and contorted facies, and/or chaotic to reflection-free seismic facies, the later case is interpreted as mud-prone in debris-flow deposits (Posamentier and Kolla, 2003). (Fig. 2.15).

This depositional element was calibrated with well-log patterns interpretation and cores from positions which correspond to the facies associations of lobes of debrites and associated flows; so these examples include debrites (as a result of cohesive and non-cohesive debris flows) and hybrid sediment gravity flow deposits (Figs. 2.13 and 2.14). The shape of these deposits (especially cohesive debrites) is controlled strongly by subtle changes in the sea floor gradient and therefore by the basin morphology (Talling et al., 2012). Seismic facies with chaotic and low-amplitude reflectors have been interpreted as debrites in a variety of forms including lobes, and channels.

7.2.3 Submarine Channels

Submarine channels have been classified based on their architectural character, and two main classification schemes have been proposed. The first one includes three types of channels: a) erosional channels, b) erosional-depositional channels and c) depositional channels; this classification was proposed by Normark (1970). The second classification was introduced by Clark and Pickering (1996), who proposed three types of channels: a) erosional, b) aggradational (resulting from levee deposition) and c) a combination of both. However, in this study, we named the channel types on the basis of their plan-view and cross-sectional geometry as follows: a) erosional channels b) meandering channel belts and c) leveed channel belts combinations of these types of channels may also occur (Fig. 2.15). These channel systems are mainly developed

on the slope; older channels also developed at the base of the slope and on the basin floor. Erosional and sinuous aggradational channels developed in confined (intraslope) basins on the slope and on basin floor settings; according to Morris and Normark, (2000) erosional channels had few or no contemporaneous levee deposits. On the other hand, when the paleotopography of the slope is less affected by topographic highs and lows, the channels tended to be shallower and exhibit distributary and meandering patterns forming channel complexes, and leveed channels; these aggradational channels included levee and channel deposits, while simultaneously the buildup over time resulted in a channel-levee complex.

In *plan-view* the features of the submarine channels in the study area reveal that: the shapes vary from straight and linear to slightly sinuous, and from meandering (highly sinuous) to distributary. In Fig. 2.17, the images illustrate channel complexes made up vertically stacked single-story elements, with little or no lateral migration and vertical aggradation: A) is a slightly sinuous channel, B) a linear channel, C) a slightly sinuous channel, and D) a sinuous channel that resembles a braided channel due switching of the channel with time. These channels have sharp boundaries. Meandering channel belts in map view images are typified by high sinuosity with regular and smoothly-curved meander loops and evidence of bend cut-offs; these channels show high to moderate amplitude reflections. The size of these channels is highly variable, but in this area there have been measured channels greater than 4 km long with widths of 350 m, and channels that were vertically and laterally stacked to form complexes measuring up to 5 km wide and more than 8 km long. Examples of meandering channels from 3D attribute maps are shown in Fig. 2.17(E, F, G). Leveed channels on maps show low to moderate sinuosities and moderate to high amplitude; erosional channels in planform are linear to slightly sinuous with moderate to low amplitude.

In *seismic cross-sections*, meandering channels may show up as single reflections associated with lateral and down dip migration of the channel forming lateral accretion packages (LAPs) on the inner side of the channel; however, these LAPs are not always recognized and instead the channels may appear as a single, laterally extensive reflection of high amplitude. Levees in these types of channels are apparently lacking; but, there is no doubt that the channelized flows were spilling out and spreading sediment in overbank areas. On the other hand, the features of leveed channels are as follows: stacked, discontinuous high-amplitude reflections (HARs) for channel fill and low-amplitude continuous reflections wedge-shaped reflections away from the channel axis toward the levees; concave upward, planar and slightly erosional bases; channel fills with distinct lateral terminations (parallel and shingled); channel-fill terminations against the levees, and low-relief and high-relief channel-levees. Leveed channels have lower sinuosity than meandering forms. Some constructional features such as gull-wing geometry ("gull wing" shape formed by proximal levee deposits.) are observed in seismic profiles. Finally, the features of erosional channels are as follows: few or no associated overbank-levee deposits, although levees may occur in smaller channels belts; V- or S- shaped features with erosional bases; aggradational fills (some of which show HARs); channel-fill sediments that onlap against the erosional surface; and discontinuous high-amplitude reflections. Some erosional channels are truncated by younger channels, especially when they are stacked within channel complexes.

In the study area, erosional channels were formed by cut-and-fill processes, with little or no evidence of levees, and with the last-stage channel fill typically composed of mud-prone heterolithic deposits probably recording channel abandonment ; the older erosional channels identified were observed cutting the mass-transport deposits. Furthermore, younger erosional

channels probably also evolved by incision of incipiently meandering or leveed channels as a result of slumping and erosion. According to Clark and Pickering (1996), the stacking architecture of channelized sand bodies results from the interaction between lateral and vertical amalgamation processes that operated during the growth of the channel system. For Mayall and Stewart (2000) the sinuosity of channels is the result of a combination of several factors including erosion from bypassing flows, lateral stacking and lateral accretion of channels, and local fault-induced sea-floor topography. Peakall, McCaffrey, and Kneller (2000) stated that sinuous channels migrate laterally, only until equilibrium point is reached and the channel position stabilizes. Finally Abreu, Sullivan, Pirmez and Mohrig (2003) mentioned that aggradational sinuous channels could form by lateral migration (swing) and migration in the down-current direction (sweep). The formation of channel-levees requires overbanking of channelized flows; at least three types of overbanks flow have been documented in the literature to explain the formation of this type of channels, and they are as follows: a) inertial overspill (Hay, 1987); b) flow stripping (Piper and Normark, 1983); and 3) overspill (Peakall et al., 2000). Seismic examples of similar submarine channels are documented in offshore Angola (Abreu et al., 2003; Sikkerna and Wojcik, 2000) and the northern Gulf of Mexico (Posamentier and Kolla, 2003) among other places.

This depositional element is related with facies association 1 (Table 2.2); leveed channels were calibrated with well-log patterns (Fig. 2.11) and cores interpretations (Fig. 2.12B).

7.2.4 Frontal splays

In the study area, frontal splays were identified in lower and middle slope settings from the lower Miocene, while in middle Miocene; they were identified in confined settings in the

middle and upper slope, and in the upper Miocene in unconfined topographic settings on the upper slope. In confined settings, lateral contacts onlap or pinch out against salt bodies or structural highs and down-dip along the reflectors, frontal splays can be thin and lap out against a pre-existing depositional surface. In unconfined settings, frontal splays have downlap terminations in lateral contacts. This element is areally widespread in both confined and unconfined topographic settings; however, its areal extent depends on the paleotopography of the receiving basin.

The shape of frontal splays revealed from 3D seismic data varies due to confinement, in intraslope basins they are rounded, or have a lobate form; while in unconfined settings; distributary channel-pattern and elongate shapes are common. In plan-view, the size of the frontal splays varies up to 4 km wide and 8 km long. Examples of frontal splays are shown in Figs. 2.18 and 2.19.

In seismic profiles, this element is recognized by its medium to high amplitude reflections, mounded external appearance, continuous convex reflectors with bidirectional downlap and planar bases; channelized and tabular geometries are characterized by parallel continuous reflections that are concordant at the base are also observed (Fig. 2.15).

This depositional element is related with facies association 2 (Table 2.2), and well-log patterns of frontal splays in proximal fans exhibit coarsening upward and blocky with serrate log-motifs, and in distal fans, frontal splays show a serrate log-motif. Fig. 2.11 (Core 1 and 4); and Fig. 2.12.

During the upper Miocene, frontal splays could be formed by small distributary channels named in this work frontal splay complexes. This type of frontal splays is characterized in seismic cross-section by parallel laterally continuous, to slightly discontinuous reflections of

high amplitude, which are generally tabular and flat topped. In map view, they have an elongated geometry and present a distributary-channel pattern. Examples of frontal-splay complex are shown in Figs. 2.20 and 2.21.

These deposits are also referred in the literature as frontal-splay complexes (Posamentier and Kolla, 2003), channelized lobes (Demityttenaere, et al., 2000; Oluboyo, et al., 2014) and distributary –channel complexes (Twichell, et al., 1991).

8. Discussion

The interpretation from different data sets, allowed us to characterize the Miocene deep-water depositional systems as well as the depositional elements. As a result, during the early Miocene the predominant depositional element was the mass-transport complex, which was distributed throughout the study area within topographic lows (northern and central parts), but was absent on structural highs related to salt bodies (southern and eastern parts) (Figs. 2.4, 2.22 and 2.23). The thickness of this unit decreases towards the south and it considerably increases toward the central and northern part of the area in which a large depocenter was developed during this time. The mass-transport deposits were easily recognized on seismic data, due to their chaotic and contorted expression, as well as by their low-frequency, semi-continuous to continuous reflections of medium to high amplitude that pinch out to topographic highs (Fig. 2.15). This deposit is a mixture of slumps, slides and debris flows, towards the northeast it is composed by extra-formational clasts of cobble/boulder size of carbonate material (mudstone and grainstone) supported by a muddy matrix and fragments of corals and shells; this unit also includes heterolithic sediments. The deposition of this element created the accommodation where later turbidites and hybrid sediment gravity flow deposits were accumulated mostly filling the

topographic lows (wedges). Overlying these deposits, the second unit of chaotic deposits was distributed in the flank of a salt body located on the central and eastern of the area; towards the west and north of the area the internal reflection configuration of this unit changed to hummocky to mounded irregular discontinuous reflections of variable amplitudes, and cut-and-fill geometries, this most likely correspond to channelized deposits (Fig. 2.16). The early Miocene succession ended with the deposition of hemipelagic and pelagic sediments which were distributed across the entire study area and are represented by two parallel and continuous reflections of high amplitude. The formation of the mass-transport deposits may have been triggered by sea-level fall, and by the tectonic contractional event that occurred during the Eocene-Oligocene, which triggered the emplacement of allochthonous salt from this time until the Miocene (Angeles-Aquino et al., 1994); Cruz Mercado et al.,2009).

According to the interpretation from well-log, cores and seismic data for the middle Miocene succession, the predominant deposits are turbidites of high and low density deposited in channels and frontal splay depositional elements. The distribution of these deposits occurred in the northern and central parts of the area, where a large thickness is observed. The entry of sediments to this depocenter is mainly from the southeast. The thickness of these deposits decreases considerably towards the south and eastern parts of the area, where mudflows and grain flows were deposited in lobes, these deposits being the second most abundant type for this time (Figs. 2.22 and 2.23). The entry of sediments in these deposits comes from the south. Seismically, the turbidites deposited in frontal splays are characterized by parallel continuous to semi-continuous reflections of medium to high amplitude and high frequency, and in some cases are mounded; these deposits have onlap, toplap and downlap terminations and pinch out against topographic highs, the last one especially to the northwest part of the area (Fig. 2.15). Like the

top of the early Miocene, the middle Miocene succession ended with pelagic and hemipelagic deposits. The tectonics of the area played an important role in the distribution of the sediments, in the paleobathymetry (Fig.2.4); and in the directions of the sediment input which were from the south to north and from the southeast. This complex paleotopography was revealed by the high thickness variability of the deposits accumulated in small and large depocenters and in topographic highs; this paleotopography was the result of the main compressional event occurred in the area (Chiapanecan orogeny) as well as the emplacement of allochthonous salt.

Finally, for the late Miocene succession, the turbidites remain the most abundant type. Specifically the low-density turbidity deposits, which are presented in channel-levee (Fig. 2.10B), frontal splays (Figs 2.12A, and B) and frontal splay complex (Figs 2.20 and 2.21) depositional elements. For the early part of the late Miocene in the southern part, semi-discontinuous hummocky and mounded reflections of medium to low amplitude and chaotic deposits of low amplitude are commonly observed (Figs. 2.22 and 2.23); these deposits according to well-log patterns (Fig. 2.13 well K) and core interpretations correspond to debris flow and hybrid sediment gravity flow deposits (Fig. 2.14). On the other hand, areas with continuous reflections of high frequency and medium to high amplitude (especially the central and northern part) correspond to turbidite deposits (Figs 2.22 and 2.23). In the upper part of the late Miocene the occurrence of hemipelagic and pelagic deposits increases especially in the southern part of the area.

For the late Miocene the confinement of the sediments in depocenters formed by the salt movement decreases because the emplacement of allochthonous salt ceased at this time and an extensional deformation event began in the area. The increment of pelagic and hemipelagic

deposits in the southern part of the area evidenced the general water shallowing that reflects the progradation of the continental margin in the late Miocene (Fig. 2.4).

9. Conclusions

The paleobathymetric maps constructed in this work show general basin-ward movement of paleobathymetry over the time, varying from the lower slope to outer shelf, which reflects the overall progradation of the continental margin during the Miocene. These maps show bathymetric variations, with shallow bathymetries related to topographic highs and deeper bathymetries related to topographic lows. These fluctuations were interpreted to be the result of tectonic and sedimentation effects in the area more than sea level variation. In these maps, the coexistence of microfauna of different bathymetries was also observed, and these mixtures were probably the result of benthic fauna transported by turbidity currents. To conclude, sedimentation during the Miocene mainly occurred in a slope with bathymetric variations as a result of syndepositional tectonics (salt bodies, folds and faults) (Fig. 2.4).

From the sedimentary facies description, the main sediment gravity flows responsible for the deposition and transport of sands in the area were turbidity currents and debris flows. The most abundant sedimentary facies in cores are massive sands, massive sands with intraclasts or pebbles and massive shale (Figs. 2.7, C, D and J). The vertical and lateral distributions of these facies revealed seven facies associations in terms of the depositional elements; these facies associations were the building blocks for characterizing the depositional elements recognized using seismic data. These depositional elements were mass-transport complexes, submarine channels, frontal splays and lobes of debrites (Fig. 2.15).

The integration of different data sets supported the interpretation that during the Miocene, submarine fans were developed and evolved from confined topographic settings to unconfined topographic settings, as a result of the regional and local tectonics of the area. In general, sedimentation during the Miocene began with the deposition of a mass-transport complex, the residual paleotopography of them provided the accommodation for the deposition of turbidity currents of high density and debris flows and was finalized with the deposition of low-density turbidity currents and deposition from suspension fallout of pelagic and hemipelagic particles.

Acknowledgements

This research was completed as part of the doctoral project carried out by the first author fully sponsored by PEMEX- Exploración y Producción and other funds for Fondo Sectorial Conacyt-Sener-Pemex.

We thank the editor, Shane Tyrrell, as well as Jose Daudt and an anonymous reviewer, for their constructive comments which helped improve the manuscript during the peer review process.

References

Abreu, V., Sullivan, M., Pirmez, C., and Mohrig, D., 2003. Lateral Accretion packages (LAPs): an important reservoir element in deep water sinuous channels. *Marine and Petroleum Geology* 20, 631-648.

Amy, L.A., Talling, P.J., Peakall, J. Wynn R.B., and Arzola Thynne, R.G., 2005. Bed geometry used to test recognition criteria of turbidites and (sandy) debrites. *Sedimentary Geology* 179. 163-174.

Amy, L., Talling, P.J., Edmonds, V.O., Sumner, E.J., and Leseuer, A., 2006. An experimental investigation of sand-mud suspension settling behaviour: implications for bimodal mud contents of submarine flow deposits. *Sedimentology*, 53, 1411–1434.

Ángeles-Aquino, F., Reyes-Núñez, Quesada-Muñeton and Meneses Rocha, J.J., 1994. Tectonic Evolution, Structural Styles and Oil habitat in Campeche sound, Mexico: Gulf Coast Association of geological Societies Transactions. V 44, pp 53-62.

Aquino-Lopez J.A., 2004. Sureste Basin, Mexico and Associated Sub-basins: An update and Future Potential. AAPG International Conference: October 24-27; Cancun México.

Baas, J.H., Best, J.L., and Peakall, J., 2011. Depositional processes, bedform development and hybrid flows in rapidly decelerated cohesive (mud-sand) sediment flows. *Sedimentology*, 58, 1953–1987.

Bagnold, R.A., 1954. Experiments on a gravity-free dispersion of large solid spheres in Newtonian fluid under shear. *Proceedings of the Royal Society of London, A*, 225, 49-63.

Bannerjee, I., 1977. Experimental study on the effect of deceleration on the vertical sequence of sedimentary structures in silty sediments. *Journal of Sedimentary Petrology*, 47, 771–783.

Bouma A.H., 1962. Sedimentology of some Flysch Deposits: A graphic Approach to Facies Interpretation (pp.68). Amsterdam: Elsevier.

Bouma A.H., 2000. Fine-grained, mud-rich turbidite systems: model and comparison with coarse-grained, sand-rich systems. In: Bouma CG, Stone CG, editors. *Fine-grained turbidite systems*, American Association of Petroleum Geologists Memoir 72, SEPM Special Publication, vol. 68; pp. 9-20.

Bouma, A.H., 2004. Key Controls on the Characteristics of Turbidite Systems. In Lomas, S. A. and Joseph, P. (Eds.) 2004. *Confined Turbidite Systems*. Geological Society, London, Special Publications, 222, pp. 9-22.

Buffler, R.T., and Sawyer D.S., 1985. Distribution of crust and early history Gulf of Mexico Basin. *Gulf Coast Association of Geological Societies Transactions*. 35.333-344.

Chapin, M.A., Davies, P., Gibson, J.L., and Pentigill, H.S., 1994. Reservoir Architecture of turbidite sheet sandstones in laterally extensive outcrops, Ross Formation, western Ireland. In P. Weimer, A.H.

Bouma, and B.F.Perkins (Eds.). Submarine fans and turbidite systems. Gulf Coast Section SEPM Foundation 15th Annual Research Conference, pp.53-68.

Clark, J.D., and Pickering, K.T., 1996. Architectural elements and growth patterns of submarine channels: application to hydrocarbon exploration. American Association of Petroleum Geology Bulletin, 80, 194-221.

Corliss, B.H., and Fois E., 1990. Morphotype analysis of deep-sea benthic Foraminifera from northwestern Gulf of Mexico: Palaios v.5.589-605.

Cruz-Mercado M.A., Reyes-Tovar E., López-Cespedes, H.G., Peterson-Rodríguez R.H., Sánchez-Rivera, R., Flores-Zamora, J.C et al., 2009. Estudio Interregional Tectónica Salina y sus implicaciones en la Exploración Petrolera Pemex. Unpublished report.

Dasgupta, P., 2003. Sediment gravity flow- the conceptual problems. Earth-Science Reviews. 62, 265-281.

Demmytenaere, R., Tromp, J.P., Ibrahim, A., Allman-Ward, P., and Meckel, T., 2000. Brunei Deep Water Exploration: From Sea Floor Images and Shallow Seismic Analogues to Depositional Models in a Slope Turbidite Setting., in P. Weimer, R.M. Slatt, J.L.Coleman, N. Rosen, C.H. Nelson, A. H Bouma, M. Sytzen, and Lawrence, (Eds.),Global deep-water reservoirs: GCS-SEPM Foundation 20th Annual Bob. F. Perkins Research Conference, 304-317.

Doranzo D.M., and Dellino, P., 2013. Hydraulics of subaqueous ash flows as deduced from their deposits: Water entrainment, sedimentation, and deposition, with implications on pyroclastic density current deposit emplacement. Journal of Volcanology and Geothermal Research 258. 176-186.

Duranti, D., and Hurst A., 2004. Fluidization and Injection in deep-water sandstones of the Eocene Alba Formation (UK North Sea). Sedimentology 51, 503-529.

Elliot, T., 1998. A renaissance in the analysis of turbidite systems: Implications for reservoir development and management. EAGE/AAPG Research conference, Developing and managing turbidite reservoirs: Case histories and experiences. Almeria, Spain, October 1-8.

Escalera- Alcocer, A., and Hernández-Romano, U., 2009. Provincias Petroleras de México. WEC México. Schulmberger.

Felix, M., and Peakall, J., 2006. Transformation of debris Flows into Turbidity Currents: Mechanisms Inferred from Laboratory Experiments. *Sedimentology* 53, 107-123.

Fillon, R.H., 2007. Biostratigraphy and Condensed Sections in Deepwater Settings in Weimer, P. and Slatt, R. Introduction to the Petroleum Geology of Deepwater Settings. American Association of Petroleum Geology Studies in Geology 57, American Association of Petroleum Geology /Datapages Discovery Series 8.

Gani, M.R., 2004. From Turbid to Lucid: A Straightforward Approach to Sediment Gravity Flows and their deposits. *The sedimentary Record*, v.2, no.3, 4-8.

Gee, M.J.R., and Gawthorpe, R.L., 2006. Submarine Channels controlled by salt tectonics: examples from 3D seismic data offshore Angola. *Marine Petroleum Geology*, 23, 443-458.

Gomez-Cabrera, P.T., and Jackson, M.P.A., 2009. Neogene stratigraphy and salt tectonics of the Santa Ana area, offshore Salina del Istmo Basin, southeastern Mexico, in Bartolinni C. and Roman Ramos J.R, (Eds.). *Petroleum systems in the southern the Gulf of Mexico* American Association of Petroleum Geology Memoir 90 .237-255.

Hampton, M.A., 1975. Competence of fine grained debris flows. *Journal of Sedimentary Petrology*, 45, 833–844.

Haughton, P.D.W., Barker, S.P., and McCaffrey, W.D., 2003. Linked debrites in sand-turbidites systems—origin and significance. *Sedimentology* 50, 459–482.

- Haughton, P., Davis, C., McCaffrey W., and Barker, S., 2009.** Hybrid sediment gravity flow deposits- Classification, origin and significance. *Marine and Petroleum Geology*, 26, 1900-1918.
- Hay, A.E., 1987.** Turbidity current and submarine channel formation in Rupert Inlet, British Columbia: 2. The roles of continuous and surge-type flow. *J. Geophysical Research*, 92, 2883–2900.
- Hiscott, R.N., 1994.** Traction-carpet stratification in turbidites fact or fiction. *Journal of Sedimentary Research*, 64, 204–208.
- Johansson, M., and Stow, D.V., 1995.** A classification scheme for shale clasts in deep-water sandstones in Hartley, A.J. and Prosser, D.J., (Eds.). *Characterization of Deep Marine Clastic Systems*, Geological Society Special Publication, n.94, pp.221-241.
- Johnson S.D., Flint, D., Hinds and Deville Wickens H., 2001.** Anatomy, geometry and sequence stratigraphy of basin floor to slope turbidite systems. Tanqua Karoo, South Africa: *Sedimentology*, 48,987-1023.
- Kneller, B., and Branney, M.J., 1995.** Beyond the turbidite paradigm: physical models for deposition of turbidites, and their implications for reservoir prediction. In Hartley, A.J., Prosser, C. (Eds.), *Characterization of deep Marine Clastic Systems*. Special Publication, V.94. Geological Society of London, London, UK, 31-49.
- Kuenen, P.H., 1966.** Experimental turbidite lamination in a circular flume. *Journal of Geology*, 74, 523–545.
- Loubere, P., Gary, A., and Lagoe, M., 1993.** Sea-bed biochemistry and benthic foraminiferal bathymetric zonation of the slope of the northwestern Gulf of Mexico: *Palaios*, 8, 439-449.
- Lowe, D.R., 1982.** Sediment gravity flows: depositional models with special reference to the deposits of high-density turbidity currents. *Journal of Sedimentary Petrology*, 52(1), 0279-0297.

Lowe, D.R., and Guy, M., 2000. Slurry flow deposits in the Brittania Formation (Lower Cretaceous) North Sea: a new perspective on the turbidity current and debris flow problem. *Sedimentology*, V.47, 31-70.

Lowe, D. R., Guy, M., and Palfrey, A., 2003. Facies of slurry-flow deposits, Brittania Formation (Lower Cretaceous) North Sea: Implications for flow evolution and deposit geometry. *Sedimentology*, 50, 45-80.

Lucchi, F.R., and Valmori, E., 1980. Basin-wide turbidites in a Miocene, over-supplied deep-sea plain: a geometrical analysis. *Sedimentology*, 27, 241-270.

Mahaffie, M.J., 1994. Reservoir classification for turbidite intervals at the Mars discovery, Mississippi canyon 807, Gulf of Mexico. In P. Weimer, A.H.Bouma, and B.F. Perkins (Eds.). *Submarine fans and turbidite systems* (pp.183-213). Coast section-SEPM special publication 42.

Marton, G., and Buffler, R.T., 1994. Jurassic Reconstruction of the Gulf of Mexico Basin. *International Geology Review*, 36, 545-586.

Mayall, M., and Stewart, I., 2000. The Architecture of Turbidite Slope Channels, in P. Weimer, R.M. Slatt, J.L. Coleman, N. Rosen, C.H. Bouma, M. Styzen, and D.T. Lawrence, (Eds.), *Global deep-water reservoirs: Gulf Coast section SEPM Foundation 20th Annual Bob F. Perkins Research conference*, 578-586.

Morris, W. R., and Normark, W.R., 2000. Scaling, sedimentologic and geometric criteria for comparing modern and ancient sandy turbidite elements, in P. Weimer, R. M. Slatt, J. L. Coleman, N. Rosen, C. H. Nelson, A.H. Bouma, M. Styzen, and D. T. Lawrence, (Eds.), *Global deep-water reservoirs: Gulf Coast Section–SEPM Foundation 20th Annual Bob F. Perkins Research Conference*, p. 606–628.

Moscardelli, L., Wood, L., and Mann, P., 2006. Mass transport complexes and associated processes in the offshore area of Trinidad and Venezuela. *American Association of Petroleum Geologists Bulletin*, 90, (7), 1059-1088.

Mulder, T., and Alexander, J., 2001. The physical character of subaqueous sedimentary density flows and their deposits. *Sedimentology*, 48, 269-299.

Mutti, E., and Nielsen, T. H., 1981. Significance of intraformational rip-up clasts in deep sea fan deposits. International Association of Sedimentologists, 2nd European Regional Meeting Bologna, Italy.

Mutti, E., and Normark, W.R., 1987. Comparing examples of modern and ancient turbidite systems. Problems and concepts. In J.K.Legget & G.G. Zuffa (Eds.), *Marine clastic sedimentology* (pp.1-38). London: Graham and Trotman.

Mutti, E., and Normark, W.R., 1991. An integrated approach to the study of turbidite systems. In P.Weimer, and M.H.Link (Eds.). *Seismic facies and sedimentary processes of submarine fans and turbidite systems* (pp.75-106). New York: Springer-Verlag.

Nielsen, T.H., and Kerr, R., 1978. Turbidites, Red beds, Sedimentary Structures, and Trace fossils. Leg 38 Cores and Sedimentary History of the Norwegian Basin: DSDP Leg 38. Doi:10.2973/dsdp.proc.383940.119.1978.

Oluboyo, A.P., Gawthorpe, R.L., Bakke K., and Hadler-Jacobsen F., 2014. Salt tectonics controls on deep-water turbidite depositional systems: Miocene, southwest Lower Congo Basin, offshore Angola. *Basin Research*, 26,597-620.

Padilla y Sánchez, R.S., 2007. Evolución geológica del sureste de mexicano desde el Mesozoico al presente en el contexto regional del Golfo de México. *Boletín de la Sociedad Geológica Mexicana*. Tomo LIX, N. 1. 19-42.

Peakall J., McCaffrey B., and Kneller B., 2000. A process model for the evolution, morphology, and architecture of sinuous submarine channels. *Journal of Sedimentary Research*, V.70.No 3 434-448.

PEMEX-IPM., 2000. Proyecto de Integración Bioestratigrafía. Informe Inédito.

Pickering K.T., and Corregidor J., 2005. Mass transport complexes and tectonic control on confined basin-floor submarine fans, Middle Eocene, south Spanish Pyrenees. In: Hodgson, D.M. and Flint, S.S. (Eds.) 2005. Submarine Slope Systems: Processes and Products. Geological Society, London, Special Publications, 244. The Geological Society of London.

Pindell, J.L., 1985. Alleghenian reconstruction and subsequent evolution of the Gulf of Mexico, Bahamas and Proto-Caribbean. *Tectonics*, 4, 1-39.

Pindell, J.L., and Kennan, L., 2002. Análisis Paleogeográfico Mesozoico-Cenozoico y Dinámica de las cuencas en el Golfo de México Profundo y Márgenes. Informe Final. Tectonic Analysis Inc. and Pemex Exploration and Production. Inédito.

Pindell, J. L., and Kennan, L., 2009. Tectonic Evolution of the Gulf of Mexico, Caribbean and Northern South America in the Mantle Reference Frame: an update. In James, K.H., Lorente, M.A and Pindell, J. L. (Eds.). *The Origin and Evolution of the Caribbean Plate*, Geological Society of London, Special Publications 328.1-55.

Piper, D.J.W., and Normark, W.R., 1983. Turbidite depositional patterns and flow characteristics, Navy submarine fan, California Borderland. *Sedimentology*, V. 30, 681–694.

Posamentier, H.W., 2003. Depositional elements associated with a basin floor channels-levee system: Case study from the Gulf of Mexico. *Marine and Petroleum Geology*, 20, 667-690.

Posamentier, H.W., and Kolla V., 2003. Seismic geomorphology and stratigraphy of depositional elements in deep-water settings. *Journal of Sedimentary Research*, 73,367-388.

Posamentier, H.W., and Walker, R.G., 2006. Deep-water turbidites and submarine fans. In Posamentier, H. W., and Walker, R.G. (Eds.). *Facies Models Revisited*. Special Publication, SEPM (Society for Sedimentary Geology). no.84, 397-520.

Postma, G., Nemec, W., and Kleinspehn, K.L., 1988. Large floating clasts in turbidites: a mechanism for their emplacement. *Sedimentary Geology*, 58, 47-61. (In Johansson, M and Stow, D.V. (1995). A classification scheme for shale clasts in deep-water sandstones. in Hartley, A.J. and Prosser, D.J., (Eds.). *Characterization of Deep Marine Clastic Systems*, Geological Society Special Publication, N.94.221-241)

Prost, G., and Aranda, M., 2001. Tectonics and Hydrocarbon Systems of the Veracruz Basin, Mexico, in Bartolini, C., Buffler, R. T. and Cantu- Chapa, A., (Eds.). *The Western Gulf of Mexico Basin: Tectonics, Sedimentary Basins and Petroleum Systems: American Association of Petroleum Geology Memoir 75*, p. 271-291.

Pyles, D. R., and Jeannete, D.C., 2009. Geometry and architectural associations of cogenetic debrites-turbidite beds in basin-margin strata. Carboniferous Ross Sandstone (Ireland): applications to reservoirs located on the margins of structurally confined submarine fan. *Marine and Petroleum Geology*, 1974-1996.

Richards, M., Bowman, M., and Reading, H., 1998. Submarine-fan systems I: Characterization and stratigraphic prediction. *Marine and Petroleum Geology*, 15, 687-717.

Robles-Nolasco, J., Pliego-Vidal, E., Toledo-Bante, C., Pimienta-Lugo, M., Ortega-González, V., Martínez-Pena, B., et al., 2004. Offshore Neogene plays, Salina del Istmo Basin, southeast of Mexico: Tulsa, Oklahoma, E.U.A., American Association of Petroleum Geologists, International Conference, October 24-27, Cancun, Mexico, 5p.

Rogers, R., Mann, P., and Emmet, P.A., 2007. Tectonic terranes of the Chortis block base on integration of regional aeromagnetic and geologic data. In Mann, P., (Eds.), *Geologic and Tectonic development of the Caribbean plate in northern Central America: Geological Society of America, Special paper 428*, 65-88.

Ross, M.I., and Scotese, C.E., 1988. A hierarchical model of the Gulf of Mexico and Caribbean Region: *Tectonophysics*, 155, 139-168.

Salomón-Mora, L.E., Aranda-García, M., and Román-Ramos, J.R., 2009. Contractional growth faulting in the Mexican Ridges, Gulf of Mexico, in Bartolini, C. and Roman- Ramos, J.R. (Eds.). Petroleum systems in the southern Gulf of Mexico: American Association of Petroleum Geology Memoir 90, 93-115.

Salvador, A., 1987. Late Triassic- Jurassic Paleogeography and Origin of Gulf of Mexico. American Association of Petroleum Geology Bulletin, 71, 419-451.

Salvador, A., 1991. Triassic-Jurassic in Salvador, A. (Eds). The Gulf of Mexico Basin: Geological Society of America. The Geology of North America, V.J., 131-180

Sánchez, R. M-A., González, L. J-C., Ayala, N.M., Padilla, A. P., Del Valle, R, A., Sánchez, D. M-J., Urbano, G. D., and Martínez, N. M., 2002. Bioestratigrafía de Alta Resolución del Terciario en Pozos de la Cuenca de Veracruz y la Sonda de Campeche. Instituto Mexicano del Petróleo. Informe Inédito.

Sánchez -Hernández Hilarion., 2013. Stratigraphic characterization and evolution of Mid-Tertiary age Deep water system, Holok área, SW Gulf of Mexico. PhD Thesis, University of Aberdeen.

Sánchez-Montes de Oca, R., 1980. Geología petrolera de la Sierra de Chiapas. Boletín de la Asociación Mexicana de Geólogos Petroleros, 31(1-2), 67-77.

Sanders, J.E., 1960. Primary sedimentary structures formed by turbidity currents and related re-sedimentation mechanisms. The Society of Economic Paleontologists and mineralogists (SEPM) Primary Sedimentary Structures, (SP12), 192-219.

Shanmugam, G., 1996. High-density turbidity currents: are they sandy debris flows? Journal of Sedimentary Research, 66, 2-10.

Shanmugam, G., 2006. Deep-Water Processes and Facies Models: Implications for Sandstone Petroleum Reservoirs. Amsterdam: Elsevier, p. 47.

Shanmugam G., 2012. New Perspectives on Deep-water Sandstones, Volume 9: Origin, Recognition, Initiation and Reservoir Quality (Handbook of Petroleum Exploration and Production). Elsevier. 544p.

Sikkema, W., and K. M. Wojcik., 2000. 3D visualization of turbidite systems, Lower Congo Basin, offshore Angola, in P. Weimer, R. M. Slatt, J. L. Coleman, N. Rosen, C. H. Nelson, A. H. Bouma, M. Styzen,, and D.T. Lawrence, (Eds.). Global deep-water reservoirs: Gulf Coast Section–SEPM Bob F. Perkins 20th Annual Research Conference, p. 928–939.

Slatt, R. M., Jordan, D.W., and Davis, R. J., 1994. Interpreting formation microscanner log images of Gulf of Mexico Pliocene turbidites by comparison with Pennsylvanian turbidite outcrops, Arkansas, in P. Weimer, A. H. Bouma and B. F. Perkins, eds., Submarine fans and turbidite systems: Gulf Coast Section–SEPM Foundation 15th Annual Research Conference, p. 335–348.

Slatt, R. M., C. G. Stone., and Weimer, P., 2000. Characterization of slope and basin facies tracts, Lower Pennsylvanian Jackfork Group, Arkansas, with applications to deepwater (turbidite) reservoir management, in P. Weimer, R. M. Slatt, J. L. Coleman, N. Rosen, C. H. Nelson, A. H. Bouma, M. Styzen, and D. T. Lawrence, (Eds.). Global deep-water reservoirs: Gulf Coast Section–SEPM Foundation 20th Annual Bob F. Perkins Research Conference, p. 940–980.

Sohn, Y.K., 2000. Depositional processes of submarine debris flows in the Miocene fan deltas. Pohang Basin, SE Korea with special reference to flow transformation. *Journal of Sedimentary Research*, 70.491-503.

Sumner, E.J., Amy, L., and Talling, P.J., 2008. Deposit structure and processes of sand deposition from a decelerating sediment suspension. *Journal of Sedimentary Research*, 78, 529–547.

Sumner, E.J., Talling, P.J., and Amy, L.A., 2009. The deposits of flows transitional between turbidity currents and debris flow. *Geology*, 37, 991–994.

Sumner, E.J., Talling, P.J., Amy, L.A., Wynn, R.B., Stevenson, C., and Frenz, M., 2012. Facies architecture of individual basin-plain turbidites: comparison to existing models and implications for flow processes. *Sedimentology*, doi: 10.1111/j.1365-3091.2012.01329.x

Talling, P.J., Wynn, L.A., Peakall, J., and Robinson, M., 2004. Beds comprising debrite sandwiched within cogenetic turbidite: Origin and widespread occurrence in distal depositional environments: *Sedimentology*, 51, 163-194.

Talling, P.J., Amy, L.A., Wynn, R.B., Blackbourn, G., and Gibson, O., 2007c. Turbidity current evolution deduced from extensive thin turbidites: Marnoso-arenacea Formation (Miocene), Italian Apennines. *Journal of Sedimentary Research*. 77, 172–196.

Talling, P. J., Masson, D. G., Sumner, E. J. and Malgesini, G., 2012. Subaqueous sediment density flows: Depositional processes and deposit types. *Sedimentology*, 59(7), 1937-2003.

Twichell, D.C., Kenyon, N.H., Parson, L.M., and McGregor, B.A.M., 1991. Depositional patterns of the Mississippi Fan surface: evidence from GLORIA II and high-resolution seismic profiles, in Weimer, P., and Link, M.H., (Eds.). *Seismic facies and sedimentary processes of submarine fans and turbidite systems*: New York, Springer-Verlag, p. 349–364.

Villamil, T., Arango, C., Weimer, P., Waterman, A., Rowan, M.G., Varnai, P.... Crews, J.R., 1998. Biostratigraphic techniques for analyzing benthic biofacies, stratigraphic condensation, and key surface identification, Pliocene and Pleistocene sediments, Northern Green Canyon and Ewing Bank (offshore Louisiana), northern Gulf of Mexico. *American Association of Petroleum Geology Bulletin*, 82,961-985.

Vrolijk, P.J., and Southard, J.B., 1997. Experiments on rapid deposition of sand from high-velocity flows. *Geosci. Can.*, 24, 45–54.

Walker, R.G., 1978. Deep-water sandstone facies and ancient submarine fans; models for exploration for stratigraphic traps. *Bulletin of the American Association of Petroleum Geologists* 62: pp. 932-966.

Walker, R.G., 1992. Turbidites and submarine Fans.. In Walker, R. G. and James N. P., Facies Models, Response to sea level change Geological Association of Canada, pp. 239-263.

Weimer P., 1989. Sequence stratigraphy of the Mississippi Fan (Pliocene-Pleistocene) Gulf of Mexico. Geo-Marine Letters, 9,185-272.

Weimer, P., and Slatt, R.M., 2004. Petroleum Systems of Deepwater Settings. Distinguished Instructor Series, No.7.EAGE. Tulsa, OK. USA.

Witton-Barnes, E. M., Hurley, N. F. and Slatt, R. M., 2000. Outcrop characterization and diagnostic criteria for confined vs. unconfined deep-water sandstones using outcrops and borehole images, Lewis Shale, Wyoming, in P. Weimer, R. M. Slatt, J. L. Coleman, N. Rosen, C. H. Nelson, A. H. Bouma, M. Styzen, and D. T. Lawrence, (Eds.), 2000, Global deep-water reservoirs: Gulf Coast Section–SEPM 20th Annual Research Conference, p. 1087-1105.

Figures

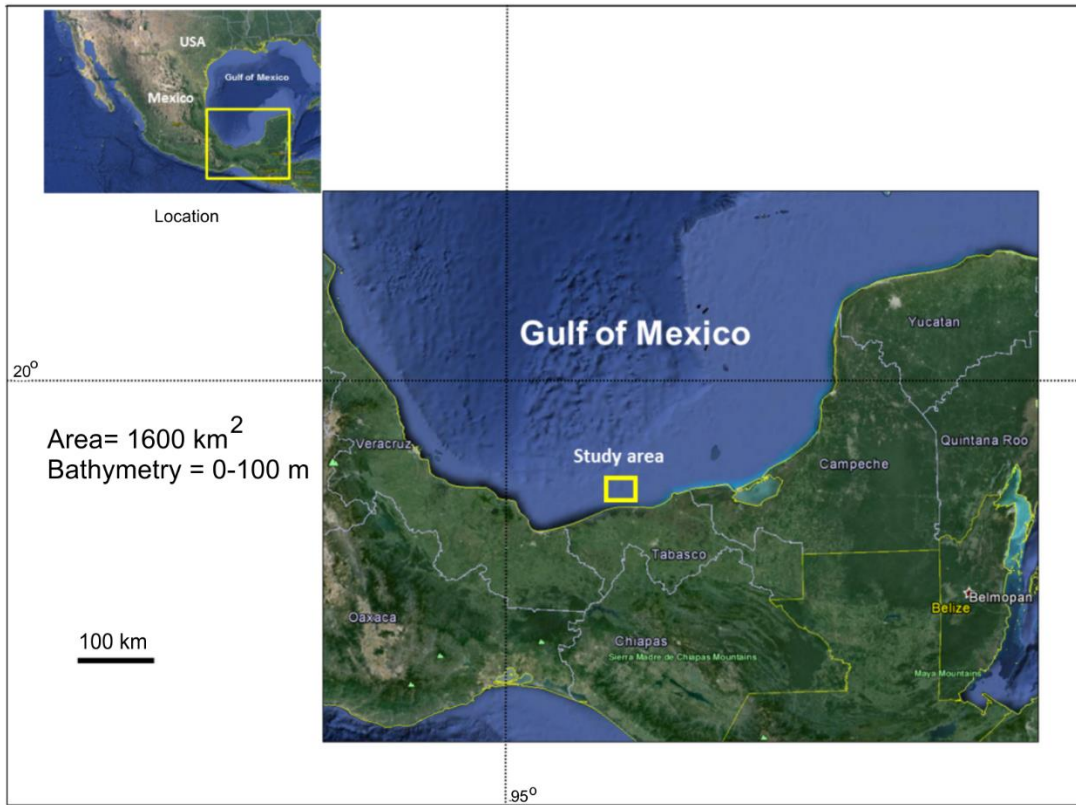


Figure 2.1 Location map of study area in the southern Gulf of Mexico

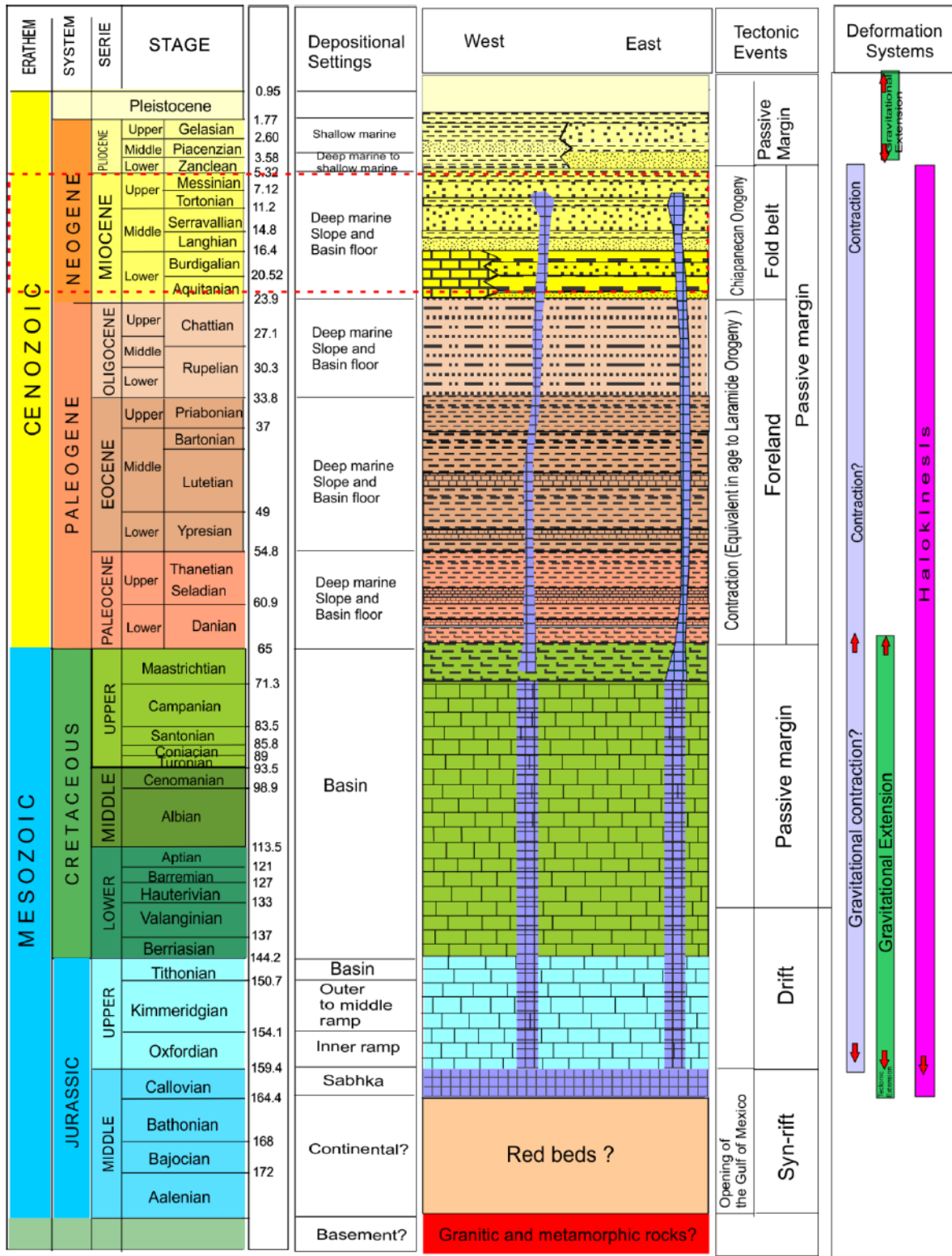
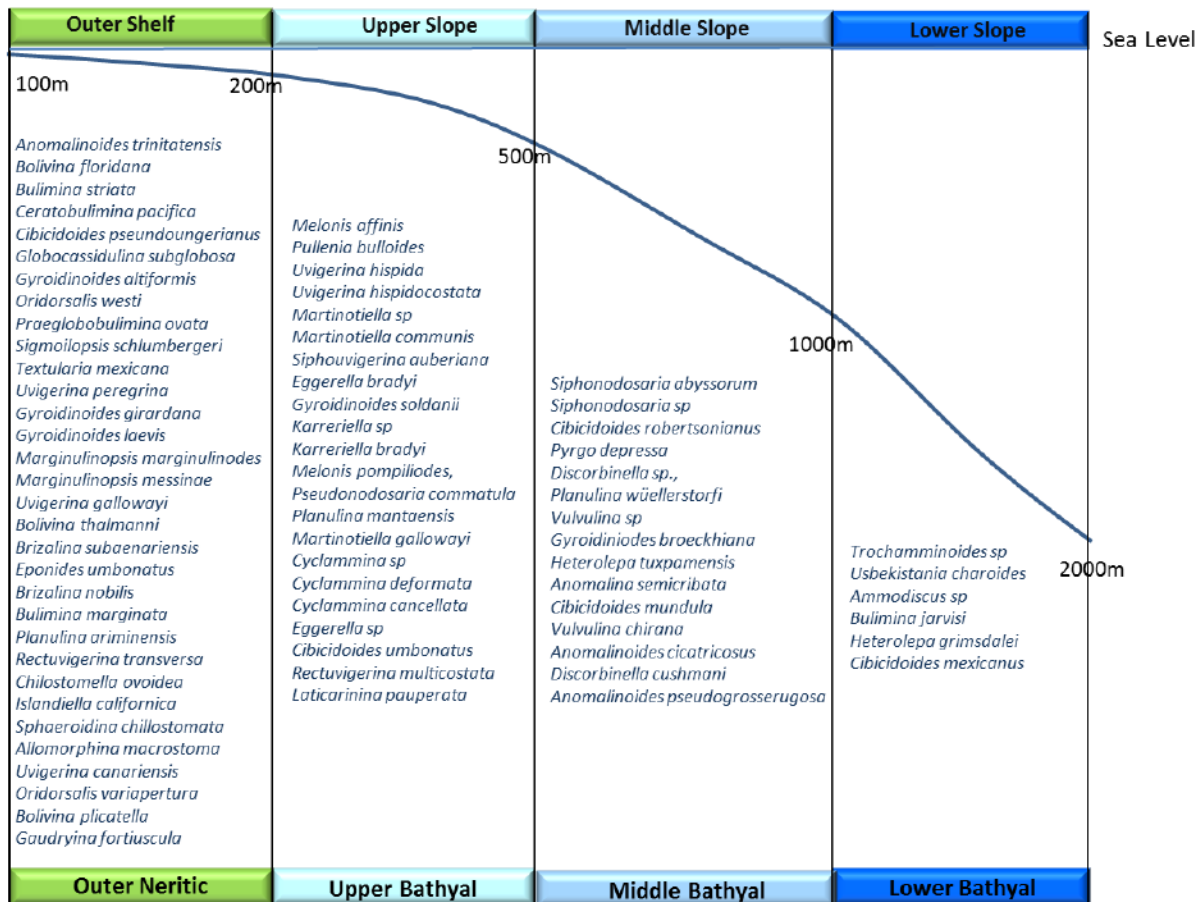


Figure 2.2 Stratigraphic chart showing the main regional tectonic and deformational events present in the study area. The focus of this study is exclusively on the Miocene units.



Modified from Proyecto de Integración Bioestratigráfica PEMEX-IMP, 2000

Figure 2.3 Paleobathymetric profile defined by benthic foraminifera assemblages established for the Mexican basins. Modified from PEMEX-IMP, (2000).

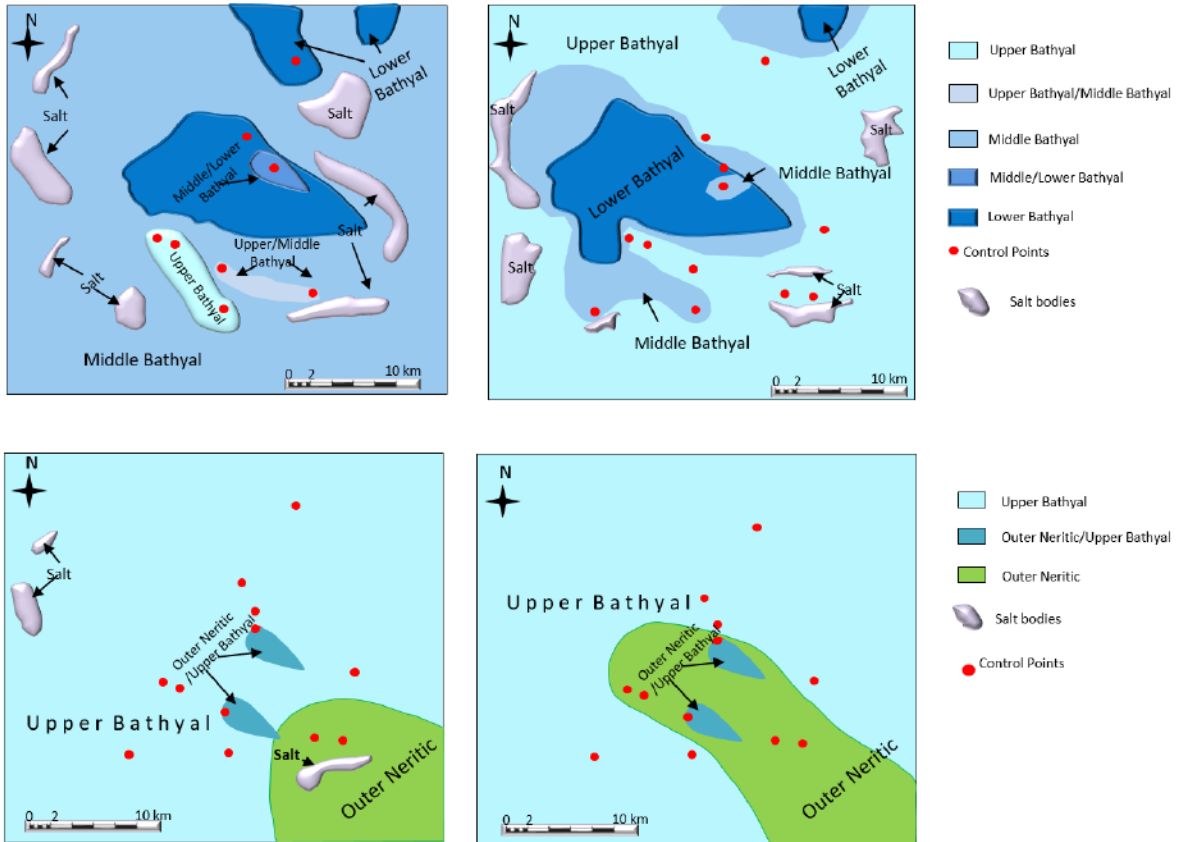


Figure 2.4 Paleobathymetric maps show general water shallowing that reflects the progradation of the continental margin. These maps also show shifts in the paleoenvironments that reveal the strong control of the tectonics and sedimentation on the paleobathymetry.

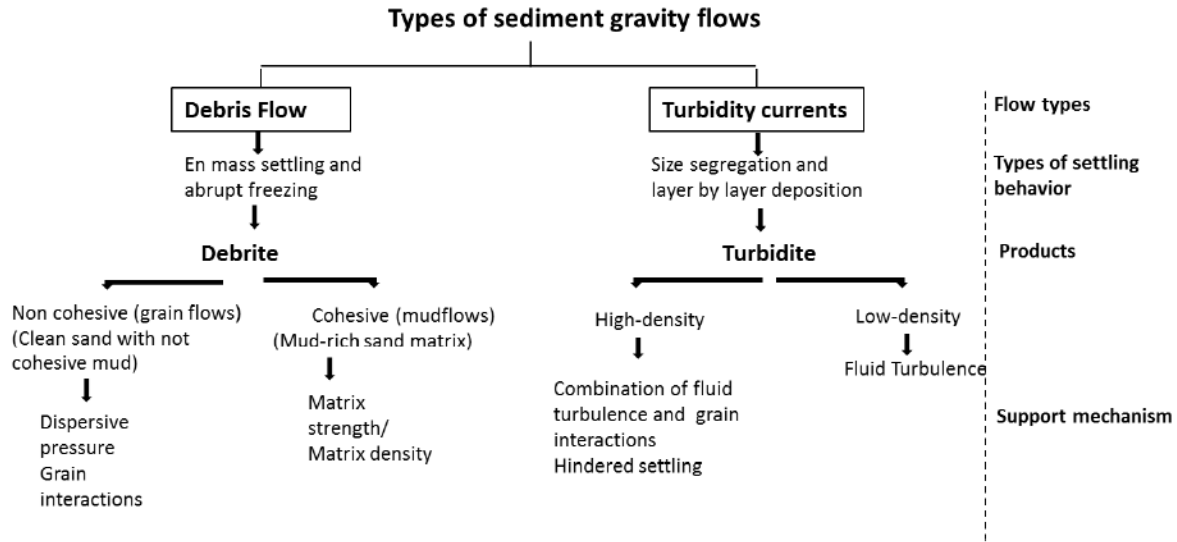


Figure 2.5 Main sediment gravity flows recognized in this study, including for each one the types of settling behavior, products and grain support mechanisms.

Classification scheme for shale clasts occurring with sandstones beds (Johansson and Stow, 1995)

A (Basal Erosion or disruption of underlying or laterally adjacent beds during the flow)	B (Erosion and Transport. Clasts modify by transport with flow)	C (Post-depositional processes)
A1 Shale clast breccia (Slump debris flow)	B1 Shale clast conglomerate (Non-cohesive sandy debris flow)	C1 Rip-down clasts (Rip-down process)
A2 Scour-lag clasts (Traction at the bed of the flow)	B2 Isolated clasts (Buoyancy)	C2 Injection clasts (Ripping process due to sand injection and post-depositional disturbance)
A3 Rafted clasts (Rip-up process)	B3 Clustered clasts (Floating and Inertia layer)	
A4 Amalgamation clasts (Amalgamation surfaces)	B4 Dispersed clasts (High-concentration turbidity currents)	
A5 Flame clasts (Loading and Injection)	B5 Lamination clasts (Traction at the base of the flow)	

Figure 2.6 Summary of the classification scheme for shale clasts occurring with sandstone beds, proposed by Johansson and Stow (1995).



Figure 2.7 Core photographs illustrating the different types of lithofacies interpreted in this study. The examples come from five wells.

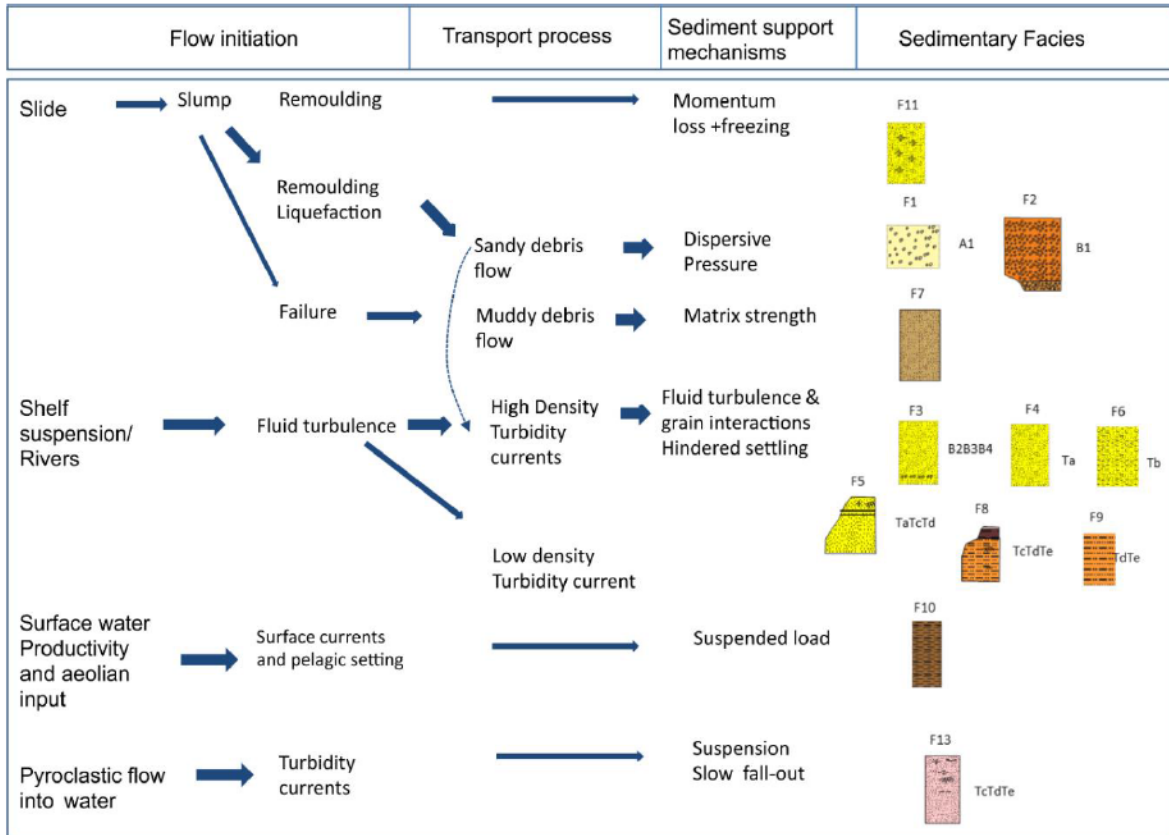


Figure 2.8 Sedimentary facies recognized in this study, which result from deposition by different processes, different mechanisms for initiation and transport, and post-depositional modifications. The color in the facies represent the size of the sediments; yellow color in facies in F11F3F6F5 represent sand, light yellow in F1 represent breccia, orange in F2 conglomerate, light brown in F7 muddy sand, light orange silt, and dark brown mud. (Modify from Walter, 1978).

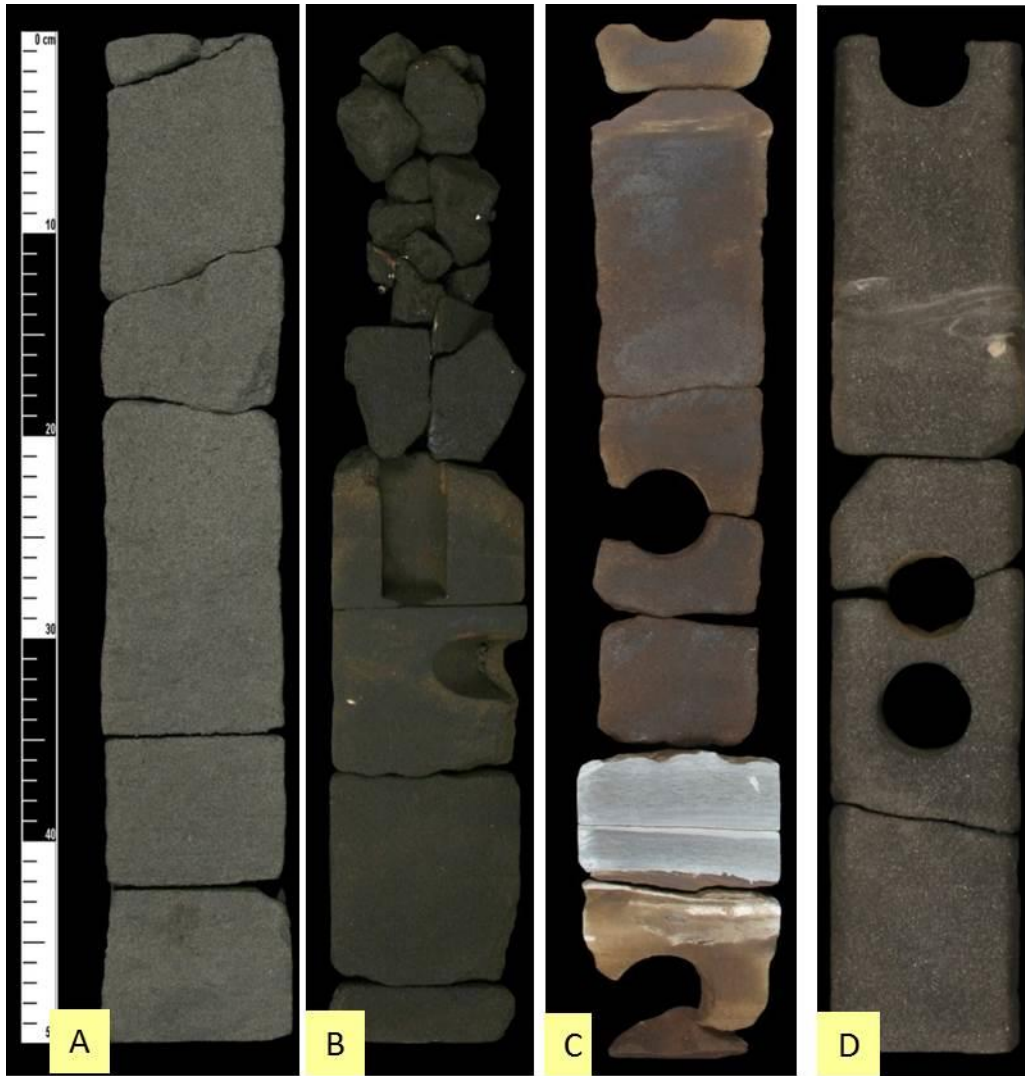


Figure 2.9 Core photographs showing examples of massive sands A) This photograph illustrates internally homogenous unconsolidated sands; B) Structureless sands with oil impregnation; C) Massive sands with siltstone partings; and D) Structureless sand with a flame structure.

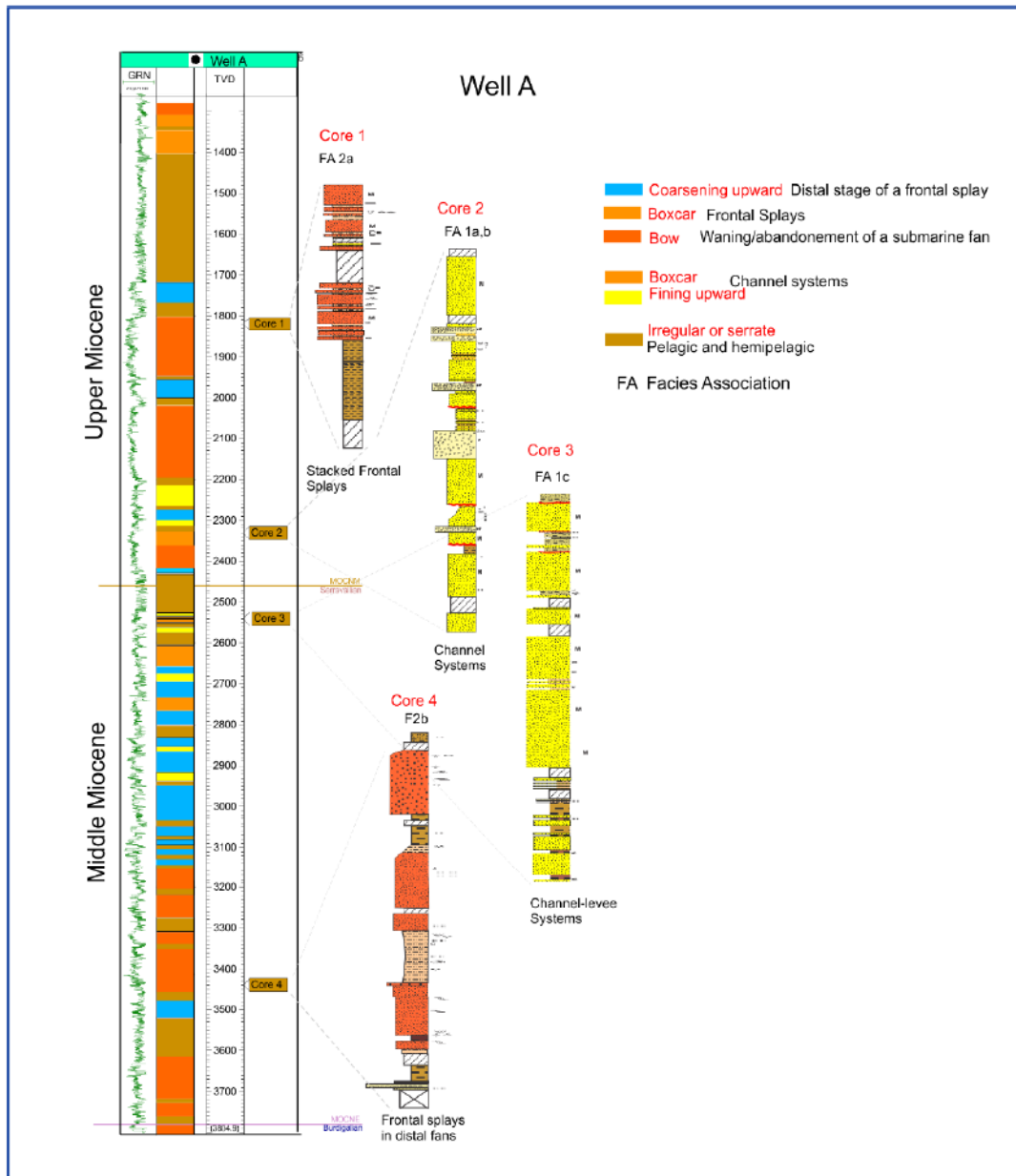


Figure 2.11 shows the interpretation of well logs patterns and cores for well A, which is located in the central part of the study area. In this well are predominant turbidites deposited in channel systems (facies association (1a and b), channel levees (facies association 1C) and frontal splays (Facies association 2a and 2b).

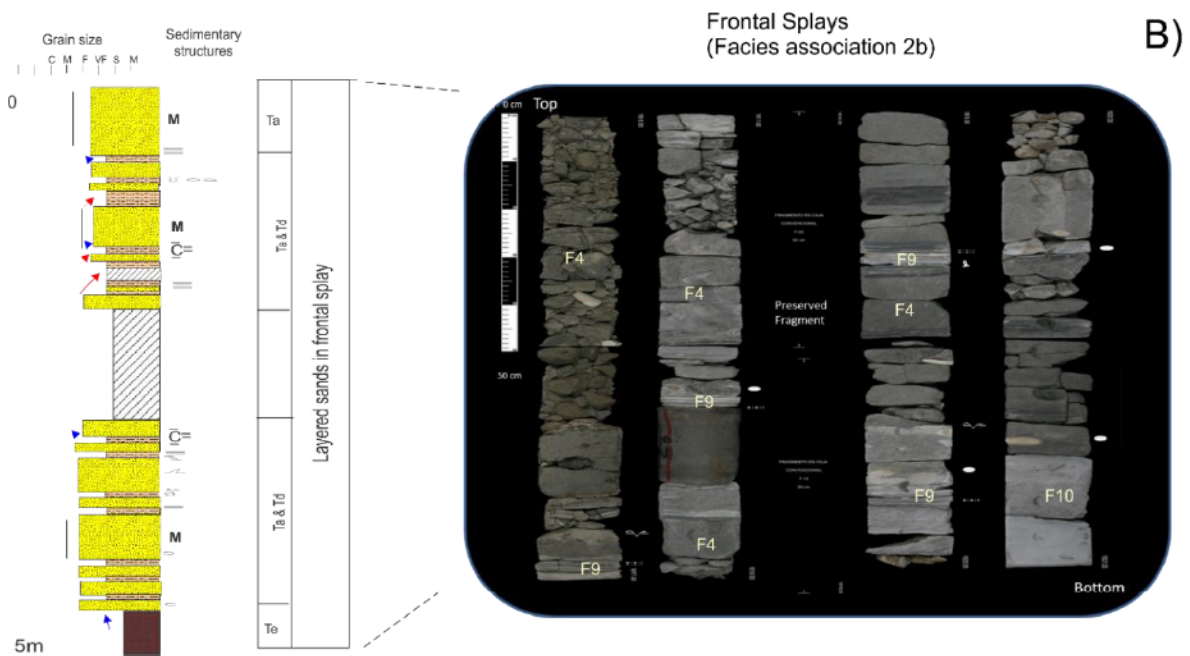
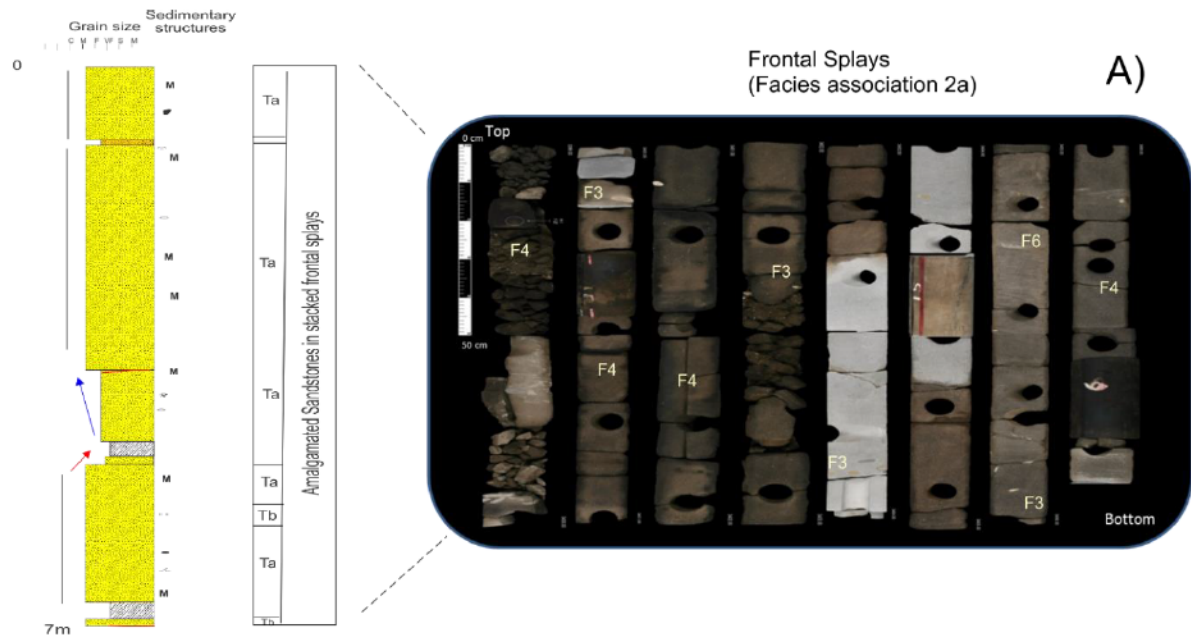


Figure 2.12 A) Core photographs illustrating the frontal-splay facies association from amalgamated sandstones in stacked proximal frontal splays; this example comes from well J, located in the southern of the area. B) Core photographs illustrating layered sands in a distal frontal splay; this example comes from well A core 1. Blue arrow indicated coarsening-upward pattern, red arrow fining-upward, and black line boxcar pattern.

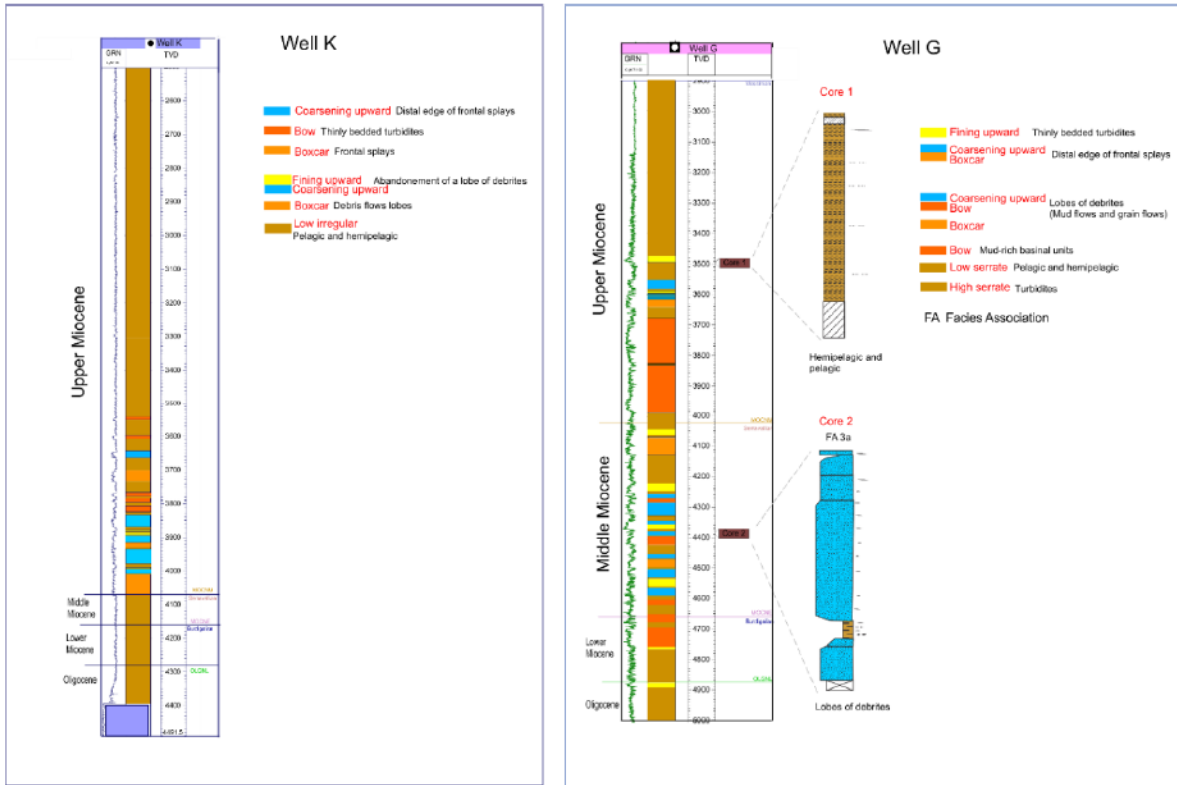


Figure 2.13 shows two wells located in the southern area. The well-log patterns in well K exhibit frontal splays, channels and lobes of debris. The thin thicknesses of the lower and middle Miocene units are due to a salt body cut at 4400meters. On well G the interpretation was also based on cores interpretation, in the middle Miocene we have lobes of debris (facies association 3b) and frontal splays for the upper Miocene.

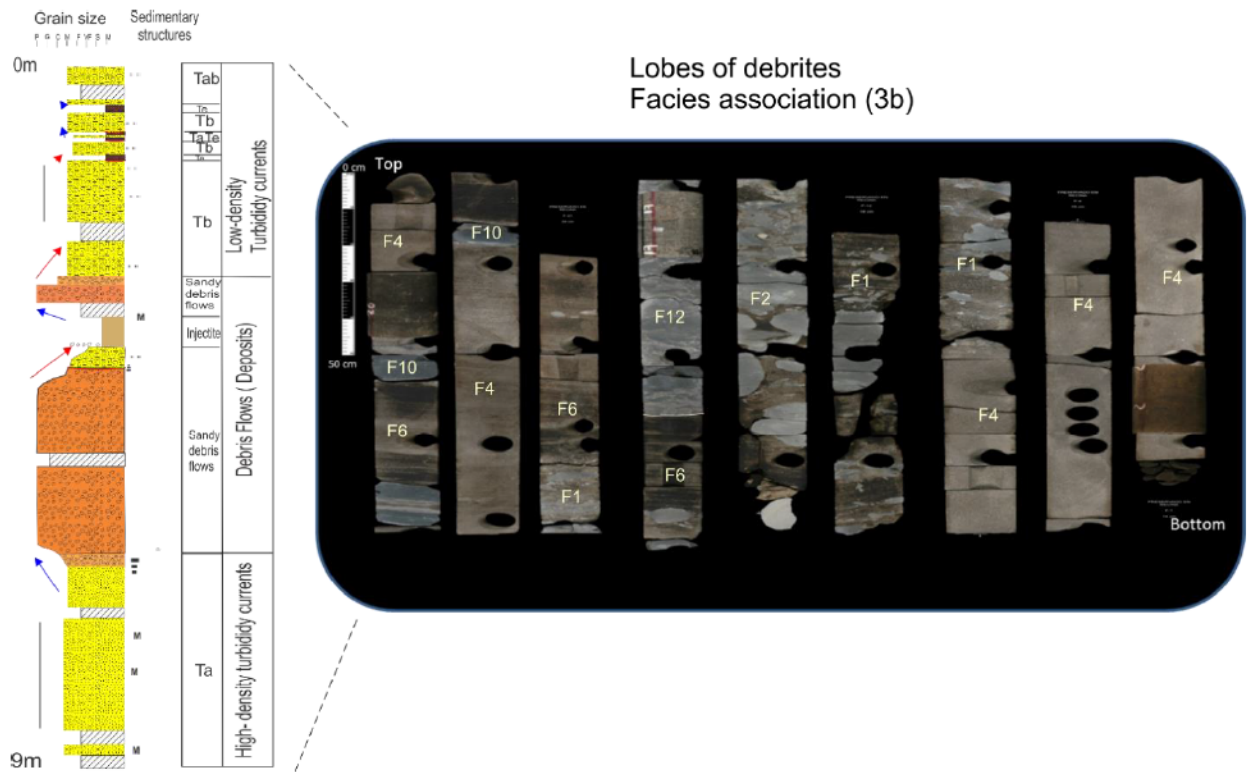


Figure 2.14 Core photographs illustrating debrisites encased in turbidites. This example comes from well J, located in the southern of the area. Blue arrow indicated coarsening-upward pattern, red arrow fining-upward, and black line boxcar pattern.

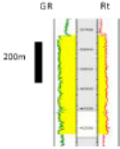
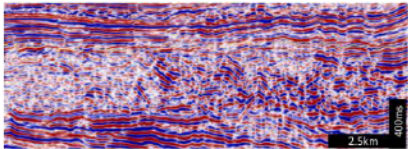
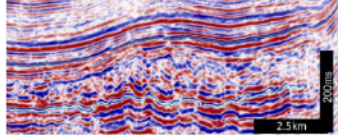
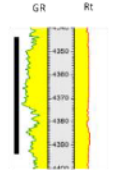
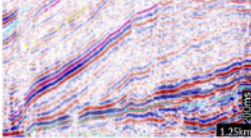
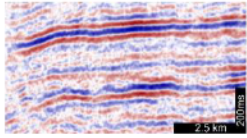
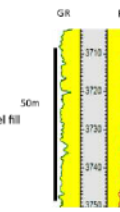
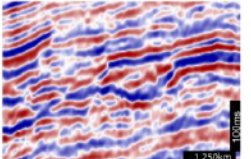
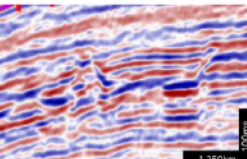
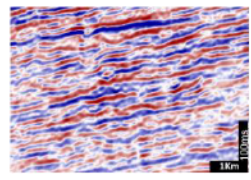
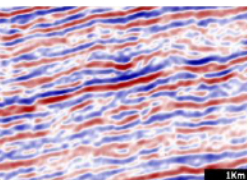
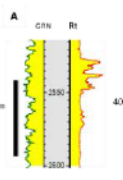
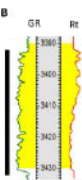
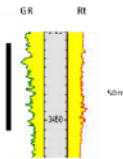
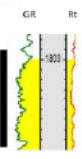
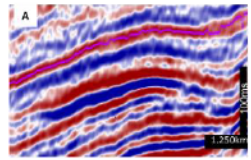
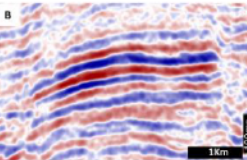
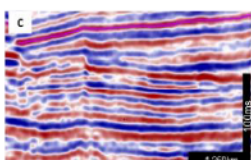
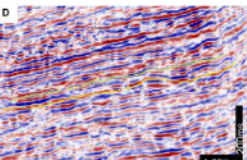
Depositional Element	Characteristics	Welllog motifs	Seismic
Mass-Transport complexes	<ul style="list-style-type: none"> Variable amplitude, chaotic, contorted seismic facies Erosive Base Calibrated example has carbonate breccia and shale fill Blocky log motif 		 
Lobes of debrites and associated flows	<ul style="list-style-type: none"> Medium to low amplitude Lateral pinch out Mounded externally Internally mounded and discontinuous In map view straight and narrow Coarsening-upward to box-shape Facies association 3 (a and b) 		 
Submarine Channels	<p>1) Meandering Channels</p> <ul style="list-style-type: none"> Erosional bases Channel fill has distinct lateral terminations V- or U-shaped features High-sinuosity and smoothly curved meander loops Vertical and lateral stacked Discontinuous high amplitude reflectors <p>2) Leveed channels</p> <ul style="list-style-type: none"> Concave upward and planar slight erosional base Channel fill terminations (parallel and shingled) Gully-wing geometry Vertical and lateral stacked Discontinuous high amplitude reflectors (HARs) to channel fill Low amplitude continuous reflectors for the levees Braided-distributary to sinuous Ratty and thins upward log motifs Facies association 1C 		   
Frontal-Splays	<p>1) Frontal splay (Amalgamated sands)</p> <ul style="list-style-type: none"> High to medium amplitude Mounded externally appearance Continuous convex-up reflectors with bidirectional/downlap Coarsening and thickening upward Facies association 2a. <p>2) Frontal Splay (Layered sands)</p> <ul style="list-style-type: none"> High amplitude Parallel/continuous reflectors Tabular and flat topped Elongated shaped geometry or distributary in plan-view Blocky and coarsening upward With serrate character Facies association 2b. 	   	   

Figure 2.15 shows the characteristics (seismic features, well-log patterns and facies associations) of the main depositional elements recognized in this study, as well as examples of seismic profiles.

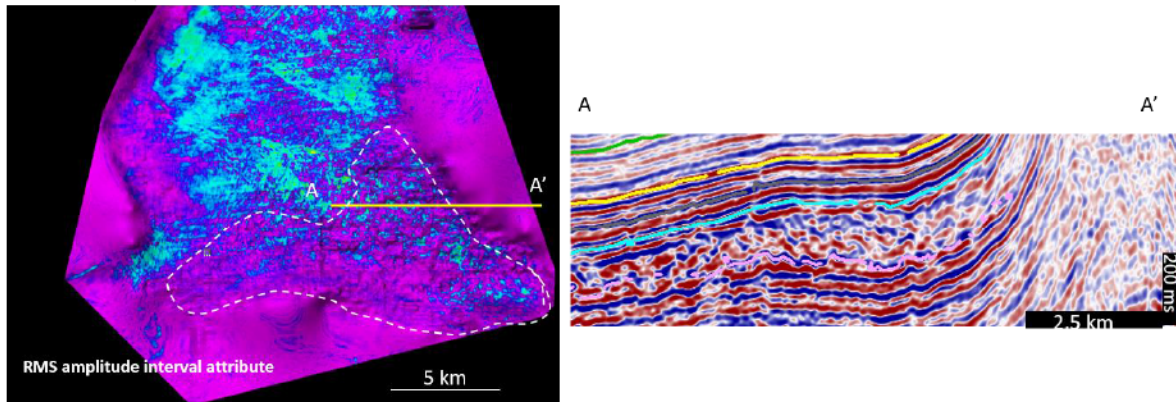


Figure 2.16 RMS amplitude map and one seismic profile illustrating mass-transport deposits. The 3D RMS amplitude map was extracted 20 ms below the top of the MTD (blue interval in seismic profile A). This depositional element occurred in the lower Miocene.

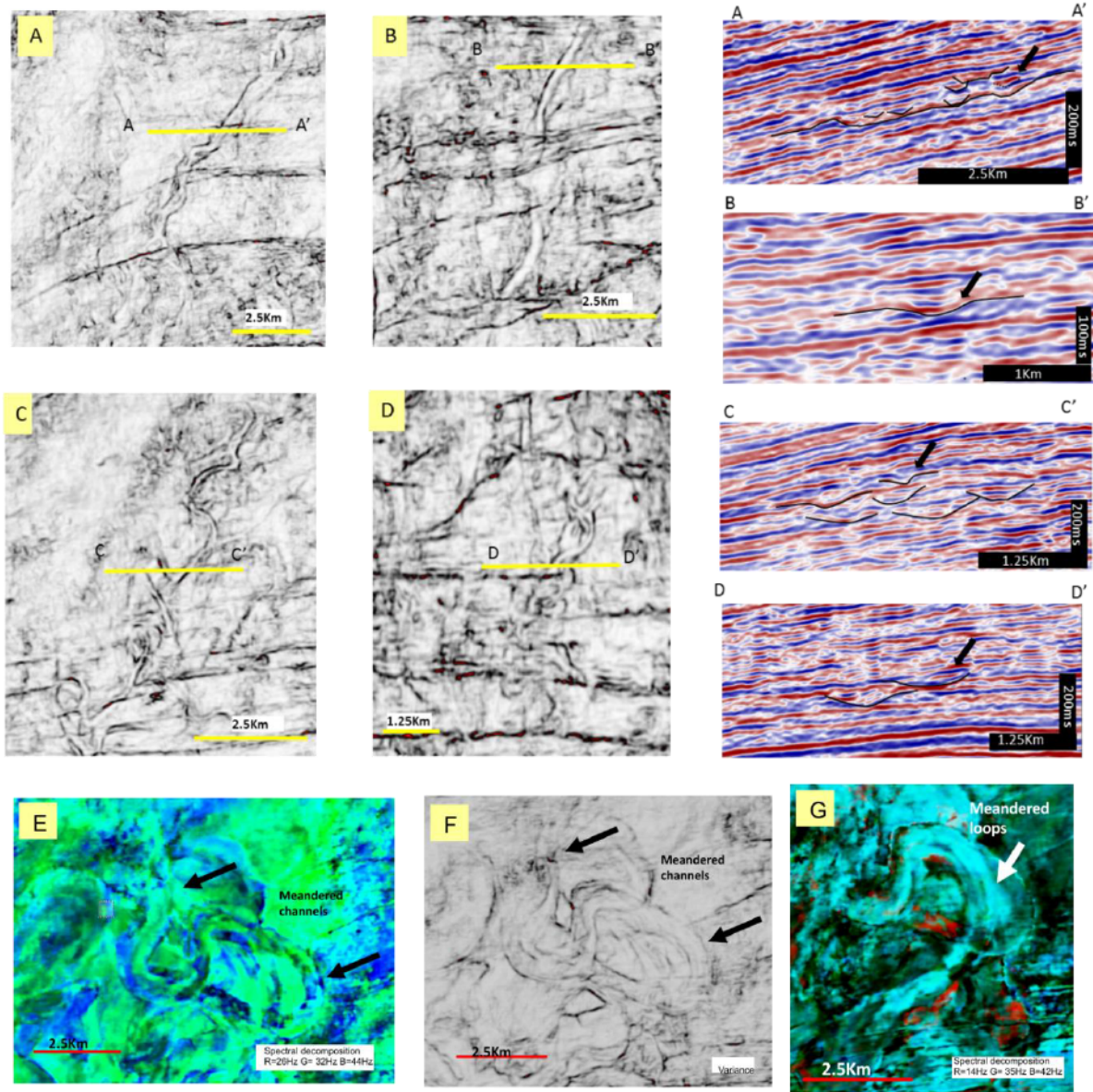


Figure 2.17 Examples of 3D seismic-derived plan-view images for submarine channels using seismic attributes. A, B, C and D are examples from the upper Miocene, and E, F and G from the middle Miocene. Some of the images show channel complexes made up of vertically stacked single-story elements, with little or no lateral migration and vertical aggradation which is observed in the seismic profiles. A) Slightly sinuous channel; B) Linear channel; C) Slightly sinuous channel, and D) Sinuous channel that resembles a braided channel due to lateral migration of the channel with time. E) and G) Examples of 3D seismic-derived plan-view images for meandering channels from spectral decomposition and F) meandering channels obtained from variance attribute.

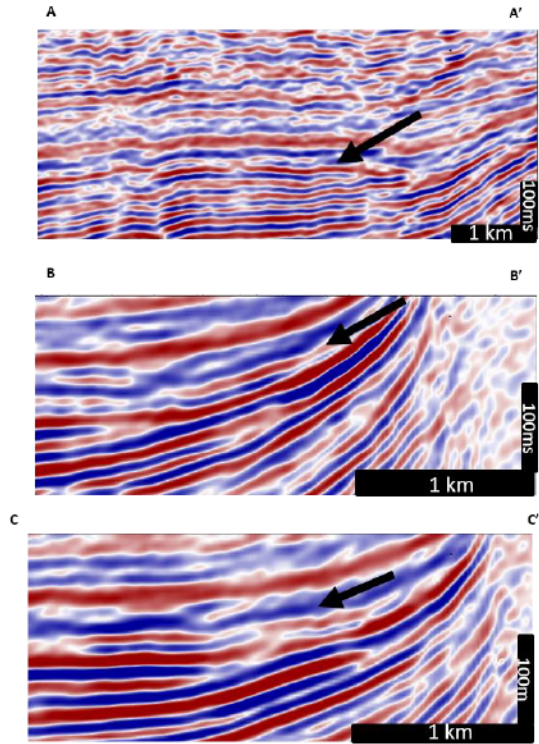
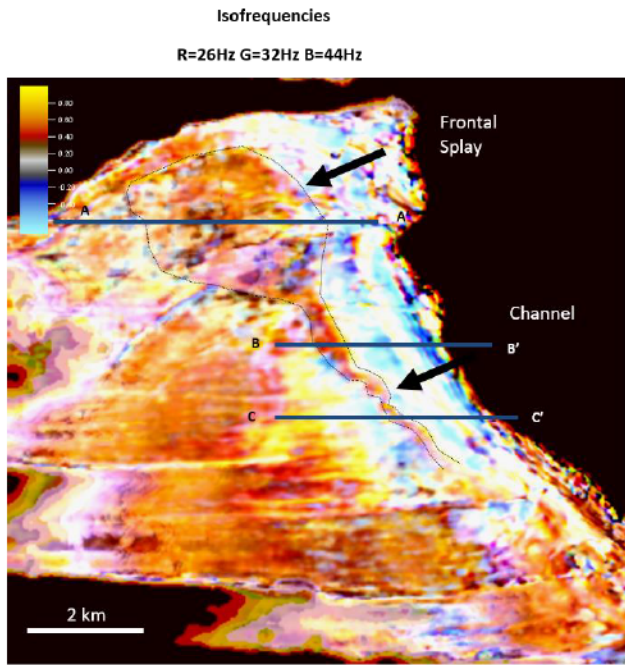


Figure 2.18 Examples of 3D seismic-derived plan-view images and seismic profiles to illustrate frontal splays for the upper Miocene. On the map at the left a younger channel and frontal splay are overlapping an older frontal splay calibrated with two wells.

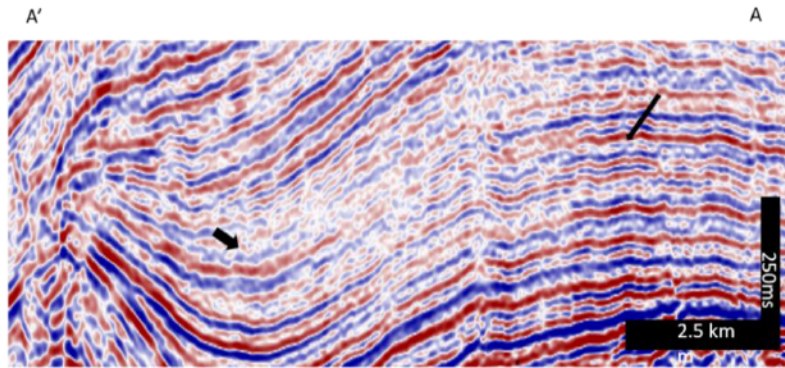
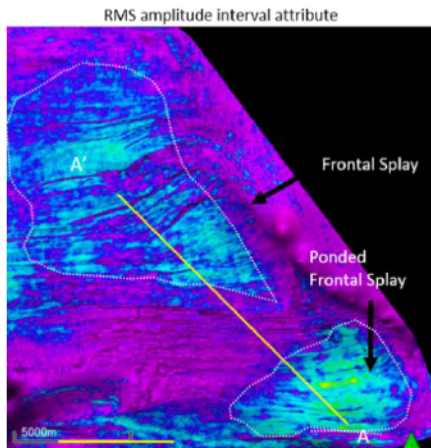


Figure 2.19 Example of 3D seismic-derived plan-view image and seismic profiles for frontal-splay and ponded frontal splay for the middle Miocene.

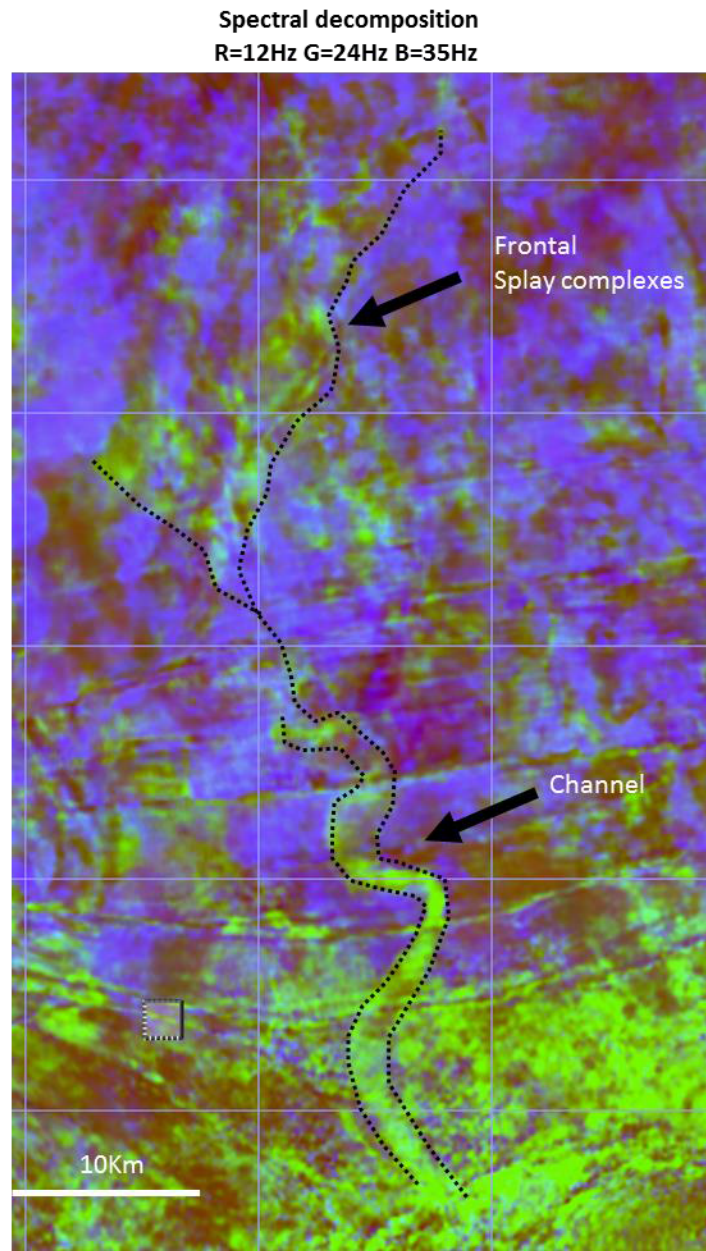


Figure 2.20 Example of 3D seismic-derived plan-view image for frontal splay complexes deposited during the upper Miocene. The frontal splay is internally composed of small distributary channels.

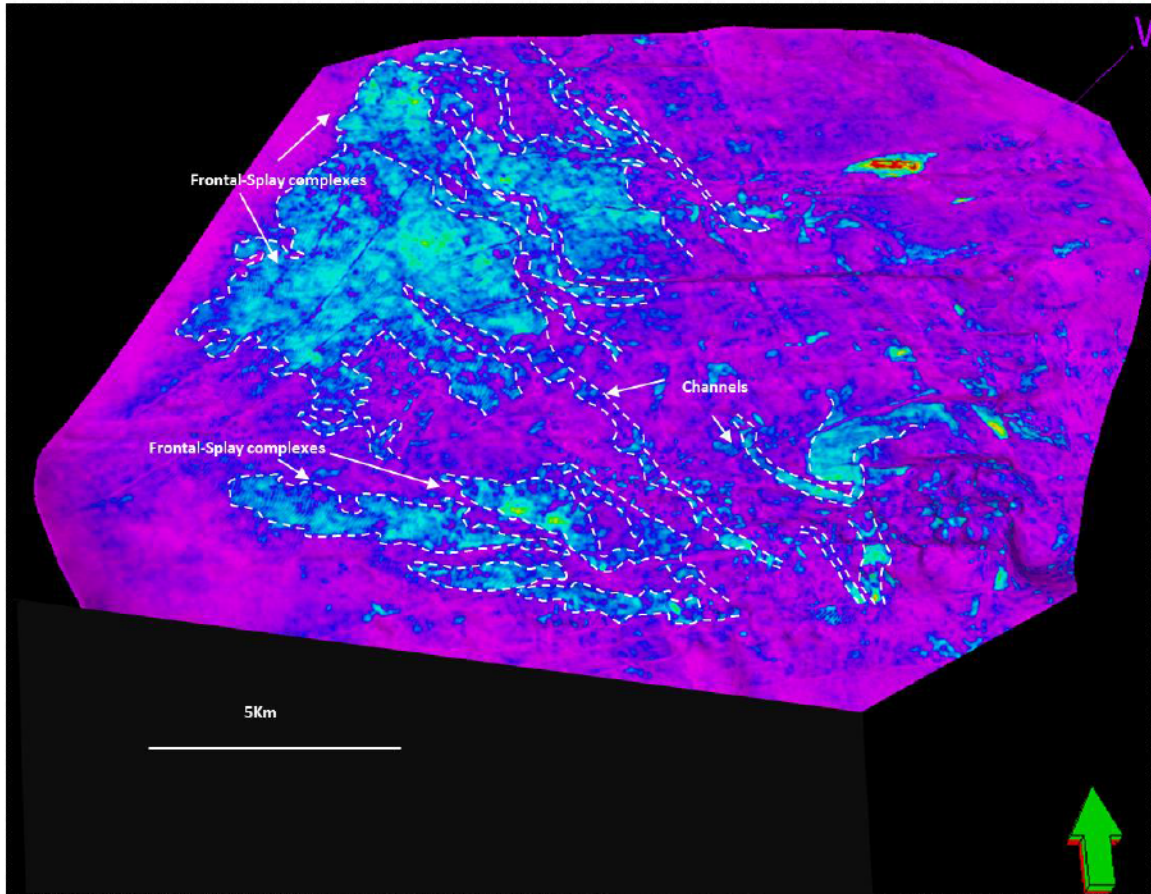


Figure 2.21 3D seismic-derived plan-view image using RMS attribute extraction to illustrate frontal splays complexes, and channels.

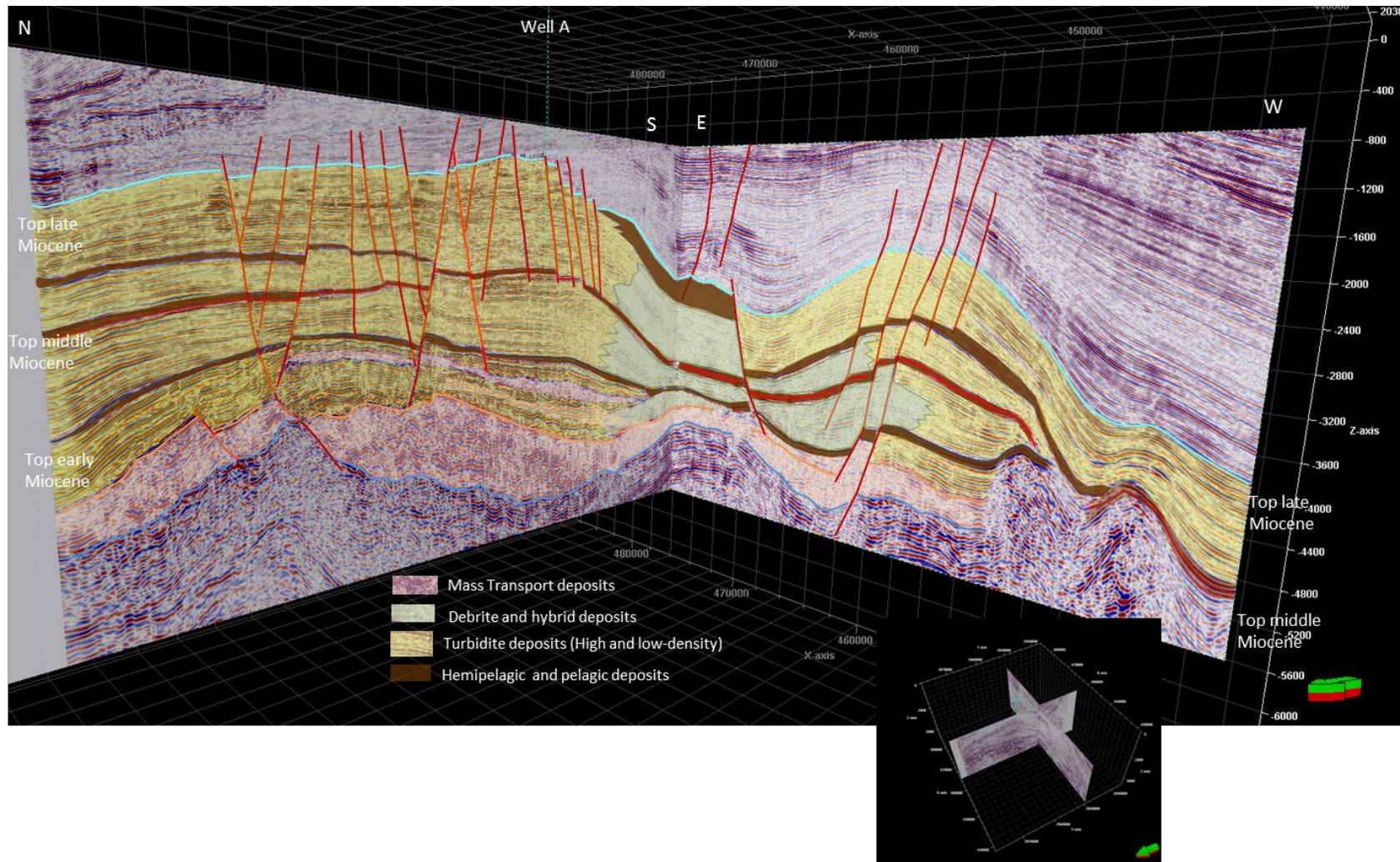


Figure 2.22 seismic lines illustrating the distribution of the depositional elements in the study area. The line where is located well A shows mass-transport deposits during the Oligocene and lower Miocene and turbidite deposits for the middle and upper Miocene; towards the south for the middle and on the base of the upper Miocene debris flows and hybrid deposits.

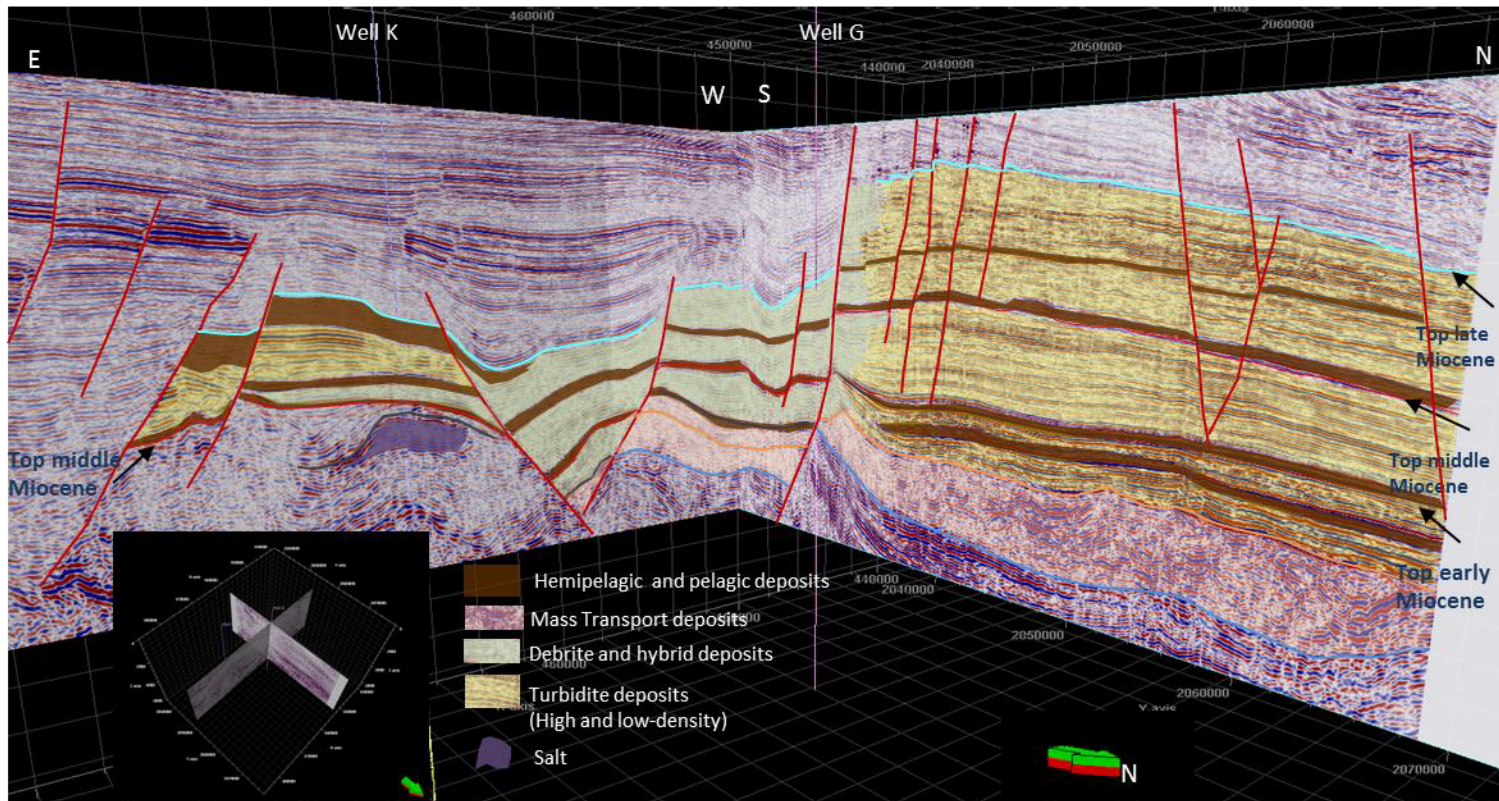


Figure 2.23 The seismic lines in this image show the distribution of the depositional elements in the study area. The line where is located the well K shows a body of allochthonous salt thinning the lower and middle Miocene units; on the other hand, the well G shows the mass-transport deposits for the Oligocene and lower Miocene and the increment in thickness of these units towards the north. Well G also illustrates the debrite deposits and the change to turbidite deposits toward the central and northern parts of the area.

Table 2.1 Sedimentary facies and depositional processes interpreted from the Miocene cores

Sedimentary Facies and depositional processes					
Facies Designation	Facies	Description	Sedimentary Structures	Facies Model	Process
F1	Intraclast mudstone breccia	Disorganized and very poorly sorted boulder-sized mudstone intraclasts supported by fine sand and muddy matrix. The clasts are angular to subangular and irregular shaped. This facies is associated with massive sandstone	Structureless	A1 Johanson and Stow	Debris flow
F2	Intraclast mudstone conglomerate	Disorganized and very poorly sorted boulder-sized mudstone intraclasts supported by fine sand and muddy matrix. The clasts are subrounded and oval-shaped. This facies could be associated with muddy sandstone and massive sandstone. Inverse grading in the base of the deposit	Structureless	B1 Johanson and Stow	Debris flow
F3	Massive sandstone with floating pebbles or intraclasts	Massive sandstone with scattered pebbles or intraclasts. The clasts range in size from granules to pebbles. Pebbles are rounded and mainly composed by quartz and lithic fragments, their orientation is parallel and subparallel. The intraclasts are subangular and irregular shaped, compositionally the clasts may be claystone-mudstone, siltstone or fine sandstone. Both pebbles and intraclasts are located on the base of the beds.	Structureless	and B4 (Johanson and Stow)	Hindered settling and turbulence. High-density turbidity currents
F4	Structureless sandstone	Homogeneous coarse to fine grained and grey consolidated and unconsolidated sand. Internally this facies is homogeneous and occasionally shows normal grading. These sandstones are very thick bedded (20 cm to 1.5m). Amalgamation surfaces are common	Structureless. Occasionally flame structures and load casts	Ta (Bouma)	High-density turbidity currents
F5	Normally graded sandstone	Normally graded thin to medium bedded sandstone that changes from massive medium to very fine grained sandstone at the base into parallel and rippled laminated siltstone and mudstone in the top.	N/A	TaTcTd (Bouma)	High to low-density turbidity current
F6	Laminated sandstone	Medium to fine grained sandstone. Bed thickness range from 13 cm to 1.30 m. The upper and basal contacts are sharp. With lamina of organic matter.	Irregular lamination	Tb (Bouma)	Waning Turbulent flow. Low-density turbidity currents
F7	Muddy sandstone	clay-rich sandstone and thinly intercalations of silty sandstone., with mudstone chips at the base	Structureless and ungraded	N/A	Cohesive Debris Flow
F8	Rippled, parallel and cross laminated heterolithic units	fine-grained sandstone and siltstone interbedded with mudstone of turbiditic or hemipelagic origin. This facies occurs in beds of 5 to 80 cm thick. The lower contact of this facies is planar and sharp	Planar tabular bedding, tangential laminations, climbing ripples, trough cross-stratification and occasionally hummocky cross-stratification, less common lenticular structures, bioturbation and deformation structures (load casts, and flame structures)	Tc, Td, Te (Bouma)	1) Low-density turbidity currents 2) Deposition from fallout of suspended hemipelagic mud particles
F9	Laminated siltstone and mudstone	Grey to greenish grey, structureless to thin bedded mudstone interbedded by siltstone and silty mudstone. Silt-mud couplets either as discrete beds or as interlaminated units are common in this facies	Parallel, and inclined lamination, lenticular and irregular lamination, load casts, and bioturbation	Td-Te (Bouma)	Deposition from suspension from a low-density turbidity current
F10	Massive mudstone	Massive dark, and grey-green mudstone with faint horizontal laminae. Zones of bioturbational mottling may be developed. Pyrite nodules, coal laminae, planktonic foraminifera, shell material and other organic material bedded or chaotic are present.	Irregular laminations and bioturbation	N/A	Deposition from hemipelagic muds
F11	Distorted heterolithic units	Fine grained sediments (fine grained sandstone, siltstone and mudstone). The bed thickness is usually thin from 0.25 to 1m. The upper and lower contacts are sharp irregular. Occasionally present ichnofossils.	Convolute beds, slumps, contorted packets	Tc (Bouma)	1) Local origin from slumping of unstable walls of channels/overbank deposits. 2) Transformation flow from more distal slumps into debris flows
F12	Mudstone clasts breccia with sand injections.	Mudstone clasts breccia incorporated into a matrix of structureless sandstone. Breccia margins are dentate and discordant to sand host. Adjacent mudstone clasts are linked together with thin mudstone connections named roof pendants.	N/A	N/A	Breaching of mudstone accompanied by sand fluidization
F13	Heterolithic units of Rippled and Parallel laminated volcanic siltstone and fine grained sandstone	Very fine sand to silt-sized ash tuff with concretions a slightly cemented with silice.	Laminations, cross-stratification, prograding ripples, tabular sigmoidal, trough cross-lamination, convolute structures and less commonly gutter casts and flame structures.	Tb, Tc, Td and Te (Bouma)	Suspension fallout of volcanic ash

N/A Not applicable

Depositional elements		Facies association	General Gamma Ray response
1) Submarine Channels	a) Channel fill (axis)	F1,F4,F5	Blocky
	b) Channel margin	F3,F5,F8,F9, F10 and F11	Fining-upward
	c)Channel levee	F4, F5,F6 ,F8 and F10 less F3 and F11	Fining-upward
2) Frontal Splay	a) Proximal	F4 and F6 minor F3, F9	Coarsening and thickening upward
	b) Distal	F10,F11, F13	Coarsening and fining upward with serrate character
3) Lobes of Debrites and associated flows	a)Debrite flow deposits	F7,F9 and F10	Coarsening- upward and box-shaped pattern
	b) Hybrid sediment gravity flow deposits	F1,F2,F6 and F12	Coarsening- upward and box-shaped pattern

Table 2.2 Facies associations in terms of depositional elements recognized in Miocene cores.

Chapter 3

Sequence stratigraphy of the Miocene section, southern Gulf of Mexico

1. Introduction

This study focuses on the interpretation of stratigraphic sequences through the integration of biostratigraphic, well log and 3D seismic data. Sequence analysis is used to identify significant surfaces, systems tracts, and sequences for the Miocene succession. The depositional systems in this area are dominantly represented by submarine fans deposited on the slope and the basin floor. The main depositional elements that characterize these depositional settings are channel systems (channel-fills, channel-levee systems), frontal splays, frontal splay complexes, lobes of debrites and mass-transport complexes. Five genetic sequences were identified, and eleven stratigraphic surfaces interpreted and correlated through the study area. The Oligocene to lower Miocene, lower Miocene and middle Miocene sequences were deposited in bathyal water depths, whereas the upper Miocene sequences (Tortonian and Messinian) were deposited in bathyal and outer neritic water depths. The bulk of the Miocene succession, from the older to younger deposits consist of mass-transport deposits (Oligocene lower Miocene); mass-transport deposits and turbidite deposits (lower Miocene); debrite deposits and turbidite deposits (middle Miocene); and debrite deposits, turbidite deposits and pelagic and hemipelagic sediments (upper Miocene). Cycles of sedimentation are delineated by regionally extensive maximum flooding surfaces within condensed sections of hemipelagic mudstone which represent starved basin floors. These condensed sections are markers for regional correlation, and the maximum flooding surfaces, which they include, are the key surfaces for the construction of the Miocene stratigraphic

framework. The falling-stage system tract forms the bulk of the Miocene sequences. Individual sequence geometry and thickness were controlled largely by salt evacuation and large-scale sedimentation patterns. For the upper Miocene, the older sequence (Tortonian) includes sandy deposits, whereas the overlying younger sequence (Messinian) includes sandy facies at the base and muddy facies at the top; this trend reflects the change from slope to shelf settings.

Over recent decades, sequence stratigraphy has changed the methods of facies and stratigraphic analyses and introduced a new component of facies predictability, giving the petroleum industry a powerful analytical and correlation tool for petroleum exploration. Additionally, sequence stratigraphic studies combine different sets of data (e.g., biostratigraphic, well-log and seismic patterns) and methods of data analysis to understand the relationships among rock layers, their seismic expression and their depositional environments for a more accurate prediction of reservoirs, source rocks and seals (e.g., De Gasperi and Catuneanu, 2014; Vander Merwe et al., 2010). Furthermore, the application of sequence stratigraphy has also been expanded to the Precambrian rock record (Catuneanu et al., 2005; Eriksson et al., 2005, 2006, 2007, 2013).

Notwithstanding the growing application of this method, its applicability in deep-marine settings be difficult for reasons that have been identified by several authors (Catuneanu, 2003; 2006; Catuneanu et al., 2009; Galloway, 2001; Muto et al., 2002; Porebski et al., 2003; Sinclair et al., 2002; Shannon et al., 2005; Shanmugam, 2007). Moreover, the sequence stratigraphic method could be risky if used dogmatically; observations are forced to fit inadequate interpretational templates provided by standard models. For this reason, a process-based approach to the method is recommended, based on the geological circumstances and available data sets for each particular case. An inherent difficulty in the interpretation of deep-water

sequences is that facies changes respond to complex and varied controls. For example, local controls such as dispersal patterns, sediment supply, changes in energy flux, and accommodation caused by local tectonic events play an important role in the facies distribution (Galloway, 2001; Shannon, et al., 2005; Shanmugam, 2007; Sinclair et al., 2002). Furthermore, Carvajal, et al. (2009); Muto et al. (2002), and Porebski et al. (2003), showed that sediment supply may become more important than sea-level changes to shelf-margin growth, because it controls the rates of progradation and aggradation, and thus sediment delivery to the deep-water settings; even during highstand periods, high-supply river-delta systems are capable of prograding to the shelf edge, particularly in the case of narrow continental shelves. Shanmugam (2007) also mentioned that in areas with narrow shelves, sediment supply to deep-water environments may be high enough to develop sediment gravity flow deposits during all stages of the relative sea-level (RSL) cycle. However, in relative terms, cycles of grain-size changes are still expected during the development of stratigraphic sequences (Catuneanu et al., 2009, 2010, 2011).

The patterns of sediment delivery to deep-water settings are typically complex, due to the fact that clastic sediments may be derived from a diverse set of sources, and because sediment failures into the continental slope may be triggered by a wide variety of mechanisms such as earthquakes, tectonic and depositional oversteepening, depositional and hydrostatic loading, tropical cyclones, tsunamis, submarine volcanic slope failure, glacial processes, current redistribution and activity of land-derived sources, salt movements, biological erosion, and gas hydrate decomposition (Shannon, et al., 2005; Shanmugam, 2007).

Other issues are concern what model is best suited for sequence stratigraphic studies and which stratigraphic surface should be considered as the sequence boundary; Catuneanu et al.

(2009, 2011) presented the timing of the systems tracts and sequence boundaries for the five sequence stratigraphic models that have been proposed.

This study builds on previous stratigraphic studies performed by the Mexican petroleum company (PEMEX); it presents a sequence stratigraphic analysis focusing on the Miocene in an area of the southern Gulf of Mexico. This work was based on data gathered from several sources, including paleontological, well and seismic data. The aims of this study were to update the chronostratigraphic framework; to propose an integrated seismic, well-log and core-based sequence stratigraphic framework; and finally, to place the depositional environments in the context of sequence stratigraphy for a more accurate prediction of reservoirs, source rocks and seals.

2. Geological Setting

The study area is located offshore in the southern portion of the Gulf of Mexico (Fig. 3.1) in a present-day continental platform setting; where water depths range from 0 to 100m. The tectonic evolution of this area is related to the regional tectonic events of the evolution of the Gulf of Mexico (Buller and Sawyer, 1985; Pindell, 1985; Salvador, 1988, 1991), the subduction of the Farallon Plate under the North American Plate (Laramide Orogeny) (Pindell and Kennan, 2002) and the lateral movement of the Chortis Block and the subduction of the Cocos Plate against the southern end of the North American Plate (Angeles-Aquino et al., 1994; Morán-Zenteno et al., 2000; Padilla y Sánchez, 2007) and local tectonic events (salt tectonics) (Angeles-Aquino et al., 1994; Cruz-Mercado et al., 2009; Robles-Nolasco et al., 2004). The Mesozoic tectonic events will not be described here because this study focuses only on the Miocene. During the Cenozoic, the sedimentation changed from carbonate to siliciclastic as a result of the

Laramide Orogeny; during the Paleocene, sea-level rise exceeded subsidence and deep-water sediments began to backstep the carbonate slope (Angeles-Aquino et al., 1994). As a result of Paleogene clastic sedimentation in the southern Gulf of Mexico, the Chiapas Massif still produced large volumes of sediments deposited in large depocenters, whereas in the Yucatan Block the deposition of shallow water carbonates continued (Padilla y Sánchez, 2007). In the study area, the Miocene succession is mainly sand-prone and it originates from deposition within submarine fan systems infilling local topography under bathyal paleobathymetric conditions. As a result, this stratigraphic unit is characterized by mass-transport, debrite, turbidite deposits and pelagic and hemipelagic sediments. Angeles-Aquino et al. (1994) suggested that the salt movement combined with the lowering of the sea level probably produced a regional unconformity that could be detected by the absence of some biozones in the middle and late Oligocene. The same sedimentary patterns continued until the early Miocene, but during the middle Miocene the maximum deformation that folded and upthrust the rocks in the southern Gulf of Mexico occurred (Chiapanecan Orogeny, Sánchez-Montes de Oca, 1980), resulting from the lateral movement of the Chortis Block and the subduction of the Cocos Plate, beneath the North American Plate, forming the Chiapas-Reforma-Akal belt over a decollement at the level of the Callovian salt (Angeles-Aquino et al., 1994; Padilla y Sánchez, 2007). At this time, the deposition of submarine fans and pelagic and hemipelagic sedimentation occurred. Following the middle Miocene contractional event, during the Pliocene-Pleistocene, a gravitational system was developed due to the extension triggered by the high rate of sedimentation related to great volumes of salt evacuation, and increased tilting of the basement; as a result, extensional basins were formed (Padilla y Sánchez 2007; Robles-Nolasco et al., 2004).

The tectonic events previously mentioned define the Gulf of Mexico basin as a passive margin in which most of the basement subsidence related to plate tectonics had ceased by the Cenozoic (Buffler, 1985); leaving a deep marine environment over much of the area. Much of the rapidly deposited late Cenozoic fill occurred in an overall progradational pattern that was accommodated by this bathymetric deep. This pattern was complicated by local loading onto mobile salt; in some locations forming salt-controlled sub-basins, in which the subsidence was controlled by large diapir-related contemporaneous expansion faults or fault zones. The sedimentary section on the downthrown side of the fault zone is thicker than its age equivalent section on the upthrown side. The patterns of deposition were controlled by contemporaneous extension faulting, allowing the slope depositional environment to evolve into a shelf depositional environment.

3. Methods and Data Sets

To develop the sequence stratigraphic framework of the Miocene, a multidisciplinary approach was undertaken, and diverse data sets such as biostratigraphic data, core data, well logs and 3D seismic data were integrated.

This study used information from twelve wells, which includes the facies description of twelve cores (each core of nine meters length) of the upper and middle Miocene section; as well as the facies association and depositional elements recognized in previous studies performed in the study area (Gutierrez-Paredes et al., 2017).

To build the chronostratigraphic framework we use the biostratigraphic information, especially the biozones, which are in the petroleum industry widely applied to determine the last occurrence (extinction), or the first appearance of their index fossil content or the concurrence of

a group of microfossils. In particular, the last extinction of a given species ("Last Appearance Datum" or LAD) represents the top of a sedimentary unit. To update the stratigraphic framework, this study used three wells with foraminifera (benthic and planktonic) and calcareous nannoplankton information and nine exploratory wells with only foraminifera data. We used the biozones of planktonic foraminifera and calcareous nannoplankton proposed for the Mexican basins by Lugo et al. (2005); they established the biozone tops based on the first appearance in the sense of drilling of the planktonic foraminifera biozones defined by Blow (1979); Bolli and Saunders (1989), and Berggren et al. (1995). For calcareous nannoplankton, this study used the biozones defined by Martini (1971), Perch-Nielsen, K (1985) and Aubry (1984-1987, 1993, 1997, 1999).

The study area is 1600 km² and is totally covered by 3D seismic information. The 3D seismic survey version is post-stack time migration with a record length of 5s two-way time (TWT) and it was processed close to zero phase. The seismic quality is good between 0 and 3000 ms, and the display polarity is the normal SEG (Society of Exploration Geophysics) convention. A set of log templates was designed in Petrel to display and interpret well-log profiles. The lithology was interpreted from well logs, cuttings and cores by applying different cut-offs of the well-log values derived from the core-to-log calibration. Well-log templates were printed on a scale of 1:2000 and then were interpreted with the support of lithological, core, and biostratigraphic data. Annotated paleontological information in well logs showing the paleobathymetries helped to interpret log patterns and to select the candidates for regional markers, maximum flooding surfaces and/or condensed sections and to assign absolute ages to key surfaces for a preliminary sequence stratigraphic framework.

As recommended by Catuneanu et al. (2009), a model-independent framework was applied in this study, with the identification of all of the genetic units and bounding surfaces present in the Miocene successions. Following this, well-log templates were interpreted to identify the stacking patterns and the stratigraphic surfaces such as correlative conformities, maximum flooding surfaces, and basal surfaces of forced regression.

Once key surfaces were identified in the wells and calibrated with nannofossils and foraminifera data, they were extended to the rest of the wells through well-log cross-section correlations. Then, well-log data and key surfaces were tied to seismic data for seismic stratigraphic correlation and mapped across the seismic survey. The seismic horizons were interpolated in order to convert the interpreted mesh into a surface. Chronostratigraphic control of the seismic horizons was also achieved, using the available biostratigraphic data. After the preliminary framework was established, seismic sequence interpretation was employed to more accurately delineate the stratigraphic cycles.

4. Depositional Environments

Previous studies (Gutierrez-Paredes et al., 2017b) interpreted the Miocene depositional environments, processes and depositional elements in the study area based on the integration and interpretation of different data sets (biostratigraphic data, cores, well-log and seismic data). In that work, the paleontological interpretation (benthic assemblages) established that the sedimentation during the Miocene occurred in paleo-environments that varied from the lower slope to the outer shelf; this general basinward shift of the paleobathymetry over time reflects the overall progradation of the continental margin from the south to the north during the Miocene. From the early to middle Miocene slope and basinfloor depositional settings prevail in the study

area; at this time topographic variations were observed with shallow bathymetries related to topographic highs and deeper bathymetries related to topographic lows. These fluctuations were interpreted to be the result of tectonics and sedimentation effects in the area, more than sea level variation (Gutierrez-Paredes et al., 2017). The sediment input for the early to middle Miocene came mainly from the south (SW and SE, from two different sources). For the late Miocene slope and outer shelf settings prevail; at this time in the onshore part of the study area unstable shelf-edge deltas were formed, thus providing the sediment input (from south to north) to deepwater settings. From core descriptions, we established that the main depositional processes during the middle and upper Miocene were related to turbidity currents (high and low density) and debris flows (mudflows and grain flows), as well as deposition from fallout of suspended hemipelagic mud particles. From the description of the available cores, we also recognized thirteen sedimentary facies, the most abundant being structureless (massive) sandstone and massive mudstone. Rippled, parallel and cross-laminated sandstone and siltstone were found in minor proportions. Fig. 3.2 shows some examples of these sedimentary facies recognized from cores, which are massive sands with intercalations of rippled, laminated siltstone and mudstone. From the middle Oligocene to lower Miocene, the main depositional element is mass-transport deposits; at this point to avoid confusion in the terminology, in this study we used the term mass-transport deposits (MTD) for any undifferentiated mass-failure deposits (i.e., when different types are mixed, or when their exact origin is unclear).

The vertical and lateral distributions of facies linked to depositional environments were the building blocks to calibrate the depositional elements recognized through the use of seismic data. As a result, the depositional elements identified were mass-transport complexes, lobes of

debrites, submarine channels, and frontal splays. Examples of these depositional elements recognized by the integration of cores, well logs and seismic data are shown in Figs. 3.3 and 3.4.

Many cycles of repeating successions are observed in any vertical column through the Miocene, recording relative changes in sea-level and sediment supply, which facilitated the development of a sequence stratigraphic framework. In this work, the lateral and vertical distribution of the main deposits and depositional elements for the Miocene succession are illustrated with stratigraphic cross-sections. The cross-sections exhibit log trends that illustrate coarsening-upward (funnel) patterns, interpreted as the distal edge of seaward-building frontal splay deposits (cf., Posamentier et al., 1999). Moreover, the coarsening-upward log motif is commonly part of a bow (symmetrical) trend associated with an increase in the sand percentage of thinly bedded turbidites, and the fining-upward trend (bell) may show a decrease in the sand percentage of thinly bedded turbidites, and so it may record the waning/abandonment period of a submarine fan deposition or a sediment gravity flow (Emery and Myers, K.J, 1996). Fining-upward log patterns are also associated with blocky and serrated and less commonly with coarsening-upward log motifs, all of them embedded within a thick blanket of fine-grained deposits. Fining-upward trends are also related to channel-fills. Isolated boxcar (blocky or cylindrical) patterns with more serrate character (due to thin intercalations) embedded in fine-grained sediments represent turbidites in frontal splays and boxcar trends at the base and fining upward tops are related to channels, especially the beginning of a channel abandonment. Boxcar trends could also represent debris flow deposits in lobes. The bow (symmetrical) trend is associated with waxing and waning in a basinal setting, as for example, mud-rich basinal units tend to show a symmetric bow response, whereas sand-prone units tends to show a boxcar trend (Emery and Myers, K.J, 1996). Finally, highly irregular or serrate trends represent alternations of

high- and- low energy deep-water turbidity flows and are related to heterolithic lithofacies in distal deep-marine slopes. These trends could also be interpreted as the aggradation of shaley or silty sediment in deep-water and shelfal settings, whereas a low irregular pattern is related to pelagic and hemipelagic deposits.

Fig. 3.5 shows a stratigraphic cross-section for the middle Miocene orientated in the strike direction; its interpretation was based on the interpretation of well-log patterns and cores. The length of the section is approximately 16 km, and the datum is the maximum flooding surface of the lower Miocene. The paleontological information in these wells showed that deposition during the middle Miocene occurred on the slope (upper bathyal). The main deposits in this section correspond to lobes formed by debris flows (mudflows and grain flows) encased by fine-grained sediments; the thickness of the unit decreases toward the east, varying from 450 to 150 m, and it is absent in well K.

The example shown in Fig. 3.6 is a cross-section for the upper Miocene succession orientated in the strike direction. The length of the section is approximately 21 km, and the datum is the maximum flooding surface of the middle Miocene. The sedimentation began with the deposition of lobes of debrites; its thickness is constant, and this deposit is absent in the western-most well (E). Overlying these deposits are turbidites deposited in channel systems and frontal splays; in these wells, the Messinian (upper Miocene) is represented by fine-grained deposits of hemipelagic and/or turbiditic origin.

5. Chronostratigraphic Framework

Biostratigraphic data were essential in the construction of the geologic-time framework, providing time lines for biostratigraphic zonation; this was significant for defining the age control in the stratigraphic analysis of the sequences. Furthermore, it was helpful in identifying the maximum flooding surface and in some cases the basal surface of forced regression.

Although the main focus of the study was on the Miocene, the stratigraphic interval studied was 22.18 Ma in duration and ranges from the middle Oligocene (33.7 Ma) to the upper Miocene (5.32 Ma).

According to unpublished paleontological reports (PEMEX-IMP internal reports), the boundary between the lower Pliocene and the upper Miocene is identified by the appearance in the sense of drilling of *Discoaster quinquerramus*, *Globorotaloides variabilis* and *Sphaeroidinellopsis disjuncta*. The upper Miocene is defined by the biozone associations of *Globorotalia humerosa* (N17), *Globorotalia acostaensis* (N16), *Globorotalia menardii* (N15), *Discoaster quinquerramus* (NN11), *Discoaster hamatus* (NN10) *Discoaster calcaris* (NN9) and *Catinaster coalitus* (NN8). Biozone (N17) follows with the appearance of *Globorotaloides variabilis* and *Sphaeroidinellopsis disjuncta* biozone (N16) with the presence of *Sphaeroidinellopsis multiloba*.

The boundary between the upper Miocene and middle Miocene is set by the appearance in the sense of drilling of *Globorotalia mayeri*. The middle Miocene is defined by the biozone associations of *Globorotalia mayeri* (N14), *Globigerinoides ruber* (N13), *Globorotalia foshi robusta* (N12), *Globorotalia foshi foshi* (N9), *Globorotalia foshi peripheroronda* (N9), *Praeorbulina glomerata* (N8), *Discoaster exilis* (NN6) and *Discoaster heteromorphous* (NN5).

The *Praeorbulina glomerosa* (N8) biozone is determined by the appearance of *Globigerinoides diminutus* and *Globorotalia suteri*. The boundary between the lower Miocene and the middle Miocene is given by the appearance of *Globigerinoides bisphericus*, *Praeorbulina sicana* and *Praeorbulina glomerosa curva*.

The lower Miocene is defined by the biozone associations of *Globigerinoides bisphericus* (N7), *Catapsydrax stainforthi* (N6), *Catapsydrax dissimilis* (N5), *Globigerinoides primordius* (N4), *Helicosphaera ampliapertura* (NN4), *Triquetrorhabdulus carinatus* (NN3) and *Discoaster druggi* (NN2).

The boundary between the lower Miocene and the upper Oligocene is determined by the appearance of *Globigerinaciperoensis ciperoensis*.

The paleontological information allowed us to identify several discontinuities during the Miocene; however, the Messinian and Tortonian stages were recognized throughout the area. A discontinuity was identified at the base of the Tortonian stage based on the absence of the N15 and NN8 biozones. During the middle Miocene, several discontinuities occurred, and in some wells, their presence is represented only by one biozone; five wells reported the N14 biozone, which marks the top of the Serravallian. Nevertheless, this biozone was not correlatable for the whole of the area; another stratigraphic discontinuity was identified in the upper and middle part of the Serravallian by the absence of N13 to N11 biozones of planktonic foraminifera and NN7 of calcareous nannoplankton. The Langhian stage is considered absent because the N8 biozone was not recognized throughout the area; it was identified in only one well, so its presence could be local. Regarding the lower Miocene, in six wells, the N7 and N6 biozones are not correlatable; similarly, biozones N4 and NN1, which mark the Aquitanian stage, are also not correlatable. The main stratigraphic discontinuities (upper and middle Miocene and middle to

lower Miocene boundaries) in three wells tied well with the results of previous biostratigraphic studies, in which the graphic correlation method was used. Table 3.1 shows the Miocene biozones for twelve wells, the stratigraphic discontinuities, and the biozones not correlatable throughout the study area.

6. Sequence Stratigraphic Framework

6.1 Nomenclatural considerations

Currently, the sequence stratigraphic studies consider a ‘sequence’ as a succession of strata deposited during a full cycle of change in stratal stacking patterns, with the beginning and the end of one cycle marked by the same kind of event (Catuneanu et al., 2009; Catuneanu and Zecchin, 2013). The sequence should also be distinguished from component systems tracts, which are formed during specific stages of the relative sea-level cycle. In this study, we used the four systems tracts recognized in modern sequence stratigraphy (Catuneanu et al., 2009; Hunt and Tucker, 1992): the falling-stage systems tract, the lowstand systems tract, the transgressive systems tract and the highstand systems tract.

Not all types of data are always available for sequence stratigraphic analysis, and not all stratigraphic surfaces are present in deep-water environments. Catuneanu (2006) and Catuneanu et al. (2009) showed that in deep-water environments, only four of the seven sequence stratigraphic surfaces which define the four main events of a reference relative sea-level (RSL) cycle, can be recognized (maximum flooding surface, maximum regressive surface, the basal surface of forced regression, and the correlative conformity), as the other three form in subaerial or shallow-water environments. However, the maximum regressive surface is typically cryptic in the deep-water setting (Catuneanu, 2006), so the sequence stratigraphic framework is essentially

defined by only three sequence stratigraphic surfaces: the maximum flooding surface (MFS), the basal surface of forced regression (BSFR) and the correlative conformity (CC). These surfaces mark changes in the stratal stacking pattern and all of them are systems tract boundaries.

The criteria employed in this study for selecting the stratigraphic-surfaces and systems tracts using the subsurface data are described in the following section.

6.2 Stratigraphic surfaces

6.2.1 Basal surface of forced regression (BSFR)

This surface marks the base of the marine deposits accumulated during forced regression, which include the bulk of the basin floor and slope fans. The criteria followed in this work to place this surface in well logs and seismic data are as follows:

- 1) Forced regressive units typically start with mud-dominated gravity flow and mass-transport deposits associated with the onset of high sediment supply to the deep basin; considering this, the BSFR is placed at the base of the mass-transport deposits as the scour cut by the earliest gravity flows of forced regression (Hunt and Tucker, 1992 Posamentier and Allen, 1999). It may also be placed at the base of sand-prone units of the submarine fan complex, where slumps and grain flow deposits are missing (Fig. 3.7, or mass-transport deposits in that figure).
- 2) Following the criteria of Loutit et al. (1988), this surface was identified by abrupt shifts in biofacies assemblages from deeper paleo-bathymetries below to shallower above the surface. In five wells, it was possible to identify these shifts in biofacies assemblages mainly from middle bathyal to upper bathyal paleo-bathymetries (Fig. 3.8).

- 3) This surface is marked by a decrease in both microfossil abundance and diversity, due to the onset of rapid accumulation of sediment (Armentrout, 1996). This criterion was identified in three wells (Fig. 3.8).
- 4) In almost all the available wells, the BSFR shows an abrupt change in lithology and shift from mud to sand.
- 5) On seismic data, this surface typically corresponds to a high-amplitude reflection at the base of the submarine fan complexes, or mass-transport complexes, often with overlying onlap and downlap terminations, and underlying toplap terminations (often developed during forced regressions and associated with minimum erosion undetectable on seismic lines).

An integration of all of these criteria is ideal, in order to produce a reliable interpretation.

Four basal surfaces of forced regression were recognized in this work: the oldest at the base of the middle Oligocene, the second in the lower Miocene (Burdigalian), the third at the base of the Serravallian, and the last at the base of the Tortonian. In some places, the BSFRs converge toward the underlying MFS, which occur within an interval of condensed section.

6.2.2 Correlative Conformities (CC)

In this study, we use the term “correlative conformity” following the definition of Hunt and Tucker (1992), to define the surface that separates forced regressive from overlying lowstand normal regressive strata (i.e., the end of the RSL fall at the shoreline). Catuneanu (2006) noted that this correlative conformity has a high preservation potential because it is followed by a stage of RSL rise, when aggradation is the prevalent depositional trend.

The criteria to place this surface include: 1) within submarine fan systems, the correlative conformity is placed at the top of the coarsest sediment delivered to deep water; and 2) the CC is commonly the limit between high- and low-density turbidites (Catuneanu 2006).

In our data set, this stratigraphic surface was placed at the top of mass-transport deposits (in the Aquitanian and Burdigalian sequences) and at the top of the coarsest sediment of the submarine fan complex (in the Serravallian and Tortonian sequences). In the case of the youngest correlative conformity (Tortonian), this surface may coincide with an abrupt lithological change with a decrease in the sand/mud ratio; this circumstance was confirmed by seismic data and occurred in three wells (Fig. 3.9).

On seismic data, this surface typically corresponds to medium to high-amplitude semicontinuous reflections, often with overlying and underlying onlap and downlap terminations. The stratal terminations above and below of the CCs vary with local paleotopography in the study area, especially the correlative conformities of the lower Miocene and middle Miocene sequences. These surfaces may be expressed as onlap surfaces against salt bodies and structural highs; and also, could be downlap surfaces in areas less confined by salt bodies (more often during the upper Miocene).

In this study, four correlative conformities were recognized: two in the lower Miocene (Aquitanian and Burdigalian), one in the middle Miocene (Serravallian) and one in the upper Miocene (Tortonian).

6.2.3 Maximum Flooding surfaces with condensed sections (MFS/CS)

This surface separates retrograding strata below (TST) from prograding strata above (HST) and marks the timing of the minimum sediment delivery to deep-water settings; it is placed within regionally extensive condensed sections (Catuneanu et al., 2011). Loutit et al.

(1988) defined condensed sections as thin marine stratigraphic intervals rich in calcareous nannoplankton and foraminifera fossils that are related to maximum flooding surfaces. Condensed sections also comprise pelagic to hemipelagic sediments characterized by very low sedimentation rates. Due to the abundance and diversity of planktonic and benthonic microfossil assemblages that the condensed section contains, it is an excellent correlation surface and it is most extensive in areal extent at the time of maximum regional transgression. Moreover, Wynn (1996) recognized that this stratigraphic surface provides the key chronostratigraphic horizon for sequence analysis and in delineating sequences. Stratigraphic sequences bounded by MFSs are referred to a “genetic stratal sequences” (Galloway, 1989).

The criteria used in this work to identify this surface on well logs and seismic data are mentioned in the literature by Armentrout (1996); Catuneanu (2006); Fillon (2007); Loutit et al. (1988); Mitchum et al. (1993), and include:

- 1) In well logs, this surface was placed at the top of fining-upward (transgressive deposits). As such, condensed sections correspond to the highest gamma ray values and the lowest resistivity values, indicating the most clay-rich shale, and may be points of maximum separation between the neutron and density log curves compared to their surroundings.
- 2) MFSs correspond to peaks in the abundance and diversity of planktonic and benthic fossils and calcareous nannoplankton and are marked by the deepest-water biofacies assemblage. This criterion is exemplified in three wells (Fig. 3.8).

On seismic profiles, maximum flooding surfaces within condensed sections exhibit a reflection of high amplitude, good lateral continuity and good regional correlation that drape the underlying units; at the base of the mass-transport deposits the BSFR converges toward to the MFS/CS

(lower Miocene MFSs). Downlap and onlap terminations are common above the MFSs/CSs observed occurring in the Oligocene and lower Miocene (Fig. 3.10).

The maximum flooding surface exhibits a change between transgression and regression with a subtle increase in sediment supply to the basin, following the time of maximum transgression. Armentrout (1996) mentioned that condensed sections also represent local condensed intervals formed during sediment starvation on the abandonment surface of the basin floor and slope fans. Similarly, Posamentier et al. (1988) noted that condensed sections represent a cut-off in sediment supply and may be a result of autocyclic sediment switching on the submarine fan, a change from basin floor fan to slope fan or a cessation of basinal deposition during a phase of rising relative sea-level (Emery and Myers, 1996). Therefore, the mere observation of a condensed section is not enough to identify a MFS, and different criteria need to be integrated for a reliable interpretation.

In this project, six MFSs were observed. The first one was identified as being in the middle Oligocene, the second and third ones in the Burdigalian (lower Miocene), the fourth one in the Serravallian (middle Miocene), the fifth in the Tortonian and the last one in the Messinian (both in the upper Miocene). The last two MFSs are less reliable with the data set.

6.3 Systems Tracts

The systems tracts were identified and correlated based on the mapping of the three prominent stratigraphic surfaces: the maximum flooding surface, the basal surface of forced regression and the correlative conformity, which represent changes in the dominant depositional elements and the stacking patterns that relate to changes in shoreline trajectories on the shelf.

LST and TST are grouped together because the MRS is cryptic in deep-water setting (no change in the types of gravity flows, commonly low-density turbidite below and above; Catuneanu, 2006).

The system tracts are defined by their bounding surfaces as shown in Fig. 3.11.

The systems tracts identified in this study are shown in the cross-sections of Figs. 3.12 and 3.13 and in the seismic line of Fig. 3.14.

6.3.1 Highstand systems tract (HST)

The HST is related to the late stages of RSL, during which the rates of rise drop below the sedimentation rates, generating a normal regression of the shoreline. It is bounded by the maximum flooding surface at the base, which correspond to the time of maximum flooding of the shelf and by the basal surface of forced regression at the top. The highstand systems tract in deep-water systems is mainly mud-prone; in this area, the HSTs include thin intervals of pelagic and hemipelagic sediments and in some cases these intervals are below seismic resolution.

6.3.2 Falling-stage systems tract (FSST)

The FSST includes all the strata that accumulate in the marine portion of the basin during a forced regression. It is bounded by the basal surface of forced regression at the base, which is placed above or within the maximum flooding surface, and a correlative conformity at the top. It is frequently marked by upward-thickening units (Catuneanu 2006; Catuneanu et al., 2009).

This study identified four falling-stage systems tracts; the oldest FSST, in the Oligocene to lower Miocene, was formed entirely by mass transport complexes; the next one, in the Burdigalian was composed by mass transport complexes, channels and frontal splays; the third one at the base of

the Serravallian comprises lobes of debrites, channels and frontal splays; and the last one at the base of the Tortonian, is also composed of lobes of debrites and frontal splay complexes. The deposits of the FSST are well expressed in well logs and in seismic cross-sections with an abrupt increase of sand or the presence of mass-transport complexes. This systems tract is mainly sand-prone, with the highest thickness of sand in the Serravallian and Tortonian sequences, especially in the center and northern end of the study area.

6.3.3 Lowstand Systems Tract (LST) and Transgressive systems Tract (TST)

The LST forms when the early stage of base-level rise is outpaced by the sedimentation rate (normal regression); it is bounded by its marine correlative conformity at the base, and by the maximum regressive surface at the top. In contrast, the TST is deposited during the part of relative sea-level rise when the rates of rise outpace the sedimentation rates, at the shoreline. It is bounded by the maximum regressive surface at the base and by the maximum flooding surface at the top. However, as mentioned earlier, the MRS is cryptic in deep-water setting, so it was not possible to differentiate the lowstand systems tract from the transgressive systems tract.

In this project, four LST+TSTs were recognized; they are underlain by correlative conformities and overlain by maximum flooding surfaces. For these systems tracts, the interpretation from different data sets allowed the identification of depositional elements of channel-fill, channel-levee, and frontal splay complexes. These systems tracts were formed predominantly by low-density turbidity currents.

6.4 Sequences

6.4.1 Middle Oligocene (*Rupelian*)-lower Miocene (*Burdigalian*) (27.1-18.3 Ma.)

This succession has duration of 8.8 million years, and it was deposited in a lower bathyal to middle bathyal paleobathymetry. The lower boundary of this sequence is diachronous and is well expressed on seismic data, in well logs and in two wells with foraminifera and nannofossils information; it corresponds to a high-amplitude reflection that has a regional extent. This seismic reflection in some locations represents the basal surface of forced regression that converges toward the underlying maximum flooding surface which occurs within an interval of condensed section. Paleontological information confirms that this MFS corresponds to the top of the middle Oligocene and marks an increase in the diversity and abundance of foraminifera and nannofossils. In well logs and seismic data, above this boundary we recognized a mass-transport complex (MTC). The upper boundary of this sequence is a MFS; the paleontological information indicated that the age of this surface is given by the (NN3) biozone; this surface was identified by an increase in the abundance and diversity of foraminifera and nannofossils in two wells.

This sequence is distributed in most of the study area, increasing its thickness toward the central and north part of the study area. Although, this sequence includes the highstand, the falling-stage, and the lowstand + transgressive systems tracts; it is best represented by the deposits of the falling-stage systems tract, which include the mass transport complex. This FSST reaches a thickness of more than 500 m in the northern part and decreases considerably toward the south, where it is locally very thin or absent on topographic highs (related to salt bodies), just as, in the western part of the area it is absent where a listric fault is present. Seismically, the MTC is easily recognized by its semi-discontinuous reflections of variable amplitude, with low-amplitude internally chaotic facies and high-amplitude contorted seismic facies (Fig. 3.15).

Examples from wells indicated that the composition of this MTC in the NE part is constituted by extra-formational clasts of cobble/boulder sized carbonate (mudstone-wackestone) clasts supported by a muddy matrix and fragments of coral and shells, and towards the central and southern parts are heterolithic deposits (mudstone and siltstone). The irregular upper surfaces of this MTC created a local accommodation with depressions upon which thin packets of heterolithic sediments infilled the residual topography. The formation of this sequence was probably controlled by a combination of the relative sea-level fall (earliest portion) and local tectonics (contractional tectonic event and beginning of the emplacement of allochthonous salt); both factors were probably responsible for the slope destabilization.

The lowstand and the transgressive systems tracts are bounded by the correlative conformity for which the age is given by (N4) biozone (this biozone is not correlatable in the entire well set); and the MFS for which the age is given by the (NN3) biozone. In seismic data and well logs, the correlative conformity is well identified, marking the end of deposition of the mass-transport complex; this upper surface is mounded and irregular, which indicates the bathymetry after a time of erosion. The LST and TST include the deposition of high-to low-density turbidites in channels and frontal splays. Toward the south the thickness of these systems tracts decreases considerably.

6.4.2 Lower Miocene (Burdigalian) 18.3-16.4 Ma

The lower Miocene has duration of 1.9 million years; the lower boundary is the MFS for which the age is assigned by the NN3 biozone as previously mentioned. Paleontologically this surface shows an increase in the abundance and diversity of foraminifera and nannofossils in two wells. This MFS is represented by a seismic reflection of medium to high amplitude and low frequency. A basal surface of forced regression converges toward this underlying MFS in some

locations; in the southern part of the area this surface onlaps a structural high, and it has overlying onlap and downlap terminations, and underlying toplap terminations.

The upper boundary of the sequence is the MFS at the top of the lower Miocene and its age is assigned by the N7 biozone. This maximum flooding surface is well documented by the entire data set (paleontological information, well logs and seismic data). This surface is represented by a seismic reflection of high amplitude, low frequency and good lateral continuity that could be correlated in the entire study area.

This sequence is thin with a thickness that no more than 100 milliseconds; it is distributed in most of the study area and is only absent in the eastern part due to the presence of normal faults. This sequence includes the following systems tracts: at the base the highstand systems tract which includes pelagic and hemipelagic sediments in a condensed interval; followed by the falling-stage systems tract that comprises mass-transport deposits, and for which distribution is limited only to the central and eastern parts of the area in the flank of a salt body; toward the south this FSST includes lobes of debrites and frontal splays and to the north channel systems. These different types of deposits during the falling-stage system tracts are contemporaneous and they reflect the influence of salt movement on sedimentation. The next systems tracts are the lowstand and the transgressive systems tracts, which include turbidite deposits of high to low density. This sequence infills the residual topography of the previously deposited MTC (Fig. 3.15).

An example of the mass-transport deposits present in the falling-stage systems tract in this sequence is shown in Fig. 3.16 seismic line B-B'.

6.4.3 Middle Miocene (Serravallian) 16.4-11.2 M.a

This sequence has duration of 5.2 million years. It is bounded by two maximum flooding surfaces: the lower limit is the MFS at the top of the lower Miocene, and the upper limit is the MFS at the top of the middle Miocene. These two maximum flooding surfaces are the best represented in the entire data set (paleontological, well logs and seismic data). Above the MFS at the top of the lower Miocene we identified a BSFR; this surface converges toward the underlying maximum flooding surface, which occurs within an interval of condensed section in some parts of the study area. Above this MFS the correlative conformity (based on the interpretation of well logs) was placed at the top of the coarsest sediment of the submarine fan complex; in seismic data this surface corresponds to a continuous seismic reflection of medium to high amplitude, and low frequency. Finally, at the top of the middle Miocene the age of the MFS is assigned by the N14 and NN7 biozones; this surface is represented by a seismic reflection of high amplitude, low frequency and good lateral continuity that we correlated throughout the study area (Fig. 3.17).

This sequence is mainly sand-prone, and it is distributed throughout the study area with variable thickness, because the paleotopography of the area was affected by the movement of the salt; so, in this way the maximum thickness is observed in the central and north parts of the area, where a large depocenter was formed.

The middle Miocene succession comprises, from the base to the top, the highstand and falling-stage systems tracts; the last one is the best represented in the area and includes lobes of debrites (mudflows and grain flows) distributed in the southern of the area with variable thickness (from wells) ranging from 80 to 350 m. Seismically they were recognized by continuous to discontinuous reflections of medium to low amplitude and high frequency with contorted and

mounded configuration and onlap and downlap terminations; the lower limit can be grooved. According to Pickering et al. (2005) these types of deposits are the products of flow transformations that resulted from multiphase granular flows, and their shape is controlled strongly by subtle changes in the seafloor gradient and therefore by the basin morphology (Talling et al., 2012). Toward the central and northern part of the area, we interpreted turbidite deposits of high and low-density deposited in channel systems (mainly meandering channels) and frontal splays; the thickness of these deposits is thicker over 500 m, and they are confined to a large depocenter formed by salt withdrawal. Seismically, the meandering channels show up single reflections associated with lateral and downdip migration of the channel forming lateral accretion packages (LAPs) on the inner side of the channel; however, these LAPs are not always recognized and instead may appear as a single, laterally extensive reflection of high amplitude. On the other hand, frontal splays in seismic profiles are recognized by their medium to high amplitude, mounded external appearance, continuous convex reflectors with bidirectional downlap and planar bases. An example of the types of frontal splays recognized in the falling stage system tract of this sequence is shown in Fig. 3.18.

The next systems tracts are the lowstand and the transgressive systems tracts, which comprise turbidites (mainly low density). They are distributed throughout the entire area. In the southern part of the area their average thickness is 100 m, in seismic profiles these systems tracts are included in seismic reflections of medium to high amplitude, low frequency and good lateral continuity. Locally these turbidites fill small depocenters formed by the movement of the salt, and in this particular case include continuous to semicontinuous reflections of medium to high amplitude and high frequency. In the central and north part of the area these systems tracts have an average thickness of 200 m; and frontal splays complexes are recognized in cores, well logs

and seismic data. In seismic cross-sections are characterized by parallel laterally continuous, to slightly discontinuous reflections of high amplitude (Fig. 3.19).

6.4.4. Upper Miocene (Tortonian) 11.2-7.12 Ma.

The Tortonian sequence has a duration of 4.08 million years; the lower limit is given by the maximum flooding surface at the top of the middle Miocene, the age of this surface is assigned by the NN9 biozone, which is followed by a BSFR; above this surface there is a correlative conformity placed at the top of the coarsest sediment of the slope fan, followed by a maximum flooding surface placed in the boundary between the Tortonian and Messinian stages, and given by the N16 biozone; this surface corresponds to the upper limit of this sequence.

This sequence is mainly sand-prone and it is distributed throughout the study area with thickness varying from 300–1000m; this thickness variation reflects the paleotopography of the area at the time of deposition.

The Tortonian sequence comprises, from the base to the top, firstly the highstand systems tract with hemipelagic and pelagic sediments distributed over the entire study area, and they are easily identified in well logs and seismic data. Seismically, these deposits are recognized by continuous parallel reflections of low frequency and high amplitude. The next systems tract is the falling-stage systems tract, which includes lobes of debrites (grain flows), channel systems and frontal splays; all of them are distributed in the southern part of the area. Toward the central and northern parts turbidites prevail, which are deposited in channel-levee systems and frontal splay complexes. Seismically, lobes of debrites tend to be narrow and are encased by two continuous reflections of medium to high amplitude that pinch out laterally, these surfaces with steep-edges can give the appearance of mounding, and their basal surfaces can be grooved. The

internal configurations of these deposits are contorted and chaotic. On the other hand, channel systems are represented by stacked, discontinuous high amplitude reflections for channel fills and low-amplitude continuous reflections wedge-shaped away from the channel axis toward the levees; concave upward, planar and slightly erosional bases, and other features such as gull-wing geometry are also observed in seismic profiles. Finally, frontal splays are recognized by their medium to high amplitude, mounded external appearance, continuous convex reflectors with bidirectional downlap, whereas frontal splay complexes are characterized by laterally continuous to slightly discontinuous reflections of high amplitude; in map view, they have an elongated geometry and some present a distributary-channel pattern. Examples of these types of deposits are shown in Figs 3.3 and 3.4.

The next systems tracts are the lowstand and transgressive systems tracts. Both comprise low-density turbidites and they are distributed throughout the study area. The thickness of these systems tracts is thin compared with the thickness of the FSST.

Fig. 3.20 shows examples of the systems tracts and depositional elements formed during the upper Miocene.

6.4.5. Upper Miocene (Messinian) 7.12-5.32 Ma

The Messinian sequence has a duration of 1.8 million years. This sequence is bounded by two maximum flooding surfaces, the older MFS is placed in the boundary between the Messinian and Tortonian given by the N16 biozone, and the younger MFS probably corresponds to the boundary between the upper Miocene and lower Pliocene; the criteria to place this MFS were mainly based on the interpretation of the stratigraphic stacking patterns in well logs.

This sequence is mainly mud-prone and it is distributed throughout the study area with variable thickness; in two wells located in the southern part of the study area, this sequence was deposited in a shelf setting.

For the Messinian succession it was not possible to identify stratigraphic surfaces other than the maximum flooding surfaces that bounded this sequence; as a result it was not subdivided into systems tracts. However, this sequence comprises the following deposits: in the south pelagic and hemipelagic sediments are distributed, and towards the north, channel-levee systems are found. The seismic lines in Fig. 3.20 show examples of the depositional elements formed during the upper Miocene.

7. Discussion

As was mentioned before, the basal surface of forced regression, the correlative conformity and the maximum flooding surface provide the basis to identify systems tracts, as well as different types of sequences. The stratigraphic chart in Fig. 3.21 exhibits the sequence stratigraphic framework of the study area. It was possible to establish the age of some of these stratigraphic surfaces by paleontological data, especially the maximum flooding surfaces and some correlative conformities, as shown in Fig. 3.21.

The systems tracts and the different types of sequences are illustrated in the seismic section of Fig. 3.22.

Within the study area, the most reliable surfaces for regional correlation are the MFSs; therefore, the model that best fits the reality of the studied section is the model of genetic sequences (Frazier, 1974 and Galloway, 1989 and 2001). Using the MFSs, it was possible to identify five complete sedimentation cycles. Each sedimentation cycle includes three

recognizable events, namely the onset of relative sea-level fall, the end of relative sea-level fall, and the end of transgression. In general terms, each genetic sequence starts with hemipelagic and pelagic sediments, within condensed sections above MFSs (which are the most reliable regional markers), followed by the deposits of relative sea-level fall, which are represented by mass-transport deposits, debris flows and turbidites, all deposited in bathyal paleobathymetries, from lower to upper slope environments. Mass-transport complexes commonly develop during early stages of relative sea-level fall, when sediment supply to the shelf edge is high and water overburden weight is being reduced over shelf regions (Posamentier and Kolla, 2003). Although Beaubouf and Friedman (2000) agree that mass wasting and mass transport of muddy slope materials could occur during the early portion of RSL fall, and typically precede the major influx of sand during the forced regression (extra-basinal MTC), they also argue that this is not always the case, as MTCs could (intrabasinally) occur in response to local processes unique to each basin, at any time during the basin evolution, (e.g., slumps or slides from oversteepened, collapsed basin margin areas regardless of the relative sea-level stage). The extra-basinal MTCs tend to be the most laterally extensive and have point-sourced, fan-like plan-view patterns. The oldest MTC (middle Oligocene - lower Miocene) is the best example to illustrate the deposits occurring during the forced regression. At this time, even though the shoreline was far from the shelf edge, the erosion triggered by exposure of the continental portion of the basin as a result of a contractional deformation event (Eocene - Oligocene) delivered large amounts of sediments to deep-water settings. Another example of the deposits that occurred during the forced regression is represented by lobes of debrites (mudflows, grain flows and associated deposits); this depositional element is mainly distributed in the southern portion of the study area at the base of the middle Miocene and the base of the upper Miocene. Finally, the last example of this type of

deposit correspond to the large amounts of sand transferred into the basin via high-density turbidity currents; this type of deposit occurred mainly at the base of the middle and upper Miocene in more distal areas (central and northern portions of the study area), where channel systems and frontal splays developed.

At the end of the relative sea-level fall the deposition of turbidites prevailed with a change from high to low density across the correlative conformities; this change implies not only a decrease in the volume of sediment delivered to deep-water settings but also a decrease in grain size and the sand/mud ratio of the sediment involved in the flow. As a result, channel-levee complexes and frontal splay complexes were developed at the end of the middle Miocene and during the upper Miocene in the whole area. According to the seismic data, the channel-levees continued to develop toward the central and northern part of the study area; while some mudflow entrenched channels were generated in the southern portion.

Tectonics played an important role on sedimentation, by forming topographic lows and highs as a result of sydepositional processes (movement of salt and normal faults). This complex paleotopography was revealed by the high thickness variability of the deposits accumulated in small and large depocenters and in topographic highs; this complex paleotopography was the result of the main compressional event that occurred in the area during the middle Miocene (Chiapanecan orogeny); as well as the emplacement of allochthonous salt, which movement began during the middle Oligocene.

The sequence stratigraphic framework allowed the reconstruction of the relative sea-level curve for this area, which combines the effects of eustasy and tectonics (Fig. 3.23). The biostratigraphic information from three wells was incorporated, allowing us to calibrate and to verify the position of key stratigraphic surfaces within the sequence stratigraphic framework.

The relative sea-level curve matches the long-term trend of the global eustatic chart of Haq et al. (1988); however, local tectonism also played an important role in controlling the timing of sequences and bounding surfaces, which explains the departures from the predictions of the global cycle chart, which can observe at smaller scales.

The relative sea-level curve of the study area shows that a major drop in relative sea-level lasted for six million years, from the lower Oligocene to Aquitanian (lower Miocene); this major drop was also reported by Davis et al. (2011). Three other minor drops in the relative sea level occurred during the Miocene and lasted less than 2 My. These drops in the sea level are related to tectonic events; for instance, during the Oligocene and lower Miocene, the sea-level fall combined with the beginning of the salt movement in the study area was mainly responsible for the slope destabilization, triggering the mass transport deposits. Additionally, the Chiapanecan orogeny that occurred mainly during the middle Miocene resulted in the dominance of falling-stage deposits during this time.

8. Conclusions

The new information on the chronostratigraphic framework of the Miocene in the southern Gulf of Mexico allows the identification of several regional discontinuities and maximum flooding surfaces, which are used to establish the sequence stratigraphic framework that can provide a genetic context for observed depositional elements. The sedimentary sequences of the lower and middle Miocene are dominated by the deposits of the falling-stage, lowstand and transgressive systems tracts, while the sediments of the highstand systems tract are reduced to a thin condensed interval interbedded between sandy sediments.

This analysis shows that a framework based on the use of maximum flooding surfaces as sequences boundaries is most adequate for the studied area, due to the ease of recognition and regional mappability of these surfaces. As a result, the genetic sequence model was applied in this paper.

Four stages of relative sea-level fall were recognized within the Miocene succession; during these stages, the fall in relative sea level exposed the shelf to erosion and/or bypass, making it possible for rivers to discharge most of their sediment load directly onto the head of the continental slope or to build unstable shelf-edge deltas (e.g., in the onshore part of the study area, during the upper Miocene). The deposits of relative sea level fall overlie the basal surface of forced regression, and are represented by a range of gravity flows, from muddy (early forced regression) to coarse-grained sandy (late forced regression). During the Oligocene - lower Miocene, the major relative sea level fall occurred; during this time, the main deposits were the thicker mass-transport deposits and a few thinner sand-prone units. Finally, the thicker sand-prone units accumulated from the Serravallian to the Tortonian, forming a falling-stage systems tract. Additional sand units are found within the lowstand and transgressive systems tracts and are overlain by a mud-prone interval that corresponds to the transgressive and/or highstand systems tract in the Messinian. Subsequent increase in accommodation on the shelf, accompanied by sedimentation in fluvial to shallow-water systems, triggered a decrease in the sediment delivery to deep-water environments during the Pliocene.

Acknowledgments

This research was completed as a part of the doctoral project carried out by the first author, sponsored by Pemex Exploración and Producción and other funds by Fondo Sectorial Conacyt-Sener-Pemex.

We thank the editor, Massimo Zecchin, as well as Jose Daudt and Patrick Eriksson, for their constructive comments which helped to improve the manuscript during the peer review process.

References

- Ángeles-Aquino, F., Reyes-Núñez, J., Quesada- Muñeton, J.M., and Meneses-Rocha, J.J., 1994.** Tectonic Evolution, Structural Styles and Oil habitat in Campeche sound, Mexico: Gulf Coast Association of Geological Societies Transactions. 44, 53-62.
- Armentrout, J. M., 1996.** High resolution sequence biostratigraphy: examples from the Gulf of Mexico Plio-Pleistocene. Howell J.A and Aitken J.F. (Eds.), High Resolution Sequence Stratigraphy: Innovations and Applications, Geological Society Special Publication No.104, 65-86.
- Aubry, M.P., 1984-1987, 1993, 1997 and 1999.** Handbook of Cenozoic Calcareous Nannoplankton. Micropaleontology Handbook series. Vols. I, II, III, IV and V.
- Beaubouf, R.T., and Friedman, S.J., 2000.** High resolution seismic/sequence stratigraphic framework for the evolution of Pleistocene intraslope basins, western Gulf of Mexico: depositional models and reservoir analogs. In P. Weimer, R.M., Slatt, J.L. Coleman, N. Rosen, C.H., Nelson, A.H., Bouma, M., Styzen, and D.T Lawrence, (Eds.), Global deep-water reservoirs: Gulf Coast Section-SEPM Foundation 20th Annual Bob. F. Research Conference, 40-60.

Berggreen, W.A., Kent, D.V., Swisher, C. C., and Aubry, M.P., 1995. A revised Cenozoic Geochronology and Chronostratigraphy. Geochronology Time Scales and Global Stratigraphic Correlation, SEPM Special Publication No. 54.

Blow, W.H., 1979. The Cenozoic Globigerinida: A Study of the Morphology, Taxonomy, Evolutionary Relationships and the Stratigraphical distribution of some Globigerinida (mainly Globigerinacea): Leiden, E.J.Brill (3 vols), 1462 p.

Bolli, H.M., and Saunders, J.B., 1985. Oligocene to Recent low latitude planktic foraminifera. In: Bolli, H.M., Saunders J.B. and K. Perch-Nielsen (Eds.) Plankton Stratigraphy. Cambridge University, Press New York: 155-262.

Buffler, R.T., and Sawyer D.S., 1985. Distribution of crust and early history Gulf of Mexico Basin: Gulf Coast Association of Geological Societies Transactions.35. 333-344.

Carvajal, C.R., Steel, R.J., and Peter, A., 2009. Sediment supply: The main driver of shelf margin growth. Earth-Science Reviews, 96,221–248.

Catuneanu, O., 2003. Sequence Stratigraphy of Clastic Systems, vol.16. Geological Association of Canada, Short Course Notes p248.

Catuneanu, O., Martins-Neto, M., and Eriksson, P.G., 2005. Precambrian sequence stratigraphy. Sedimentary Geology, v.176, Issues 1-2, p.67-95.

Catuneanu, O., 2006. Principles of sequence stratigraphy. Elsevier. Oxford Uk

Catuneanu, O., Abreu, V., Bhattacharya, J.P., Blum, M. D., Dalrymple, R.W., Eriksson, P. G., et al., 2009. Towards the standardization of sequence stratigraphy. Earth-Science Reviews, 92.

Catuneanu, O., Bhattacharya, J.P., Blum, M.D., Dalrymple, R.W., Eriksson, P.G., Fielding, C.R., Fisher, W.L., Galloway,W.E., Gianolla, P., Gibling, M.R., Giles, K.A., Holbrook, J.M., Jordan, R., Kendall, C.G.St.C., Macurda, B., Martinsen, O.J.,Miall, A.D., Nummedal, D., Posamentier, H.W.,

Pratt, B.R., Shanley, K.W., Steel, R.J., Strasser, A., and Tucker, M.E., 2010. Sequence stratigraphy: common ground after three decades of development: *First Break*, 28, 21-34.1–33.

Catuneanu O., Galloway W.E., Kendall C G.St. C., Miall A.D., Posamentier H.W., Strasser A., and Tucker M.E., 2011. Sequence Stratigraphy: Methodology and Nomenclature. *Newsletters on Stratigraphy*, 44/3, 173-245.

Catuneanu, O., and Zecchin, M., 2013. High-resolution sequence stratigraphy of clastic shelves II: controls on sequence development: *Journal of Marine and Petroleum Geology*, 39, 26-38.

Cruz-Mercado, M.A., Flores-Zamora, J. C., León-Ramírez R., López-Céspedes, H. G., Peterson-Rodríguez, R. H., Reyes-Tovar E, Sánchez-Rivera, R et al., 2011. Salt Provinces in the Mexican Portion of the Gulf of Mexico Structural Characterization and Evolutionary Model: *Gulf Coast Association of Geological Societies Transactions*, v.61, p.93-103.

Davis, R. A., 2011. *Sea-Level Change in the Gulf of Mexico* Texas A&M University Press. 192p.

De Gasperi, A., and Catuneanu, O., 2014. Sequence stratigraphy of the Eocene turbidite reservoirs in Albacora field, Campos Basin, offshore Brazil. *American Association of Petroleum Geologists (AAPG) Bulletin*, 98/2, 279-313.

Emery, D., and Myers, K.J., 1996. *Sequence Stratigraphy*. Blackwell Oxford, U.K., p.297.

Eriksson, P.G., Catuneanu, O., Sarkar, S., and Tirsgaard, H., 2005. Patterns of sedimentation in the Precambrian. *Sedimentary Geology*, v. 176, Issues 1-2, p. 17-42.

Eriksson, P.G., Mazumder, R., Catuneanu, O., Bumby, A.J., and Ilondo, B. O., 2006. Precambrian continental freeboard and geological evolution: A time perspective. *Earth-Science Reviews*, vol. 79, p. 165-204.

Eriksson, P.G., Porada, H., Banerjee, S., Bouougri, E., Sarkar, S., and Bumby, A.J., 2007. Mat-destruction features. In: Schieber, J., Bose, P.K., Eriksson, P.G., Banerjee, S., Sarkar, S., Altermann, W.

and Catuneanu, O. (Eds.) Atlas of microbial mats features preserved within the siliciclastic rock record. Atlases in Geosciences, V. 2, p. 76-105.

Eriksson, P.G., Banerjee, S., Catuneanu, O., Corcoran, P.L., Eriksson, K.A., Hiatt, E.E., Laflamme, M., Lenhardt, N., Long, D.G.F., Miall, A.D., Mints, M.V., Pufahl, P.K., Sarkar, S., Simpson, E.L., and Williams, G.E., 2013. Secular changes in sedimentation systems and sequence stratigraphy. Gondwana Research, V. 24, p. 468-489.

Frazier, D.E., 1974. Depositional episodes: their relationship to the Quaternary stratigraphic framework in the northwestern portion of the Gulf Basin: The University of Texas at Austin, Bureau of Economic Geology, and Geological Circular 74-1, 28p.

Fillon, R.H., 2007. Biostratigraphy and Condensed Sections in Deepwater Settings in Weimer P and Slatt R. Introduction to the Petroleum Geology of Deepwater Settings. AAPG Studies in Geology 57 AAPG/Datapages Discovery Series 8.

Galloway, W.E., 1989. Genetic stratigraphic sequences in basin analysis; I, Architecture and genesis of flooding-surface bounded depositional units: American Association of Petroleum Geology Bulletin, 73, no.2, 125-142.

Galloway, W.E., 2001. The many faces of submarine erosion: theory meets reality in selection of sequences boundaries. American Association of Petroleum Geology. Hedberg Research Conference on Sequence Stratigraphic and Allostratigraphic Principles and Concepts, Dallas, August 26-29, Program and Abstracts. V, 28-29.

Gutierrez-Paredes, H.C., Catuneanu, O., and Hernández-Romano, U., 2017. Miocene depositional environments, processes, and depositional elements in the southern Gulf of Mexico. Geological Journal.2017; 1-30. <https://doi.org/10.1002/gi.2948>.

Haq, B.U., Hardenbol, J., and Vail, P.R., 1988. Mesozoic and Cenozoic chronostratigraphy and cycles of sea-level change. In Sea Level Changes- An Integrated Approach C.K. Wilgus, B. S Hastings,

C.G.St.C. Kendall, H.W.Posamentier, C.A. Ross J.C.Van Wagoner, (Eds.), pp 125-154. SEPM Special Publication 42.

Hunt, D., and Tucker, M.E., 1992. Stranded parasequences and the forced regressive wedge systems tract: deposition during base-level fall. *Sedimentary Geology*, 81, 1-9.

Hunt, D., and Tucker, M.E., 1992. Stranded parasequences and the forced regressive wedge systems tract: deposition during base-level fall-reply. *Sedimentary Geology*, 95, 147-160.

Loutit, T. S. Hardenbol, J., and Vail, P. R., 1988. Condensed sections: the key to age determination and correlation of continental margin sequences, in Wilgus, C. K., Hastings, B. S., Kendall, C. G. St. C., Posamentier, H. W., Ross, C. A., and Van Wagoner, J. C., eds., *Sea-level Changes: An Integrated Approach*: SEPM Special Publication No. 42, pp. 183–213.

Lugo, R. J.E, Granados, M.O.J, Segura, T.A., Castillo, D.R., Villanueva, G.L.I., Jiménez, B.D., Berlanga J.A et al., 2005. Carta de Biozonas y Bioeventos de microfósiles del Cenozoico de las Cuencas del Golfo de México. PEMEX. Informe Inédito.

Martini, E., 1971. Standard Tertiary and Quaternary calcareous nannoplankton zonation. En A. Farinacci (i). In: *Proceedings 2nd Planktonic Conference*, Roma, 1970, vol. 2, pp739-785.

Mitchum, R.M., Sangree, J. B. Vail, P. R., and Wornardt, W., 1993. Recognizing sequences and systems tracts from well logs, seismic data, and biostratigraphy: examples from the Late Cenozoic of the Gulf of Mexico, in P. Weimer and H. Posamentier, (Eds.), *Siliciclastic sequence stratigraphy: recent developments and applications*: American Association of Petroleum Geology Memoir 58, 163–197.

Morán-Zenteno, D. J., Martiny, B., Tolson, G., Solís Pichardo, G., Alba Aldave, L., Hernández-Bernal, M. del S., Macías Romo, C., Martínez Serrano, R.G., and Silva Romo, G., 2000. Geocronología y características geoquímicas de las rocas magmáticas terciarias de la Sierra Madre del Sur: *Boletín de la Sociedad Geológica Mexicana*, T. LIII, No. 1, p. 27-58.

Muto, T. and Steel, R.J., 2002. In defense of shelf-edge delta development during falling and lowstand of relative sea level. *Journal of Geology* ,110 (4), 421–436.

Padilla y Sánchez, R.J., 2007. Evolución Geológica del Sureste Mexicano desde el Mesozoico al Presente en el Contexto Regional del Golfo de México. *Boletín de la Sociedad Geológica Mexicana*, tomo LIX, no 1, p. 19-42.

Perch-Nielsen, K., 1985. Cenozoic Calcareous Nannofossils in Bolli, H.M. Saunders J.B & Perch-Nielsen (Eds.) *Plankton Stratigraphy*. Cambridge University, Press New York: pp 427-545.

Pyles, R.D., and Slatt, M.R., 2000. A High Frequency Sequence Stratigraphy Framework for Shallow Trough Deep-Water deposits of the Lewis shale and Fox Hill sandstone, Great Divide and Washakie Basins, Wyoming. GCSSEPM Foundation 20th Annual Research Conference Deep-Water Reservoirs of the World, December 3-6, 2000.

Pindell, J.L., 1985. Alleghenian reconstruction and subsequent evolution of the Gulf of Mexico, Bahamas and Proto-Caribbean. *Tectonics*, 4, 1-39.

Pindell, J.L., and Kennan, L., 2002. Análisis Paleogeográfico Mesozoico-Cenozoico y Dinámica de las cuencas en el Golfo de México Profundo y Márgenes. Informe Final. Tectonic Analysis Inc. and Pemex Exploration and Production. Reporte Inédito.

Porebski, S. J., and Steel, R., 2003. Shelf-margin deltas: their stratigraphic significance and relation to deepwater sands. *Earth-Science Reviews*, 1282, 1-44.

Posamentier, H.W., and Vail, P.R., 1988. Eustatic controls on clastic deposition II-sequence and systems tract models. In *Sea Level Changes- An Integrated Approach* C.K. Wilgus, B.S Hastings, C.G.St.C. Kendall,H.W. Posamentier, C.A.Ross and J.C.Van Wagoner, (Eds.), pp 125-154. SEPM Special Publication 42.

Posamentier, H.W., and Allen, G.P., 1999. Siliciclastic sequence stratigraphy: concepts and applications. SEPM Concepts in Sedimentology and Paleontology No.7, p.210.

Posamentier, H.W., and Kolla V., 2003. Seismic geomorphology and stratigraphy of depositional elements in deep-water settings: Journal of Sedimentary Research, 73, 367-388.

Robles Nolasco, J., Pliego- Vidal, E., Toledo-Bante, C., Pimienta-Lugo, M., Ortega-González, V., Martínez-Peña, B., et al., 2004. Offshore Neogene plays, Salina del Itsmo Basin, southeast of Mexico: Tulsa, Oklahoma, E.U.A., American Association of Petroleum Geologists, International Conference, October 24-27, Cancun, Mexico, 5p.

Salvador, A., 1987. Late Triassic- Jurassic Paleogeography and Origin of Gulf of Mexico. AAPG Bulletin, 71, 419-451.

Salvador, A., 1991. Triassic-Jurassic, in A. Salvador, (Ed.). The Gulf of Mexico Basin: Geological Society of America. The Geology of North America, V.J.p.131-180.

Sánchez-Montes de Oca, R., 1980. Geología petrolera de la Sierra de Chiapas: Boletín Asociación Mexicana Geológica Petrolera. 31, Nos. 1-2, 67-77.

Shanmugam, G., 2007. The obsolescence of deep-water sequence stratigraphy in petroleum geology. Indian Journal of Petroleum Geology, 1-45.

Shannon, P.M., Stoker, M.S., Praega, D. Van Weering T.C.E., De Haasc H., Nielsend, T., Dahlgrene, K.I.T., and Hjelstuenf, B.O., 2005. Sequence stratigraphic analysis in deepwater underfilled NW European Passive Margin Basins, Marine and Petroleum Geology, 22, 1185–1200.

Sinclair, H.D., and Tomasso, M., 2002. Depositional Evolution of Confined Turbidite Basins, Journal of Sedimentary Research, 72, No. 4, 451–456.

Talling, P. J., Masson, D. G., Sumner, E. J., and Malgesini, G., 2012. Subaqueous sediment density flows: Depositional processes and deposit types. Sedimentology, 59(7), 1937-2003.

Vander Merwe W.C., Flint, S., and Hodgson D.M., 2010. Sequence stratigraphy of an argillaceous, deepwater basin-plain succession: Vischkuil Formation (Permian), Karoo Basin, South Africa: Marine and Petroleum Geology, v. 27 p321-333.

Wynn, J. R., 1996. Micropaleontology in Petroleum Exploration Oxford Science Publications, 432p.

Figures

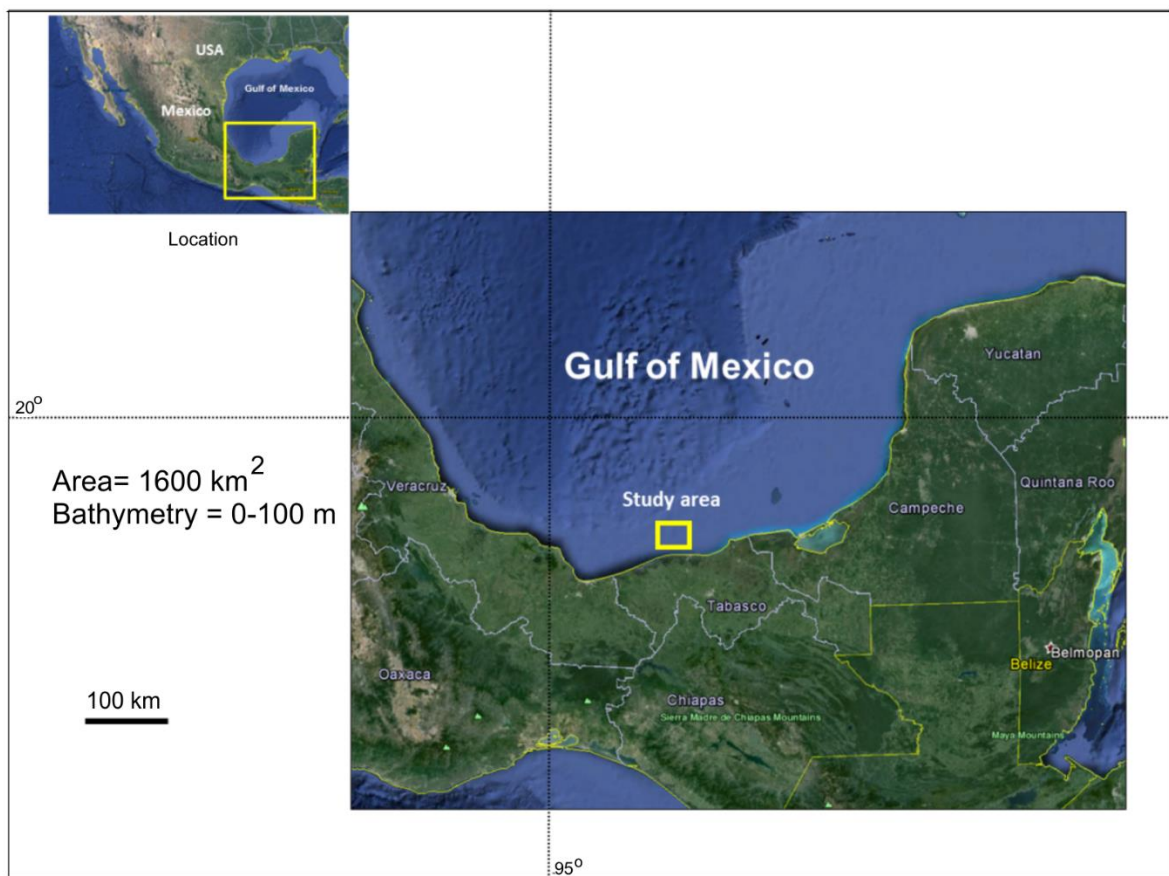


Figure 3.1 Location map of study area in the southern Gulf of Mexico.

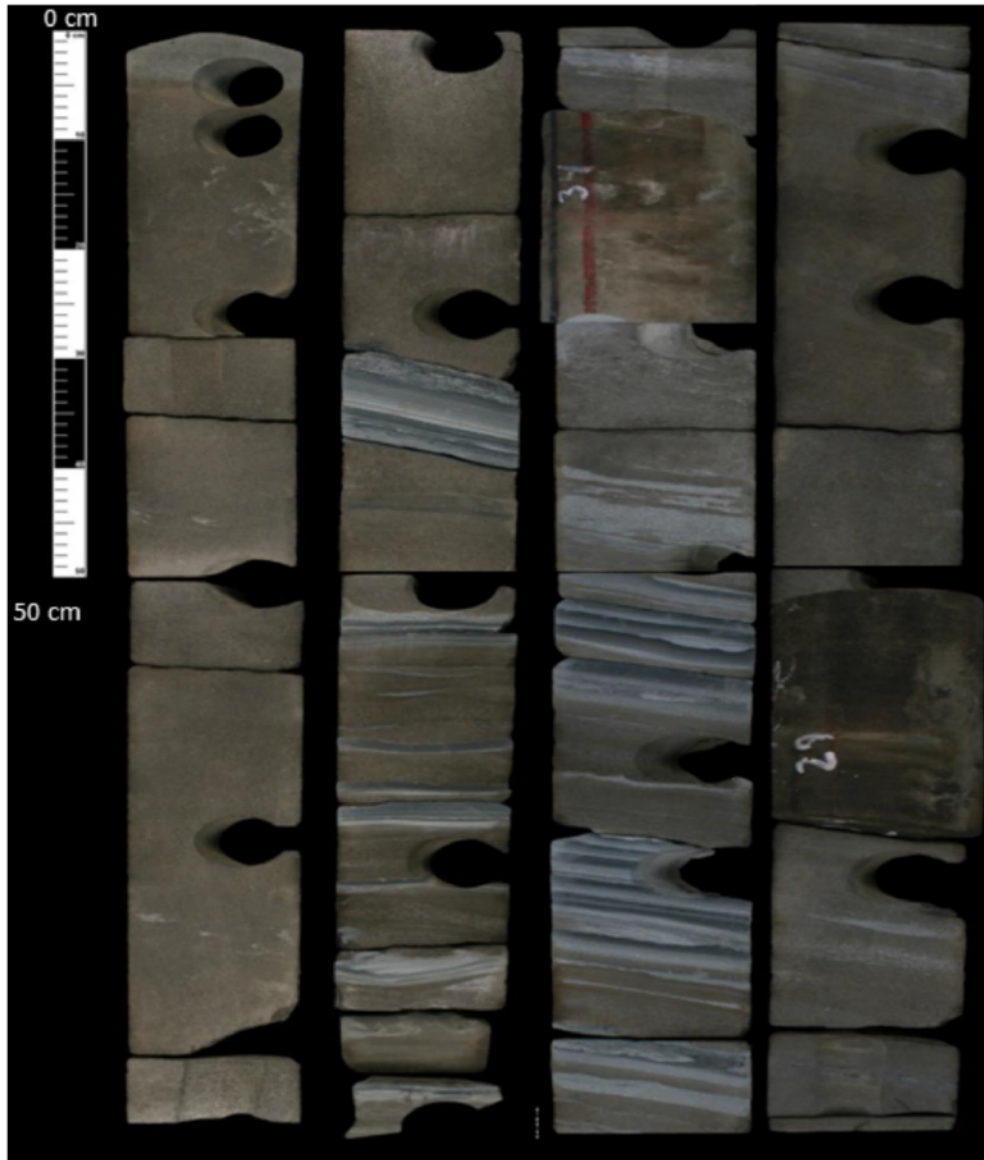


Figure 3.2 The main lithofacies recognized in the study area: massive sand with intercalations of rippled, laminated siltstone and mudstone. In this example the facies association represents channel-levee depositional elements.

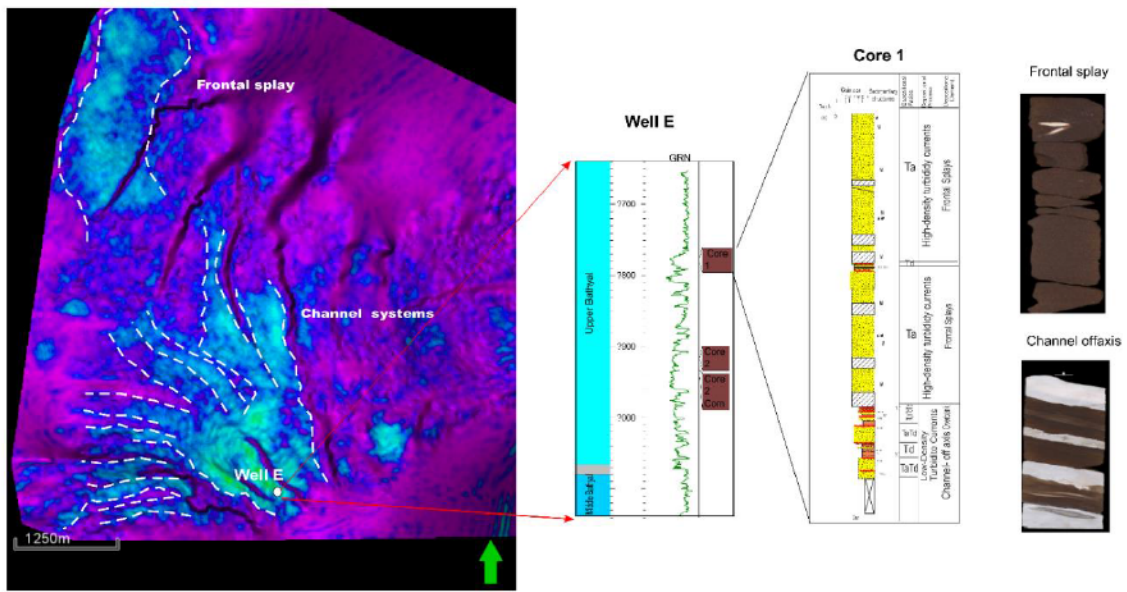


Figure 3.3 The integration of different data sets to identify the depositional elements in the area. This example corresponds to the overlap of frontal splay and channel systems deposited during the upper Miocene.

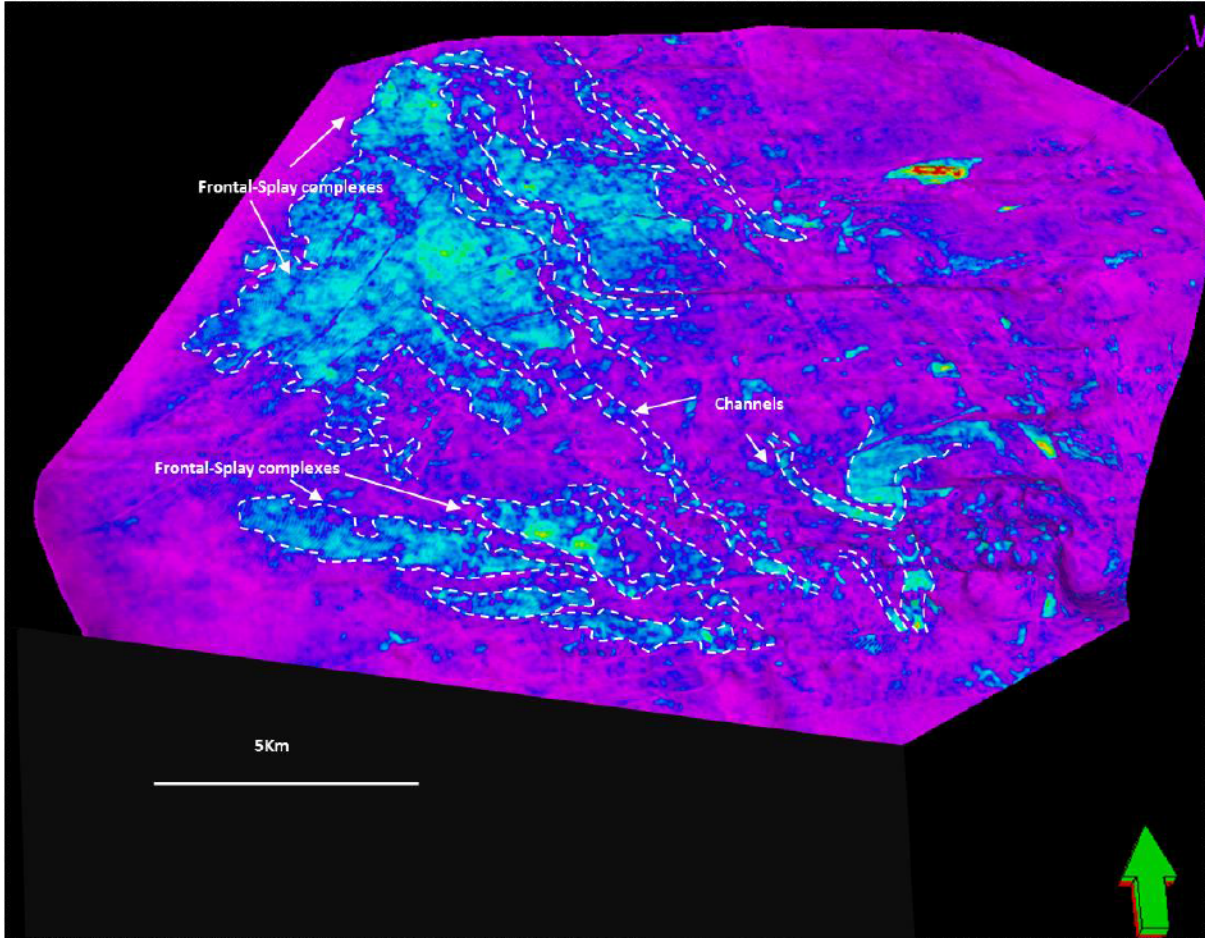


Figure 3.4 3D seismic- derived plan view image using RMS attribute extraction to illustrate frontal splay complexes and channels present in the upper Miocene.

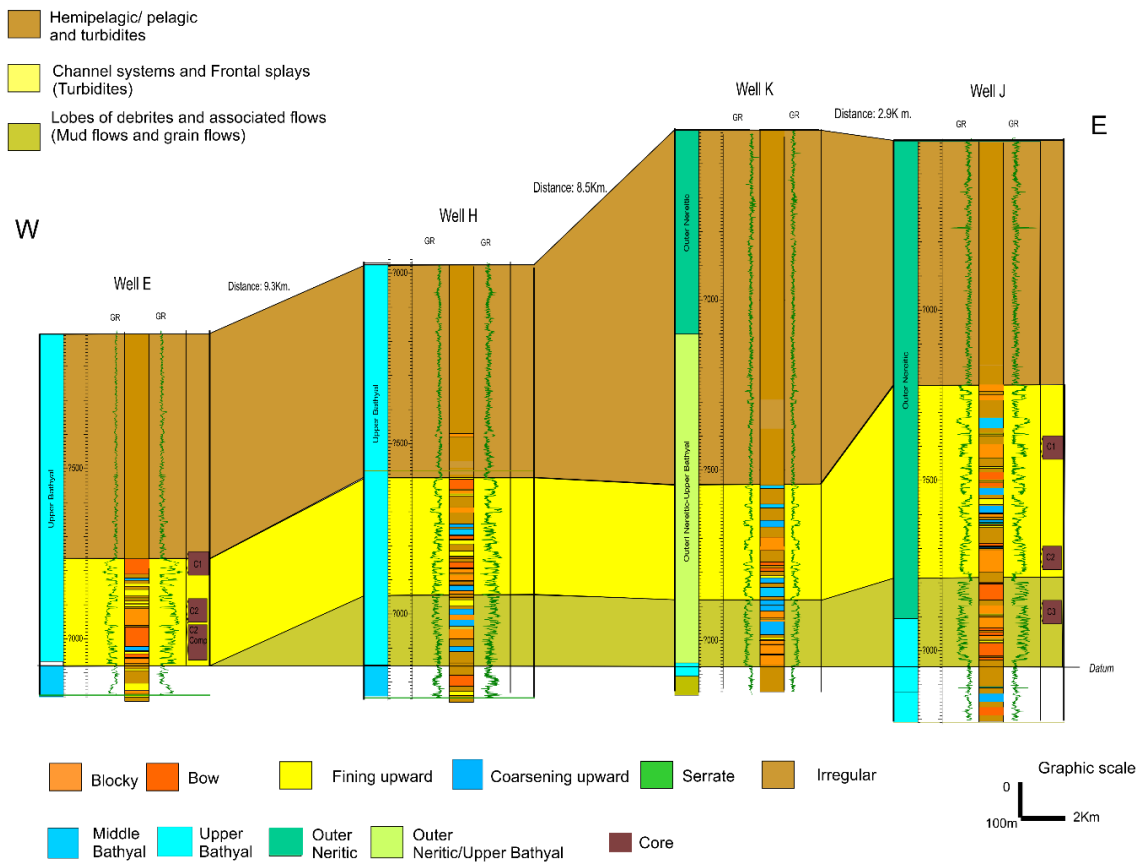


Figure 3.6 Stratigraphic section showing the vertical and lateral distribution of depositional environments during the upper Miocene. This section is orientated in the strike direction.

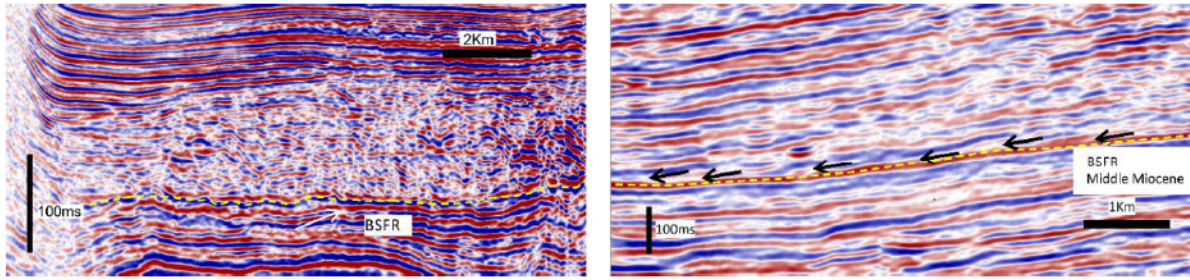


Figure 3.7 Two seismic sections showing some of the criteria for placing the basal surface of forced regression; the seismic line on the left illustrates a basal surface of forced regression (BSFR) placed on the base of mass-transport deposits; the seismic profile on the right shows the basal surface of forced regression placed on the base of a submarine fan complex. The right section also shows the downlap terminations above the BSFR, which are associated with the progradation of the submarine fan complex.

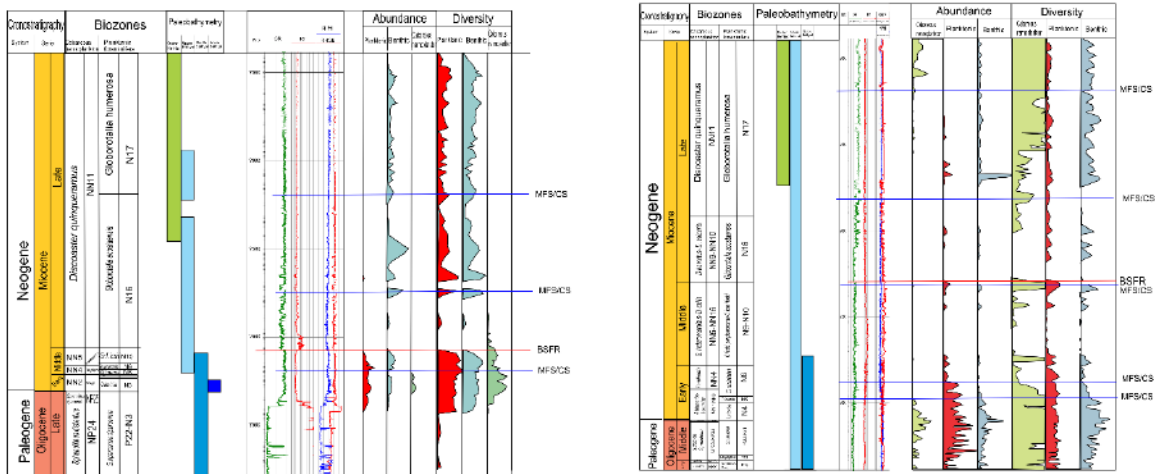


Figure 3.8 The biostratigraphic information from two wells shows abrupt shifts in biofacies assemblages from deeper paleo-bathymetries below to shallower above, and a decrease in both microfossil abundance and diversity above the BSFR; in contrast, the MFSs within the condensed sections (CS) show an increase in fossil abundance and diversity by the deepest-water biofacies assemblage.

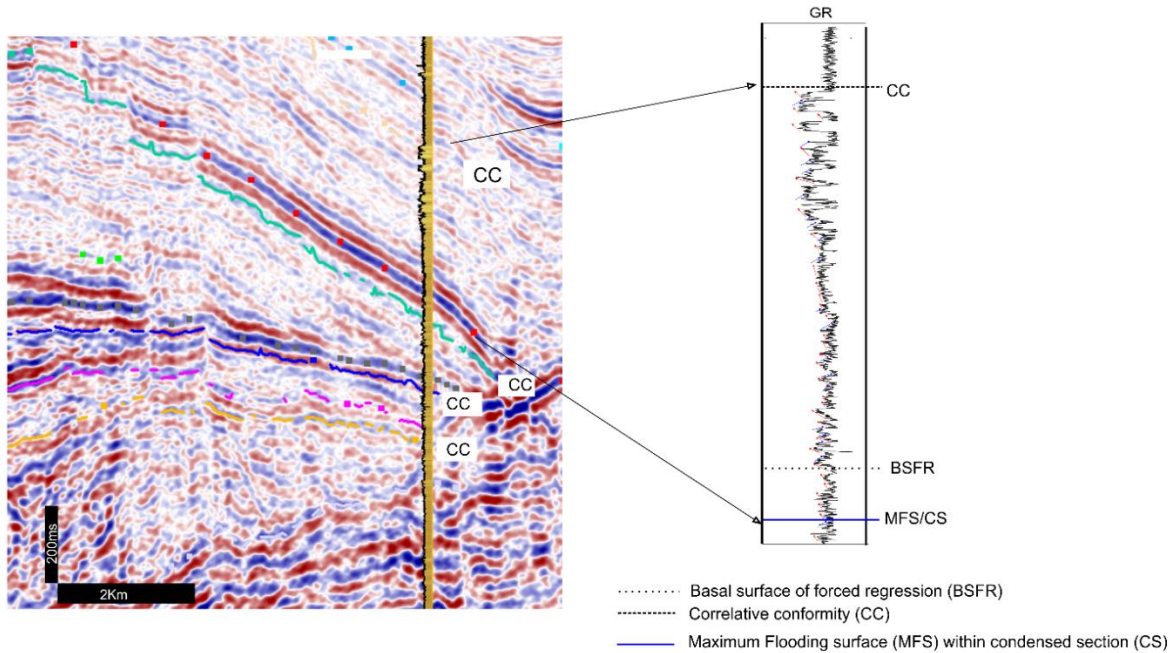


Figure 3.9 The example shows the criteria used to place the correlative conformity on well data and seismic section; in this well, this surface was marked at the top of the coarsest sediment of a submarine fan complex, in this particular case the correlative conformity coincided with an abrupt lithological change with a decrease in the sand/mud ratio; this correlative conformity was confirmed by seismic data and could be correlated regionally.

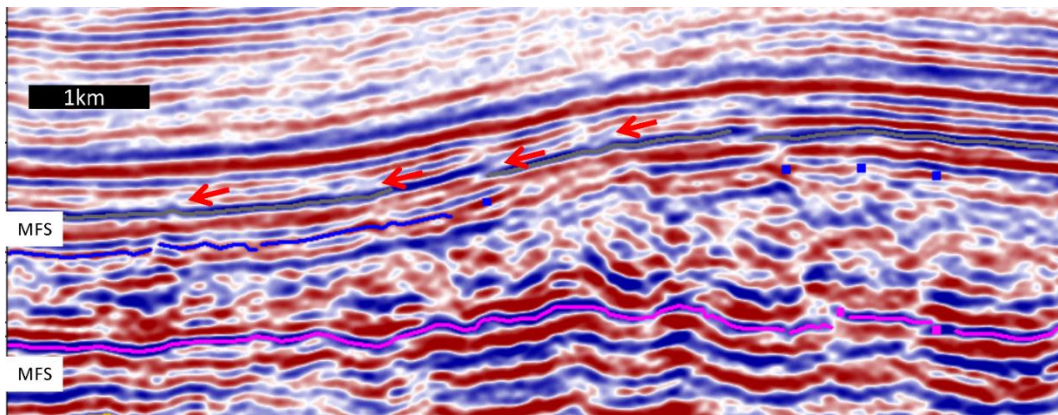


Figure 3.10 This seismic profile illustrates downlap terminations above the maximum flooding surface interpreted at the top of the lower Miocene. The older BSFR converges toward the MFS at the base of mass-transport complex.

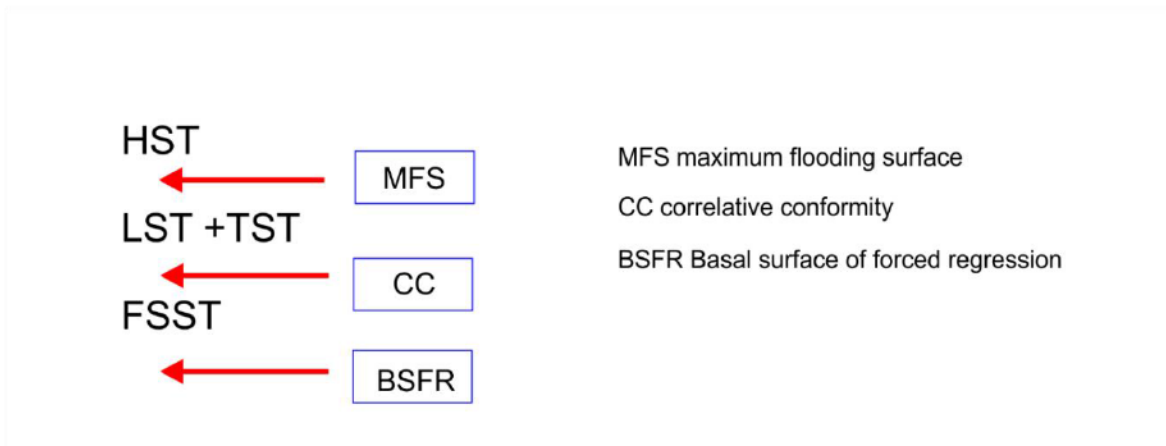


Figure 3.11 This diagram shows the systems tracts recognized in this study, as well as their bounding surfaces; note that the LST and TST are not differentiated because the MRS is cryptic in a deep-water setting.

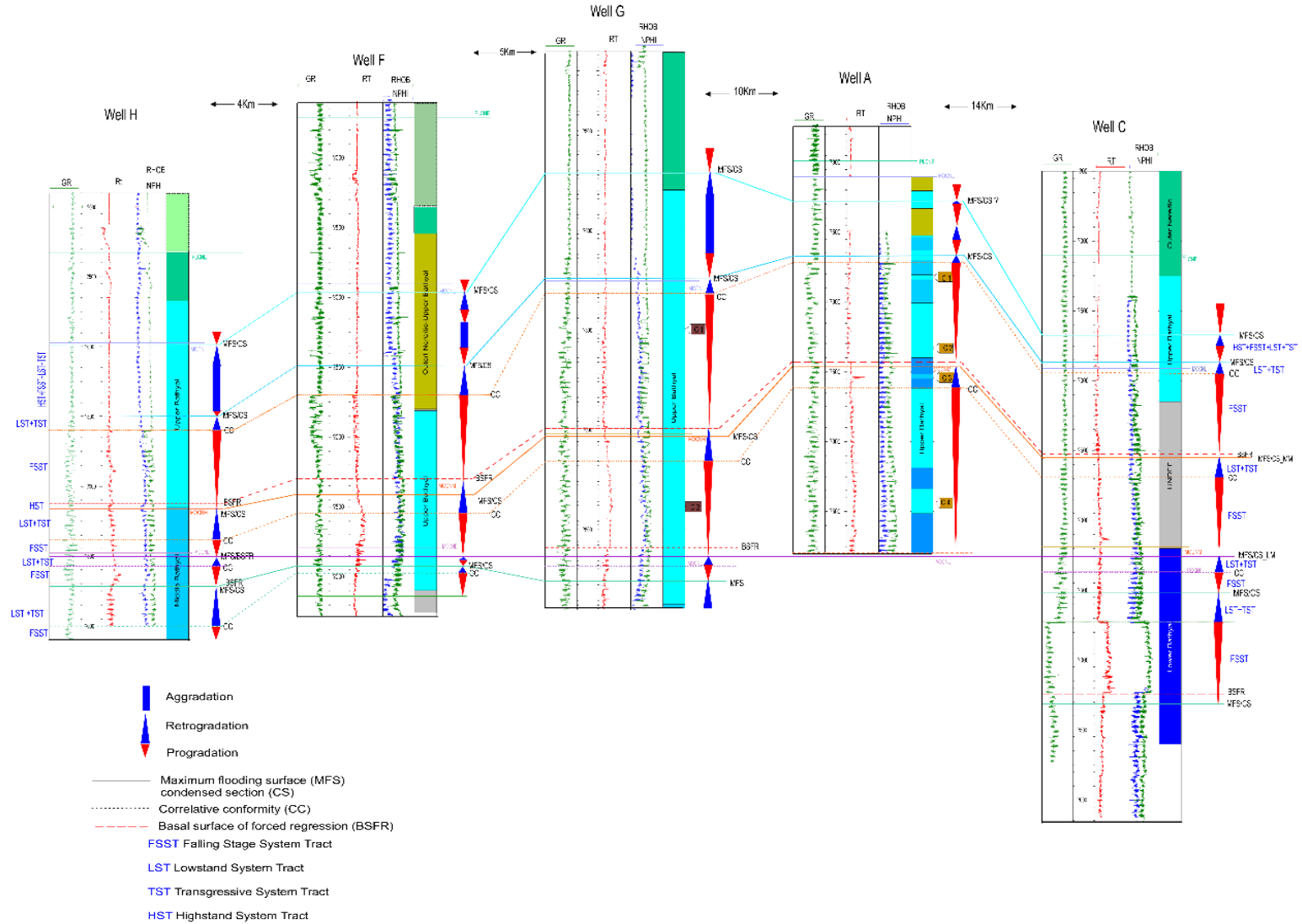


Figure 3.12 Stratigraphic section showing the sequence stratigraphic framework for the middle Miocene.

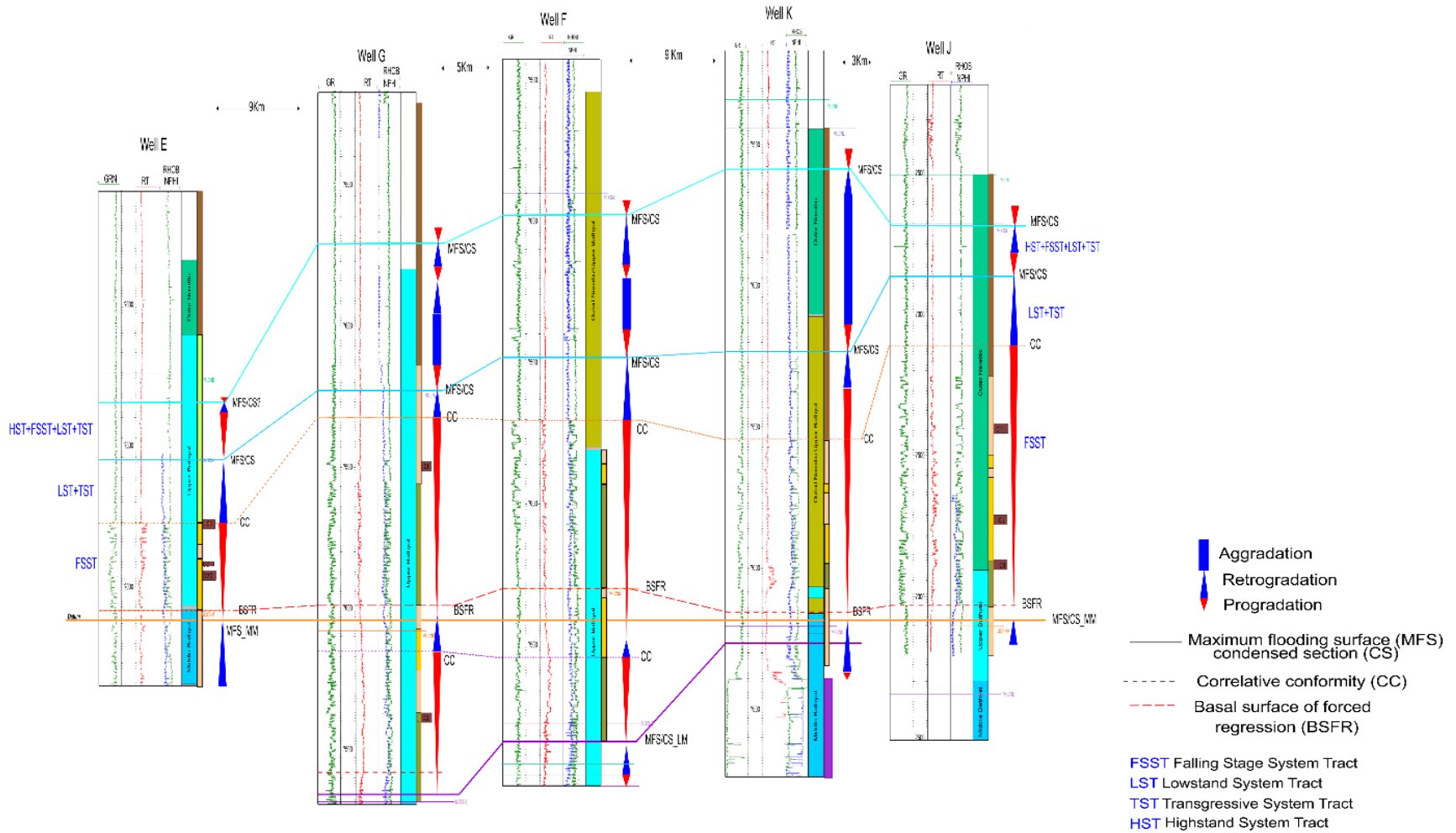


Figure 3.13 Stratigraphic section showing the sequence stratigraphic framework for the upper Miocene.

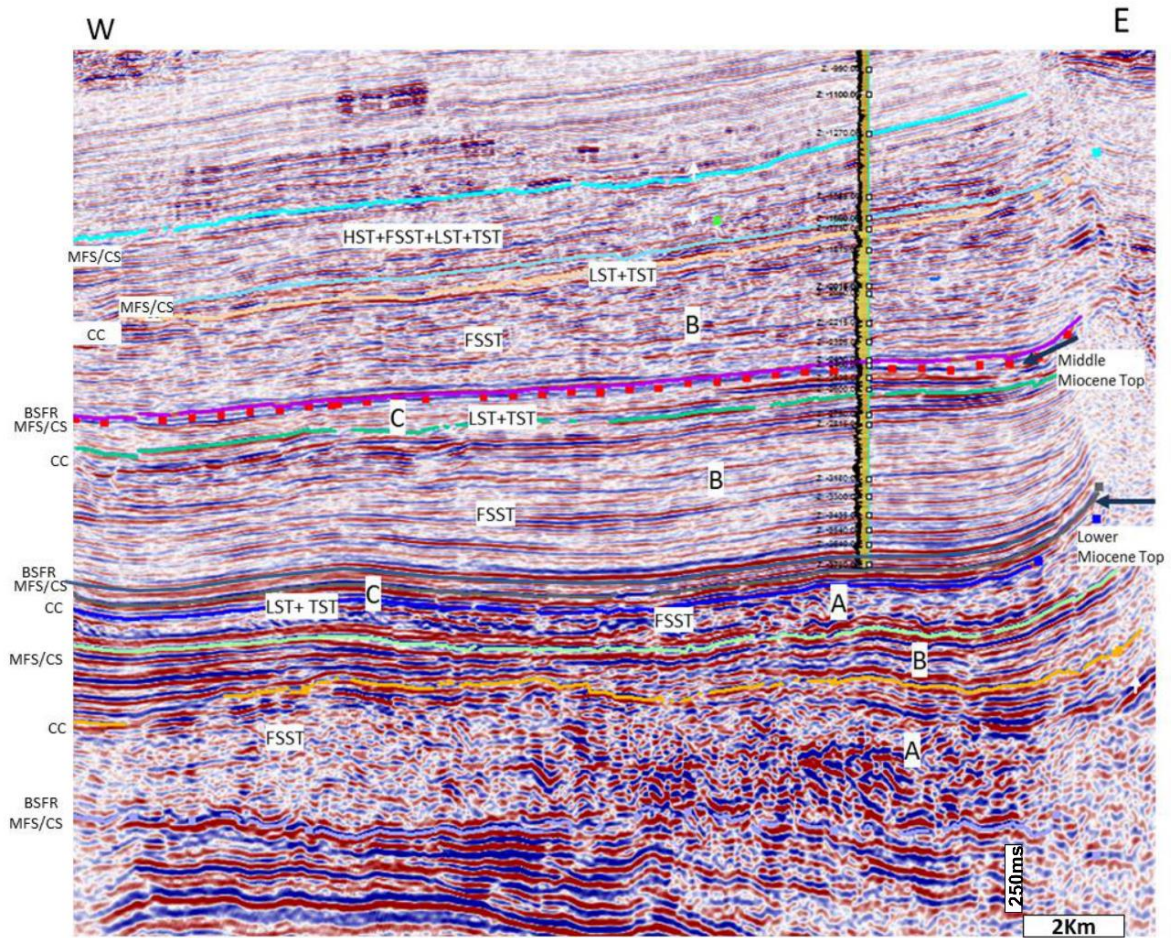


Figure 3.14 Seismic profile that illustrates the stratigraphic surfaces and systems tracts, as well as the type of deposits identified in this study in the Miocene succession; A: mass transport complex, B: High-density turbidity current deposits, C: Low-density turbidity current deposits.

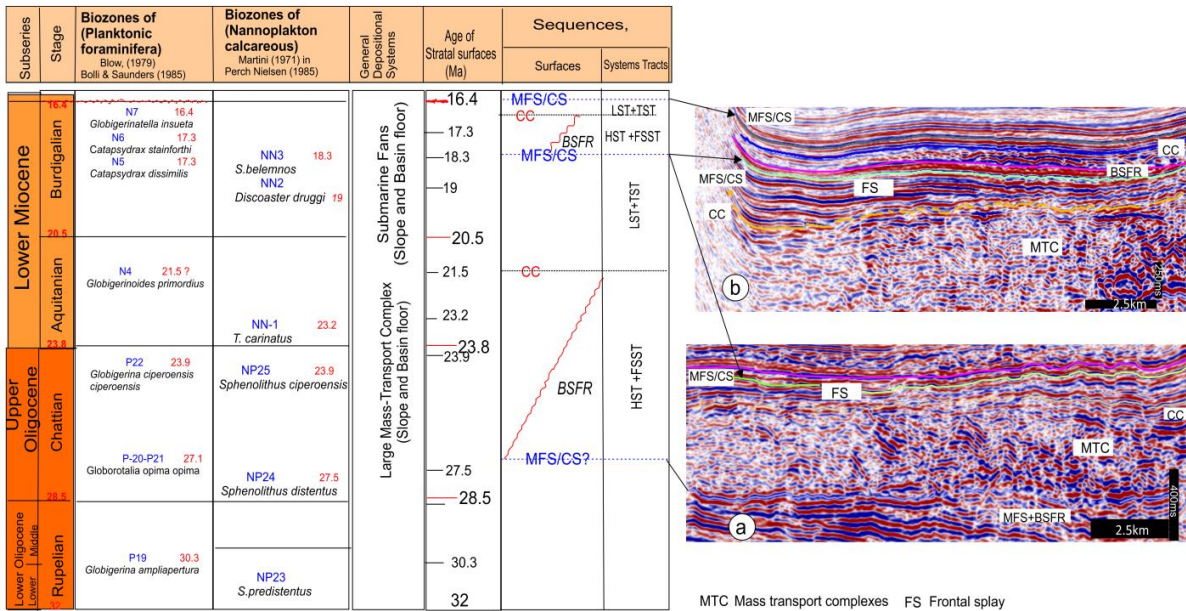


Figure 3.15 Examples of seismic lines showing the bounding surfaces, and deposits (mass transport complexes and frontal splays) present during the Oligocene and lower Miocene sequences. The seismic line “a” shows the deposits of the middle Oligocene-lower Miocene sequence bounded by two MFSs point by the black arrows. The seismic line “b” shows the deposits of the lower Miocene (Burdigalian) sequence, the black arrows point the bounding surfaces.

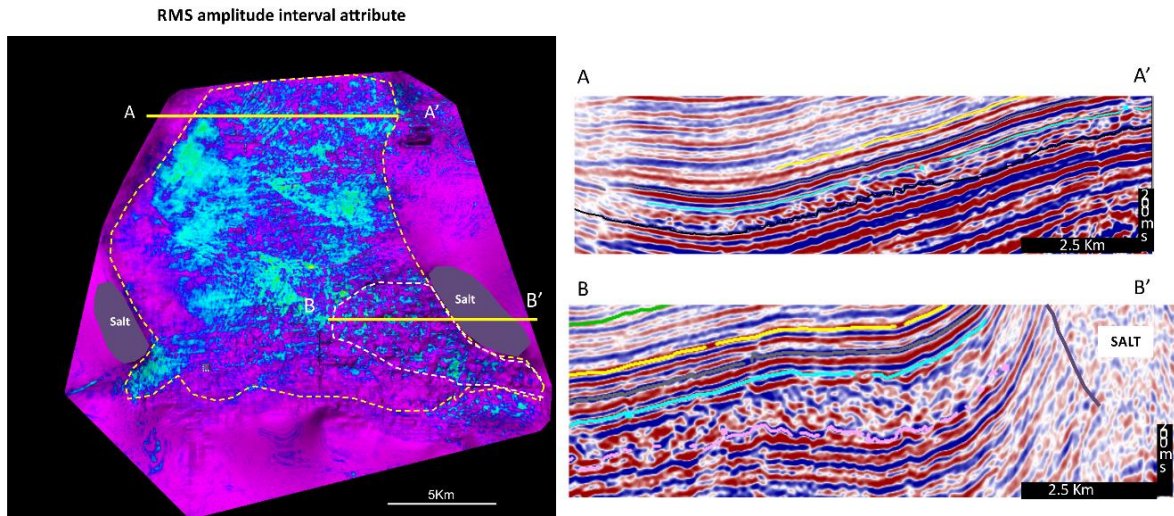


Figure 3.16 Examples of deposits during the falling stage systems tract. In plan view the yellow dotted line represents a main depocenter, and the white dotted line shows the area of the mass-transport deposits; the yellow lines represent the seismic profiles A-A' and B-B'. The seismic profile A-A' shows overbank deposits and the seismic profile B-B' mass-transport deposits.

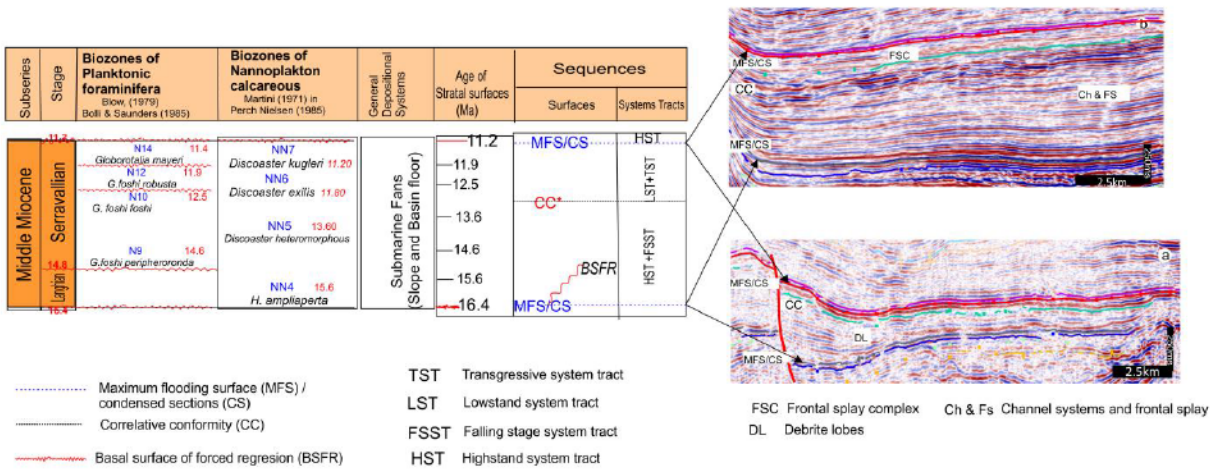


Figure 3.17 Examples of two seismic lines showing the bounding surfaces, and the deposits accumulated during the middle Miocene. Seismic line “a” illustrates the lobes of debris deposited during the FSST in the south of the study area; seismic line “b” illustrates channels and frontal splays in the FSST and frontal splay complexes in the LST +TST.

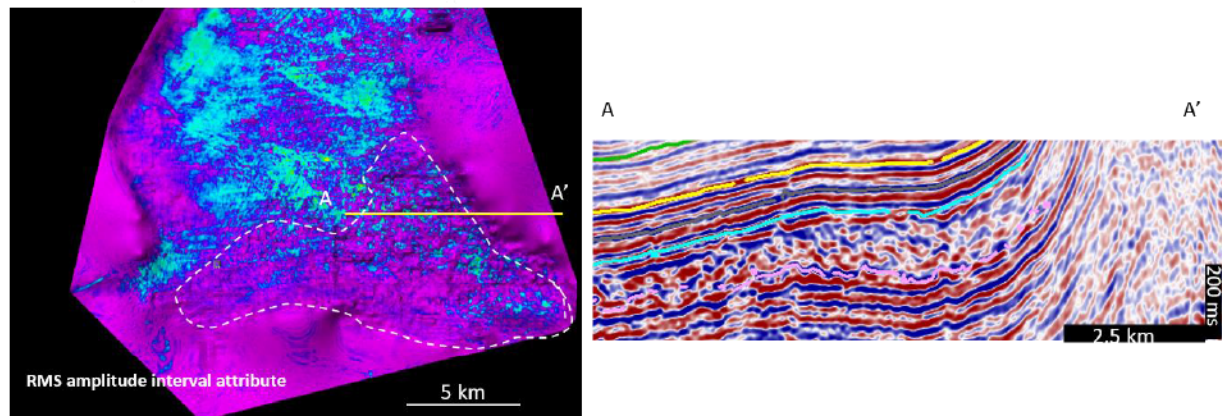


Figure 3.18 Examples of frontal splays deposited during the falling stage systems tract in the middle Miocene sequence. The yellow line represents the seismic line A-A’, and the black arrows in the seismic profile point the two types of frontal splays showed in map view.

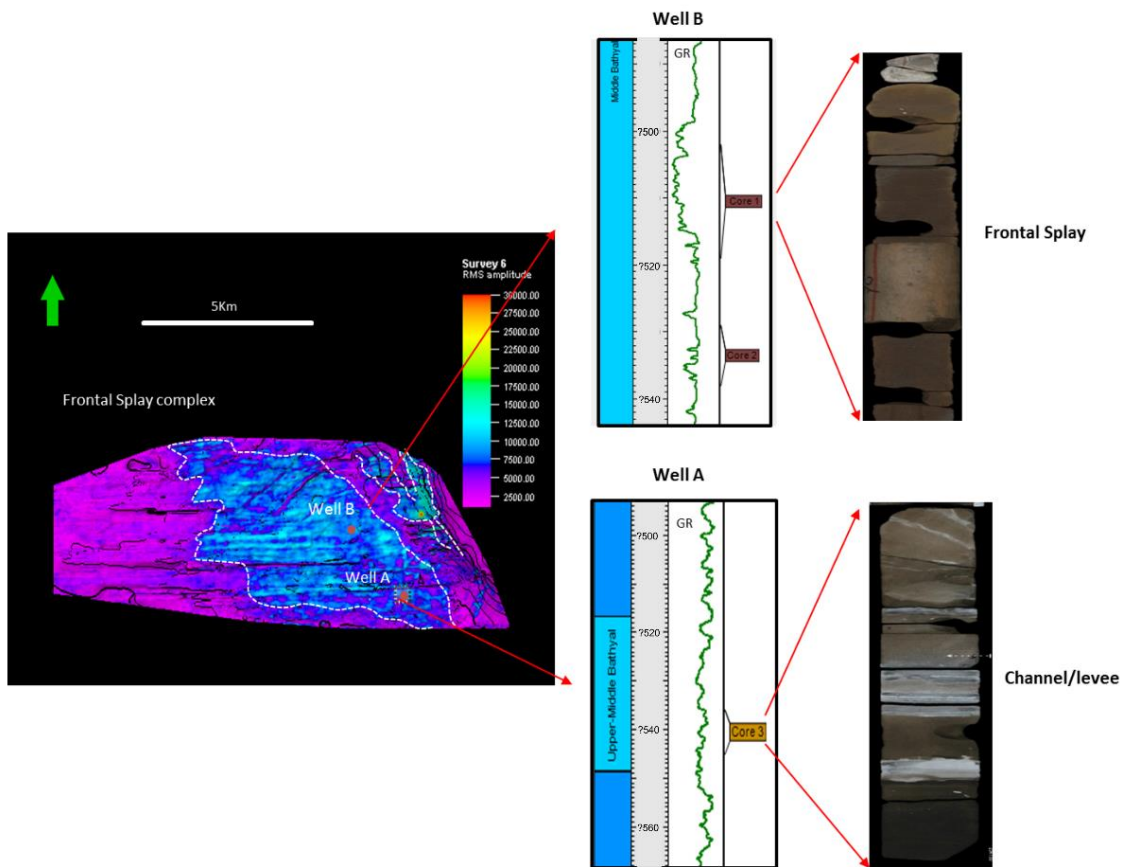


Figure 3.19 An example of frontal splay complex, with seismic attributes (RMS) and calibrated with well-logs and cores from two wells.

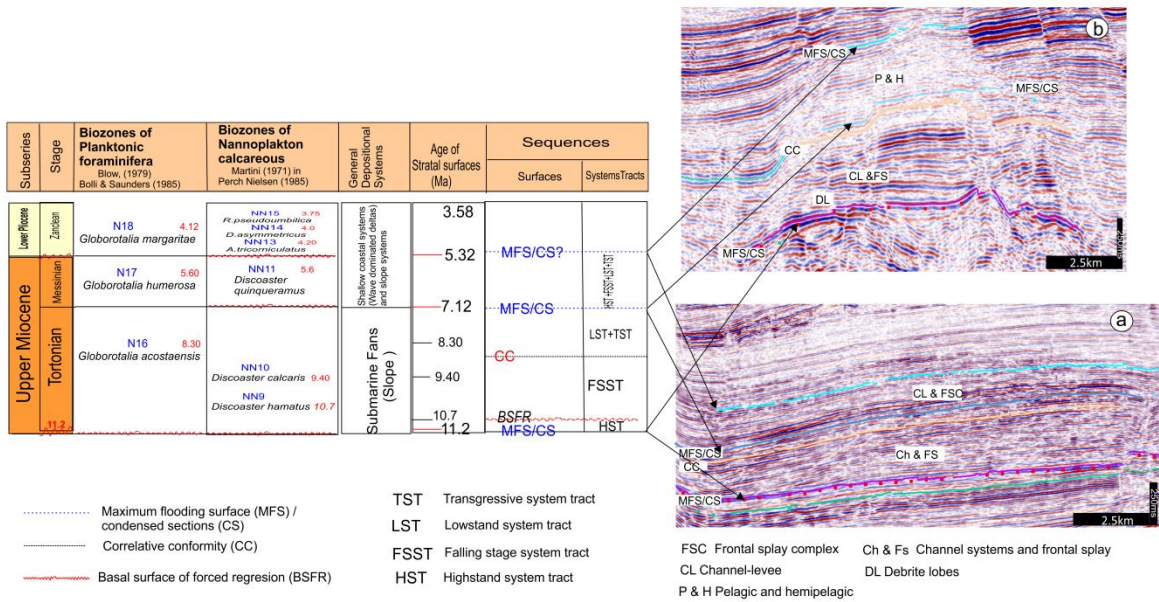


Figure 3.20 Examples of seismic lines showing the bounding surfaces, and deposits of lobes of debrites, channels, channel-levees, frontal splays and frontal splay complexes present accumulated during the FSSTs within the upper Miocene sequences.

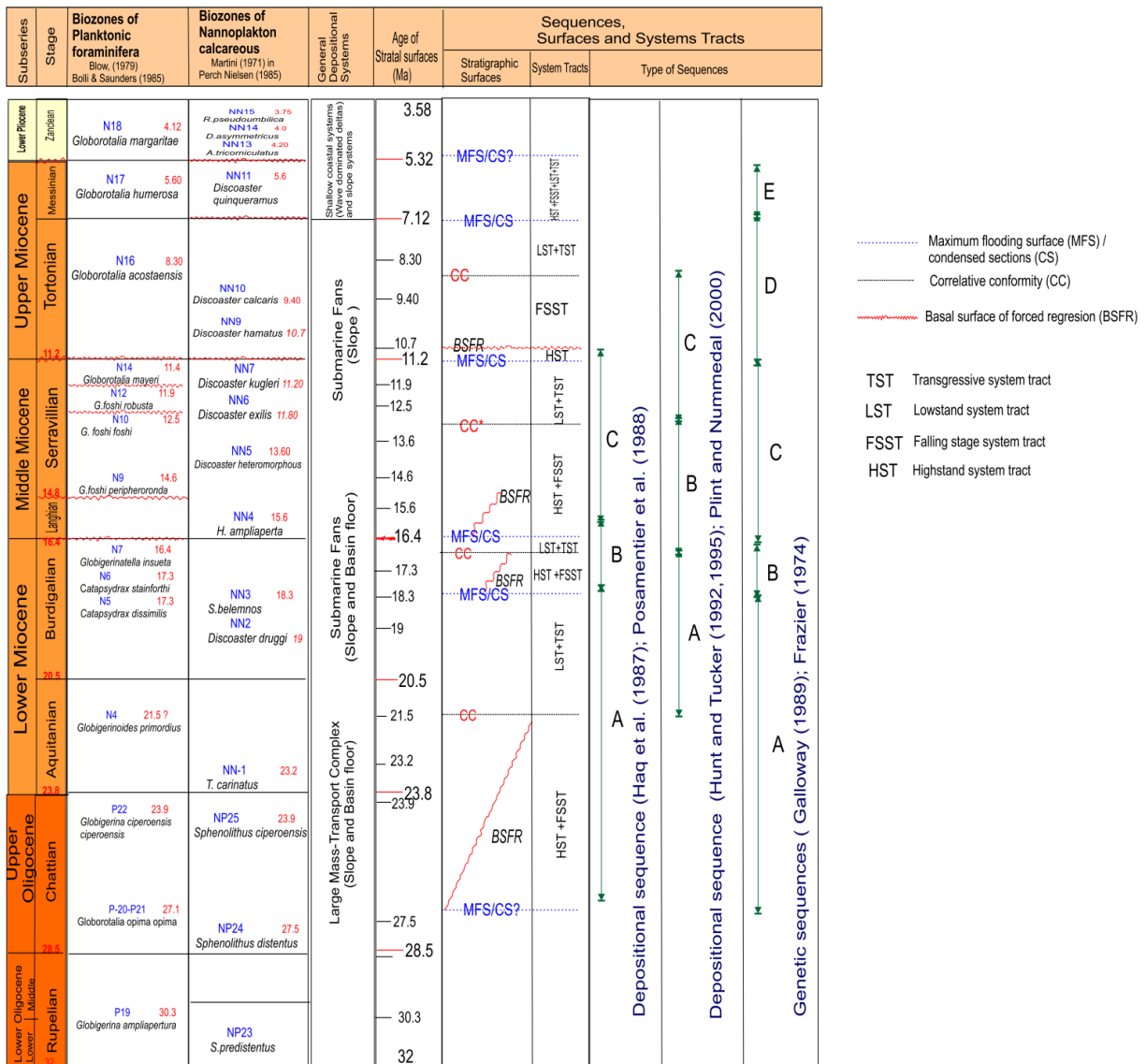


Figure 3.21 The sequence stratigraphic framework for the Miocene sequences in the study area.

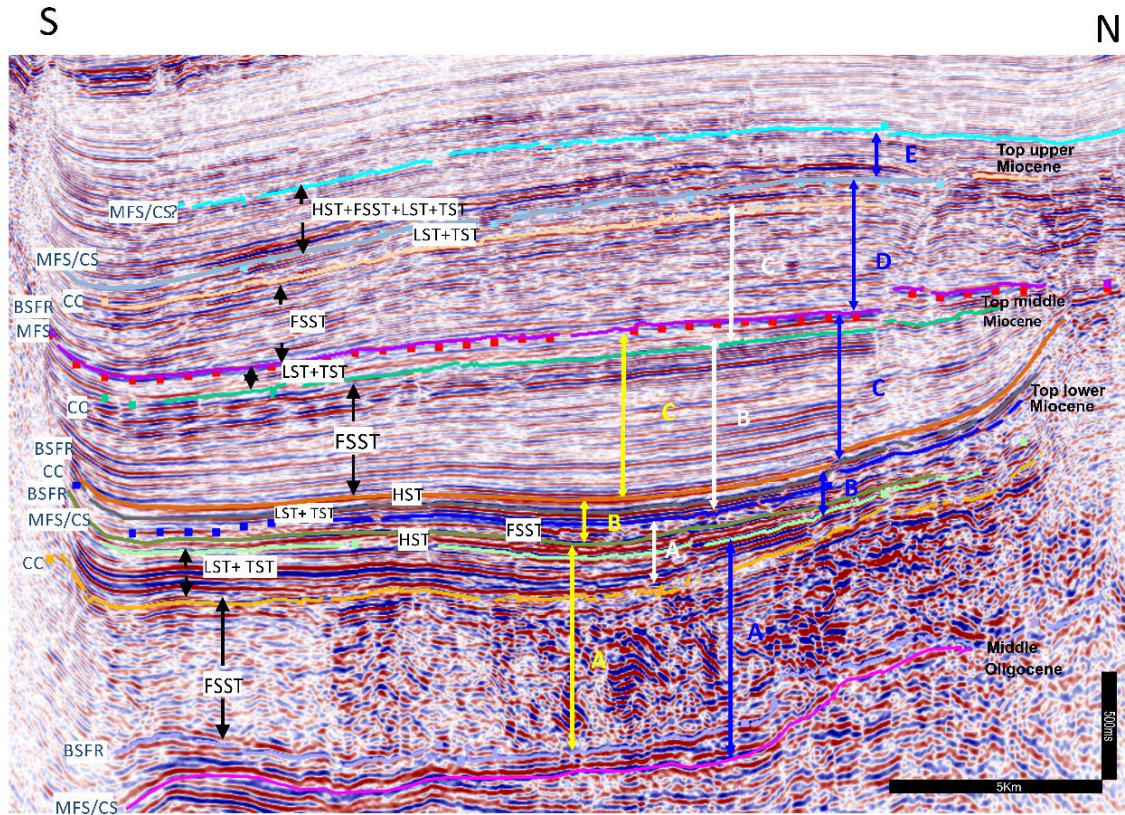


Figure 3.22 Seismic profile illustrating the sequence stratigraphic framework in the study area; this section also shows the types of sequences. Yellow arrows depositional sequences in accordance to Haq et al. (1987); Posamentier et al. (1988). White arrows sequences in accordance to Hunt and Tucker (1992,1995); Plint and Nummedal, (2000). Blue arrows genetic sequences in accordance to Frazier, (1974) and Galloway (1989).

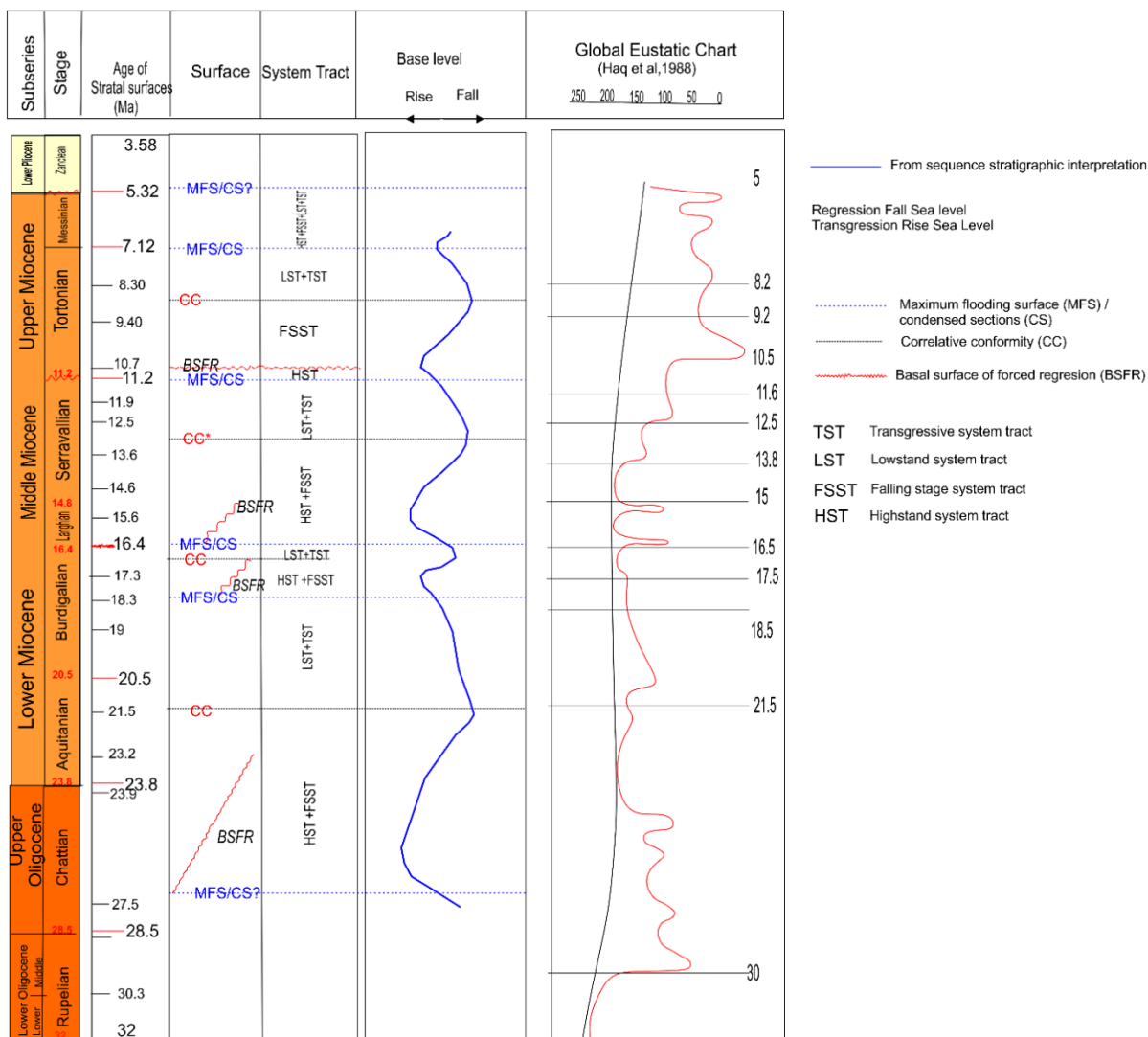


Figure 3.23 Relative sea-level curve proposed for the study area; this curve is compared with the global eustatic chart proposed by Haq et al. (1988). The relative sea-level curve matches the long-term trend of the global eustatic chart; however, differences are recorded as well, reflecting the local tectonics of the area.

	subseries	Stage Ma	Planktonic foraminifera (PF)	Biozones	Calcareous Nannoplankton (CN)	WELLS																
			Bolli and Saunders, 1985			M.P.Aubry, Berggren et al, 1995 Martini, 1971			A	B	C	D	E	F	G	H	I	J	K	L		
			PF						PF	CN	PF	PF	PF	PF	CN	PF	PF	CN	PF	PF	CN	PF
MIOCENE	UPPER	5.32																				
		MESSINIAN 7.12	Globorotalia humerosa	N 17	NN 12 5.60 D. quinquemurmus 5.90 NN 11																	
		TORTONIAN	Globorotalia acostaensis	N 16	D. quinquemurmus/berggrenii 6.0 NN 10 D. calcans 9.40																	
	MIDDLE	11.20	Globorotalia menardii	N 15	C. calliculus/D. hamatus 10.70 NN 9																	
			Globorotalia mayeri	N 14	C. coalitus 11.20 NN 8																	
			Globorotalia fohsi robus	N 13	D. kugleri 11.80 NN 7																	
			Gt. fohsi lobata	N 11	D. exilis 11.80 NN 6																	
			Gt. fohsi foehsi	N 10	S. heteromorphus 13.60 NN 5																	
		LANGHIAN	Praeorbulina glomerosa	N 9																		
	14.80																					
	16.40																					
		BURDIGALIAN	Globigerinatella insueta	N 7	NN 4 H. ampliapertura																	
		Catapsydrax stainforthi	N 6	NN 3 S. helemus 18.30																		
LOWER	20.52																					
UPPER	23.8																					
LOWER	28.5																					
33.7																						

TD Total depth

- - - Discontinuities - - - Not correlatable

Table 3.1 Stratigraphic discontinuities and non correlatable biozones throughout the study area for the Miocene and Oligocene units.

Chapter 4

Tectonic influence on the morphology and distribution of Miocene reservoirs, southern Gulf of Mexico

1. Introduction

In the southern Gulf of Mexico, deepwater sediments were affected during deposition by contractional and extensional deformation events and halokinesis. The Miocene reservoirs in this area were deposited in slope and basinal settings during the falling-stage systems tracts and the lowstand systems tracts, where channel and frontal splay depositional elements were the most important. The integration of the structural analysis with seismic data, seismic attributes and isochron maps allows us to evaluate how the deformational events (especially the contractional event D3) controlled the distribution of sediments and the external geometry of their deposits. This interplay between deformation and sedimentation occurred in two main ways. First, the structural elements modified the paleobathymetry of the basin and created accommodation space for clastic deposition. Second, the structural features controlled the entry of sediments. During the Oligocene and early Miocene, the depocenters were bounded by diapirs, salt sheets and structural highs formed by older salt anticlines; on the other hand, for the middle Miocene, the depocenters were controlled by the presence of folds in the southern part of the study area and by shortened diapirs and salt sheets in the periphery; the formation of these depocenters provided the accommodation space for sediment deposition; as a result, during the early and middle Miocene, the frontal splays were confined to these

depocenters. At the end of the middle Miocene, these depocenters were filled, and channel levee systems and frontal splay complexes predominated. Finally, during the late Miocene, the depocenters formation was controlled by the extensional event, which provided the accommodation space for sediment deposition in half-grabens, where frontal splays complexes and channel levee systems were the most important depositional elements. All of these structural elements had significant implications for the architecture and internal organization of the turbidite systems.

Turbidite plays are increasingly the focus of hydrocarbon exploration in deepwater basins and are prolific in terms of hydrocarbon production, particularly in the Gulf of Mexico, offshore Brazil and West Africa. However, turbidite plays present significant difficulties in terms of successful exploration and production. Sediment supply, tectonism and relative sea-level change are the three main controls on deep-water depositional systems. However, as sediments reach the shelf margin or beyond, the sediment delivery system and the configuration of the receiving basin become the controlling factors of submarine fan morphology and lithofacies distribution. In particular, salt tectonics plays an important role in many deep-marine settings (Alves et al., 2009; Brun and Fort, 2004; Fort et al., 2004; Isaksen, 2004; Rowan and Weimer 1998; Rowan et al., 1999, 2003; Yin and Groshong, 2007). For example, in passive continental margins, as in the northern Gulf of Mexico, deformation by salt diapirs and/or faults, forming complex continental slope topography, can control the sediment architecture and distribution; another example of the influence of salt tectonics is the formation of minibasins that capture large volumes of sediment and can hold important hydrocarbon accumulations; in the northern Gulf of Mexico, these structures have captured the attention of geoscientists not only for their prolific hydrocarbon nature but also for improving knowledge of sediment-salt dynamics and their driving processes

(Beaubouf and Friedmann, 2000; Prather et al., 1998; Rowan and Weimer 1998; Winker, 1996). In addition, the appreciation of the effects of seafloor deformation on submarine channel systems is important in terms of our understanding of reservoir potential and distribution. For all of these reasons, a better understanding of the various factors enables geoscientists to identify scenarios that predict the risk in reservoirs in deep-water environments.

The study area is one example of the hydrocarbon potential in Neogene rocks, with reservoirs found principally in the Miocene units where sedimentation was strongly controlled by tectonics.

The purpose of this work is to discuss the influence of the deformational events on sedimentation during the Miocene and to assess their influence on the distribution and geometry of the reservoirs.

We briefly describe the local tectonic framework and place it in a larger tectonic context to better understand the role of the deformational systems in sedimentation; then, we use structural and isochron maps to illustrate how the structural styles have influenced the sediment-transport systems and/or the formation of the depocenters. Finally, we discuss the implications of salt-sediment interactions for the stratigraphic architecture of the depositional elements.

2. Geological Setting

2.1 Regional Tectonic-sedimentary framework

The study area is located offshore in the southern portion of the Gulf of Mexico (Fig. 4.1) in a present-day continental platform setting, where water depths range from 0-100 m. This area belongs to the Province Cuencas del Sureste Marino, which is the most important Mexican petroleum province since the mid-seventies with the discovery of the Mesozoic onshore light oil

province (Chiapas-Tabasco) and the offshore province (Campeche Sound). Guzman and Marquez-Dominguez (2001).

The tectonic-sedimentary evolution of this area is related to the regional tectonic events of the Gulf of Mexico evolution (Buffler and Sawyer, 1985; Pindell,1985; Salvador, 1988 and 1991), including the subduction of the Farallon Plate under the North American Plate (Laramide Orogeny) (Pindell and Kennan,2002), the lateral movement of the Chortis Block and the subduction of the Cocos Plate against the southern end of the North American plate (Angeles-Aquino et al., 1994; Morán Zenteno et al., 2000; Padilla y Sánchez,2007), as well as local salt tectonic events (Angeles-Aquino et al., 1994; Cruz Mercado et al., 2011; Robles-Nolasco et al., 2004) (Fig. 4.2). The tectonic events previously mentioned define the Gulf of Mexico basin as a passive margin originating from a rift basin, which began opening in the Late Triassic followed by a marine flooding episode during the Middle Jurassic (Salvador, 1987). This event resulted in evaporation, salt precipitation and the deposition of a salt layer known as the mother autochthonous salt. This accumulation was controlled by pre-existing rift topography resulting in variable thickness across the basin. Following its deposition, the salt played a primary role in controlling structural styles, sediment deposition/trapping and hydrocarbon systems. In the northern Gulf of Mexico basin, most of the basement subsidence related to plate tectonics had ceased by the Paleogene period (Buffler, 1985); according to Cruz-Mercado et al. (2011) the subsidence related to salt tectonics in the southern Gulf of Mexico occurred until the Neogene, leaving a deep marine environment across much of the area. Much of the rapidly deposited Late Cenozoic fill occurred in an overall progradational pattern that was accommodated by this bathymetric deep. This pattern was complicated by local loading onto mobile salt, in some

locations forming salt-controlled sub-basins in which the subsidence was controlled by large diapir-related contemporaneous expansion faults or fault zones.

Regarding the stratigraphy in this area, the pre-rift and syn-rift deposits are inferred from the neighboring onshore areas. According to Angeles-Aquino, et al. (1994) and Escalera-Alcocer and Hernández-Romano (2009), the basement rock could be similar to those found in the Sierra de Chiapas (Chiapas Massif) and the Yucatan Block, which are composed of granitic and metamorphic rocks; the ages of these rocks range from late Silurian to Permian. The syn-rift deposits comprise red beds derived from basement rock erosion and volcanic rocks deposited in grabens during the Late Triassic and Early Jurassic (Buffler and Sawyer, 1985; Salvador, 1987). At the southern margin of the Gulf of Mexico, the continental syn-rift deposits are represented by the Todos Santos Formation, which crops out in the Sierra de Chiapas and eastern Oaxaca. Thicker salt deposits of Callovian age overlie these rocks. Salvador (1987 and 1991) mentioned that these deposits mark the end of the rift stage and are contemporaneous with the Louann Salt. Angeles-Aquino et al. (1994) suggested that the Callovian salt in Campeche Sound was mobilized during the Oligocene and that related deformation continued until the early Miocene. Overlying the autochthonous salt, drift-related deposits characterize a marine transgression that ranged from shallow to deep marine environments. Consequently, during the Oxfordian and Kimmeridgian, siliciclastic rocks were deposited along the littoral zones; carbonate rocks, on the ramps; thin beds of shale and carbonates, in open marine conditions. During the Tithonian, a maximum marine transgression occurred that triggered the deposition of the main source rocks (bituminous shales) in the whole area. From the late Jurassic until the late Cretaceous, carbonate rocks were deposited in outer ramp and basinal settings. During the Cenozoic, the sedimentation changed from carbonate to siliciclastic as a result of the Laramide Orogeny; during the

Paleocene, sea-level rise exceeded subsidence, and deep-water sediments began to backstep the carbonate slope (Angeles-Aquino et al., 1994). During the resultant Paleogene clastic sedimentation in the southern Gulf of Mexico, the Chiapas Massif still produced large volumes of sediment deposited in large depocenters, whereas in the Yucatan Block, the deposition of shallow-water carbonates continued (Padilla y Sánchez, 2007); in the study area, mass-transport complexes, debrites and turbidite deposits accumulated in lowerto mid-bathyal paleobathymetry. Angeles-Aquino et al. (1994) suggested that the salt movement combined with the decreasing sea level probably produced a regional unconformity that could be detected by the absence of some biozones in the middle and late Oligocene. The same sedimentary patterns continued until the early Miocene, but during the middle Miocene, the maximum deformation that folded and thrust up the rocks in the southern Gulf of Mexico occurred (Chiapanecan Orogeny, Sánchez-Montes de Oca,1980); this event resulted from the lateral movement of the Chortis Block and the subduction of the Cocos Plate beneath the North American plate, forming the Chiapas-Reforma-Akal belt over a decollement at the level of the Callovian salt (Angeles-Aquino et al., 1994; Padilla y Sánchez, 2007). At this time, the deposition of submarine fans and pelagic and hemipelagic sedimentation occurred. Following the middle Miocene contractional event, during the Pliocene-Pleistocene, a gravitational system developed due to extension propagated by the high rate of sedimentation related to great volumes of salt evacuation and increased tilting of the basement; as a result, extensional basins were formed (Padilla y Sánchez 2007; Robles Nolasco et al., 2004).

In the study area, the Miocene succession is mainly sand-prone and originates from deposition within submarine fan systems infilling local topography mainly in bathyal paleobathymetric

conditions. As a result, this stratigraphic unit is characterized by mass-transport deposits, debris flow deposits, turbidite deposits and pelagic and hemipelagic deposits.

2.2 Sequence stratigraphic framework

In previous studies, Gutierrez-Paredes et al. (2017a) provided the sequence stratigraphic framework for this area; they based their sequence analysis on the recognition of basal surfaces of forced regression (BSFR), correlative conformities (CC) and maximum flooding surfaces (MFS). The cycles of sedimentation were delineated by regionally extensive maximum flooding surfaces within condensed sections of hemipelagic mudstone. These condensed sections were the markers for regional correlation, and the maximum flooding surfaces, which they include, were the key surfaces (most reliable for regional correlation) for the construction of the Miocene stratigraphic framework. As a result, five genetic sequences were interpreted, with the MFSs as the sequence boundaries for each sequence (Fig. 4.3). Each cycle of sedimentation comprises the onset of relative sea-level fall, the end of relative sea-level fall and the end of transgressive events; the end of regression was not identified because the maximum regressive surface (MRS) is cryptic. Each sequence began with hemipelagic and pelagic sedimentation, which resulted in the development of condensed intervals into the maximum flooding surfaces in the continental slope and basin-floor portions of the basin, followed by the deposits related to the onset of relative sea-level fall, which are represented by debris flow deposits (mudflows and grain flows) and turbidite deposits (high to low density). At the end of the relative sea-level fall, the deposition of low-density turbidites prevailed; this change from high to low density implies a decrease in the volume of sediment delivered to deepwater settings as well as a decrease in the sand/mud ratio of the sediments involved in the flow. The falling stage system tracts are the most important and abundant system tracts in the Miocene sequences.

3. Data and methodology

We performed a detailed study of Miocene deepwater systems in an area measuring 40 x 40 km², located offshore in the southern Gulf of Mexico. The study used a time-migrated 3D seismic survey; these data were processed near zero phase and displayed using the SEG normal polarity.

To analyze the salt-sediment interaction, we used the sequence stratigraphic framework proposed for this area by Gutierrez-Paredes et al. (2017a); as a result, we interpreted and mapped five genetic sequences in the 3D seismic survey. Stratal terminations and abrupt major changes in seismic facies were used to correlate these sequences that were mapped as horizons using Schlumberger's Petrel software. Within these seismic units, seismic facies were described on the basis of reflection character (amplitude, continuity, geometry and external form) in cross-section and plan-view geometry on seismic attribute maps. The isochrons of the genetic sequences were integrated with TWT structure maps and cross-sectional geometry to determine structural style and evolution. The thickness variations on isochron maps were used as proxies for syndepositional subsidence and uplift variations around individual structures and/or variations in sediment accumulation. Horizon-based extractions from the RGB spectral decomposition volumes and RMS amplitude provided clarity for the depositional elements, particularly frontal splay complexes. An important part of the workflow for the interpretation of the depositional elements was the integration of map-view observations extracted from the seismic attributes with seismic reflection characteristics obtained from cross-sections.

4. Depositional elements and their seismic facies

Gutierrez Paredes et al.(2017b) defined the depositional elements that formed the Miocene deep-water depositional systems in the study area. These depositional elements have diagnostic seismic facies defined by external geometries and internal facies and in some cases, characteristic upper and lower surfaces. Furthermore, the analysis of the depositional elements integrated stratigraphic, geomorphologic and facies observations based on seismic, core and borehole data.

A summary of the main depositional elements and their seismic characteristics is shown in Figure 4.4. In the next paragraphs is provided a brief description of these depositional elements.

4.1 Mass-transport complexes (MTC)

Two types of MTCs are recognized in this area. The first type ranges in thickness from 440 to 540 m and comprises mainly extra-basinal carbonate platform deposits. The erosive nature of this MTC type is clearly observed in seismic profiles. Detailed correlation and mapping show that the base of the MTC is diachronous; the upper surface is mounded and irregular, which indicates the bathymetry after the time of erosion. On seismic data, this element is recognized by its variable amplitude, with low-amplitude internally chaotic and high-amplitude contorted seismic facies. In map view, it has a lobate shape that reflects the relative confinement of the basin. The irregular upper surfaces of the MTCs created local ponded accommodation space in depressions within which thin packets of heterolithic sediments infilled the residual topography. The second type of MTC is thinner in comparison with the previous one, and it has a variable thickness of up to 60 ms TWT. Its composition is quite variable and depends on the nature of the sediment that failed but often consists of muddy sediment. The base and the top of

these units are planar with little apparent erosion; and they pinch out laterally. In seismic cross-sections, this element is identified by discontinuous reflections of medium to low amplitude; externally, it is mounded, and internally, it has contoured and hummocky facies with small thrust faults and compressional structures. This deposit is overlain by two continuous parallel reflections of high amplitude that correspond to a condensed interval of pelagic deposits. On an RMS amplitude extraction map, a mottled appearance is observed. Fig.4.4a

4.2 Lobes of debrites and associated flows.

Lobes of this type have variable thickness but not more than 100 ms TWT; their composition can be quite variable and depends on the nature of the sediment that failed but often consists of heterolithic sediments that tend to contain the greatest portion of sand-grade sediment. In cross-sections, this type of lobe is frequently encased by two reflections of medium to high amplitude that pinch out laterally; these surfaces with steep edges can give the appearance of mounding (Fig.4.4b). In general, their basal surfaces in some cases are grooved, and in plan view, these grooves are long and linear. Internally, these lobes have chaotic and contorted facies and/or chaotic to reflection-free seismic facies; the latter case is interpreted as mud in debris-flow deposits (Posamentier and Kolla, 2003).

4.3 Submarine Channels

The channel types, on the basis of their observed plan-view and cross-sectional geometries are 1) erosional channels, 2) meandering channel belts and 3) leveed channel belts a combination of these types of channels may also occur (Fig. 4.4c). These channel systems are mainly developed on the slope; older channels are also developed at the base of the slope and on the basin floor. Erosional and sinuous aggradational channels are developed in confined

(intraslope) basins on the slope and in basin floor settings. On the other hand, when the paleotopography of the slope is less affected by topographic highs and lows, the channels tend to be shallower and exhibit distributary and meandering patterns, forming channel complexes and leveed channels.

In plan view, the features of the submarine channels in the study area reveal shapes that vary from straight and linear to slightly sinuous and from meandering (highly sinuous) to distributary. Meandering channel belts in map view images are typified by high sinuosity with regular and smoothly curved meander loops evidence bend cut-offs; these channels show high to moderate amplitude. The leveed channels on maps show low to moderate sinuosities and moderate to high amplitudes; erosional channels in planform are linear to slightly sinuous with moderate to low amplitudes.

In *seismic cross-sections*, meandering channels may appear as single reflections associated with lateral and downdip migration of the channel, forming lateral accretion packages (LAPs) on the inner side of the channel; however, these LAPs are not always recognized and instead appear as a single laterally extensive reflection of high amplitude. The features of leveed channels are as follows: stacked, discontinuous high-amplitude reflections (HARs) for channel fill; low-amplitude continuous reflections wedge-shaped away from the channel axis toward the levees; concave upward, planar and slightly erosional bases; channel fills with distinct lateral terminations (parallel and shingled); channel-fill terminations against the levees, and low-relief and high-relief channel levees. Leveed channels have lower sinuosities than meandering forms. Some constructional features such as gull-wing geometry are observed in seismic profiles (Fig.4.4c). Finally, the features of erosional channels are as follows: few or no associated overbank-levee deposits, although levees may occur in smaller channels belts; V- or S-shaped

features with erosional bases; aggradational fills (some of them show HARs); channel-fill sediments that onlap against the erosional surface; and discontinuous high amplitude reflections. Erosional channels can be truncated by younger channels, especially when they are stacked within channel complexes.

4.4 Frontal splays

In the study area, frontal splays were identified in confined settings in the middle and upper slope and in unconfined topographic settings on the upper slope. In confined settings, lateral contacts onlap or pinch out against salt bodies or structural highs, and downdip along the reflectors, they thin and lap out against a pre-existing depositional surface. In unconfined settings, frontal splays have downlap terminations of lateral contacts. This element is areally widespread in both confined and unconfined topographic settings; however, its areal extent depends on the paleotopography of the receiving basin.

The shape of frontal splays revealed from 3D seismic data varies; in intraslope basins, they are rounded or have a lobate form due to confinement, while in unconfined settings, distributary channel-pattern and elongate shapes are common. In plan view, the size of the frontal splays varies up to 4 km wide and 8 km long. In seismic profiles, this element is recognized by its medium- to high-amplitude reflections, mounded external appearance, continuous convex reflectors with bidirectional downlap, and planar bases; channelized and tabular geometries characterized by parallel continuous reflections that are concordant at the base are also observed. Fig. 4.4d.

Some frontal splays are also formed by small distributary channels. This type of frontal splays is characterized in seismic cross-section by parallel laterally continuous to slightly

discontinuous reflections of high amplitude, which are generally tabular and flat-topped. In map view, they have an elongated geometry and present a distributary channel pattern. Fig.4.4d.

5. Ages of the deformational events

The ages of the deformational events are named according to the classification proposed by Cruz-Mercado et al., 2011 and Peterson-Rodríguez et al., 2013. These events were recognized by analyzing the geological sections, thickness variation and the structural traps in the Cuencas del Sureste Province on the continental platform and in the basin. According to this interpretation, the structural styles and the ages assigned to the structures are defined, as well as the tectonic events related to these deformational events. The stages of deformation are named and described as D0, Middle Jurassic (not observed in the study area), related to the rift stage; D1, Late Jurassic to Late Cretaceous, associated with the Mesozoic gravitational event; D2, Paleogene (Eocene-Oligocene), related to the Paleogene contractional event; D3, Neogene (middle Miocene to late Miocene), related to the contractional tectonic event; and finally D4, Neogene (Pliocene-Pleistocene) related to the Neogene gravitational event (Fig. 4.5).

5.1 Deformational event D1 (Late Jurassic-Late Cretaceous)

The D1 deformational event is related to the opening of the Gulf of Mexico. Since the Kimmeridgian the basin was subject to a subsidence (to the NW) by the drift of the Yucatan Block towards the SE. From the Valanginian the basin became a passive margin establishing a gravitational tectonics, with a tilting basinward, and developing of the Mesozoic structures (Pindell and Kennan, 2002). At the regional scale, the salt movement occurred by a combination of sediment loading and extension; and in the study area, the movement of the autochthonous salt was mainly triggered by sediment loading. The main driver for the formation of the structures

formed during this stage was a down-building process, which was attributed to the thermal subsidence. The thickness analysis suggested the presence of structures with an irregular orientation and distribution; these are common features of saline structures. Examples of these structures include salt pillows, salt anticlines, and passive diapirs. In Fig. 4.6A a thickness variation in the Jurassic sequence is observed, which suggests the early evacuation of the autochthonous salt by sediment loading and the formation of a primary basin; salt anticlines or pillows and passive diapirs can also be observed.

5.2 Deformational event D2 Paleogene (Eocene-Oligocene)

This stage is characterized by contraction and halokinesis, it was also associated with the activity of the tectonic plates in the Pacific margin and it was younger than the Laramide event. The D2 event is considered the first stage of shortening of the structures formed during D1 and the first overlapping of deformational events (D1 and D2). The structures formed during this event are folded salt anticlines, shortened diapirs, salt sheets and contractional folds. These structures were formed by a combination of contraction and down-building processes during a thin-skinned tectonic detachment from the allochthonous salt. Some of the diapirs formed by down-building process changed to active diapirs by the contraction during the D2 event. The presence of welds and salt canopies evidenced the emplacement of allochthonous salt during the Eocene and Oligocene (Fig.4.6). This event is difficult to recognize since it is masked by the deformational event D3, which formed similar structures. In the seismic line of the Fig. 4.6A we also observed that the early Miocene sequence are post-kinematic to D2, with a thickness variation related to salt withdrawal and the collapse of a salt diapir and the formation of a small mini basin.

5.3 Deformational event D3 Neogene (middle Miocene-late Miocene)

This event comprises contraction related to the movement of the margin of the Pacific tectonic plates and Chortis block migration (Chiapanecan orogeny) and halokinesis. The structures formed at this stage were detachment folds, fault bend folds, fault propagation folds (outside of the study area), and allochthonous salt sheets. These structures were formed by a contractional system during a thin-skinned tectonic detachment from the allochthonous salt. The structures formed during this stage include shortened diapirs, welded diapirs, sheets and refolded of salt anticlines formed in previous events. Examples of them are shown in Fig. 4.6.

This event is considered the most important because it developed and deformed several structures in the continental platform; some of these structural traps hold important hydrocarbon accumulations.

5.4 Deformational event D4 Neogene (Pliocene-Pleistocene)

This extensional system was the last event identified in the structures of the continental platform. It was the result of gravitational tectonics, which was attributed to a high rate of sedimentation related to great volumes of salt evacuation and increased tilting of the basement. The structures formed by this event corresponded to normal faults and lateral faults. Some structures formed during the D1, D2 and D3 events were affected by the normal faulting during D4 (Fig. 4.6). Also, in Fig. 4.6B we observed a large anticline bounded by faults; this turtle structure was formed by the collapse of the collapse of the salt structures triggered by extensional forces.

6. Tectono-sedimentary development

The genetic sequences interpreted in the study area by Gutiérrez Paredes et al. (2017a) were mapped and used to describe the tectono-sedimentary units of the Miocene succession in this area. Based on attribute analysis of a series of intervals within these seismic units, major sediment transport pathways related to the deposition of frontal splays, channel-levee complexes and frontal splay complexes have been identified. In this section, we describe each genetic sequence, and then outline the relationships among structural evolution, sediment transport, and deposition.

6.1 Sequence middle Oligocene-lower Miocene (27.1-18.3 Ma)

The study area during the Oligocene and early Miocene was bounded towards the north by canopies, to the west and southeast by sheets and to the south by antiforms (Fig. 4.7). In the northern and central parts of the area, mass-transport complex was deposited in a large depocenter formed by a combination of contraction and halokinesis. According to the paleontological data, this sequence has duration of 8.8 million years, and it was deposited in a lower bathyal to middle bathyal paleobathymetric environments. The lower boundary of this sequence is diachronous and easily observed on seismic data as a high-amplitude reflection that has a regional extent. This sequence is distributed across most of the study area with its major thickness of 500 to 800 m in the central and northern parts, and it decreases towards the south, where it is very thin or absent on topographic highs (salt bodies and folds). Seismically, the MTC is easily recognized by its semi-discontinuous reflections of variable amplitude, with low-amplitude internally chaotic facies and high-amplitude contorted seismic facies (Fig. 4.4).

Moscardelli et al. (2006) mentioned that MTCs occur at any time during basin evolution, but are most commonly found in the early phases of basin fills, during the falling on sea-level when the sedimentation at the shelf edge is at its peak. In the study area, the deposition of this deposit was controlled by a combination of the relative sea-level fall (earliest portion) and tectonics (contractional event and the beginning of the emplacement of the allochthonous salt); both factors were probably responsible for the slope destabilization. The geometry of this type of deposit can vary extensively as well as the lithology, which often consists of muddy sediments showing a degree of deformation, dipping beds, and stratal blocks of varying sizes. However, the main control of the lithology of MTCs is the nature of the original sediment that failed (Moscardelli, 2007). In the study area, this deposit is a mixture of slumps, slides and debris flows. The composition of this MTD in the NE part of the area is constituted by extraformational clasts to cobble/boulder sized carbonate (mudstone-wackestone) clasts supported by a muddy matrix and fragments of corals and shells, these clasts probably came from the Mesozoic highs that were exposed by the relative sea-level fall and destabilized by the salt movement. Towards the south, the MTD is composed of heterolithic deposits (mudstone and siltstone).

The irregular upper surface of this MTC created a local accommodation with small depressions upon which thin packets of heterolithic sediments infilled the residual topography. These deposits comprise high-to low-density turbidites in channels and frontal splays. The alteration of seafloor topography by mass transport affected sediment pathways on the depocenter and probably the distribution of zones of erosion, bypass, and deposition from turbidity currents, the latter occurring within relative bathymetric lows or in association with negative gradient changes. Thus, the location, nature, and geometry of depositional systems

dominated by sediment gravity flow, in specific turbidite systems, may be profoundly affected by the presence of MTDs (Kneller et al., 2016).

6.2 Sequence “B” lower Miocene (18.3-16.4 Ma)

During the early Miocene, the study area was still bounded towards the north by canopies, to the west and southeast by sheets and to the south by antiforms. According to the paleontological data, this sequence has duration of 1.9 million years; the lower and upper boundaries are represented by seismic reflections of medium to high amplitude, low frequency and good lateral continuity that were correlated across the entire study area. In the southern part of the area, this surface onlaps a structural high, and it has overlying onlap and downlap terminations and underlying toplap terminations.

This sequence was deposited during a tectonic quiescence, and it was only affected by halokinesis. For example, the isochron map shows less variation in thickness, with the maximum thickness located in small depocenters formed by salt movement (Figs. 4.8 and 4.6). This sequence is distributed throughout the study area and is only absent in the eastern part due to the presence of normal faults. We observe in this sequence chaotic facies of high amplitude that correspond to a mass-transport deposit which distribution is only limited to the flank of a salt body; this MTD occurred in response to salt movement. Towards the south, there are mainly lobes of debrites composed by muddy sandstone; to the north, channels are composed by turbidites. These different types of deposits are contemporaneous, and they reflect the influence of the salt tectonics on sedimentation and sediment pathways; the entry of sediments mainly came from the southeast.

6.3 Sequence C Middle Miocene (16.4-11.2 Ma)

The study area is bounded to the north by shortened diapirs and to the east by a folded minibasin; towards the SE, there is a canopy, and to the SW, there is an antiform. According to the paleontological data, this sequence had duration of 5.2 million years. It is bounded by two seismic reflections of high amplitude, low frequency and good lateral continuity that we correlated throughout the study area. This sequence is distributed throughout the study area with variable thickness; the maximum thickness (800 m) is observed in the central and northern parts of the area where the main depocenter is located. Towards the south, the thickness varies from 300-400m (Fig. 4.9). During the middle Miocene, the formation of the depocenters was controlled by contraction and halokinesis. The thick layers of the middle Miocene are found in the center of the synclines, and the thin sequences that onlap the pre-kinematic sequences of the D3 event define the flanks of the anticlines formed during this event.

At this time, even though the shoreline was far from the shelf edge, the erosion triggered by exposure of the continental portion of the basin (as a result of the relative sea-level fall and the Chiapanecan orogeny) delivered large amounts of sediments to the basin; as a result, this sequence is mainly sand-prone. It comprises, from the base to the top, lobes of debrites (mudflows) distributed in the southern part of the area with variable thickness (from wells) ranging from 80 to 350 m. Seismically, they are recognized by continuous to discontinuous reflections of medium to low amplitude and high frequency with contorted and mounded configuration and onlap and downlap terminations; the lower limit can be grooved, and the shape is strongly controlled by subtle changes in the seafloor gradient and therefore by the basin morphology (Talling et al., 2012). Toward the central and northern part of the area, high density turbidites were deposited in frontal splays; in seismic profiles these depositional elements are

recognized by their medium to high amplitude, mounded external appearance, continuous convex reflectors with bidirectional downlap and planar bases. The shape of these deposits was controlled by the confinement of the basin (Fig.4.4d). Due to the confinement of the basin the main entry of sediments came from the SE. At the top of this sequence, meandering channels were deposited in the NW part (Fig. 4.4c) and frontal splays complexes in the NE part (Fig 4.4d). Seismically, the meandering channels appear as single reflections associated with lateral and downdip migration of the channel, forming lateral accretion packages (LAPs) on the inner side of the channel; however, these LAPs are not always recognized and instead may appear as a single laterally extensive reflection of high amplitude. On the contrary, frontal splay complexes in seismic cross-sections are characterized by parallel laterally continuous to slightly discontinuous reflections of high amplitude (Fig. 4.4d). The orientation of the meandering channels (SW-NE) suggested and entry of sediments from the south, this change in the sediment pathways also revealed that the basin was less confined at the top of the middle Miocene.

6.4. Sequence “D” upper Miocene (11.2-7.12 Ma).

During the late Miocene, the study area was bounded to the north and NE by shortened diapirs; to the west by a fault and to the east there were no structural elements bounding the sediments deposited at this time (Fig. 4.10). According to the paleontological data, this unit had duration of 4.08 million years.

This sequence is mainly sand-prone, and it is distributed throughout the study area with thickness varying from 100–1000 ms; this thickness variation reflects the paleotopography of the area at the time of deposition. The main depocenters are located in the southeast part of the area (Fig 4.10).

From the base to the top, this sequence includes lobes of debrites (hybrid deposits) distributed in the southern part of the area. Towards the central and northern parts, turbidites prevail and are deposited in leveed channels and frontal splays. Seismically, the lobes of debrites tend to be narrow and are encased by two continuous reflections of medium to high amplitude. The internal configuration of these deposits is chaotic or reflection free. On the other hand, leveed channel is represented by stacked discontinuous high-amplitude reflections for channel fills; low-amplitude continuous reflections wedge-shaped away from the channel axis toward the levees; other features such as gull-wing geometry are also observed in seismic profiles. Finally, frontal splay complexes are characterized by laterally continuous to slightly discontinuous reflections of high amplitude; in map view, they have an elongated geometry, and some present a distributary-channel pattern.

At this time the salt tectonics end, as a result, the basin was less confined and the direction of the sediment entry came from the south and southeast.

6.5. Sequence “E” upper Miocene (7.12-5.32 Ma)

This sequence is bounded to the north and NE by shortened diapirs; to the west by fault and to the east there are no structural highs bounding the sediments deposited at this time (Fig. 4.11). The Messinian sequence had duration of 1.8 million of years, and it is distributed throughout the study area with thickness varying from 100 to 600 ms. The depocenters shift to the south and their formation was controlled by normal faulting. This sequence is mainly mud-prone and comprises the following deposits: in the south, pelagic and hemipelagic sediments are distributed, and towards the north, channel-levee systems are found. This change not only implies a decrease in the sediment delivered to the basin but also a decrease in grain size and the

sand/mud ratio. This was probably related to the progradation of the shelf margin from the south to the north, and with the change to shallow-marine depositional settings.

Finally, during the early and middle Pliocene the D4 extensional event occurred, and the syncline formed during the middle Miocene was inverted, developing an anticline (turtle structure) (Fig. 4.6B). This turtle structure was formed due to the collapse by extension of the salt structures located at the east and west of the depocenter. This collapse triggered the migration of depocenters outside of the study area during the Pliocene-Pleistocene.

7. Discussion

7.1 Structural controls on deposition

In this section, we discuss the influence of structural features on sedimentation. Establishing the correct timing of this interaction was a key factor in predicting the depositional response to active deformation of the slope. Moreover, the interplay between sedimentation and tectonics was critical in controlling sediment trapping and spatial distribution, as well as the sediment pathways on the slope and the geometry of the deposits. In this study, we use the term ponding to indicate a situation in which sediment gravity flows fill the floor of an enclosed depression and are unable to surmount the bounding slopes (or ‘sills’) around the depositional area (‘mini-basin’, ‘silled subbasin’ or ‘ponded depocenter’). The term ‘confinement’ is used to describe situations where sediment gravity flows and their deposits are appreciably affected by the presence of significant basin floor topography but without the connotation of complete containment (Lomas and Joseph, 2004). The origin of the confining topography is tectonic: large-scale structural features such as anticlines or more subtle perturbations of basin-floor

gradients associated tilting and faulting. In other instances, basin-floor relief is the result of slope collapse masses and tectonics.

According to Gutierrez Paredes et al., 2017b in the study area tectonic activity influenced the paleobathymetric environments by creating paleobathymetric highs and lows that were related to salt structures, salt withdrawal, anticlines and normal faults. These abrupt bathymetric variations were more susceptible to syndepositional tectonics than sea-level changes; as a result, the slope paleotopography was constantly changing in association with sedimentation and deformation in this area. This influence is observed in the maps of Fig. 4.12., where for the early Miocene, the predominant paleobathymetry was middle bathyal, with the upper bathyal zone represented in areas with topographic highs and the lower bathyal zone represented in areas with topographic lows. For the middle Miocene, the prevalent paleobathymetry was upper bathyal, with areas of middle bathyal and lower bathyal zones in topographic lows.

The deposition of the mass-transport complex also affected the paleotopography during the early Miocene. This alteration influenced the sediment pathways on the slope and the distribution of zones of erosion, bypass, and deposition from turbidity currents, which occurred within relative bathymetric lows. These relative bathymetric lows on and around the MTD constituted local accommodation spaces in the sense that they formed available space within, in which sediments were deposited. Thus, the location, nature, and geometry of depositional elements dominated by turbidite systems were affected by the presence of the mass-transport complex deposited in sequence A.

On the other hand, for the middle Miocene (sequence “C”), the contraction and salt movement occurred during the deformational event D3; this event and the relative sea-level fall controlled the accommodation space, and the large volumes of sediments entry to the basin. As a result

turbidite deposits were accumulated in the depocenters with ponded and wedged external geometries due to the confinement of the basin. The sediment dispersal pattern was affected by pre-existing or developed basin-floor relief, so the turbidity currents were not free to spread radially. Based on isochron maps of more detailed subdivisions, we observed that depocenters were not simply stacked, instead these were shifted laterally; this effect is also observed in the well-log correlations where the frontal splays shifted laterally. The new lobe deposits occupied the lows created by the previous lobe deposits. This type of lobe sedimentation thus occurred by compensation. This control is also well expressed in the proximal part of lobe deposits, where sharp lateral changes are observed from onlap terminations to hemipelagic sedimentation. The channels were also affected by this confinement (the restriction of the course of a channel and its overbank deposits as a result of pre-existing structures). This confinement limited the channel's ability to migrate laterally and develop sinuous planform geometry, as well as it limited the thickness and the development of channel levee deposits since the available accommodation space was restricted by the enclosing structures. At the end of the middle Miocene, the confining structures were no longer active, and then the degree of confinement decreased as the deposits infilled the accommodation space. This change precipitated the development of channels in unconfined settings, which allowed the lateral migration of the channel and resulted in the growth of highly meandering channels in the western part of the area. At this time, in the SW part of the study area, the topographic highs (anticlines) obstructed the flow pathway, so the channels flowed around the structures; once the channel had been diverted around the structure, it could resume its original downslope course.

For the upper Miocene sequence, the accommodation space was controlled by the extensional event, which was also related to the formation of Comalcalco basin located to the south. At this

time, the channel development was unaffected by underlying deformation; as a result, leveed channel predominated.

8. Conclusions

The salt-withdrawal synclines played a key role in controlling both sediment trapping and spatial distribution. Particularly in the study area, large volumes of sediment gravity flows accumulated in the large depocenter located in the central and northern parts, assuming ponded and wedged external geometries. The depocenters were formed as result of the deformational systems that affected this area.

The sedimentation in the study area during the Miocene occurred on a topographically complex slope as a result of the interaction between deformational events (extension, contraction, and halokinesis) and sedimentation. These structures impacted the seafloor's morphology by creating bathymetric relief, and at the depocenter scale, the effect of overburden vertical movement due to salt withdrawal, salt diapirism, folding, and faulting created accommodation space for the deposition of clastics during the Miocene. The resulting paleotopography also affected the sediment pathways and controlled the external geometry of the deposits by promoting the confinement of the deposits.

Acknowledgements

This research was completed as part of the doctoral project carried out by the first author fully sponsored by PEMEX- Exploración y Producción and other funds for the Fondo Sectorial Conacyt-Sener-Pemex

References

Alves, T. M., Cartwright, J., and Davies, R. J., 2009. Faulting of salt-withdrawal basins during early halokinesis: effects on the Paleogene Rio Doce Canyon system (Espírito Santo Basin, Brazil). *AAPG Bulletin*, 93, 617–652.

Ángeles-Aquino, F., Reyes-Núñez, Quesada- Muñeton and Meneses Rocha, J.J., 1994. Tectonic Evolution, Structural Styles and Oil habitat in Campeche sound, Mexico: *Gulf Coast Association of Geological Societies Transactions*. V 44, pp 53-62.

Beaubouf, R.T., and Friedman, S.J., 2000. High resolution seismic/sequence stratigraphic framework for the evolution of Pleistocene intraslope basins, western Gulf of Mexico: depositional models and reservoir analogs. In P. Weimer, R.M., Slatt, J.L. Coleman, N. Rosen, C.H., Nelson, A.H., Bouma, M., Styzen, and D.T Lawrence, (Eds.), *Global deep-water reservoirs: Gulf Coast Section-SEPM Foundation 20th Annual Bob. F. Research Conference*, 40-60.

Brun, J.P., and Fort, X., 2004. Compressional salt tectonics (Angolan margin). *Tectonophysics*, 382, 129–150.

Bursik, M.I., and Woods, A.W., 2000. The effects of topography on sedimentation from particle laden turbulent density currents. *Journal of Sedimentary Research* 70, 53–63.

Buffler, R.T., and Sawyer D.S., 1985. Distribution of crust and early history Gulf of Mexico Basin. *Gulf Coast Association of Geological Societies Transactions*.35.333-344.

Cruz-Mercado, M.A., Flores-Zamora, J. C., Leon-Ramírez R., López-Céspedes, H. G., Peterson-Rodríguez, R. H., Reyes-Tovar E, Sánchez-Rivera, R. et al..., 2011. Salt Provinces in the Mexican Portion of the Gulf of Mexico Structural Characterization and Evolutionary Model: *Gulf Coast Association of Geological Societies Transactions*, v.61, p.93-103.

Gee, M.J.R., and Gawthorpe, R.L., 2006. Submarine channels controlled by salt tectonics: examples from 3D seismic data offshore Angola. *Marine and Petroleum Geology* 23, 443–458.

Escalera-Alcocer, A., and Hernández-Romano, U., 2009. Provincias Petroleras de México. WEC México. Schulmberger.

Fillon, R.H., 2007. Biostratigraphy and Condensed Sections in Deepwater Settings in Weimer, P. and Slatt, R. Introduction to the Petroleum Geology of Deepwater Settings. AAPG Studies in Geology 57 AAPG/Datapages Discovery Series 8

Fort, X., Brun, J.P., and Chauvel, F., 2004. Salt tectonics on the Angolan margin, synsedimentary deformation processes. *AAPG Bulletin*, 88, 1523–1544.

Gee, M.J.R., and Gawthorpe, R.L., 2006. Submarine Channels controlled by salt tectonics: examples from 3D seismic data offshore Angola. *Marine and Petroleum Geology*, 23, 443-458.

Gutierrez-Paredes H.C., Catuneanu O., and Hernández-Romano U., 2017a. Sequence stratigraphy of the Miocene section, Southern Gulf of Mexico. *Marine and Petroleum Geology*, 86, 711-732

Gutierrez-Paredes H.C., Catuneanu O., and Hernández-Romano, U., 2017b. Miocene depositional environments, processes, and depositional elements in the southern Gulf of Mexico. *Geological Journal*.2017;1-30. <https://doi.org/10.1002/gj.2948>

Guzmán, A.E., and Marquez-Dominguez, B., 2001. The Gulf of Mexico Basin South of the Border: The Petroleum Province of the Twenty-First Century, in M. W. Downey, J. C. Threet and W. A. Morgan, editors, American Association of Petroleum Geologists, Tulsa.

Isaksen, G. H., 2004. Central North Sea hydrocarbon systems: generation, migration, entrapment, and thermal degradation of oil and gas. *AAPG Bulletin*, 88, 1545–1572, <http://dx.doi.org/10.1306/06300403048>.

Joseph, P. and Lomas, S.A. 2004. Deep-water sedimentation in the Alpine Basin of SE France. *Geological Society Special Publication*. No.22. VIII. 448pp.

Kneller B., Dykstra, M., Fairweather L., and Milana, J. P. 2016. Mass-transport and slope accommodation: Implications for turbidite sandstone reservoirs.

Morán-Zenteno, D. J., Martiny, B., Tolson, G., Solís Pichardo, G., Alba Aldave, L., Hernández-Bernal, M. del S., Macías Romo, C., Martínez Serrano, R.G... Silva Romo, G., 2000. Geocronología y características geoquímicas de las rocas magmáticas terciarias de la Sierra Madre del Sur: Boletín de la Sociedad Geológica Mexicana, T. LIII, No. 1, p. 27-58.

Moscardelli, L., Wood, L., and P, Mann ., 2006. Mass transport complexes and associated processes in the offshore area of Trinidad and Venezuela. American Association of Petroleum Geologists Bulletin, 90, (7), 1059-1088.

Moscardelli. L., and Wood, L., 2007. New classification system for mass transport complexes in offshore Trinidad. Basin Research 20(1), 73-98.

Oluboyo, A.P., Gawthorpe, R.L., Bakke K., and Hadler-Jacobsen F., 2014. Salt tectonics controls on deep-water turbidite depositional systems: Miocene, southwester Lower Congo Basin, offshore Angola. Basin Research, 26,597-620.

Padilla y Sánchez, R.S., 2007. Evolución geológica del sureste de mexicano desde el Mesozoico al presente en el contexto regional del Golfo de México. Boletín de la Sociedad Geológica Mexicana. Tomo LIX, núm. 1. 19-42.

Peterson-Rodríguez R.H., Hernández-Peñaloza J., Heyn T., Jiménez-Guerrero M., Ibañez-Garduño D.,Garza-Goicochea C.E Rojas-Rosas, R., 2013. Modelo de evolución estructural para entender el desarrollo de las trampas estructurales de HC's en la zona costa afuera de la porción occidental de la Sonda de Campeche, México. Congreso Mexicano del Petróleo Riviera Maya, 5-8 de Junio 2013., Cancún México.

Pindell, J.L., 1985. Alleghenian reconstruction and subsequent evolution of the Gulf of Mexico, Bahamas and Proto-Caribbean. *Tectonics*, 4, 1-39.

Pindell, J.L., and Kennan, L., 2002. Análisis Paleogeográfico Mesozoico-Cenozoico y Dinámica de las cuencas en el Golfo de México Profundo y Márgenes. Informe Final. Tectonic Analysis Inc. and Pemex Exploration and Production. Inédito.

Posamentier, H.W., and Kolla V., 2003. Seismic geomorphology and stratigraphy of depositional elements in deep-water settings. *Journal of Sedimentary Research*, 73,367-388.

Prather, B.I, Booth J.R Steffens, G. S., and Craig, P.A., 1998. Classification, lithologic calibration, and stratigraphic succession of seismic facies of intraslope basins, deepwater Gulf of Mexico, AAPG, Bulletin.82 (Ja) 701-728.

Robles-Nolasco, J., Pliego-Vidal, E., Toledo-Bante, C., Pimienta-Lugo, M., Ortega-González, V., Martínez-Peña, B., et al., 2004. Offshore Neogene plays, Salina del Itsmo Basin, southeast of Mexico: Tulsa, Oklahoma, E.U.A., American Association of Petroleum Geologists, International Conference, October 24-27, Cancun, Mexico, 5p.

Rowan M.G., and Weimer P., 1998. Salt-Sediment Interaction, Northern Green Canyon and Ewing Bank (Offshore Louisiana) Northern Gulf of Mexico. AAPG Bulletin, V.82 N05B (May 1998 Part B) p1055-1082.

Rowan, M. G., Jackson, M. P. A., and Trudgill, B. D., 1999. Salt-related fault families and fault welds in the northern Gulf of Mexico. AAPG Bulletin, 83, 1454–1484.

Rowan, M. G., Lawton, T. F., Gilles, K. A., and Ratliff, R. A., 2003. Near-salt deformation in La Popa Basin, Mexico, and the northern Gulf of Mexico: a general model for passive diapirism AAPG Bulletin, 87, 733–756, <http://dx.doi.org/10.1306/01150302012>

Salvador, A., 1987. Late Triassic- Jurassic Paleogeography and Origin of Gulf of Mexico. AAPG Bulletin, 71, 419-451.

Salvador, A., 1991. Triassic-Jurassic in Salvador, A. (Eds.). The Gulf of Mexico Basin: Geological Society of America, The Geology of North America, v.J., 131-180

Sánchez-Montes de Oca, R., 1980. Geología petrolera de la Sierra de Chiapas: Boletín. Asociación Mexicana. Geólogos. Petroleros, 31, Nos. 1-2, 67-77.

Talling, P. J., Masson, D. G., Sumner, E. J., and Malgesini, G., 2012. Subaqueous sediment density flows: Depositional processes and deposit types. Sedimentology, 59(7), 1937-2003.

Villamil, T., Arango, C., Weimer, P., Waterman, A., Rowan, M. G., Varnai, P.,...Crews, J.R., 1998. Biostratigraphic techniques for analyzing benthic biofacies, stratigraphic condensation, and key surface identification, Pliocene and Pleistocene sediments, Northern Green Canyon and Ewing Bank (offshore Louisiana), northern Gulf of Mexico. AAPG Bulletin, 82,961-985.

Winker, C. D., 1996. High-resolution seismic stratigraphy of a late Pleistocene submarine fan ponded by salt-withdrawal minibasins on the Gulf of Mexico continental slope: Offshore Technology Conference Program with Abstracts, p. 619–628.

Yin, H., and Groshong, Jr. R. H., 2007. A three-dimensional kinematic model for the deformation above an active diapir. AAPG Bulletin, 91, 343–366.

Figures

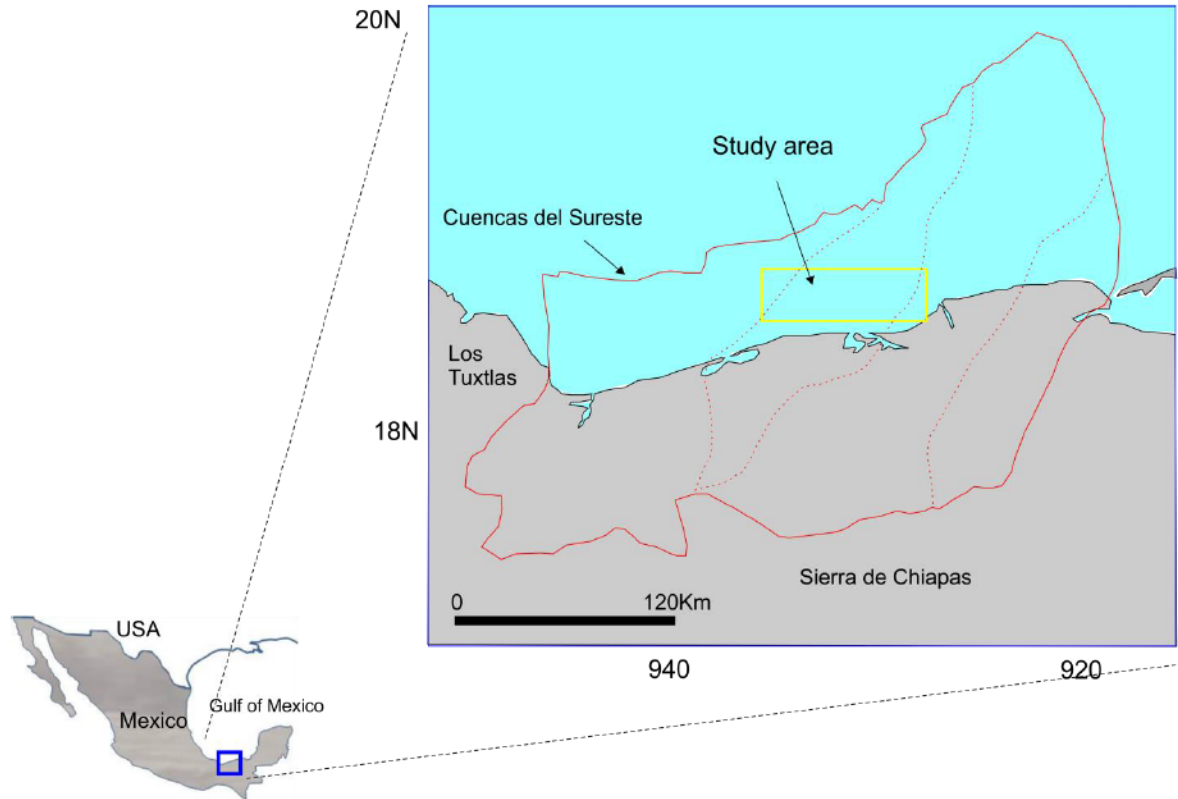


Figure 4.1. Location map for the study area in the southern Gulf of Mexico.

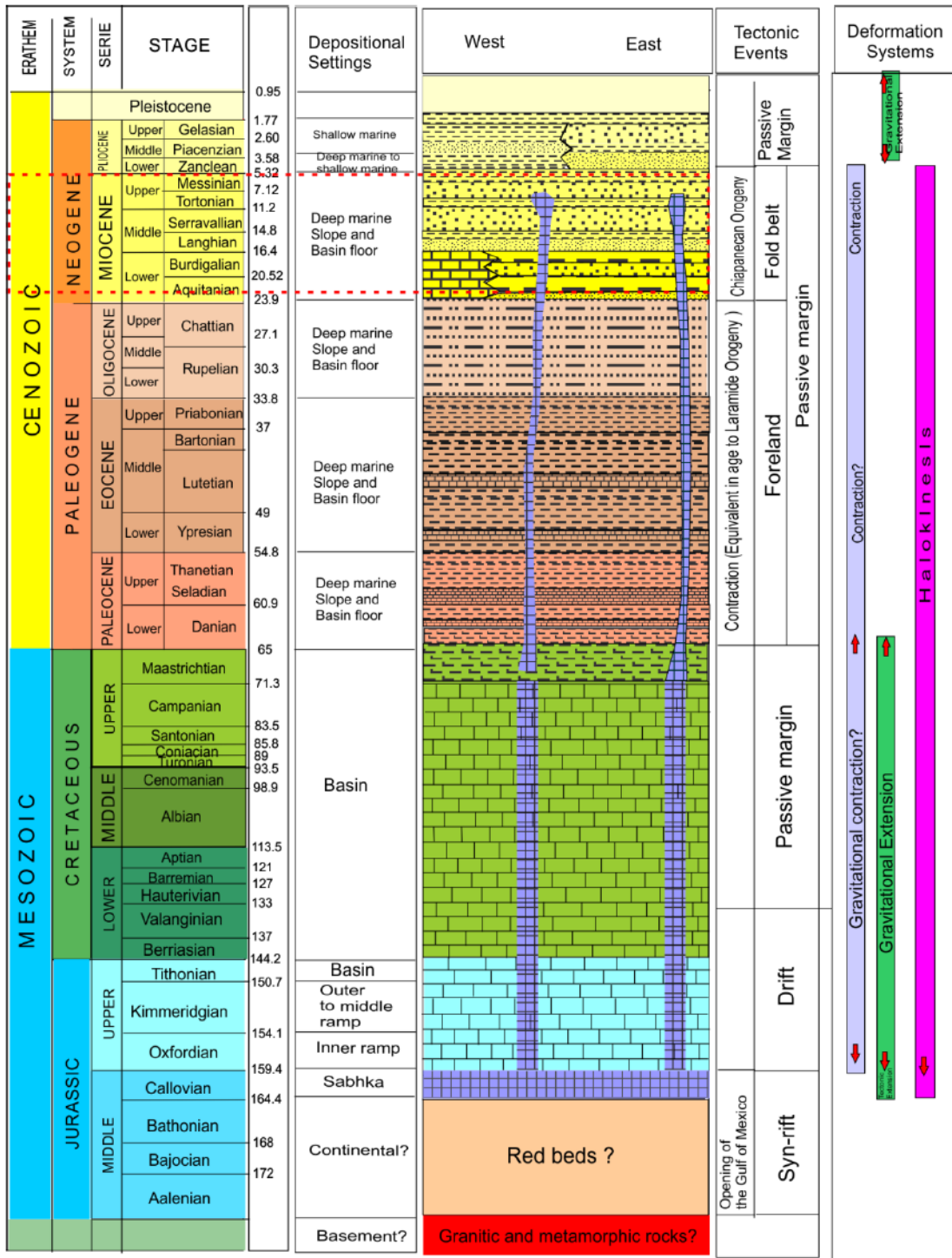


Figure 4.2. Stratigraphic chart of the study area showing the tectonic and deformation systems that affected the sequences in the study area (modified from Gutiérrez Paredes et al., 2017 b).

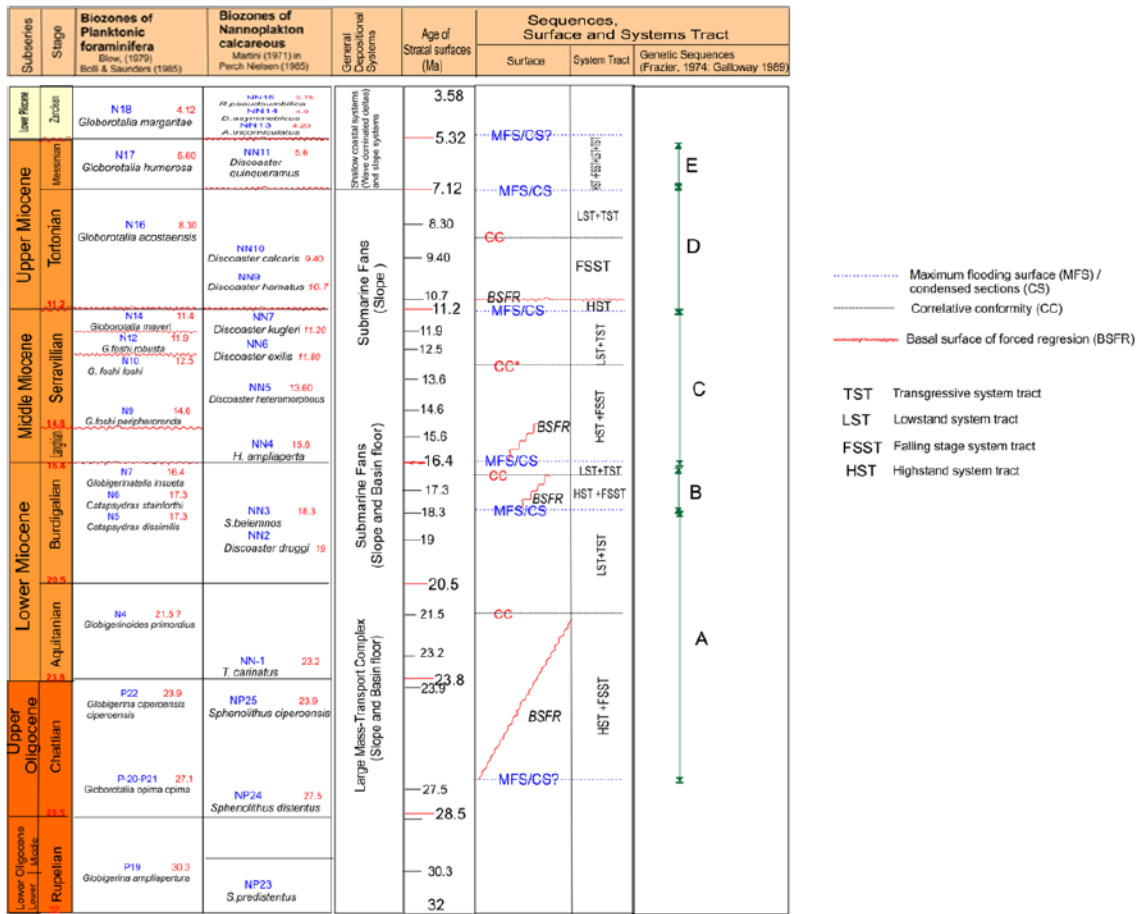


Figure 4.3 Miocene sequence stratigraphic framework for the study area (Gutiérrez Paredes et al., 2017a). The basal surface of forced regression (BSFR) according to the paleontological data is dated from the middle Oligocene to lower Miocene.

Depositional Element	Reflection character and Geometry	Seismic	Attribute map
a) Mass-Transport complexes	<ul style="list-style-type: none"> Chaotic, disorganized and contorted seismic facies Variable amplitude (low to medium) Discontinuous, semitransparent reflections Erosive basal shear surface with irregular upper surface Internally deformed mounded facies 		
b) Lobes of debris and associated flows	<ul style="list-style-type: none"> Medium to low amplitude Lateral pinch out Mounded externally Internally mounded and discontinuous In map view straight and narrow 		
c) Submarine Channels	<p>1) Meandering Channels</p> <ul style="list-style-type: none"> Erosional bases Channel fill has distinct lateral terminations V or U-shaped features High-sinuosity and smoothly curved meander loops. Vertical and lateral stacked Discontinuous high amplitude reflectors <p>2) Leveed channels</p> <ul style="list-style-type: none"> Concave upward and planar slight erosional base Channel fill terminations (parallel and shingled) Gully-wing geometry Vertical and lateral stacked Discontinuous high amplitude reflectors (HARs) in channel fill Low amplitude continuous reflectors for the levees 	 	
d) Frontal-Splays	<p>1) Frontal splay</p> <ul style="list-style-type: none"> High to medium amplitude reflections Mounded externally appearance Continuous convex-up reflectors with bidirectional downlap <p>2) Frontal Splay complex</p> <ul style="list-style-type: none"> High amplitude reflections Parallel/continuous reflectors Tabular and flat topped Elongated shaped geometry or distributary in plan-view 	 	

Figure 4.4 Depositional elements identified during the Miocene in the study area (modified from Gutierrez Paredes et al., 2017b).

STAGE	SYSTEMS AND AGES OF THE DEFORMATIONAL EVENTS IN THE STUDY AREA (Southern Marine Basins Province)				
	Deformational Events	Structural styles systems			Structures
		Contractional	Extensional	Salt Tectonics	
Holocene	D4 Extension/ gravitational		Gravitational		Normal faulting Extensional turtle Collapse of the shortened salt anticline Redeformation of the structures formed during D1, D2 and D3
Pleistocene					
Late Pliocene					
Middle Pliocene					
Early Pliocene					
Late Miocene	D3 Contraction / Halokinesis	Tectonic		Allocthonous and Contractional Salt systems	Folds, re-folded salt anticlines and diapirs Redeformation of the structures formed during D1 and D2
Middle Miocene					
Early Miocene					
Oligocene	D2 Contraction / Halokinesis	Tectonic		Allocthonous and Contractional Salt systems	Folds, shortened salt anticlines canopies, active diapirs, shortened diapirs Inverted structures Redeformation of the structures formed during D1
Eocene					
Paleocene					
Cretaceous	D1 Contraction/ Extension / Halokinesis	Gravitational ?	Gravitational	Halokinesis and Allocthonous Salt systems	Normal Faulting salt anticlines or salt pillows downbuilding diapirs
Late Jurassic					

Figure 4.5 this figure shows the systems and the ages of the deformational events and structures formed in the study area. (Modified from Cruz Mercado et al., 2011 and Peterson-Rodríguez et al., 2013).

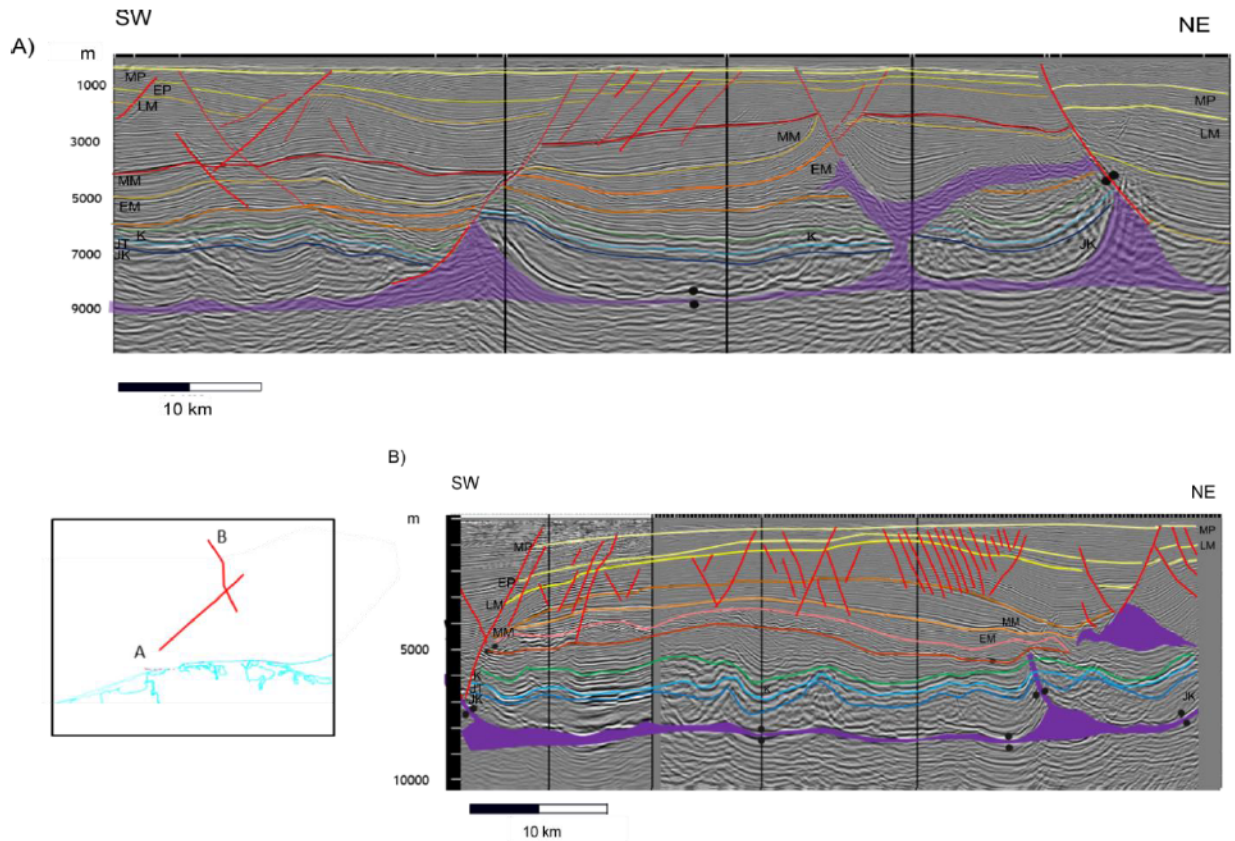


Figure 4.6 A) This section shows differences in the thickness of the Jurassic sequences suggesting and early evacuation of the autochthonous salt; as well as salt pillows or anticlines formed during D1, and canopies formed during D2. These salt structures were deformed in the deformational events D3 and D4 . The early Miocene sequences are post-kinematic to the D2 deformational event and some changes in thickness due to down-building and collapsed diapirs are also observed; on the contrary, the middle Miocene sequences are syn-kinematic to D3. B) This seismic line shows a primary basin formed during the Mesozoic by salt withdrawal. Also show salt structures formed during D1, and deformed during D2, D3 and D4 events; the last one formed a turtle structure in the Neogene sequences. Toward the south are observed salt anticlines and small depocenters formed by salt collapse as a result of the D4 extensional event. EP=early Pliocene; MP=middle Pliocene; LM = late Miocene; MM= middle Miocene; EM=early Miocene; K=Cretaceous; JT= Jurassic Tithonian; JK =Jurassic Kimmeridgian.

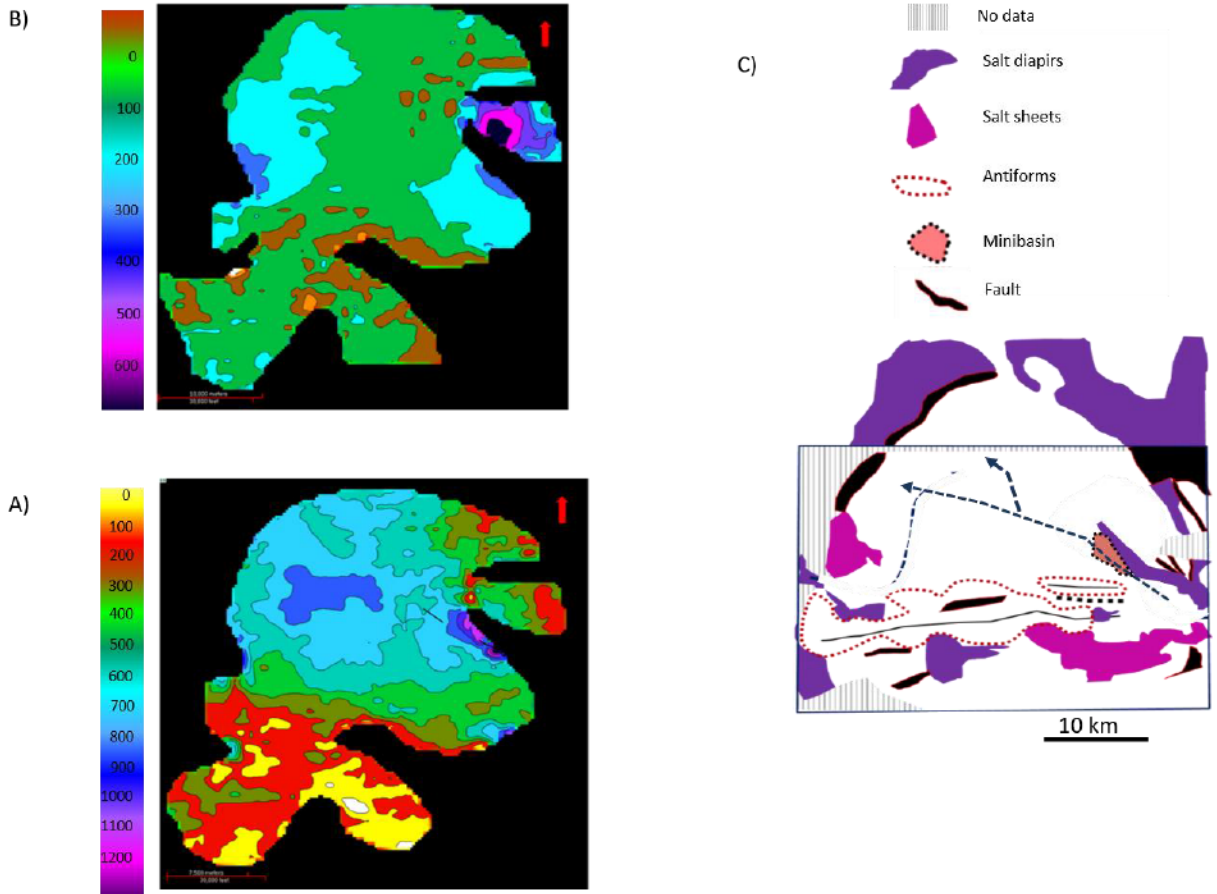


Figure 4.7 For the Oligocene-early Miocene sequence two isochron maps were done to illustrate the influence of the MTD in the paleotopography of the basin. A) This isochron map was calculated from the base to the top of the MTD, and exhibited the main depocenters located in the central and northwest parts; where large thicknesses are accumulated. Towards the south the thickness of the MTD is thin or absent due to the presence of structural highs and salt bodies. B) This map corresponds to sequence A and now the large thickness are accumulated in the depocenters formed at the end of the deposition of the MTD. C) The structural map shows that the distribution of the sediments (MTD and turbidites) occurred in a confined setting due to the structural elements present at this time; the dotted blue line represents the sediment pathways. The blue rectangle in the structural map represents the area of the isochrone maps.

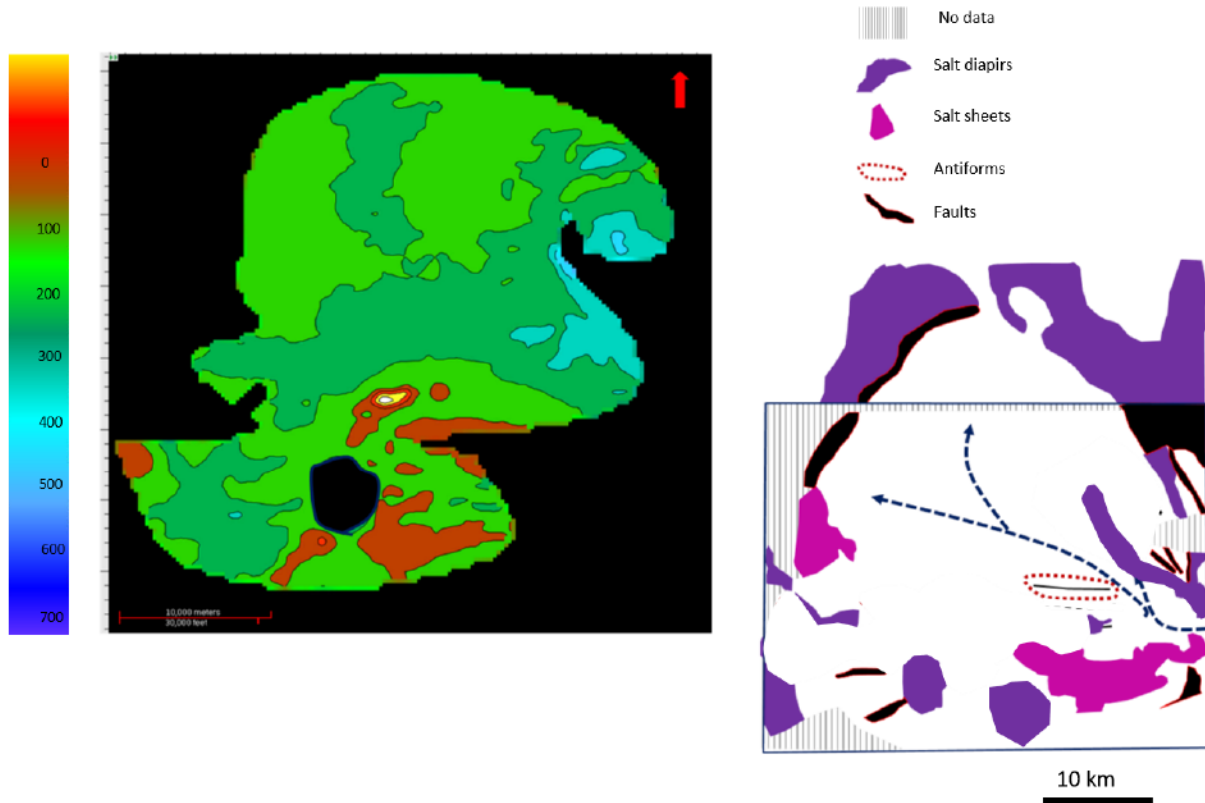


Figure 4.8 Isochron map for the early Miocene sequence shows less variability in the thickness in the central and northern part, whereas in the southeast the thin thicknesses are related to the presence of a structural high and salt bodies. The structural map showed that the confinement of the basin continues due to the structural elements present at this time. The blue dotted lines represent the sediment pathways. The blue rectangle in the structural map represents the area of the isochron map.

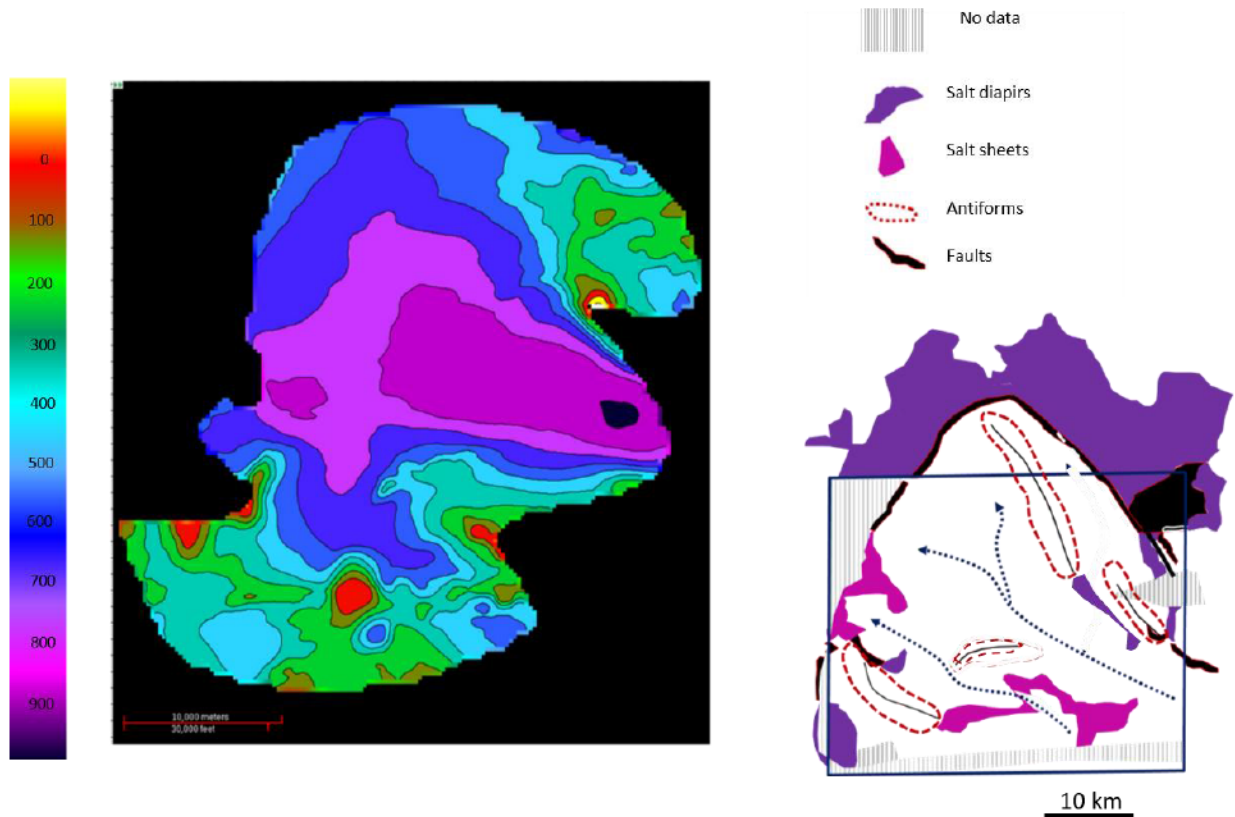


Figure 4.9 Isochron map for the middle Miocene sequence exhibits the main depocenter located in the central and northern parts where a large thickness is accumulated; whereas the areas with thin thicknesses are related to structural highs (in southern and western parts). The structural map showed that the distribution of the sediments occurred in a confined setting due to the structural elements present at this time. The blue dotted lines represent the sediment pathways. The blue rectangle in the structural map represents the area of the isochron map.

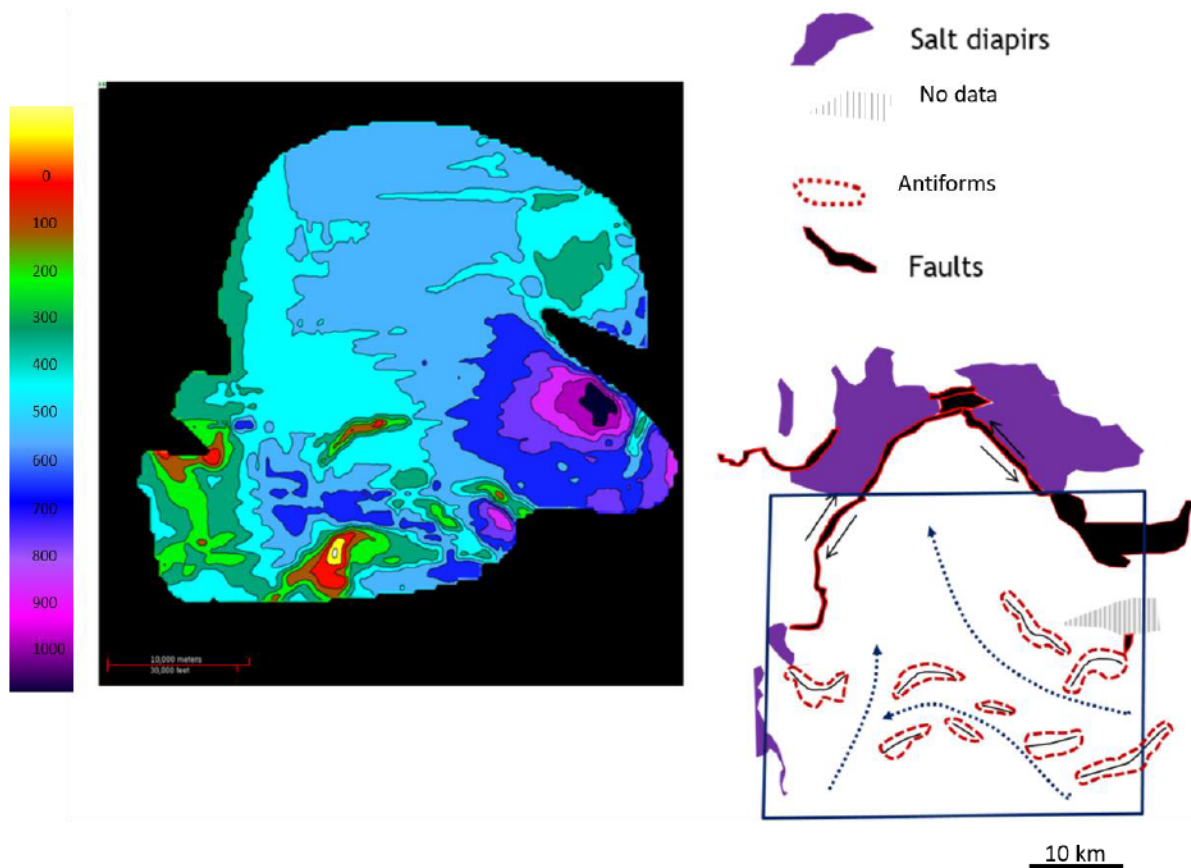


Figure 4.10 Isochron map for base of the late Miocene sequence illustrates that the main depocenters are in the eastern and southern parts with the development of small depocenters where large thicknesses are accumulated; whereas the areas with thin thicknesses correspond to the structural highs. The structural map showed small antiformal structures located in the southern and eastern parts, and faults towards the north. The blue dotted lines represent the sediment pathways. The blue rectangle in the structural map represents the area of the isochron map.

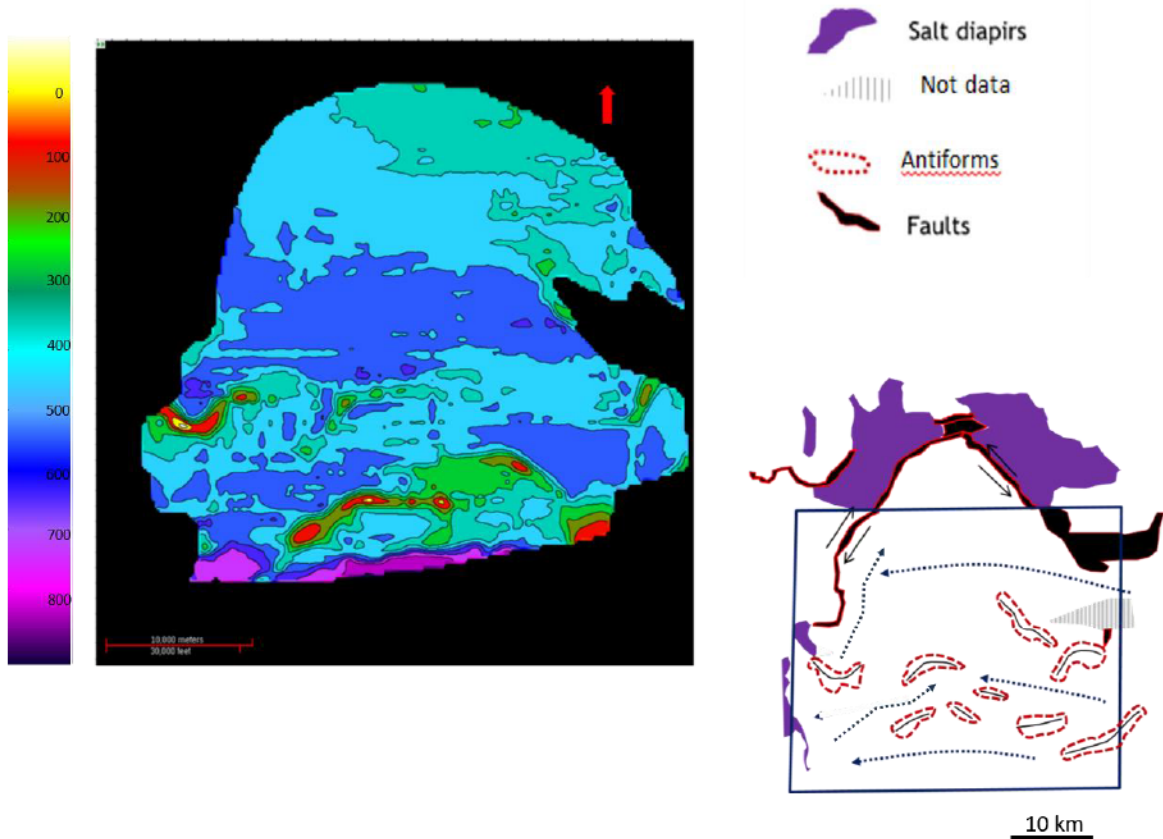


Figure 4.11 Isochron map for the upper part of the late Miocene sequence; the depocenters were located throughout the study area, and this condition reflects the non-confinement of the basin at this time. The structural map shows that in the study area there were no more salt structures. The blue dotted lines represent the main depocenters. The blue rectangle in the structural map represents the area of the isochron map.

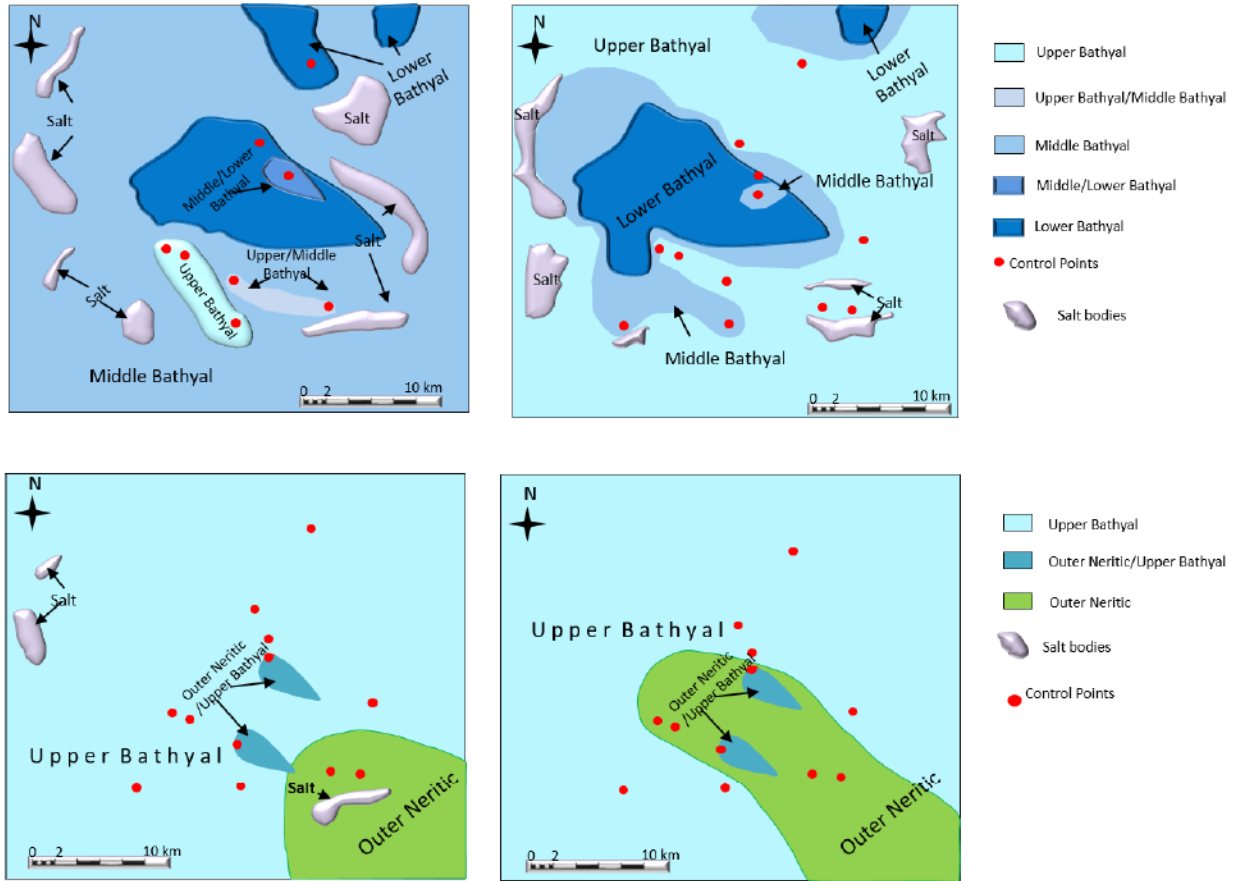


Figure 4.12. Paleobathymetric maps show a general shallowing of the water that reflects the progradation of the continental margin. These maps also show shifts in the paleoenvironments that reveal the strong control of the tectonics and sedimentation on the paleobathymetry (Gutierrez-Paredes et al., 2017b).

Chapter 5

Controls on the quality of Miocene reservoirs, southern Gulf of Mexico

1. Introduction

An investigation was conducted to determine the main controls on the reservoir quality of the middle and upper Miocene sandstones in the southern Gulf of Mexico based on core descriptions, thin section petrography and petrophysical data; as well as to explore the possible link between the sequence stratigraphic framework, depositional facies and diagenetic alterations. The Miocene deepmarine sandstones are attributed to the falling-stage, lowstand, and transgressive systems tracts. The middle Miocene falling-stage systems tract includes medium- to very fine-grained, structureless sandstones deposited in channels and frontal splays, and muddy sandstones, deposited in lobes of debrites. The lowstand and transgressive systems tracts consist of medium- to very fine-grained massive and normally graded sandstones deposited in channel systems within frontal splay complexes. The upper Miocene falling-stage systems tract includes medium- to coarse-grained, structureless sandstones deposited in channel systems and frontal splays, as well as lobes of debrites formed by grain flows and hybrid-flow deposits. The lowstand and transgressive systems tracts include fine-grained sandstones deposited in overbank deposits. The results reveal that the depositional elements with the best reservoir quality are the frontal splays deposited during the falling-stage system tracts. The reservoir quality of the Miocene sandstones was controlled by a combination of depositional facies, sand composition and diagenetic factors (mainly compaction and

calcite cementation). Sandstone texture controlled primarily by depositional facies appears more important than sandstone composition in determining reservoir quality; and compaction was more important than cementation in porosity destruction. Compaction was stopped when complete calcite cementation occurred.

In the southern Gulf of Mexico, Miocene sandstone reservoirs are important economic targets since several petroleum discoveries have occurred in deposits of this age. Reservoir quality is one of the key controls on prospectivity during petroleum exploration and one of the critical uncertainties to consider in frontier areas. For that reason, it is important to establish what controls reservoir quality in these deposits, in order to evaluate the economic viability of future petroleum discoveries in this area. Furthermore, evaluations of sandstone reservoir quality should consider porosity and permeability, as well as the factors controlling heterogeneities in sandstone reservoirs, including the depositional facies, diagenetic alterations and detrital compositions. The sequence stratigraphic framework governs to some extent the spatial and temporal distribution of depositional facies (Catuneanu, 2002, 2003; Posamentier and Allen, 1999; Van Wagoner et al., 1990). Moreover, the depositional facies control the sand body architecture and the primary porosity and permeability of sandstones (Morad et al., 2000). Diagenetic alterations reduce the porosity and permeability of sandstones by compaction and cementation or they preserve or increase the porosity and permeability by dissolution (Gier et al., 2008; Luo et al., 2009; Salem et al., 2005). Finally, the detrital composition of sandstone, which is influenced by factors such as provenance, paleoclimate and tectonics (De Ros et al., 1994; Morad et al., 2010; Ramm, 2000), exerts an influence on reservoir quality by controlling the differential compaction of framework grains and causing the cementation and dissolution of sandstones via interactions between pore water and framework grains during progressive burial

(Nentwich and Yale, 1997; Poursoltani and Gibling, 2011; Reed et al., 2005). In some cases, the sandstone reservoir quality can be also modified by fluid flow that is related to structures (Khalifa and Morad, 2012).

Despite its importance, the impact of diagenetic modifications on the Miocene reservoirs in the study area has been sparsely studied. Therefore, the aims of this paper are to determine the controls of the depositional facies on Miocene sandstone reservoir quality within the sequence stratigraphic framework, and to identify the most important diagenetic events influencing the porosity and permeability of these reservoir rocks and their quality and heterogeneity. Furthermore, linking the types and distributions of diagenetic processes to the depositional facies and sequence stratigraphic framework of these clastic successions could help to predict the diagenetic alterations controlling the quality and heterogeneity of the Neogene reservoir rocks in adjacent areas.

2. Geological Setting

The study area is located offshore in the southern portion of the Gulf of Mexico (Fig. 5.1.) in a present-day continental platform setting, where the water depth ranges from 0-100 m. According to Guzman and Marquez-Dominguez (2001), this area belongs to the Province Cuencas del Sureste, which has been the most important Mexican petroleum province since the mid-1970s following the discovery of the Mesozoic onshore light oil province (Chiapas-Tabasco) and the offshore province (Campeche Sound). The Cenozoic basins in the onshore region of this area have been producing light oil and gas since the early 1900's (Escalera-Alcocer and Hernández-Romano, 2009).

2.1 Tectonic framework

The tectonic-sedimentary evolution of this area is related to the regional tectonic events that occurred during the evolution of the Gulf of Mexico (Buffler and Sawyer, 1985; Pindell, 1985; Salvador, 1988 and 1991); the subduction of the Farallon Plate under the North American Plate (Pindell and Kennan, 2002); the lateral movement of the Chortis Block and the subduction of the Cocos Plate against the southern end of the North American Plate (Angeles-Aquino et al., 1994; Morán Zenteno et al., 2000; Padilla y Sánchez, 2007); and local tectonic events related with salt movements (Angeles-Aquino et al., 1994; Robles-Nolasco et al., 2004; Cruz Mercado et al., 2011). All of these tectonic events defined the Gulf of Mexico basin as divergent continental (passive) margin in which most of the basement subsidence related to plate tectonics ceased by the Paleogene period (Buffler and Sawyer, 1985), at which time a deep marine environment existed throughout much of the area. Much of the rapidly deposited Cenozoic fill describes an overall progradational pattern in this deep-water setting. This pattern was influenced by local loading onto mobile salt, forming salt-controlled sub-basins in some locations in which the subsidence was controlled by large, diapir-related contemporaneous g faults or fault zones. By the Neogene period, the patterns of deposition were controlled by syndepositional fault tectonics forming a slope that evolved into a shelf setting.

2.2 Stratigraphic framework

The samples of the Miocene sandstones were placed in the context of the sequence stratigraphic framework established for the study area by Gutierrez-Paredes et al. (2017a). In that study sequence analysis was used to recognize three types of stratigraphic surfaces: the basal surface of forced regression (BSFR), the correlative conformity (CC) and the maximum flooding surfaces (MFS); and to identify the systems tracts (highstand, falling-stage, lowstand and

transgressive). The analysis proposed a framework based on the use of maximum flooding surfaces as sequence boundaries, due to the ease of recognition and regional mappability of these surfaces. As a result, a genetic sequence model was applied for the study area (Fig. 5.2, Catuneanu, 2017).

Four stages of relative sea-level fall were recognized within the Miocene succession; during these stages, the fall in relative sea-level exposed the shelf to erosion and/or bypass, making it possible for rivers to discharge most of their sediment load directly onto the head of the continental slope or to build unstable shelf-edge deltas (e.g., in the onshore part of the study area, during the late Miocene). Thus, the deposits of relative sea-level fall overlie the basal surface of forced regression, and are represented by a range of gravity flows, from muddy (early forced regression) to coarse-grained sandy (late forced regression). Finally, the thicker sand-prone units accumulated in sequences C and D (Fig. 5.2), form the falling-stage systems tracts. Additional sand units are found within the lowstand and transgressive systems tracts and are overlain by a mud-prone interval that corresponds to the transgressive and/or highstand systems tracts in the sequence E (Fig.5.2). Subsequent increase in accommodation on the shelf, accompanied by sedimentation in fluvial to shallow-water systems, triggered a decrease in the sediment delivery to deep-water environments during the Pliocene (Gutiérrez Paredes et al., 2017a).

This study focuses on two genetic sequences, the middle Miocene (sequence C), and the Tortonian (sequence D) (Fig. 5.2). In this sequence stratigraphic framework, the middle Miocene reservoirs are placed into the lowstand and transgressive systems tracts (these two systems tracts are undifferentiated), and the upper Miocene reservoirs are placed into the falling-stage systems tract. Samples from non-producing intervals are also considered in this study; they are placed into the falling-stage systems tract of the middle Miocene sequence, as shown in Fig. 5.2. The

well log correlation in Fig. 5.3 shows the Miocene sandstone reservoirs (except well G) placed into the sequence stratigraphic framework, as well as the depositional elements where these sandstones reservoirs are placed.

3. Methodology

The database used in this study contains petrographic information from samples of twelve whole cores of the middle and upper Miocene, obtained from four oil-producing wells (A, B, E, and J) and one non-producing well (G). The subsurface depths of these samples range from 1810 m to 4380 m; in general, the rocks in the upper part of this depth range (1810-2500 m) are unlithified. A total of 150 thin sections of the upper and middle Miocene sandstones underwent petrographic examination; the samples were stained with blue dye epoxy to determine porosity, alizarin red for carbonates and potassium ferricyanide for other minerals, before preparing thin sections. Modal compositions were obtained using Indiana point-count data, 300 equidistant points into a grid were counted on each thin section; for this method, a petrographic microscope and an automatic point counter with 12 channels were used. Standard petrophysical nitrogen porosity and air permeability values were obtained from 275 horizontal plugs corresponding to many of the studied thin sections.

To support the petrographic and diagenetic analyses we used photographs taken with a scanning electron microscope (SEM) and the results of X-ray diffraction analysis to identify the clay minerals. For the X-ray diffraction two analyses were performed: 1) for the whole sample, clean and dried samples were broken up and dispersed in a diluted solution of sodium phosphate using a sonic probe. Later the samples were centrifuged and were grounded in fractions >2 microns, these fractions are dried and weighted to determine the loss of weight due to the

removal of the clay-size particles; later they are pulverized in distilled water using a micronized grinder. The resultant particles are disintegrated and packed in aluminum receptacles to produce random aggregates. The analysis of the X-ray diffraction is performed using a diffractometer equipped with a cobalt tube and a scintillation detector. The clay aggregates are oriented and analyzed with a variable angle of 2 to 50 degrees 2 theta with a scanning rate of 1.5 degrees per minute. The random aggregates are analyzed with a variable angle of 2 to 60 degrees theta with a scanning rate of 1 degree per minute. The weight of the clays minerals are determined by the clay aggregates of each sample and normalized to the percentage of mud/silt. The compositions of the whole sample are determined by the mathematical combination of the X-ray diffraction data of both fractions. The determination of the type of clays in the mixed plates and the percentage of the expandable plates are made by the experimental comparison of the diffraction data of the clays with the unidimensional diffraction profiles using the Newmod program of C. Reynolds. 2). for the clays, clean and dried samples were broken up and dispersed in a diluted solution of sodium phosphate using a sonic probe. Later the samples were centrifuged and were grounded in fractions >2 microns. The suspended clays are decanted and deposited in vacuum on a silver membrane to obtain oriented aggregates. The clay aggregates are mounted on glass slides and exposed to ethylene glycol vapors for 24 hours. The resultant particles are disintegrated and packed in aluminum receptacles to produce random aggregates. The clay aggregates are oriented and analyzed with a variable angle of 2 to 50 degrees 2 theta with a scanning rate of 1.5 degrees per minute. The fine fraction is analyzed by three ways air drying, saturated with glycol and heated to 375° C. The weight of the clays minerals is determined by the clay aggregates of each sample and normalized to the percentage of the weight of the clay-size mineral. The determination of the type of clays in the mixed plates and the percentage of the expandable plates

are made by the experimental comparison of the diffraction data of the clays with the unidimensional diffraction profiles using the Newmod program of C. Reynolds.

A set of spreadsheets were designed using Excel software to store petrographic and petrophysical data from these samples. With this database, several ternary discriminatory graphs were plotted like the QFL diagram of Folk (1974), and the QFL and Q_mFL_t diagrams of Dickinson et al., 1983. Diagenetic analysis employed the subdivision of diagenetic stages based on the work of Morad et al. (2000). These stages include eodiagenesis (0-2 km depth and $<70^\circ\text{C}$) that was principally affected by depositional and meteoric waters and mesodiagenesis (>2 km depth and $>70^\circ\text{C}$) which was mostly controlled by evolved formation waters.

We considered for this study the depositional facies and facies associations interpreted by Gutiérrez Paredes et al., 2017 (b).

4. Depositional Systems and Facies

The Miocene sandstones accumulated in deep-water submarine fans in slope and basin-floor settings. Gutierrez Paredes et al.(2017b) defined the sedimentary facies, which were grouped into facies associations and interpreted in terms of the depositional elements of channel systems, frontal splays, and lobes of debrites. The summary of these facies associations and the sedimentary facies included in each association are shown in Fig. 5.4.

The following paragraphs describe the main characteristics of these facies associations.

4. 1 Channel Facies Associations

These facies associations include three types: channel fill, channel margin and leveed channel.

Description: the first type, channel fill, is characterized by the amalgamation of thick-bedded structureless sandstones, normally graded sandstones, and intraclast mudstone breccias. Erosional bases of the sand beds are common, as are amalgamation surfaces. Channel-axis deposits contain sand with high net-gross value; in this facies association, the Bouma Ta division is common. In places where thin intercalations of massive sandstone with laminated sandstone, are presented, the Bouma Tad divisions are common and correspond to the channel-off axis (Fig.5.5A). The second type, channel margin, is characterized by massive sandstone with mudstone intraclasts; normally graded sandstones; ripple, parallel and cross-laminated sandstone and siltstone, laminated siltstone and mudstone and distorted heterolithic units (fine-grained sediments with convolute beds, slumps and contorted beds). The grain sizes are more variable due to the heterolithic compositions; because of this characteristic, the sand net to gross ratio decreases. In this facies association, the Bouma Td, Tc and Ta divisions are common (Fig. 5.5A). The third type is leveed channels, with massive sandstone representing channel fill, and intercalations of thinly bedded sandstones, siltstones and shales representing levee deposits. The levee sub-environment is indicated by the deposition of siltstones with climbing ripples and parallel laminations, as well as by the presence of beds with rip-up mudstone clasts and distorted heterolithic units (Posamentier and Walker, 2006). Bouma Tb, and Tcde divisions are commonly found in this association.

Interpretation: The Channel fill facies association is probably the result of repetitive and rapid deposition from high-density turbidity currents along the channel axis, which is indicated

by its thick bedding (>3 m), the absence of fine-grained facies, and the occurrence of amalgamation surfaces. The channel margin deposits represent the lateral transition from the channel offaxis, to the channel margins. This happens when the flow turbulence is not high enough to remove the fine-grained deposits; instead less erosion is inferred to have occurred from the channel axis to the margin. The presence of distorted heterolithic units further supports the interpretation of collapsed channel walls. Finally, leveed channels were deposited along the margins of the channels where low-density turbidity currents formed overbank deposits. Minor erosion occurred in the proximal levee, as a result of occasional incremental changes in sediment concentration, turbulence and the angle of the slope. According to Talling et al. (2012), thin turbidite sand layers are common on channel–levees, where levee deposits record evidence of dilute flow in the form of Tc, Td and Tb intervals if they are formed by bedwaves.

Leveed channels are frequently associated with other depositional elements, such as basal debris flows, frontal splays that are dissected and overlain by distributary channels, and hemipelagites.

4.2 Frontal Splay facies Associations

Description: Frontal splays include two types; the first one is proximal frontal splays. This facies association is represented by massive sand, laminated sandstone, although minor proportions of massive sandstone with floating pebbles, mudstone intraclasts and laminated siltstone and mudstone are present. This facies group typically exhibits several flows that are amalgamated in an ordered stacking pattern. The amalgamation surfaces are marked by floating pebbles or very thin siltstone partings. The net-gross sand ratio is high. The Bouma Ta division is predominant in amalgamated sand beds. An example of this association is shown in Fig. 5.5B. The second type is distal frontal splays; this facies association comprises beds typically (14 cm-thick) of fine-grained sandstone, intercalated with beds typically (7 cm-thick) of laminated

siltstone and mudstone; massive sandstone with floating pebbles is also present in minor proportions. The top and bottom contacts are planar. Sedimentary structures include load casts, planar features, and tabular sigmoidal and ripple laminations; some lenses of fine-grained sandstones and concretions of silt are also observed. The Ta and Td Bouma divisions are present.

Interpretation: Both facies association are mainly the result of turbidity currents.

Frontal splays also occur with distributary channels, forming frontal splay complexes (Posamentier and Kolla, 2003).

4.3 Lobes of debrites and hybrid sediment gravity flows facies associations

Description: Lobes of debrites comprise two types of lobes; the first type includes the lobes formed by muddy sandstone. Accompanying this facies there are thin intervals of ripple, parallel and cross-laminated heterolithic beds, laminated siltstone and mudstone and distorted heterolithic units; these lobes record abundant faults and fractures in their tops and contortions related to faults at their bases. The second type of lobe is formed by hybrid sediment gravity flow deposits, which include sandy debrites associated with turbidites; in this case the facies includes intraclast mudstone breccia, intraclast mudstone conglomerate associated with structureless sandstone, laminated sandstone, laminated siltstone and mudstone and heterolithic units with sand injections. The Ta, Tb and Te Bouma divisions are common in the upper parts of the deposits, whereas the Bouma Ta division is found in the lower parts (Fig. 5.6).

Interpretation: The lobes of debrites formed by muddy sandstones are the products of muddy debris flows, whereas their thin intervals are related to distal turbidites of the Bouma cde divisions. The lobes formed by hybrid sediment gravity flows that both fluid turbulence and matrix strength can act simultaneously within the same flow; as a result, turbidity currents and

debris flows are often genetically related. Multiple models have been proposed to explain the origins of these deposits. According to Sohn (2000), the transformation from debris flow to turbidity current is based on the initial flow conditions of hydroplaning and non-hydroplaning debris flows. For Felix and Peakall (2006), this transformation reflects a combination of the erosion of material from the dense mass, the breaking apart of the dense underflow, the breaking of internal waves and turbulent mixing. Talling et al. (2004) proposed that the transformation from debris flow to turbidite (and vice versa) is due to mixing and dilution, seafloor erosion, flow deceleration and the deceleration of low-coherency debris flows.

5. Detrital composition, classification and provenance

The sand of the middle and upper Miocene sequences is medium-grained to very-fine-grained, and angular to subrounded, with sorting that ranges from poor to moderate. The average values of the detrital compositions of the sandstones from both sequences are quite similar (that of the middle Miocene is $Q_{57}F_{10}L_{33}$ and that of the upper Miocene is $Q_{51}F_{16}L_{33}$), only a small increase in the feldspar content in the sandstones of the younger sequence is observed (Fig. 5.8). The mineralogical framework for these sandstones is dominated by the following mineralogy:

Quartz grains: Quartz grains are mainly monocrystalline (with an average value of 29 %; and a maximum value of 48 % for the middle Miocene sandstones, and an average value of 32 % and a maximum value of 57 % for the upper Miocene sandstones), polycrystalline quartz (with an average value of 4 %; and maximum value of 8% for the middle Miocene sandstones and average value of 6 %; and maximum value of 14 % for the upper Miocene sandstones) and chert (an average value of 4 %; and a maximum value of 7 % for the middle Miocene sandstones and average value of 3 %; and a maximum value of 9 % for the upper Miocene sandstones).

Monocrystalline and polycrystalline types exhibit grain shapes that vary from very angular to subround; monocrystalline quartz grains exhibit straight and undulose extinction, and contain embayments, internal fractures and scarce vacuoles and fluid inclusions. These features likely denote their volcanic origin. Polycrystalline quartz grains exhibit undulose extinction, internal fractures, and sutured internal crystal/boundaries, which likely reflect their origin from weakly metamorphosed sandstone or quartzite. The shapes of chert grains are mainly subrounded. The photographs in Fig. 5.7 (a, c, d, e) show examples of the different types of quartz grains in the Miocene sands.

Feldspars: Plagioclase (with an average value of 6 % and a maximum value of 9% for the middle Miocene sandstones and an average value of 15 % and a maximum value of 46 % for the upper Miocene sandstones) dominates over K-feldspar (with an average value of 1 % and a maximum value of 2 % for the middle Miocene sandstones; and average value of 7 % and a maximum value of 12 % for the upper Miocene sandstones), in most of the samples. K-feldspars are represented by microcline (characterized by its tartan twinning), orthoclase and sanidine. Plagioclase crystals have euhedral crystal outlines and exhibit single twinning, polysynthetic and lamellar twinning. Both types of feldspars are present as altered and fresh grains, which are sometimes partially or totally dissolved; this feature could indicate the presence of variable compositions or different sources of feldspars. Fig. 5.7 (b and e) illustrates examples of the different types of feldspars in the Miocene sands.

Sedimentary rock fragments: This is the most abundant group of rock fragments present in the Miocene sandstones (with an average value of 11 % in both the middle and upper Miocene sequences); they are essentially represented by fragments of shale, limonite, sandstone, and minor proportions of carbonate fragments (i.e., mudstone clasts and grainstone); the shapes of

the clasts vary from subangular to subrounded. Fig. 5.7 (d and f) shows examples of these sedimentary rock fragments.

Igneous fragments: These include plutonic and volcanic rock fragments and represent the second most abundant group of rock fragments in the Miocene sandstones (with an average value of 5 % in the middle Miocene sandstones and an average value of 11 % in the upper Miocene sandstones). Volcanic fragments include andesites, rhyolites (present as microgranular, glassy and microfelsitic pastes), and basalts. Plutonic rock fragments include granite with myrmekitic textures. Some of the volcanic rock fragments have been chloritized and kaolinitized. Fig. 5.7 (d and f) shows examples of igneous rock fragments.

Metamorphic fragments: These rock fragments are minor constituents and commonly comprise an average value of less than 1% in both the middle and upper Miocene sandstones. Some of these fragments include quartzite, schists and phyllites (Fig. 5.7e).

Accessories and heavy minerals: Micas are the major constituents of this group and are represented by muscovite, biotite (Fig. 5.7 a and c) and hornblende which are predominant among the heavy minerals (zircon, epidote and sphene). Minor proportions of authigenic pyrite (1 %) are also present in these samples. *Other constituents include:* organic matter, foraminifera and undifferentiated fossils.

The table 5.1 shows the summary of the average composition of detrital components of the middle and upper Miocene sandstone.

Based on the sandstone classification of Folk (1974), these sandstones are predominantly litharenites and feldspathic litharenites, with minor proportions of sublitharenite and subarkose (Fig. 5.8).

5.1 Sandstone provenance

The QFL ternary diagram of Dickinson et al. (1983) shows the relationships between the compositional modes and inferred provenance of detrital sandstone. The plot in Fig. 5.9 indicates that the Miocene sandstones mainly fall within the recycled orogen, and magmatic arc fields. According to Dickinson (1979), orogenic recycling occurs in regions where stratified rocks are deformed, uplifted and eroded. This type of provenance includes three tectonic subenvironments: subduction complexes, collision orogens and foreland uplift. The provenance of sediments (Fig. 5.9) is consistent with the tectonic setting and geology of southern Mexico, as well as with the presence of a wide variety of sedimentary rock fragments, abundant quartz, and minor abundances of feldspars and volcanic rocks, which are characteristics of foreland uplifts. For this reason, we assume that the most likely major sediment contributor to the Miocene sandstones was foreland uplift. Moreover, according to Dickinson (1982) the mixing of volcanic and plutonic contributions produces a spectrum of sandstones that range from feldspatholithic to lithofeldspathic in composition and which are commonly found in arc-derived debris typically deposited in forearc or interarc basins, although they may also reach foreland basins. According to these results the sediment source for the Miocene sandstones is the Chiapas fold belt and Chiapas massif, with the entry points placed in the SE and S. The second sediment entry point was placed in the southwestern portion and appears more frequently used through the late Miocene; the sediment source was probably the Chiapanecan volcanic Arc.

6. Diagenetic alterations

6.1 Compaction

In the Miocene sandstones, mechanical compaction is mainly recorded by brittle and plastic deformation and less frequently by grain slippage and rotation. Conspicuous evidence of brittle deformation includes the fractures and cleavage of individual grains of quartz and feldspar. Extreme crushing may also occur along grain-grain contacts, in which particles are spalled. Ductile grain deformation is evidenced by the squeezing of clays adjacent to rigid grains or mud intraclasts. Finally, grain slippage is observed at the edges of non-deformable grains (i.e., quartz) that slip past one another with slight rotation. Sands of the depth interval ranging from 1800-2300 m show little compaction, and it is common to observe floating grains with few grain-to-grain contacts and individual grains of fractured quartz. Sands of the depth interval ranging from 2300-3000 m show moderate to strong compaction evidenced by grain rotation and straight contacts, as well as some grain deformation and concave-convex contacts; compaction in some samples has also caused the flowage of ductile shale clasts into the surrounding pore space, producing a pseudomatrix. In sandstones at depths of more than 3000 m, chemical compaction occurred, and it is evidenced by sutured (pressure-solution) contacts, whereas mechanical compaction in these samples is represented by extreme crushing between grain-to-grain contacts and micas compressed between quartz grains. Fig. 5.10 shows examples of both mechanical and chemical compaction

6.2 Cements

Calcite cement is observed in 50 % of the studied samples, and ranges in abundance from 1-26 % according to modal analysis of the thin sections. This cement is mainly non-ferroan, and two varieties of calcite cement can be recognized: the first one exhibits a displacive texture and is observed in extensively cemented sandstone layers; the second one includes scattered patches and has a poikilotopic texture. In samples in which calcite cement is abundant, the original detrital fabric is preserved with little evidence of compaction, indicating that carbonate cementation occurred prior to significant burial; the volume of carbonate cement also increases with burial depth. In some samples, the calcite cements record evidence of recrystallization. Fig.5.11(a, b, d) illustrates examples of calcite cements.

Dolomite is observed in 5 % of the studied samples, and it ranges in quantity from trace amounts to 10 %. Sandstone samples in which, this mineral is present record partial dolomitization. Dolomite forms as either a directly precipitated pore-filling cement or a replacement of earlier carbonate cements. Fig. 5.11g shows an example of partial dolomitization.

Siderite cement is the least common of the carbonate cements observed in the samples, with abundances of less than 1%. It is characterized by its pale brownish color in plane-polarized light and its higher relief than calcite; it occurs as pore-filling and grain-coating cement (Fig. 5.11 c).

Quartz overgrowths are not commonly observed in the Miocene sandstones, and only trace amounts of quartz cement occur as discrete euhedral crystals in samples of 2700 m of burial depth. Few samples exhibit dusty rims and inclusion- poor overgrowth cements.

Feldspar cements are observed in the middle Miocene samples at burial depth of 4385 m. Only trace amounts of feldspar cement occur as overgrowths (i.e., discrete euhedral crystals) on

detrital grains. These minerals typically feature subtly different mineral chemistry and crystallography than the substrate grains, often leading to an absence of optical continuity.

Other diagenetic minerals. Minor diagenetic minerals include pyrite; although it commonly comprises <1% of the samples, it occurs in the Miocene sandstones as scattered framboids. It also occurs as cement filling the pore-spaces in bioclasts; the burial diagenetic form of pyrite is somewhat coarser than the framboids, and it is usually subhedral. Fig. 5.11h shows an example of pyrite filling pores.

6.3 Alteration

K-feldspars and plagioclase in the Miocene succession of the study area undergo two processes of alteration: sericitization and kaolinization. Incipient sericitization is first represented as scattered minerals along cleavage planes, which are identified in thin sections by their white to colorless characteristics in plane-polarized light, and bright second-order to low-third order birefringence in cross-polarized light. Kaolinization is characterized in thin sections by deep brownish and cloudy grains accompanied by the common preservation of relicts of original structures, such as cleavage and twinning planes. Where the extensive replacement of feldspars by kaolinite occurs, kaolinite commonly appears as numerous stack-like crystals and discrete booklets that penetrate the grain surface. Fig. 5.12 (a and b) reveals examples of feldspar alteration.

6.4 Dissolution

The partial or complete dissolution of unstable grains (i.e., feldspars, and lithic grains) and quartz, as well as the dissolution of authigenic cement (mainly calcite) and some bioclasts, is observed in the Miocene sandstones. In thin sections, it is common to observe honeycombed

feldspar grains and skeletal plagioclase grains in which dissolution has exploited the cleavage planes. Additionally, subtle variations in crystal compositions allow for selective grain removal, which locally creates secondary intragranular porosity. The dissolution of cement is indicated by the presence of large, oversized pores and common floating grain textures. Fig. 5.12 (b, c and d) illustrates examples of dissolution presented in the Miocene samples.

6.5 Clay minerals

Clay minerals were identified by using X-ray diffractometry and scanning electron microscope (SEM) photographs. The authigenic clay mineral content ranges from 0 to 15%; these clays include illite, mixed layer varieties of illite/smectite, kaolinite, chlorite, and minor proportions of smectite. Generally, illite is more abundant than kaolinite and chlorite in the studied sandstone samples. For the histograms shown in Fig. 5.13, we consider 29 samples for well “J”, 76 samples for well “E”, 35 samples for well “B” and 21 samples for well “G” (Fig. 5.13).

Illite/mica is the most widely distributed clay mineral in the Miocene sandstones, which occurs as both fibrous (i.e., wispy authigenic crystals lining pore spaces) and platy (i.e., boxwork) morphologies. This type of clay mainly occurs as a pore-filling mineral in void spaces. *Illite/smectite* mainly occurs as pore-filling cement forming around detrital grains and as the product of the degradation of feldspars. Fig. 5.13 shows an example of illite/smectite.

Smectite has only been observed in one well, based on the results of X-ray diffractometry. During progressive burial, most of the smectite probably changed into illite via mixed layers of illite/smectite.

Kaolinite is mostly observed as pseudomorphic replacements of feldspars and clay. Most of the kaolin clay minerals are authigenic in origin. Kaolinite clays commonly occur as aggregates of crystals ‘booklets’ and vermicular stacked pseudo hexagonal crystals. Fig. 5.13 illustrates an example of the kaolinite booklets.

Chlorite the results of the XRD analyses show that clinocllore is the most abundant type of chlorite present in these sandstones. Chlorite clays occur as crenulated flakes which, in some cases, have developed into honeycomb-like textures and rosettes. In the Miocene sandstones, chlorite was formed by the alteration of biotite and feldspars; they are also present in the sandstones as pore-filling cement.

6.6 General diagenetic sequence

The general diagenetic sequence for the middle and upper Miocene sandstones was delineated in this study, based on textural relationships observed in thin-section slides and SEM images. The diagenetic sandstone sequence is presented in Fig. 5.14. Due to the complex paragenetic relationships observed between the authigenic constituents, as well as the limitations of geochemical and geochronological data, only a schematic representation of the diagenetic evolution could be achieved; based on the relative positions of the various diagenetic products to each other. All features do not occur in all samples, so only the major diagenetic events are represented in the paragenetic sequence. The thermal gradients obtained from five wells exhibited temperatures from the lower Miocene to the upper Miocene ranged from 70° to 120°C. Diagenesis, as recognized in the upper and middle Miocene sandstones, resulted from several major processes, including compaction (both mechanical and chemical), alteration of unstable grains, cementation, dissolution, the transformation of authigenic minerals and dolomitization.

Other minor diagenetic processes were also observed such as, siderite cementation, quartz and feldspar overgrowths, recrystallization, calcitization, and pyrite formation.

Compaction and dissolution are continuous processes throughout shallow and burial diagenesis. The diagenetic processes that are attributed to eodiagenesis are mechanical compaction, the alteration of feldspars and lithic grains by sericite, the dissolution of detrital grains, Kaolinitization and calcite cementation. Mechanical compaction occurred shortly after deposition, as indicated by the abundance of deformed soft-grain rock fragments in some samples. Compaction is also indicated by the deformation of ductile grains and the presence of long, concave-convex and sutured contacts between more rigid grains (Fig. 5.10, c, d, e).

The clay replacement and dissolution of feldspar became significant after deposition due to water flushing. Leaching occurred along cleavage planes, which are the zones of weakness in these grains.

K-feldspar dissolution in sandstones commonly occurs at depths ranging from 1.5 to 4.5 km at temperatures ranging from 50 to 150°C (Wilkinson et al., 2001). Dissolution and replacement of detrital potassium and plagioclase feldspar are natural consequences of diagenesis under conditions of increasing burial and temperature. No unusual or special source of acidic pore fluids is required (Giles and deBoer, 1990). Under the most common circumstances, unstable feldspar grains react to form more stable authigenic phases (e.g., albite, kaolinite, illite) with the pore waters acting primarily as transport agents. As pore fluids reach equilibrium with the reacting feldspar phases, mass transport must occur for further reactions to proceed. The scales of mass transport determine whether reservoir porosity is indeed enhanced. Although secondary porosity due to framework grain dissolution (primarily feldspars) is almost ubiquitous, it represents a relatively minor proportion of total porosity. Morad et al. (2000) and Morad et al.

(2010) mentioned that feldspar dissolution also occurs by organic acids and CO₂ released during thermal maturation of organic matter and oil generation in source mudrock. Organic acids (mainly carboxylic) also form by the interaction of water with hydrocarbons, mineral oxidation of organic matter and by bacterial degradation of organic matter and hydrocarbons. Generation of CO₂ also occurs by thermal reduction of sulphate ions which are derived from the dissolution of evaporites.

Although we considered the feldspars alteration occurred during the eodiagenesis, the timing of the alteration of feldspars in these sandstones is uncertain, because this alteration may have occurred in the source area or during transport. Carozzi (1993) determined that is difficult to establish the precise time of feldspar alteration, because this spans the entire time interval between the onset of weathering in the source rocks and the additional processes that occur during burial.

Kaolinitization is attributed to the flux of meteoric water into the deep-water turbidite deposits as a result of a major fall in the relative sea level, when the FSST exposes the shelf, and the shoreline rapidly migrates basinward, leading to the enlargement of meteoric recharge areas. The basinward migration of the meteoric zones promotes the flushing of not only the shallow marine sediments but, in some cases, the deepwater turbidites also. (Meisler et al., 1984; Hayes and Boles, 1992; Carvahlo et al., 1995; Morad et al., 2000; Ketzer et al., 2003; Mansurbeg et al., 2006). However, other mechanisms of meteoric water influx into deep-water sand, such as hyperpycnal flow and increase in hydraulic head owing to basin margin uplift, cannot be ruled out.

Cementation by poikilotopic calcite occurs mainly below marine flooding and maximum flooding surfaces, because of the long residence time of sediments below the flooding surfaces

that enhance the diffusion of dissolved carbon and Ca^{2+} from the overlying seawater and/or to abundant intrabasinal carbonates (Al-Ramadan et al., 2005; Ketzer et al., 2003; Morad et al., 2000).

Another minor diagenetic event that is present during eodiagenesis is the precipitation of pyrite probably as the result of the microbial reduction of detrital ferric iron and typically due to the presence of seawater sulphate during earliest burial (Love, 1967). The precipitation of pyrite occurs during thermal sulphate reduction and invasion of the reservoirs by metal-rich brines. (Morad et al., 2000). The pyrite formation is also related with the presence of biotite and chlorite, the iron was released during the alteration of biotite into illite (and/or kaolinite) and chlorite. (Morad, 1986). Illitization of biotite has presumably occurred initially while the sediment was still subjected to oxic conditions, during a very early stage of burial. Part of the iron released from the earlier illitization of biotite presumably accounts for the formation of the interstitial pyrite. The iron oxides might dissolve through direct or bacterial oxidation of organic matter. Chloritization rather than Illitization of biotite occurred by rapid burial of sediments to depths below the oxic environment. Therefore, subsequent rapid decrease in redox potential prevailed and the iron released from alteration of biotite became increasingly soluble. When the chloritization of biotite occurred under conditions of high Mg^{2+} activity, pyrite is formed by the reaction of sulfide ions with excess Fe released from the biotite.

During mesodiagenesis, the most important diagenetic modifications that occurred in the sandstones were the formation of authigenic clays, calcite cementation, dolomitization, dissolution and chemical compaction. Other minor diagenetic modifications included siderite cementation, calcification (mainly observed in feldspars), and recrystallization of calcite cement, quartz and feldspar overgrowths and the formation of pyrite cement. Calcite cement is the most

volumetrically important cement, which formed early during the mesogenetic stage, due to the low Fe content deeper sandstones and the loose grain packing, and presence of undeformed ductile grains within calcite-cemented areas. According to Hein et al. (1979), in marine sandstones carbonate cements are developed through reactions between detrital aluminum-silicate minerals and the products of the breakdown of organic matter. The main source of carbonate cement is probably the pressure solution of detrital carbonate grains, smectite dissolution, and Ca-feldspar dissolution. Replacement by calcite has also occurred in the feldspar grains. Other carbonate cements are siderite cement which occurred at deep burial depths; siderite formation may be locally associated with the alteration of mica. Other mesogenetic cement in the sandstones is quartz overgrowth; it was observed in sandstones that were buried deeper than 2.5 km, corresponding to temperatures greater than 80°C. According to Bjørlykke and Egeberg (1993), quartz cement tends to form during burial diagenesis at temperatures above 70°C. The minor abundance of quartz overgrowths in the samples is probably due to a combination of different factors, such as the availability of silicate ions and the precipitation of authigenic calcite, grain coatings by clay minerals and the content of mica. Other minor cement recognized as having formed during mesodiagenesis includes pyrite cement. It is typically found to be one of the last cements to form and is especially associated with the reduction of hematite in the presence of hydrocarbons (Elmore et al., 1987). As was mentioned before dissolution continued throughout the mesogenetic stage of diagenesis and was commonly alternated with carbonate cementation.

The mesogenetic clay minerals in the sandstones are chlorite, illite/smectite and illite. Illite is exclusively burial authigenic clay, which typically begins to form at temperatures exceeding 70°C and strongly increases in sandstones buried deeper than 3 to 4 km (90–110°C). The origin

of illite is commonly associated with the alteration of kaolinite and smectite or the degradation of feldspars and micas, although it can also be formed by the breakdown of volcanic ash (Altaner and Grimm, 1990; Jeans et al., 2000) or volcanic rock fragments (Ulmer-Scholle et al., 2014). In this study, smectite is regarded as one of the main sources of illite precipitation, as indicated by the presence of a significant amount of a mixed layer of illite-smectite (Fig. 5.13 shows two examples of these illite morphologies). During progressive burial, most smectite changes into illite via mixed layers of illite/smectite (Boles and Francks, 1979; Hower et al., 1976; Perry and Hower, 1970 and 1972.). Illite begins to form from the dissolution of smectite during burial via mixed layers of illite/smectite at temperatures that have been estimated by various authors as $>70^{\circ}\text{C}$ (Bjørlykke, 1998), approximately 95°C (Perry and Hower, 1970), $90\text{--}110^{\circ}\text{C}$ (Chang et al., 1986), or $100\text{--}110^{\circ}\text{C}$ (Pearson and Small, 1988). Illite formation strongly increases in sandstones that are buried deeper than 3.8–4 km, corresponding to temperatures of $120\text{--}140^{\circ}\text{C}$ (Bjorkum and Gjelsvik, 1988; Bjørlykke and Aagaard, 1992; Ehrenberg and Nadeau, 1989; Ehrenberg, 1990; Giles et al., 1992). This transformation requires a supply of potassium and the privation of silica at the expense of aluminium (Warren and Curtis, 1989). A supply of potassium was probably transferred locally from the simultaneous dissolution of potassium feldspar. Illitization can potentially release considerable amounts of Mg^{2+} and Fe^{2+} ions that can be used for chlorite formation during later diagenetic reactions within the same rock. Other processes for chlorite formation in sandstones are the replacement of unstable grains, the replacement of authigenic clays, and the direct precipitation of chlorite from pore fluids (Anjos et al., 2003; Chang et al., 1986). Chlorite cements can be formed by the alteration of non-clay minerals such as biotite, amphibole and volcanic rock fragments, when they come into contact with iron-rich pore waters (De Ros et al., 1994b; Remy, 1994). Chlorite, however, typically varies with depth, suggesting

that an increase in authigenesis occurs at greater deep burial depths. Fig. 5.13 shows two examples of chlorite clay.

7. Reservoir quality

Miocene rocks record a wide range of porosity and permeability. Although the values of porosity and permeability are quite similar for the middle and upper Miocene sequences, the samples from the upper Miocene sandstones associated with frontal splays have the best reservoir quality.

7.1 Porosity

The types of porosity identified in the Miocene sandstones are as follows: intergranular porosity, with an average value of 15%; secondary porosity (due to the dissolution of unstable lithic grains and feldspars), with an average value of 2%; intragranular porosity (due to the dissolution of bioclasts); fracturing; with an average value of 2%. Secondary porosity generally represents a minor fraction of the total porosity. Examples of these different types of porosity present in the upper and middle Miocene sandstones are shown in Fig. 5.15.

The porosity values from core-analysis were plotted against burial depth, which revealed a general trend of decreasing porosity with increasing burial depth. The sandstones with higher porosity values have porosities ranging from 20-35%, whereas those lower values have porosities of >5%. The average core-analysis porosity is 28% at depths between 1500-3000 m (mainly unlithified sands), 18% in sandstones at depths between 3000- 4000 m and 4% in sandstones at depths between 4000-4500m. By superimposing the values of porosity versus depth for each well, the following differences in reservoir quality between sandstones of different ages or units can be determined: 1) middle Miocene sandstones at shallow depths (wells

A and B) have similar porosity values as deeper wells (wells J and E); 2) wells with the same age but at different depths show different porosity values (e.g., well A middle Miocene); 3) a wide range of porosity values is also observed in wells at the same depth and the same age (e.g., well E); 4) both middle and upper Miocene sandstones have good to excellent porosity values (20-35 %) (Fig. 5.16).

All of these differences in porosity values are probably a consequence of diagenetic effects such as mechanical compaction and cementation and depositional facies present in each well. For example lobes of debrites composed of muddy sandstone have porosity values from 0 to 10 % and permeability values ranges from 0.001 to 0.1. (Fig. 5.17 and Fig.5.19).

7.2 Permeability

Miocene sandstones record a wide range of porosity (5-35 %) and permeability (> 1- 2000 mD). In these samples, permeability values generally increase alongside the increasing porosity values (Fig.5.17). However, there is a range of porosity values (between 20-30%) in the upper Miocene samples (Fig. 5.17) that record low permeability values (< 0.1-10 mD), which indicate that complexities are involved in the permeability distribution of the Miocene sandstone reservoirs. By comparing the values of permeability versus porosity for each well, the following differences in reservoir quality between sandstones of different ages can be determined: 1) the middle Miocene samples cluster in two well-defined fields: low values of both porosity (0-10 %) and permeability (0.001- 0.1) for muddy sandstones in lobes of debrites; and high values of both porosity (24 - 36%) and permeability (10 - 1000md) for massive sandstone in channels and frontal splays. 2) The upper Miocene samples form series of more disperse clusters: high values of both porosity (25 – 35 %) and permeability (100 - 3000 mD) for massive sandstones in frontal splays and channels; moderate values of porosity (10 - 16 %) with low values of permeability (1

– 10 mD) for fine grained sandstones and siltstones in leveed channels; and low values of both porosity (0 – 10 %) and permeability (0.01 to 0.1 mD) in cemented sandstones (Fig. 5.17).

8. Discussion

The distribution of the reservoir quality of the Miocene sandstones in the study area depends upon a combination of multiple factors, including depositional facies, sandstone composition and diagenesis. The impact of these factors on the Miocene sandstone reservoir quality is discussed in this section.

8.1 Provenance controls on reservoir quality

The triangular plots show that the provenance of these sandstones is from the recycled orogen which was progressively influenced by volcanic sources (Fig.5.9). As volcanic activity increased, it was likely accompanied by tectonic uplift that rejuvenated the relief and increased the supply of sediment to the basin. As a result, the abundance of lithic fragments and the high proportions of plagioclase relative to K-feldspar suggest that the sources of these sandstones were eroded and transported in a relatively short amount of time. The detrital compositions indicate that these sands and sandstones are submature to immature. Primmer et al. (1997) mentioned that sandstones that are rich in lithic fragments are commonly chemically and/or mechanically unstable; as a result, these types of sandstones suffer rapid declines in porosity and permeability due to mechanical compaction. Moreover, Bloch et al., 2002; Pittman and Larese, 1991 argued that sandstone reservoirs with high contents of ductile grains such as shale clasts, biotite or lithic fragments experience more intensive compaction; such is the case of the rocks of wells J and B which have biotite and muscovite and shale clasts (which in some cases form pseudomatrix). The sediment composition could also affect the dissolution, for instance,

feldspars, volcanic and carbonate rock fragments are more likely to be dissolved leading to enhanced porosity.

In our data set, the $L_S L_V L_M$ plot clearly shows two sources of sediments; one is a sedimentary source and the second is a volcanic source (Fig. 5.18). The wells that come from a volcanic source contain greater content of feldspars and clays than the wells that come from a sedimentary source. As a result, these wells are more susceptible to diagenetic effects, such as feldspar alteration. Hawlader, 1990; Pirrie et al., 1994 stated that volcanic rock fragments, which are chemically unstable, tend to alter into clay minerals (smectite and chlorite), zeolites, calcite and silica during diagenesis. In the plots of the porosity vs permeability (Fig. 5.17) the wells E and B, which come from a volcanic source, exhibit a variable value of permeability with good values of porosity; this variability could be due to the sand composition. However, the impact of the sand composition could be overcome by other factors (i.e., depositional facies).

8.2 Sequence stratigraphic controls on reservoir quality

According to Morad et al. (2010), the sequence stratigraphic framework exerts a critical influence on reservoir quality by governing the depositional setting and subsequent diagenetic environment. Changes in relative sea-level exert a significant control on the types and extent of near-surface shallow burial diagenetic alterations, which in turn influence the pathways of burial diagenesis and the reservoir quality of clastic reservoirs. For example, the creation of porosity related to unconformities is because carbonate cements in sandstones undergo dissolution during uplift and weathering, as do feldspars and chert. Morad et al., 2010 also mentioned that diagenetic modifications such as dissolution and kaolinization of feldspars, micas, and mud intraclasts occur frequently along basal surface of forced regressions, especially under wet and warm climates; and the eogenetic carbonate cementation in turbidite sandstones is typically

concentrated along contacts with interbedded pelagic or hemipelagic mudrocks. This is the case of well E, which contains a major content of calcite cement; this could be related to the presence of two intervals of pelagic and hemipelagic sediments above and below of the studied samples.

In this study, we observed that the wells E, J and G, placed into falling-stage system tracts (Fig. 5.2 and Fig. 5.3), record major kaolinite contents (Fig.5.13). Finally, the wells placed in the falling stage-systems tracts record greater dissolution of feldspars and micas.

We also observed petrographic changes across the same system tracts. For example, in well J, core 3 and core 2 are both placed in the falling-stage systems tract. However, there are some differences in the abundances and types of their detrital components. In core 3, we observe carbonate and metamorphic fragments which were not observed in core 2. According to Amorosi and Zuffa (2011), these changes in arenite composition are likely to be recorded in deep-water settings, at the base of thick successions of falling-stage turbidites, in association with diagnostic changes in lithofacies patterns (e.g., an abrupt increase in the sandstone to shale ratio); furthermore, petrographic changes occurring across the sequence boundary within turbidite deposits are more likely to reflect a gradual and continuous process (not an episodic one), which may occur over a considerably long period of time. The petrographic changes observed along the same systems tracts in this area can also be related to the detritus source. For example, the sandstones of the well E and well J are placed in the falling-stage system tract of the same sequence; however the first one has a volcanic source and the second one has a sedimentary source (Fig. 5.18). This implies that distinct petrofacies may occur simultaneously within different parts of the basin across the same sequence boundary (Spadafora, 1996). As a result, arenites in the basal portion of a falling-stage systems tract can be architecturally similar, but their compositional and dispersal characteristics may be different if petrologically distinct detritus

are derived from separate sources at the same time (Lawton et al., 2003). Ryu and Niem (1999) and Marchesini et al. (2000) argued that patterns in arenite composition may be strongly affected by changes in sea level, and may thus record systematic variations within sequences, between different systems tracts. In these studies, however, compositional changes were not observed between systems tracts, which suggest that the sediment dispersal patterns on the shelf did not change significantly in response to sea-level fluctuations. Thus, these shifts in arenite composition probably developed in response to tectonic activity.

8.3 Facies controls on reservoir quality

This is an important factor in controlling the porosity and permeability of the Miocene sandstones. The sedimentary facies of the study area were interpreted to have been deposited from turbidity currents and debris flows (i.e., mudflows); however, the middle and upper Miocene deep-water systems were dominated by high- to low-density turbidite deposits, which were the most abundant deposits observed in the cored sections.

Fig. 5.19 shows the porosity and permeability cross plot for the depositional elements present in the upper and middle Miocene sequences. In these graphs, frontal splays and channel fills (which are mainly composed of massive sandstone, massive sandstone with pebbles and/or intraclasts and normally graded-sandstones) feature the highest values of porosity and permeability; whereas the fine-grained facies of overbank deposits (e.g., channel margins and levees) have lower values of porosity and permeability and thus record substantially reduced reservoir quality. Upper Miocene lobes formed by intraclast mudstone conglomerate and massive and laminated sandstone have good values of porosity and permeability, although these values are variable and sometimes decrease as a result of their mud content and poor sorting. In

contrast, lobes formed by muddy sandstones have the lowest values of porosity and permeability; these deposits represent the rocks with the poorest reservoir characteristics in this area.

Another control on reservoir quality related to the depositional facies is the grain size. The upper Miocene sandstones range from medium-grained to very fine-grained (0.064-0.261 mm) and the middle Miocene sandstones range from fine-grained to very fine-grained (0.085-0.158 mm). In this study, we observed that porosity decreases with increasing grain size. Fine- and very fine-grained sandstones have higher values of porosity and permeability than medium- and coarse-grained sandstones. The explanation for this trend is that coarser sandstones contain more ductile grains and are more poorly sorted than fine-grained sandstones; as a result, they have lower porosities. However, the role of grain size in other samples of the Miocene sandstones is overpowered by the effects of diagenetic processes, such as cementation.

8.4 Diagenetic controls on reservoir quality

Diagenetic alterations were a major factor controlling the reservoir quality of Miocene sandstones because the distribution of porosity and permeability of the sandstones could be modified by depositional processes (grain size, sorting and shale-bed distribution), or by post-depositional diagenesis (e.g., compaction, cementation, dissolution and the formation of authigenic clays).

The porosity and permeability of sandstone generally decrease with increasing depth due to compaction and cementation, although this trend may be reversed by the dissolution of grains and cements (Makowitz and Milliken, 2003). However, depth is not the only factor controlling the compaction of sandstones in this area; compaction is also affected by the proportion of ductile grains, which is a function of provenance. Makowitz and Milliken. (2003) determined that the presence of ductile grains results in greater pore-volume reduction during compaction.

Pittman and Larese (1991) showed that porosity loss is primarily due to ductile behavior; the results of these experiments also demonstrated that some lithic grains were fractured. They concluded that the amount of fractured grains varies inversely with the amount of ductile material. The rate and degree of sandstone compaction are influenced by its burial rate, sediment composition, and rock-mechanical and petrophysical properties, as well as its temperature, pressure and stress conditions. Compaction (by both ductile-grain deformation) increases with burial depth, resulting in decreases in both intergranular volume and primary porosity. The effect of sand composition on compaction exhibits a direct relationship between the content of ductile lithic grains (e.g., mudrock, argillite, phyllite, schist and glauconite) and porosity reduction by compaction (Lundegard, 1992). Furthermore, experimental studies of artificially mixed and packed clay-free unconsolidated sands have shown that original porosity and permeability are mainly determined by grain size, and the sorting and packing of grains (Fraser, 1935; Beard and Weyl, 1973). Additionally, in sands containing more than a few percent of clay, permeability is be strongly controlled by the volume and distribution of clay (Fraser, 1935).

The presence of calcite cement exerts a major control on the quality of the Miocene reservoirs by affecting the porosity values; sandstones containing less than 6% of total cement record a wide range of porosity, suggesting that the reservoir quality of these poorly cemented sandstones is controlled by other factors. However, in sandstones containing more than 10% of cement, the cement volume exerts an important control on porosity. There is a general trend of increasing cement volume with present depth that contributes to the general decrease in porosity with depth (well J). However, the samples with the highest cement volumes (26% and 19%) were not buried deeply. These sandstones, which were obtained from depths of 2,774 and 2,939 m, were probably cemented by calcite at a relatively early stage, close to the boundary between

eodiagenesis and mesodiagenesis; as a result, the abundant calcite cementation inhibited the later mechanical compaction of the sandstones, thus preserving the unfilled part of the primary porosity. An example of this occurred in well E, where early calcite cementation preserved the primary porosity; as a result, the quality of the reservoir rock in this well was not affected by the cementation.

The dissolution of detrital grains and authigenic cement is another diagenetic factor affecting the reservoir quality of the Miocene reservoir, although the contribution of secondary porosity is minor (representing no more than 2%). The dissolution of cement helps to increase the effective porosity (especially when complete dissolution occurs) by forming dissolution channels that connect adjacent pores and enlarging of pores (Fig. 5.15). On the contrary, the contribution of feldspar dissolution to the secondary porosity of the sandstones in the study area is minor. The dissolution of other detrital grains such as quartz contributes to the formation of quartz overgrowths, which could be an important factor in preserving porosity by impeding compaction (Anjos et al., 2003; Berger et al., 2009; Ehrenberg, 1993; Lander and Bonnell, 2010). However, in this area, the scarce abundance of quartz overgrowths does not affect the compaction.

Finally, in this area, the formation of authigenic clays such as kaolinite, chlorite, and illite was a major factor controlling the quality of the Miocene sandstones, due to their ability to reduce the permeability and to cause formation damage such as the migration of fine particles that can physically break away during hydrodynamic flow. Eventually, the migration of these minerals may cause accumulations in pore throats which can block fluid flow and thus reduce the overall permeability. Wilson et al. (2014) stated that kaolinite, illite, and mixed-layer illite-smectite are the major culprits in the migration of fine particles. In contrast, chlorite type minerals are not susceptible to dispersion and migration.

9. Conclusions

The studied samples in the southern Gulf of Mexico are placed within the middle Miocene and upper Miocene genetic sequences which are mainly sand-prone. These sandstones represent the falling-stage and lowstand systems tracts deposits. The sequence stratigraphic framework in this area exerted an important control on the reservoir quality of these sandstones, by governing the depositional setting, and by controlling their diagenetic environment. Moreover, calcite cementation, the dissolution of feldspars and the formation of kaolinite were related to the fall in relative sea level.

Depositional facies also exerted an influence on the reservoir quality of the Miocene sandstones. The lithofacies exhibit predictable petrophysical trends; for example, massive sands record consistently higher values of porosity and permeability than sandstones with silty and shaly lithofacies, and muddy sandstones record low values of porosity and permeability. In terms of the depositional elements, the studied samples correspond to channels, frontal splays and lobes of debrites. Upper Miocene sandstones have the best reservoir quality with the highest porosity and permeability values; they are associated with channel systems and frontal splays. These sands are dominantly unlithified, and record limited textural and mineralogical variability. Therefore, in these types of sands, mechanical compaction was the dominant porosity-reducing mechanism.

Although there is a general trend to decrease porosity and permeability with burial depth, its effect is overcome by diagenetic factors; thus, the major mechanisms of porosity reduction that have been recognized within the Miocene sandstones are mechanical compaction, calcite cementation, and the formation of authigenic clays. Nevertheless, the formation of authigenic

clay minerals exerts a major control on sandstone permeability, because to the presence of clay between pores resulted in the plugging of pore throats, hence reducing the permeability of the samples.

In conclusion, the reservoir quality of the Miocene sandstones was controlled by a combination of depositional facies, sand composition and diagenetic factors (mainly compaction and cementation). However, sandstone texture as controlled by depositional facies and their position in the sequence stratigraphic framework was more important than sandstone composition in determining reservoir quality; and compaction was more important than cementation in reducing porosity. Compaction was eventually stopped by the precipitation of calcite cement.

Acknowledgements

This research was completed as part of the doctoral project carried out by the first author. The work was sponsored by PEMEX-Exploración y Producción, additional funds from the Fondo Sectorial Conacyt-Sener-Pemex.

We thank the editor Dr. Francisco Vega, as well as Dr. Jose M. Grajales Nishimura and Dr. Jorge Moraga Benavides, for their constructive comments which helped improve the manuscript during the peer review process.

References

- Altaner, S.P., and R.E. Grimm., 1990.** Mineralogy, chemistry, and diagenesis of tuffs in the Sucker Creek Formation (Miocene), Eastern Oregon: *Clays and Clay Minerals*, V.38, p. 561-572, doi:10.1346/CCMN.1990.0380601.
- Al-Ramadan, K., Morad, S., and Proust, J.N., 2005.** Distribution of diagenetic alterations within the sequence stratigraphic framework of shoreface siliciclastic deposits: evidence from Jurassic deposits of NE France, *Journal of Sedimentary Research* 75, 943-959.
- Amorosi, A., and Zuffa, G.G., 2011.** Sand composition changes across key boundaries of siliciclastic and hybrid depositional sequences. *Sedimentary Geology* 236,153-163.
- Ángeles-Aquino, F., Reyes-Núñez, Quezada- Muñeton and Meneses Rocha J.J., 1994.** Tectonic Evolution, Structural Styles and Oil habitat in Campeche sound, Mexico: *Gulf Coast Association of Geological Societies Transactions*. V 44, p 53-62.
- Anjos, S.M.C., De Ros, L.F., and Silva, C.M.A., 2003.** Chlorite authigenesis and porosity preservation in the Upper Cretaceous marine sandstones of the Santos Basin, offshore eastern Brazil. *International Association of Sedimentology*. 34(2): 291-316.
- Beard, D.C., and Weyl, P.K., 1973.** Influence of texture on porosity and permeability of unconsolidated sand. *American Association of Petroleum Geology Bulletin* 57 (2), 349-369.
- Berger, A., Gier, S., and Krois, P., 2009.** Porosity-preserving chlorite cements in shallow marine volcanoclastic sandstones: evidence from Cretaceous sandstones of the Sawan gas field, Pakistan. *American Association of Petroleum Geology Bulletin* 93, 595-615.
- Bjorkum, P.A., and Gjelsvik, N., 1988.** An isochemical model for formation of authigenic kaolinite, k-feldspar, and illite in sediments. *Journal of Sedimentary Petrology*, V. 58, p. 506–511.

Bjørlykke, K., and Aagaard, P., 1992. Clay minerals in North Sea sandstones. In: Houseknecht, D.W., Pitman, E.D. (Eds.), Origin, Diagenesis and Petrophysics of Clay Minerals in Sandstones. SEPM Special Publication, V. 47, pp. 65–80.

Bjørlykke, K., and P. K. Egeberg., 1993. Quartz cementation in sedimentary basins: American Association of Petroleum Geology Bulletin, V. 77, p. 1538–1548.

Bjørlykke, K., 1998. Clay mineral diagenesis in sedimentary basins - a key to prediction of rock properties. Examples from the North Sea Basin. Clay Minerals 33, 15-34.

Bloch, S. Lander, R.H., and Bonnell, L., 2002. Anomalously high porosity and permeability in deeply buried sandstone reservoirs: Origin and predictability. American Association of Petroleum Geology Bulletin. 86(2): 301-328.

Boles, J.R., and Francks, G.S., 1979. Clay diagenesis in Wilcox sandstones of Southwest Texas: Implications of smectite diagenesis on sandstone cementation. Journal of Sedimentary Petrology, 49, 55-70.

Buffler, R.T., and Sawyer, D.S., 1985. Distribution of crust and early history Gulf of Mexico Basin: Gulf Coast Association of geological Societies Transactions. V.35.pp. 333-344.

Carozzi, A., 1993. Sedimentary Petrography. PTR Prentice Hall, Englewood Cliffs, New Jersey. pp. 263

Carvalho, M.V.F., De Ros, L.F., and Gomes, N.S., 1995. Carbonate cementation patterns and diagenetic reservoir facies in the Campos Basin Cretaceous turbidites, offshore eastern Brazil. Marine and Petroleum Geology 12, 741–758.

Catuneanu, O., 2002. Sequence stratigraphy of clastic systems: concepts, merits, and pitfalls. Journal of African Earth Sciences 35, 1-4.

Catuneanu, O., 2003. Sequence Stratigraphy of Clastic Systems. Geological Association of Canada, Short Course Notes Volume 16, 248 pp.3.

Catuneanu, O., 2017. Sequence Stratigraphy; Guidelines for a Standard Methodology. In; Montenari, M. (Ed.), Stratigraphy and Timescales. Elsevier. <https://doi.org/10.1016/bs.sats.2017.07.003>.

Chang, H., Mackenzie, F.T., and Schoonmark, J., 1986. Comparisons between the diagenesis of dioctahedral and trioctahedral smectite, Brazilian offshore basins. *Clays and Clay Minerals*, V. 34, p. 407–423.

Cruz Mercado, M.A., Flores Zamora, J.C; León Ramírez, R., López Céspedes H, Peterson Rodríguez, R.H.; Reyes Tovar, E., et al., 2011. Salt Provinces in the Mexican Portion of the Gulf of Mexico-Structural Characterization and Evolutionary Model. *Gulf Coast Association of geological Societies Transactions*, V.61, pp 93-103.

De Ros, L.F., Morad, S., and Paim, P.S.G., 1994. The role of detrital composition and climate on the diagenetic evolution of continental molasses: evidence from the Cambro-Ordovician Guaritas sequence, southern Brazil. *Sedimentary Geology* 92,197-228.

De Ros L.F, Anjos, S.M., and Morad, S., 1994b. Authigenesis of amphibole and its relationship to the diagenetic evolution of Lower Cretaceous sandstones of the Potiguar rift basin, northeastern Brazil. *Sedimentary Geology*. 88(3-4): 253-266.

Dickinson, W.R., 1979. Mesozoic fore-arc basin in central Oregon. *Geology*, 7, 166-170.

Dickinson, W.R., 1982. Composition of sandstones in Circum-Pacific subduction complexes and fore-arc basins, *American Association of Petroleum Geology Bulletin*.V.66, p. 121-137.

Dickinson, W. R., L. S. Beard, G.R. Bankenridge, J. L. Erjavec, R. C. Ferguson, K. F. Inman, R. A. Knepp, F. A. Lindberg, Morad et al. 1301 and P. T. Ryberg., 1983. Provenance of North American Phanerozoic sandstones in relation to tectonic setting: *Geological Society of America Bulletin*, v. 94, p. 222–235, doi:10.1130/0016-7606(1983)94< 222: PONAPS>2.0.CO;2.

- Elmore, R.D., Engel, M.H., Crawford, L., Nick, K., Imbus, S., and Sofer, Z., 1987.** Evidence for a relationship between hydrocarbon migration and authigenic magnetite. *Nature*, 325, 428–430.
- Ehrenberg, S. N. and P. H. Nadeau., 1989.** Formation of diagenetic illite in sandstones of the Garn Formation, Haltenbanken area, mid-Norwegian continental shelf: *Clay Minerals*, V. 24, p. 233–253, doi:10.1180/claymin.1989.024.2.09.
- Ehrenberg, S.N., 1990.** Relationship between diagenesis and reservoir quality in sandstones of the Garn Formation, Haltenbanken, mid-Norwegian continental shelf. *American Association of Petroleum Geologists Bulletin* 74, 1538–1558.
- Ehrenberg, S. N., 1993.** Preservation of anomalously high porosity in deeply buried sandstones by grain-coating chlorite: Examples from the Norwegian continental shelf: *American Association of Petroleum Geologists Bulletin*, V. 77, p. 1260–1286.
- Escalera-Alcocer, A., and Hernández-Romano, U., 2009.** *Provincias Petroleras de México*. WEC México Schulmberger.
- Felix, M., and Peakall, J., 2006.** Transformation of Debris Flows into Turbidity Currents: Mechanisms Inferred from Laboratory Experiments. *Sedimentology* 53, pp. 107–123.
- Folk, R.L., 1974.** *Petrology of Sedimentary Rocks*. Hemphill, Austin, Texas, p. 182.
- Fraser, H.J., 1935.** Experimental study of the porosity and permeability of clastic sediments: *Journal of Geology*, V. 43, p. 910–1010.
- Gier, S., Worden, R.H., Johns, W.D., and Kurzweil, H., 2008.** Diagenesis and reservoir quality of Miocene sandstones in the Vienna Basin, Austria. *Marine. Petroleum. Geology*. 25,681-695.
- Giles, M.R., and De Boer, R.B., 1990.** Origin and significance of redistributional secondary porosity. *Marine and Petroleum Geology* V.7, p.378-397, doi:10.1016/02648172 (90) 90016-A.

Giles, M.R., Syevenson, S., Martin, S.V., Cannon, S.J.C., Hamilton, P.J., Marshall, J.D., and Samways, G.M., 1992. The reservoir properties and diagenesis of Brent Group: a regional perspective. In: *Geology of Brent Group*. A.C. Morton, R.S. Haszeldine, M.R. Giles and S. Brown (Eds.) Geological Society Special Publication 61, p. 289–327.

Gutierrez-Paredes H.C., Catuneanu O., and Hernández-Romano U., 2017a. Sequence stratigraphy of the Miocene section, Southern Gulf of Mexico. *Marine and Petroleum Geology*, 86, 711-732.

Gutierrez -Paredes H.C., Catuneanu O., and Hernández-Romano U., Miocene depositional environments, processes, and depositional elements in the southern Gulf of Mexico 2017b. *Geological Journal*; 1-30. <https://doi.org/10.1002/gj.2948>.

Guzmán, A.E., and Marquez-Dominguez, B., 2001. The Gulf of Mexico Basin South of the Border: The Petroleum Province of the Twenty-First Century, in M. W. Downey, J. C. Threet and W. A. Morgan, editors, *American Association of Petroleum Geologists*, Tulsa.

Hayes, M.J., and Boles, J.R., 1992. Volumetric relations between dissolved plagioclase and kaolinite in sandstones: implications for aluminum mass transfer in San Joaquin Basin, California. In: Houseknecht, D.W., Pitman, E.D. (Eds.), *Origin, Diagenesis and Petrophysics of Clay Minerals in Sandstones*. SEPM Special Publication, V. 47, pp. 111–123.

Hawladar, H.M., 1990. Diagenesis and reservoir potential of volcanogenic sandstones- Cretaceous of the Surat Basin, Australia. *Sedimentary Geology*. 66(3-4): 181-195.

Hein, J.R., O'Neill, J.R., and Jones, M.G., 1979. Origin of authigenic carbonates in sediment from the deep Bering Sea. *Sedimentology*, 26, 681–705.

Hower, J., Eslinger, E.V., Hower M.E., and Perry, E.A., 1976. Mechanism of burial metamorphism of argillaceous sediments: 1. Mineralogical and chemical evidence. *Geological Society of America Bulletin*, 87, 725 737.

Jeans, C.V., D.S. Wray, R.J. Merriman., and M.J. Fisher., 2000. Volcanogenetic clays in Jurassic and Cretaceous strata of England and the North Sea Basin: *Clay Minerals*, V.35, p.25-55, doi:10.1180/000985500546710.

Ketzer, J.M., Morad, S., and Amorosi, A., 2003. Predictive clay cementation in a sequence stratigraphy framework. In: Worden, R., Morad, S. (Eds.), *Clay Cementation in Sandstones*, International Association of Sedimentologists. Special Publication, V. 34, pp. 42–59.

Khalifa, M., and Morad, S., 2012. Impact of structural setting on diagenesis of fluvial and tidal sandstones: the Bahi Formation, Upper Cretaceous, NW Sirt Basin, North Central Libya. *Marine and Petroleum Geology*. 38, 211-231.

Lander, R. H., and Bonnell, L. M., 2010. A model for fibrous illite nucleation and growth in sandstones. *American Association of Petroleum Geologists Bulletin*, 94, 1161–1187.

Lawton, T.F., Pollock, S.L., and Robinson, R.A.J., 2003. Integrating sandstone petrology and nonmarine sequence stratigraphy: application to the Late Cretaceous fluvial systems of Southwestern Utah, U.S.A. *Journal of Sedimentary. Research*. 73, 389–406.

Love, L.G., 1967. Early diagenetic iron sulphide in Recent sediments of the Wash, England. *Sedimentology*, 9, 327–352.

Lundegard, P.D., 1992. Sandstone porosity loss- a “big picture” view of the importance of compaction: *Journal of Sedimentary Research*, v.62, p. 250-260, doi:10.1306/D42678D4-2B26-11D7-8648000102C1865D.

Luo, J.L., Hall, O., Morad, S., and Ketzer, J.M., 2009. Diagenetic and reservoir-quality evolution of fluvial and lacustrine-deltaic sandstones: evidence from Jurassic and Triassic sandstones of the Ordos Basin, northwestern China. *Journal of Petroleum. Geology*. 32, 79-102.

- Makowitz, A., and Milliken, K.L., 2003.** Quantification of brittle deformation in burial compaction, Frio and Mount Simon Formation sandstones. *Journal of Sedimentary Research* 73, 1007-1021.
- Mansurbeg, H., El-ghali, M.A.K., Morad, S., and Plink-Bjorklund, P., 2006.** The impact of Meteoric water on the diagenetic alterations in deepwater, marine siliciclastic turbidites. *Journal of Geochemical Exploration* 89, 254-258.
- Marchesini, L., Amorosi, A., Cibin, U., Spadafora, E., Zuffa, G.G., and Preti, D., 2000.** Detrital supply versus facies architecture in the Late Quaternary deposits of the south- Eastern Po Plain (Italy). *Journal of Sedimentary Research*. 70, 829–838.
- Meisler, H., Leahy, P.P., and Knobel, L.L., 1984.** Effect of eustatic sea-level changes on saltwater-freshwater in the northern Atlantic coastal plain. *US Geological Survey Water-Supply Paper* 2255, 28.
- Morad, S., 1986.** Pyrite-chlorite and pyrite-biotite relations in sandstones. *Sedimentary Geology*, 49, 177-192.
- Morad, S., Ketzer, J.M., and De Ros, F., 2000.** Spatial and temporal distribution of diagenetic alterations in siliciclastic rocks: implications for mass transfer in sedimentary basins. *Sedimentology* 47, 95–120.
- Morad, S., Al-Ramadan, K., Ketzer, J.M., and De Ros, L.F., 2010.** The impact of diagenesis on the heterogeneity of sandstone reservoirs: a review of the role of depositional facies and sequence stratigraphy. *American Association of Petroleum Geologists Bulletin*. 94, 1267-1309.
- Morán-Zenteno, D.J., Martiny, B., Tolson, G., Solis Pichardo, G., Alba Aldave, L...Romo Silva., 2000.** Geocronología y características geoquímicas de las rocas magmáticas terciarias de la Sierra Madre del Sur: Boletín de la Sociedad Geológica Mexicana.

Nentwich, F.W., and Yole, R.W., 1997. Petrology and diagenetic history of deltaic litharenites, Oligocene Kugmallit sequence, Beaufort-Mackenzie basin, Arctic Canada. *Bulletin. Canadian. Petroleum Geologists* 45, 339-355.

Padilla y Sánchez, R. J., 2007. Evolución Geológica del Sureste Mexicano desde el Mesozoico al Presente en el Contexto Regional del Golfo de México. *Boletín de la Sociedad Mexicana*, tomo LIX, no1, p.19-42.

Pearson, M.J., and Small, J.S., 1988. Illite-smectite diagenesis and palaeotemperatures in northern North Sea Quaternary to Mesozoic shale sequences. *Clay Minerals*, V. 23, p. 109–139.

Perry, E., and Hower, J., 1970. Burial diagenesis in Gulf Coast pelitic sediments. *Clays and Clay Minerals*, V. 18, p. 165–177.

Perry E.A., Jr., and Hower J., 1972. Late-stage dehydration in deeply buried pelitic sediments. *American Association of Petroleum Geologists Bulletin*, 56, 2013 2021.

Pindell J.L., 1985. Alleghenian reconstruction and subsequent evolution of the Gulf of Mexico, Bahamas and Proto-Caribbean, *Tectonics*, V.4, p 1-39.

Pindell, J., and L. Kennan., 2002. Exploration Framework Atlas Series: Volume 4: Mexico and Gulf of Mexico: Tectonic Analysis, Ltd., West Sussex, England, 46 p.

Pirrie, D, Ditchfield P.W., and Marshall J.D., 1994. Burial diagenesis and pore-fluid evolution in a Mesozoic back-arc basin: The Marambio Group, Vega Island, Antarctica. *Journal of Sedimentary Research*. 64(3a): 541-552.

Pittman, E, D., and Larese R, E., 1991. Compaction of lithic sands: Experimental results and applications. *American Association of Petroleum Geologists Bulletin*. 75(8): 1279-1299.

Posamentier, H.W., and Allen, G.P., 1999. Siliciclastic sequence stratigraphy-concepts and application. *Concepts in Sedimentology. Soc. Econ. Palaeontol. Mineralogists*, Tulsa 7, 210.

Posamentier, H.W., and Kolla V., 2003. Seismic geomorphology and stratigraphy of depositional elements in deep-water settings. *Journal of Sedimentary Research*, 73,367-388.

Posamentier, H.W., and Walker, R.G., 2006. Deep-water turbidites and submarine fans. In Posamentier, H. W., and Walker, R.G. (Eds.). *Facies Models Revisited*. Special Publication, SEPM (Society for Sedimentary Geology) no.84, 397-520.

Poursoltani, M.R., and Gibling, M.R., 2011. Composition, porosity, and reservoir potential of the Middle Jurassic Kashafrud Formation, northeast Iran. *Marine and Petroleum Geologists*. 28, 1094-1110.

Primmer, T. J., Cade, C.A., Evans, J., Gluyas, J. G., Hopkins, M. S., Oxtoby, N. H., Smalley, P. C., Warren, E. A., and Worden., R. H., 1997. Global patterns in sandstone diagenesis: their application to reservoir quality prediction for petroleum exploration, in J. A. Kupecz, J. G. Gluyas, and S. Bloch, eds., *Reservoir quality prediction in sandstones and carbonates: American Association of Petroleum Geologists Memoir 69*, p. 61–78.

Ramm, M., 2000. Reservoir quality and its relationship to facies and provenance in Middle to Upper Jurassic sequences, northeastern North Sea. *Clay Mineral*. 35, 77-94.

Reed, J.S., Eriksson, K.A., and Kowalewski, M., 2005. Climatic, depositional and burial controls on diagenesis of Appalachian Carboniferous sandstones: qualitative and quantitative methods. *Sedimentary Geology*. 176, 225-246.

Remy R. R., 1994. Porosity reduction and major controls on diagenesis of Cretaceous-Paleocene volcanoclastic and arkosic sandstone, Middle Park Basin, Colorado. *Journal of Sedimentary Research*. 64(4): 797-806.

Robles Nolasco, J., Pliego- Vidal, E., Toledo-Bante, C., Pimienta-Lugo, M., Ortega-González., Martínez-Pena, B., et al., 2004. Offshore Neogene plays, Salina del Itsmo Basin, southeast of Mexico:

Tulsa, Oklahoma, E.U.A., American Association of Petroleum Geologists, International Conference, October 24-27, Cancun, Mexico, 5p.

Ryu, I., C., Niem and A.R., 1999. Sandstone diagenesis, reservoir potential, and sequence stratigraphy of the Eocene Tyee Basin, Oregon. *Journal of Sedimentary Research*. 69, 384–393.

Salem, A.M., Ketzer, J.M., Morad, S., Rizk, R.R., Al-Aasm, I.S., 2005. Diagenesis and reservoir-quality evolution of incised-valley sandstones: evidence from the Abu Madi gas reservoirs (Upper Miocene), the Nile delta basin, Egypt. *Journal of Sedimentary Research*. 75, 572-584.

Salvador, A., 1987. Late Triassic- Jurassic Paleogeography and Origin of Gulf of Mexico. *American Association of Petroleum Geologists Bulletin*, V. 71, p 419-451.

Salvador, A., 1991. Triassic-Jurassic, in A. Salvador, (Ed.) *The Gulf of Mexico Basin: Geological Society of America, The Geology of North America*, V.J. p131-180.

Sohn, Y.K., 2000. Depositional processes of submarine debris flows in the Miocene fan deltas, Pohang Basin, SE Korea with special reference to flow transformation. *Journal of Sedimentary Research* 70, 491–503.

Spadafora, E., 1996. Composizione e diagenesi delle successioni epiliguri mioceniche dell'Appennino settentrionale. PhD Thesis, Bologna, p. 136.

Talling, P.J., Wynn, L.A, Peakall, J. and Robinson, M., 2004. Beds comprising debrite sandwiched within cogenetic turbidite: Origin and widespread occurrence in distal depositional environments: *Sedimentology*, 51, 163-194.

Talling, P. J., Masson, D. G., Sumner, E. J. and Malgesini, G., 2012. Subaqueous sediment density flows: Depositional processes and deposit types. *Sedimentology*, 59(7), 1937-2003.

Ulmer-Scholle, D.S., Scholle, P.A., Schiber J., Raine R.J., 2014. A color Guide to the Petrography of Sandstones, siltstones, Shales and Associated rocks. American Association of Petroleum Geology Memoir 109.

Van Wagoner, J.C., Mitchum, R.M., Campion, K.M. and Rahmanian, V.D., 1990. Siliciclastic sequence stratigraphy in well logs, cores, and outcrops. American Association of Petroleum Geologists. Methods Exploratory. Series. 7, 220.

Warren, E.A. and Curtis, C.D., 1989. The chemical composition of authigenic illite within two sandstones reservoirs analysed by TEM. Clay Minerals, 24,137-156.

Wilkinson, M., Milliken, K.L. and Haszeldine, R.S., 2001. Systematic destruction of K-feldspar in deeply buried rift and passive margin sandstones. Journal of the Geological Society, London, 158, 675–683.

Wilson, M.J., Wilson, L. and Patey, I., 2014. The influence of individual clay minerals on formation damage of reservoir sandstones: a critical review with some new insights. Clay Minerals. 49, 147–164.

Figures

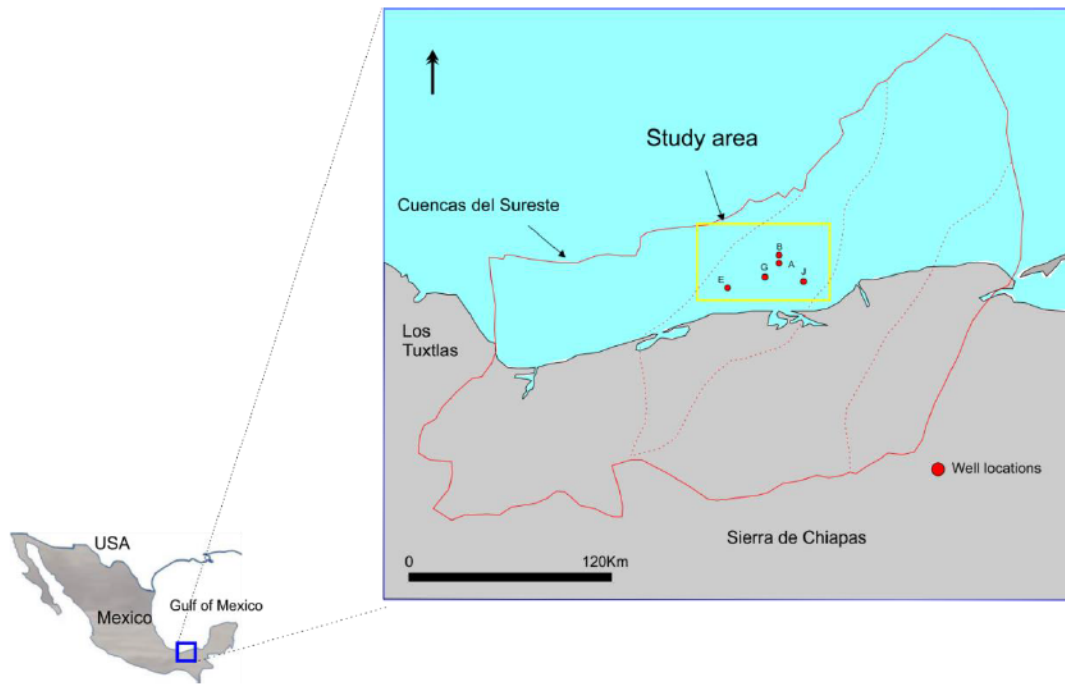


Figure 5.1. Location map of the study area in the Southern Gulf of Mexico.

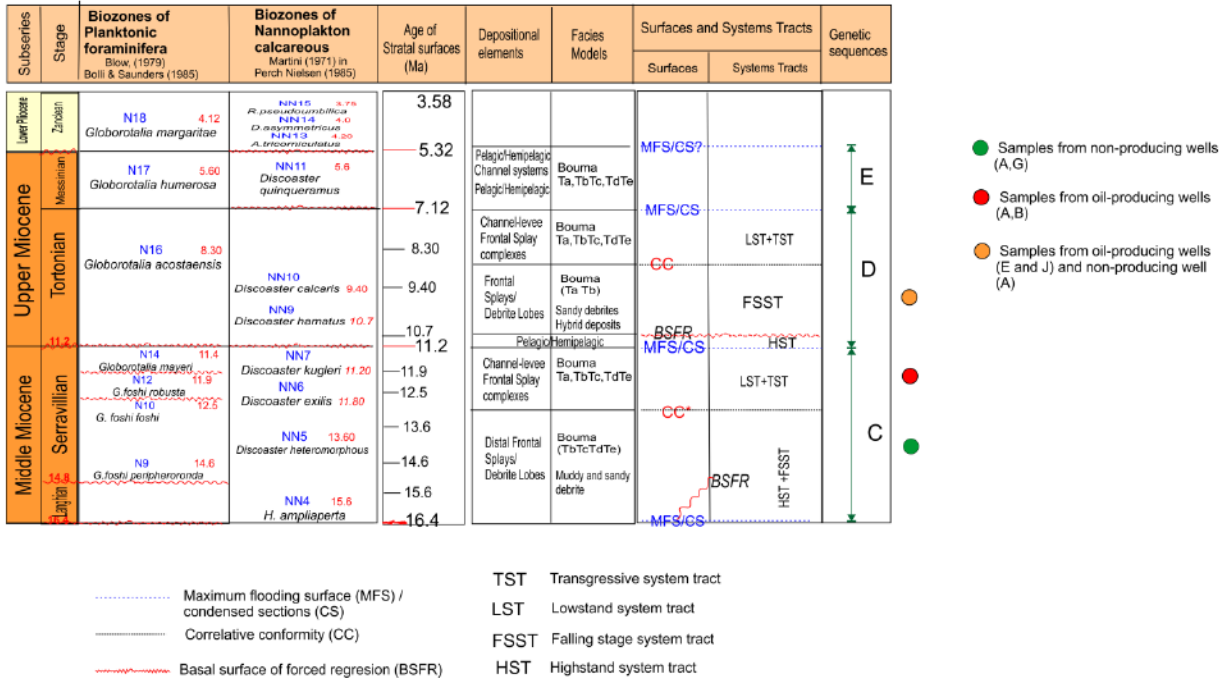


Figure 5.2 Sequence stratigraphic framework for the Miocene sands and sandstones, including samples from oil-producing wells and dry wells. (Modified from Gutierrez-Paredes et al., 2017a).

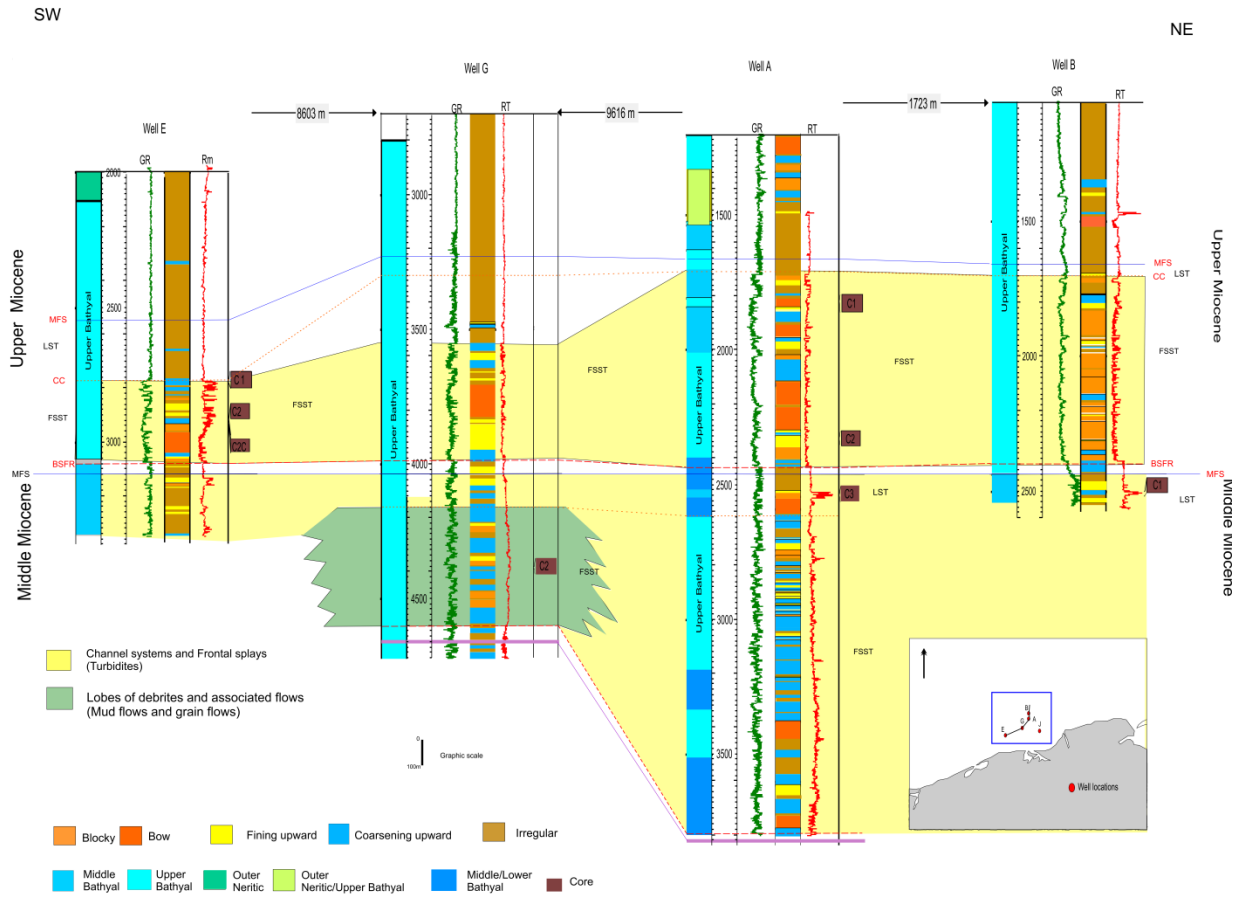


Figure 5.3 Well-log correlation showing the Miocene sandstones placed into the sequence stratigraphic framework proposed for the study area. The sandstone samples were considered from whole cores.

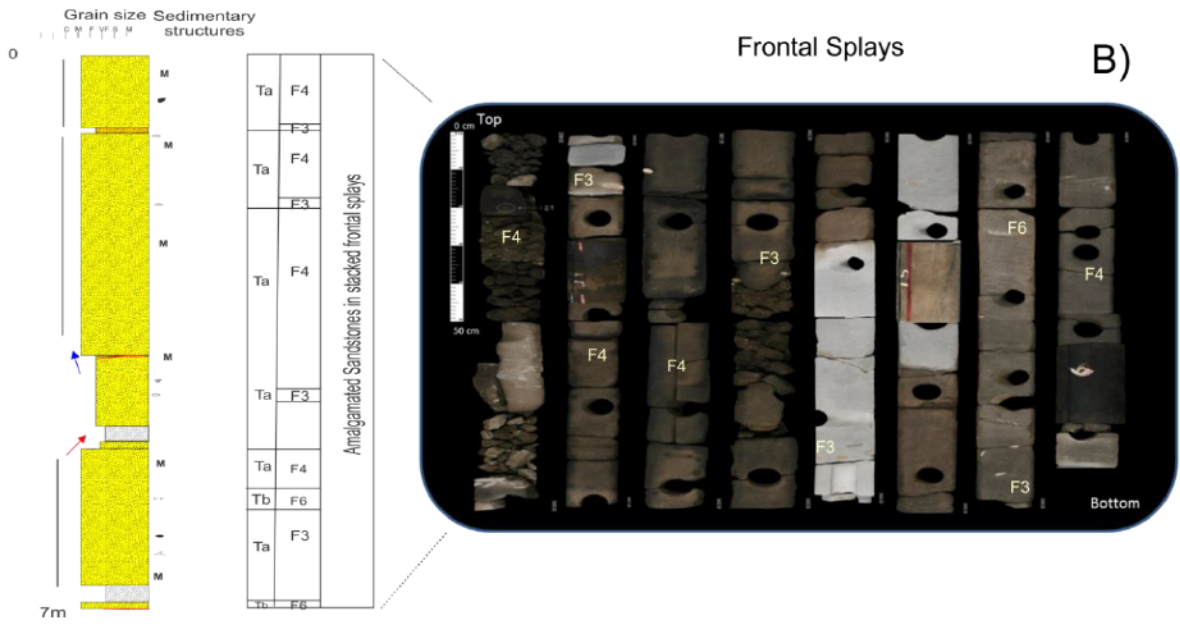
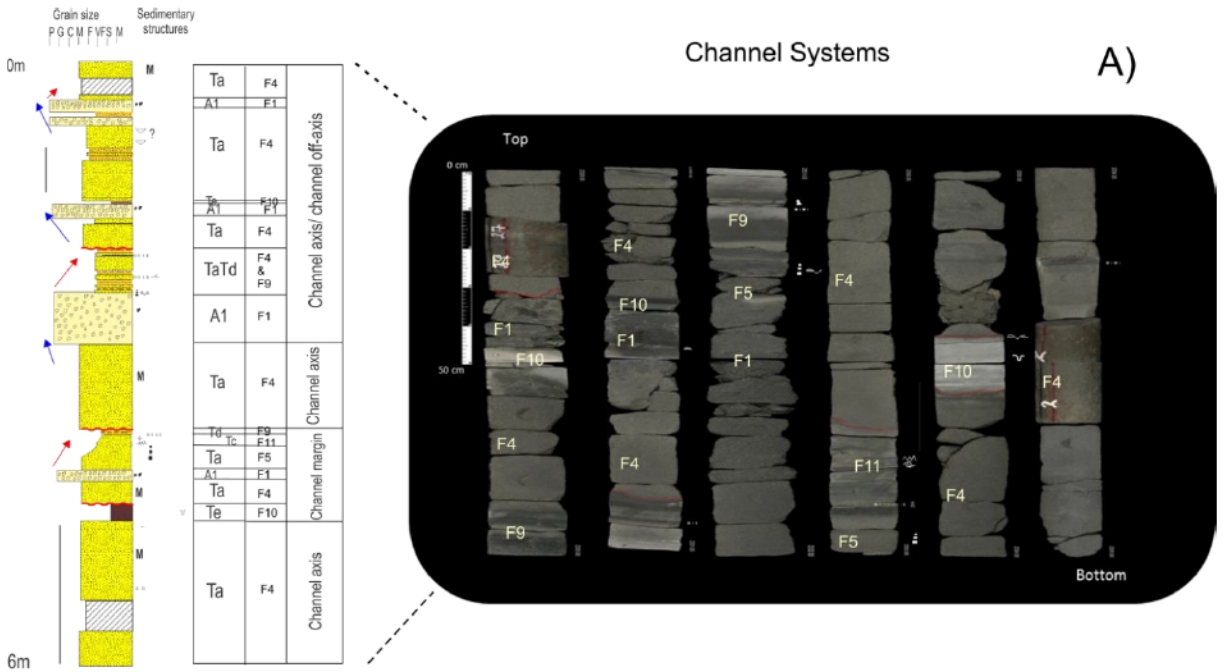


Figure 5.5 Examples of the channel facies association (A) and proximal frontal splay facies association (B). Modified from Gutierrez-Paredes et al., 2017 (b).

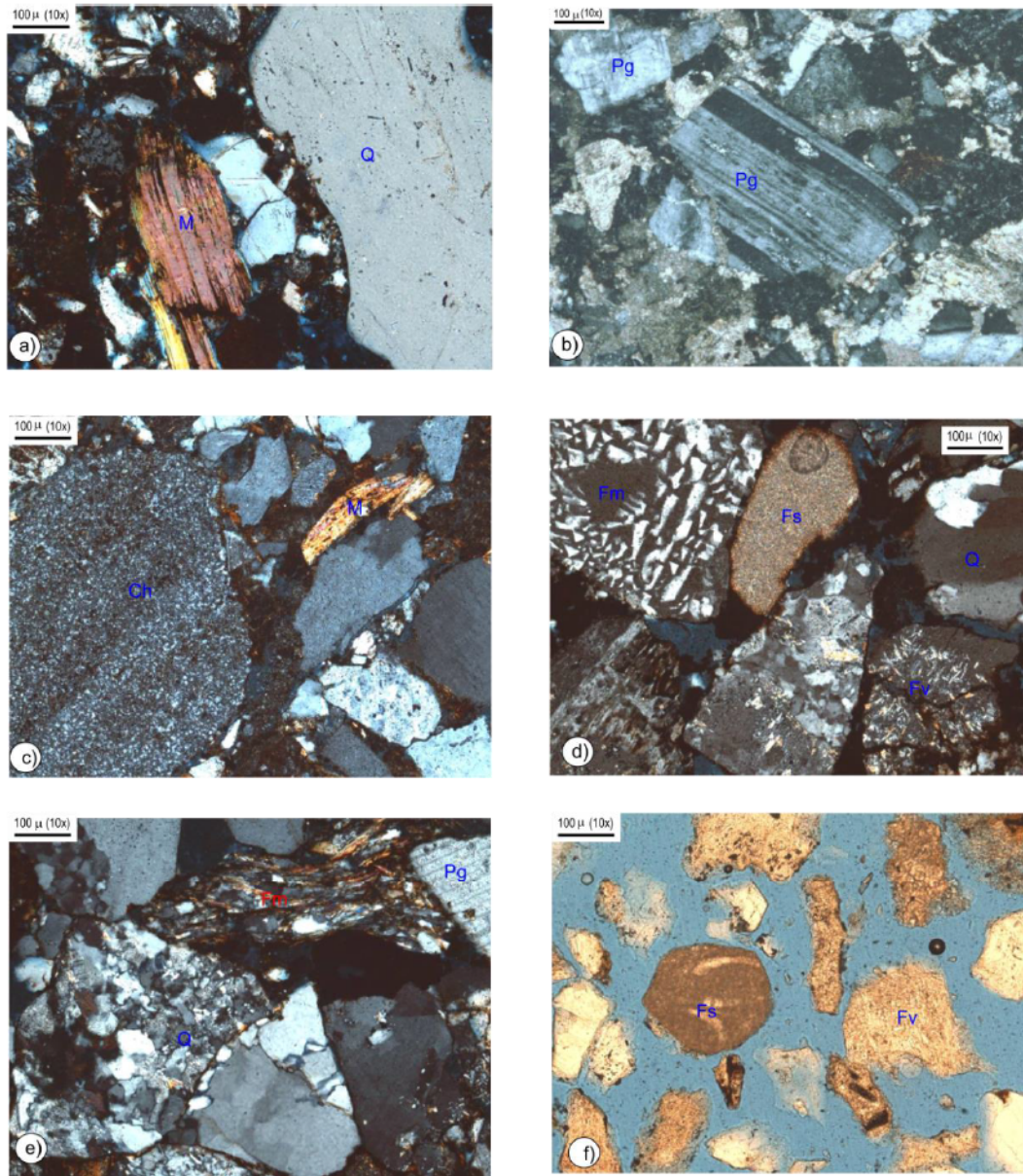


Figure 5.7 Optical micrographs showing examples of the main detrital grains of the Miocene sands in cross-polarized light (a,b,c,d and e) and plane-polarized light (f). a) Monocrystalline quartz and muscovite; b) feldspar crystals; c) chert and mica clasts; d) fragments of granite with myrmekitic texture, carbonate rock, polycrystalline quartz, and altered plagioclases; e) fragments of sandstones and schists, polycrystalline quartz and plagioclases; f) examples of sedimentary rock fragments, quartz grains and volcanic fragments, in which some of the clasts in this photo have been partially dissolved and altered. Q=quartz, M= micas, Ch=chert, Pg= plagioclase, Fs= sedimentary rock fragments, Fv= volcanic rock fragments, Fm= metamorphic rock fragments.

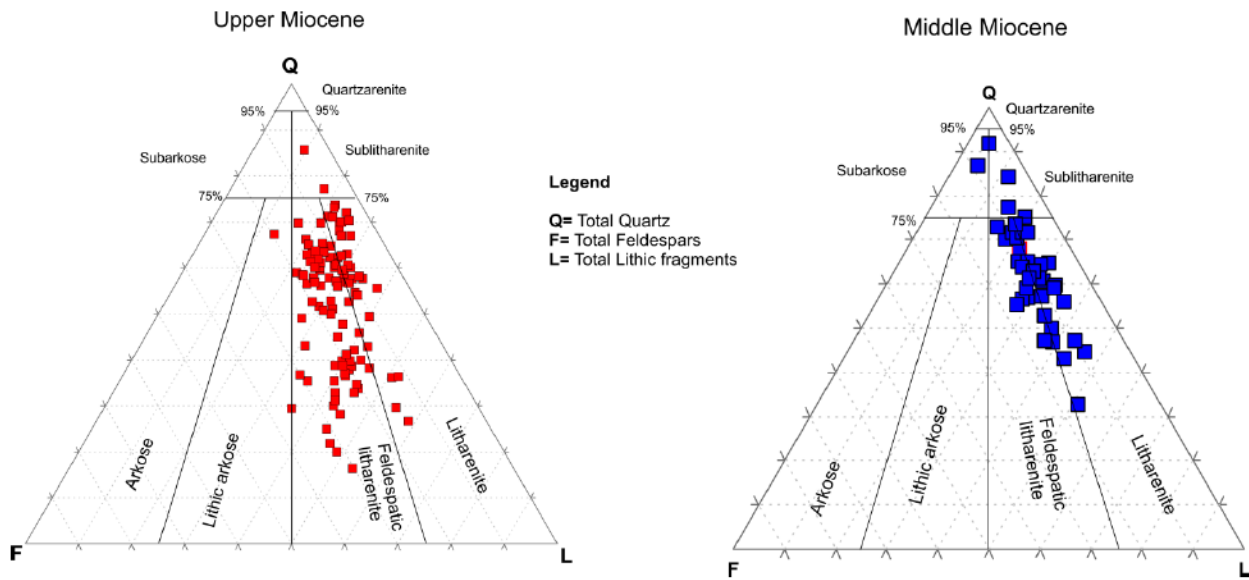


Figure 5.8 Detrital compositions of the Miocene sandstones (plotted using the classification of Folk, 1974). The average values of the detrital compositions of the sandstones from both sequences are quite similar (that of the middle Miocene is $Q_{57}F_{10}L_{33}$ and that of the upper Miocene is $Q_{51}F_{16}L_{33}$), only a small increase in the feldspar content in the sandstones of the upper Miocene sequence is observed.

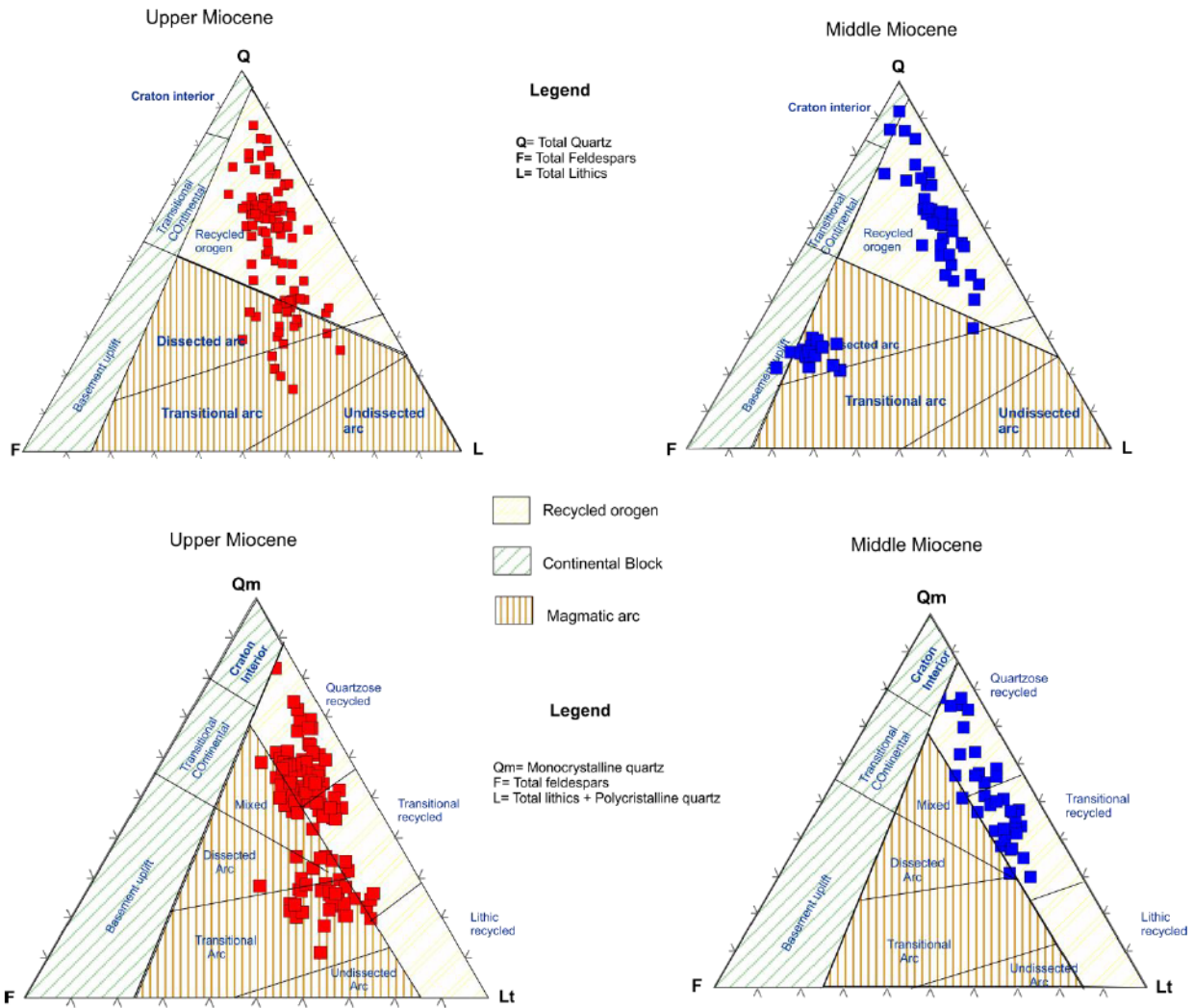


Figure 5.9 Sandstone modal data plotted in ternary plots to determine sediment provenance, using QFL plots showing provenance fields established by Dickinson et al., 1983.

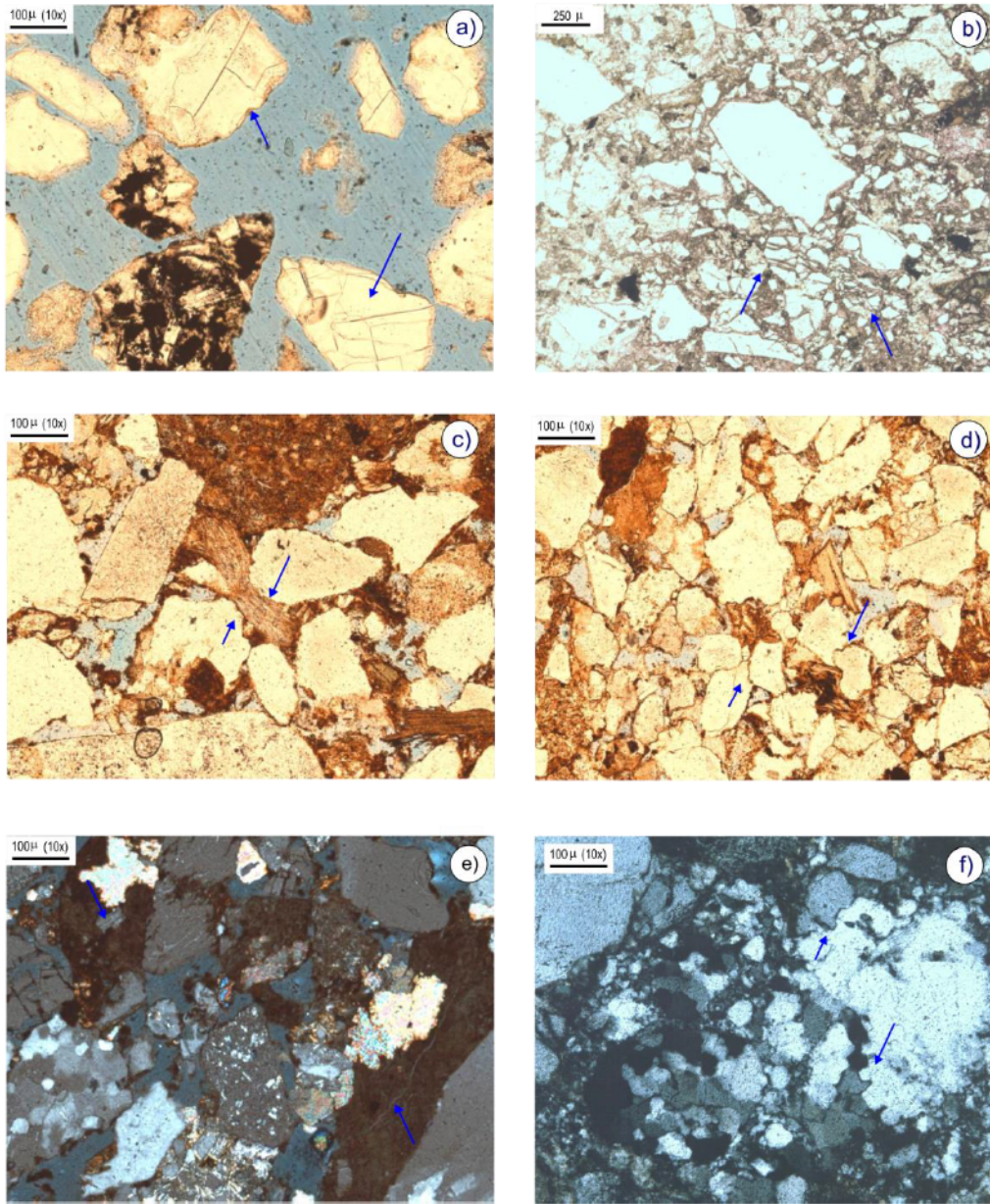


Figure 5.10 Optical micrographs showing examples of mechanical and chemical compaction in cross-polarized light and plane-polarized light. a) Floating grains, some of which contain fractures due to brittle deformation; b) crushing along grain contacts in which small particles have spalled; c) clays squeezed by ductile deformation between more rigid grains are also observed as punctual and long contacts between grains; d) grains showing concavo-convex and sutured contacts; e) flowage of ductile shale clasts in surrounding pore space, producing a pseudomatrix; f) chemical compaction as exhibited by sutured contacts.

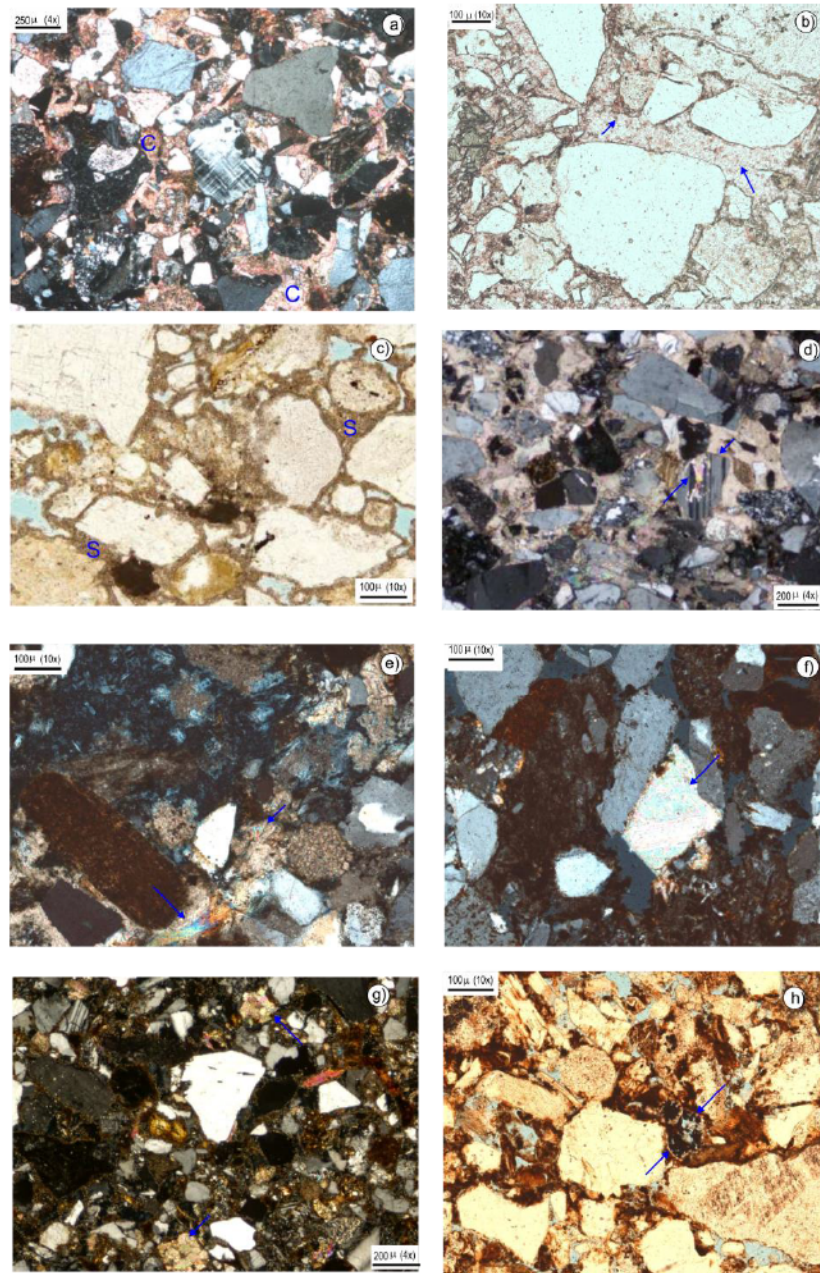


Figure 5.11 Optical micrographs showing examples of carbonate cements and other diagenetic events. a) Calcite cement in cross-polarized light; b) non-ferroan calcite cement with displacive texture, stained with alizarin in plane-polarized light; c) siderite forming grain-coating and pore-filling cements in plane-polarized light; d) calcitization of feldspars grains in well-cemented sandstones in cross-polarized light; e) calcite cement featuring recrystallization, low intergranular porosity due to cementation, and secondary porosity caused by the dissolution of grains; f) patches of calcite cement with poikilotopic texture; g) partial dolomitization; and h) pyrite filling the void spaces in foraminifera. C= calcite cement S= siderite cement.

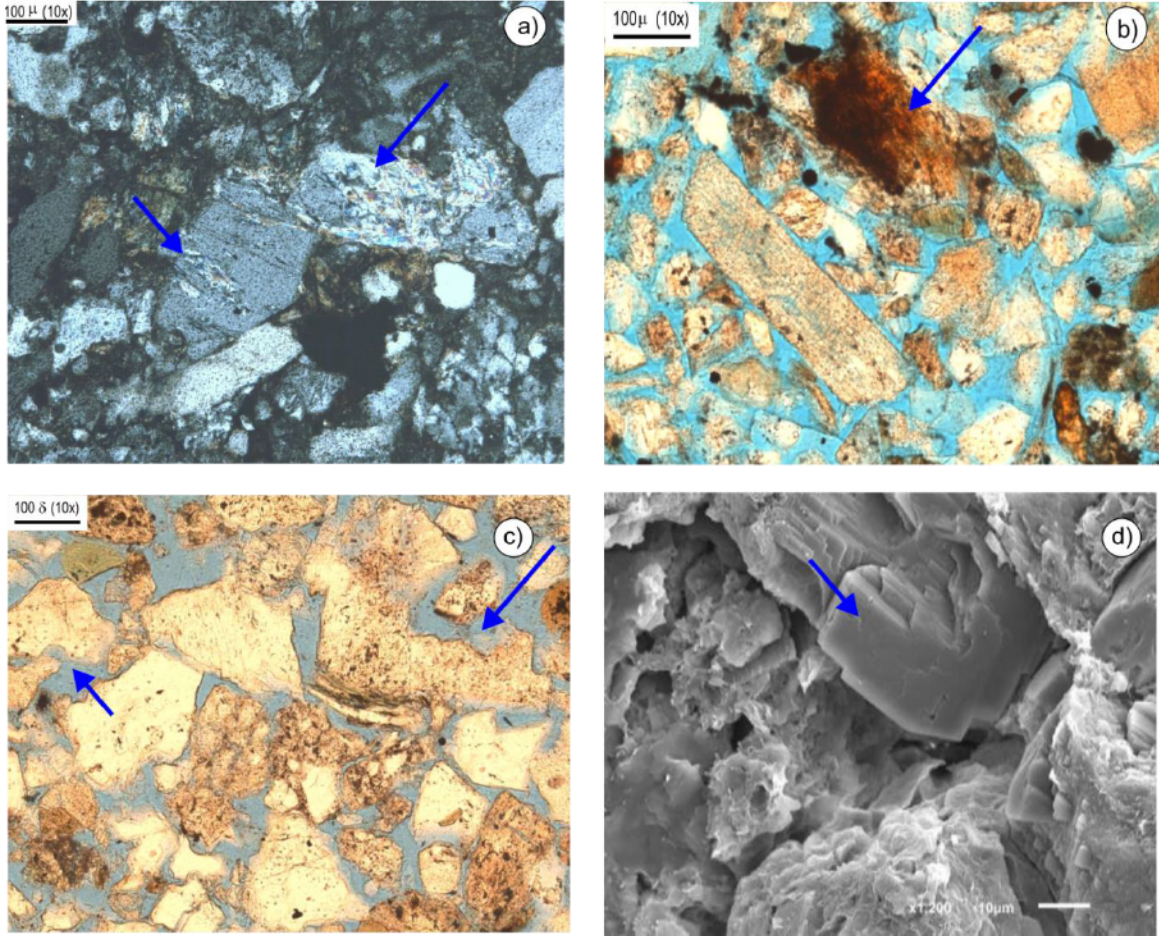


Figure 5.12 Examples of feldspar alteration and dissolution of unstable grains and cements, in plane-polarized light. a) feldspar alteration by sericite photos taken in cross-polarized light; b) feldspar alteration by kaolinite, photo taken in plane-polarized light; c) partial dissolution of grains and enhancement of pore spaces due to dissolution; d) SEM photograph showing the dissolution of feldspars.

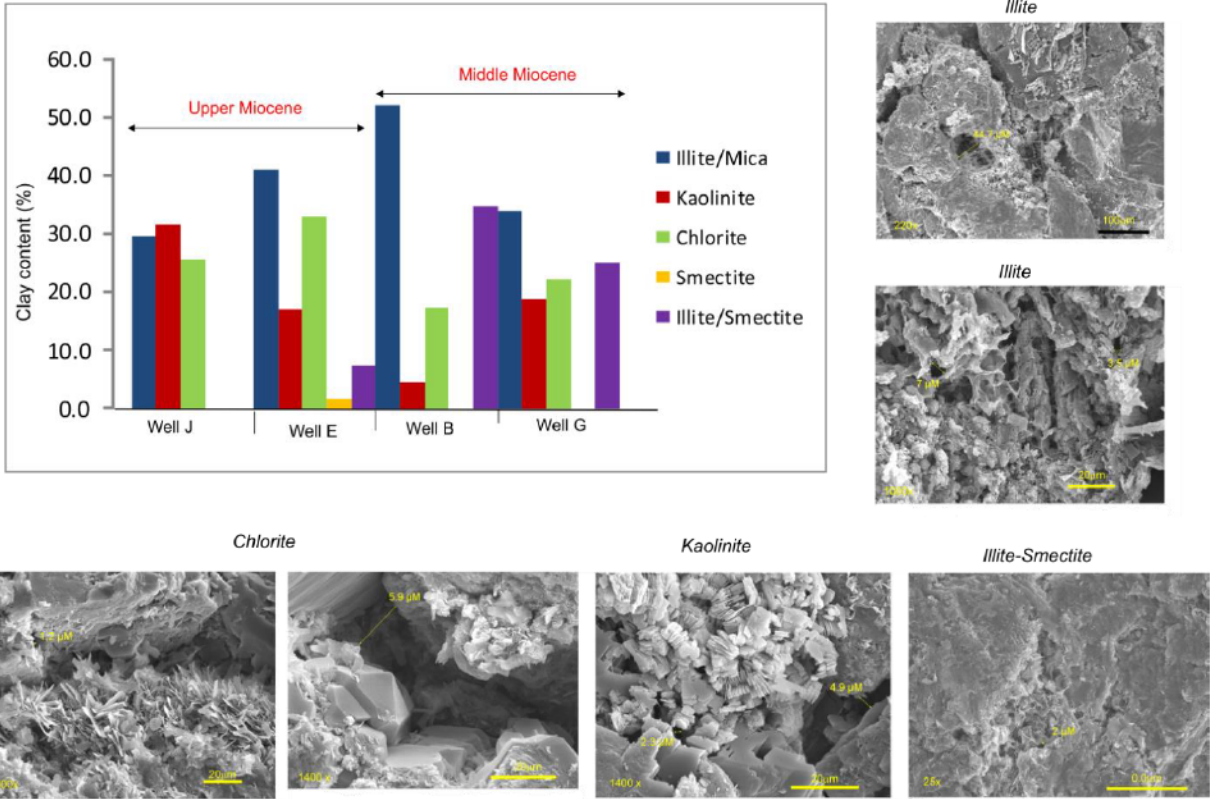


Figure 5.13 Content and SEM photographs showing the different types of clays present in the Miocene sandstones.

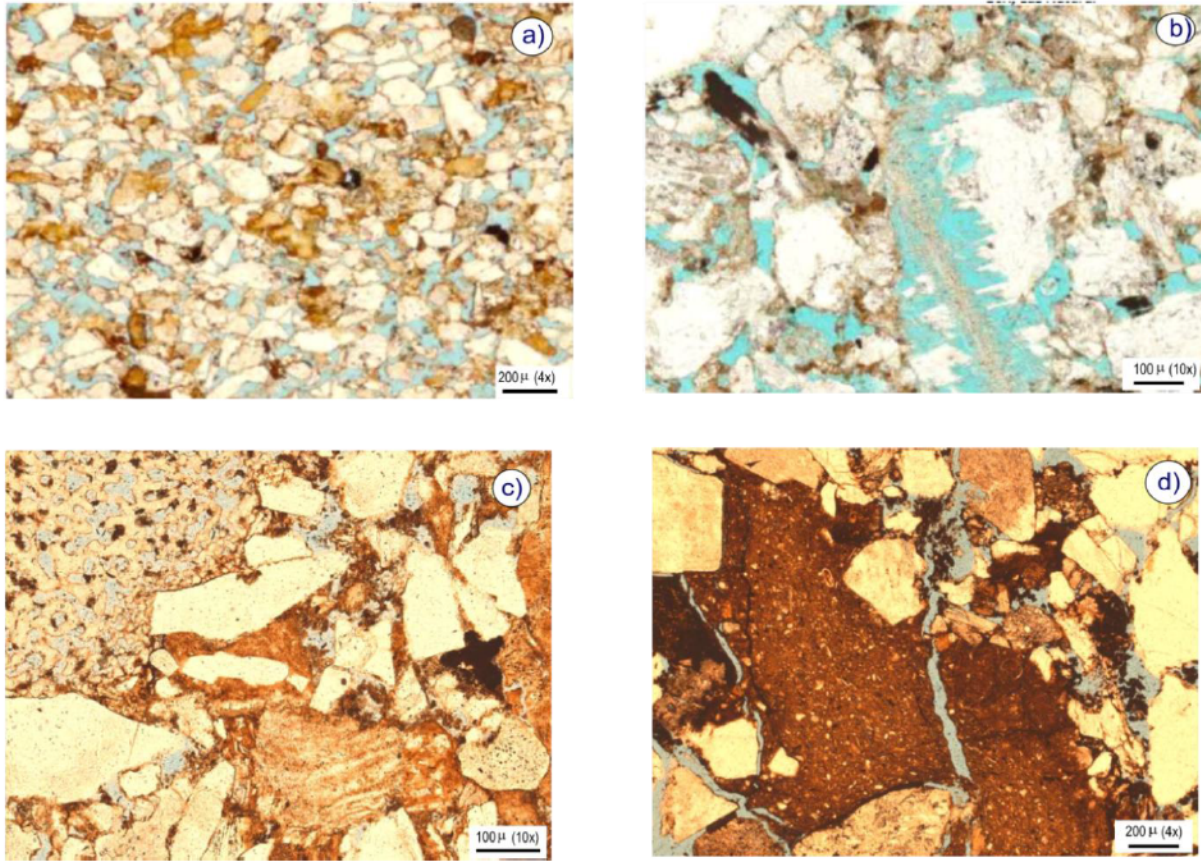


Figure 5.15 Types of porosity present in the Miocene sandstones of the study area. a) Intergranular; b) secondary porosity due to grain dissolution; c) Intragranular by the dissolution of bioclasts; and d) fracturing.

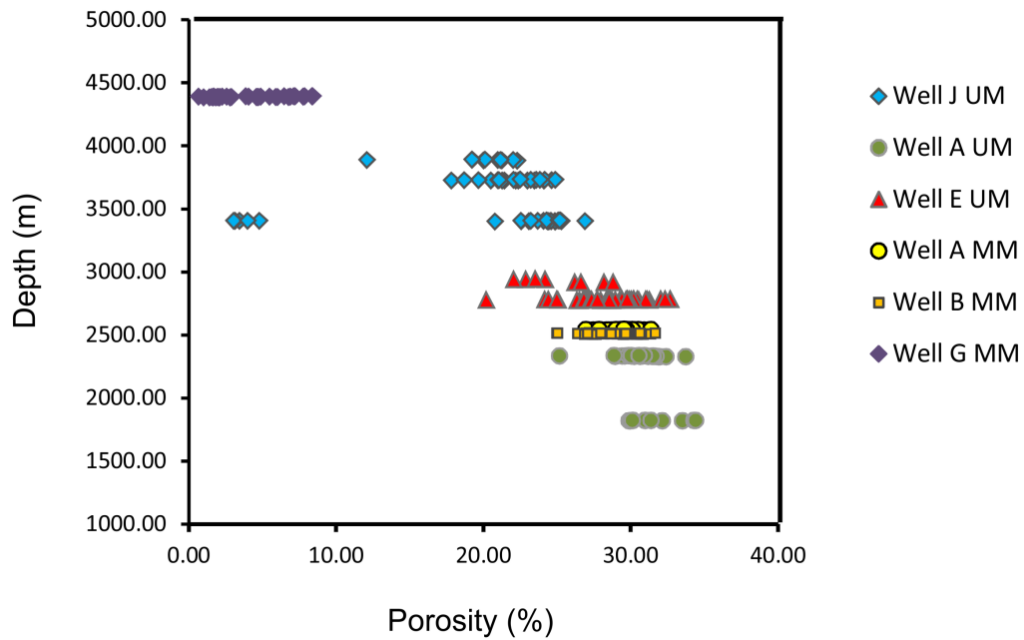


Figure 5.16 Core-analysis porosity values versus burial depth of Miocene sandstones from the southern Gulf of Mexico. These data show a general trend of gradually decreasing porosity with increasing depth. However, the effect of burial depth in the porosity is overcome by other factors such as depositional facies and diagenetic events. In this graph, UM refers to the samples of the upper Miocene and MM to the samples of the middle Miocene.

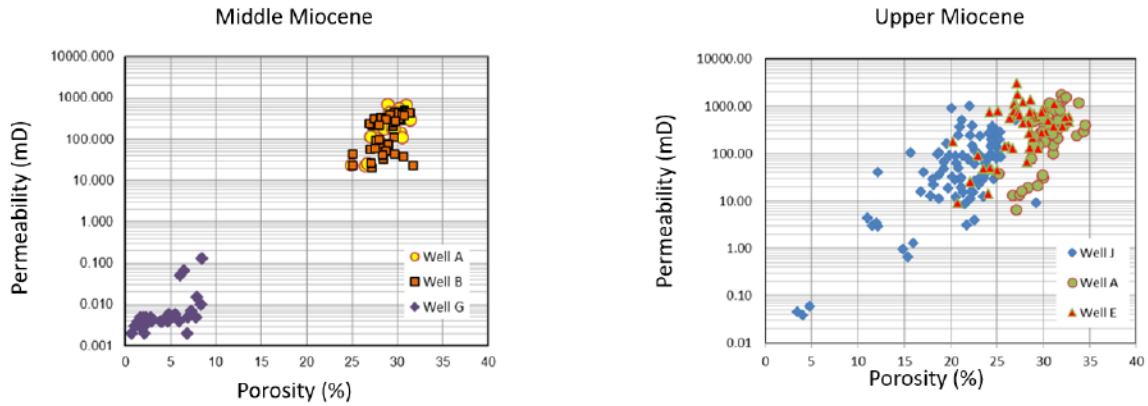


Figure 5.17 Permeability versus porosity plot for Miocene sandstones from the southern Gulf of Mexico. It should be noted that the upper Miocene sandstones have the best quality reservoir rocks, with values of permeability that are greater than 1000 mD.

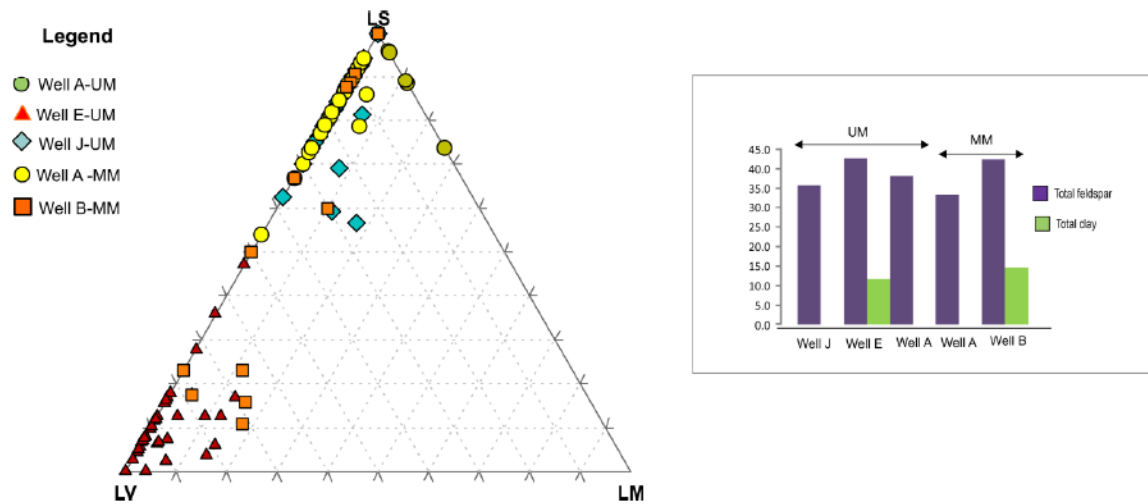


Figure 5.18 LSLVLM plot of the Miocene sandstones shows two sources of sediment: one is a sedimentary source, and the second is a volcanic source. The graph on the right shows that the wells E and B from a volcanic source, or reflecting a volcanic influence, contain higher contents of total feldspar and total clay than the wells A and B from the sedimentary source.

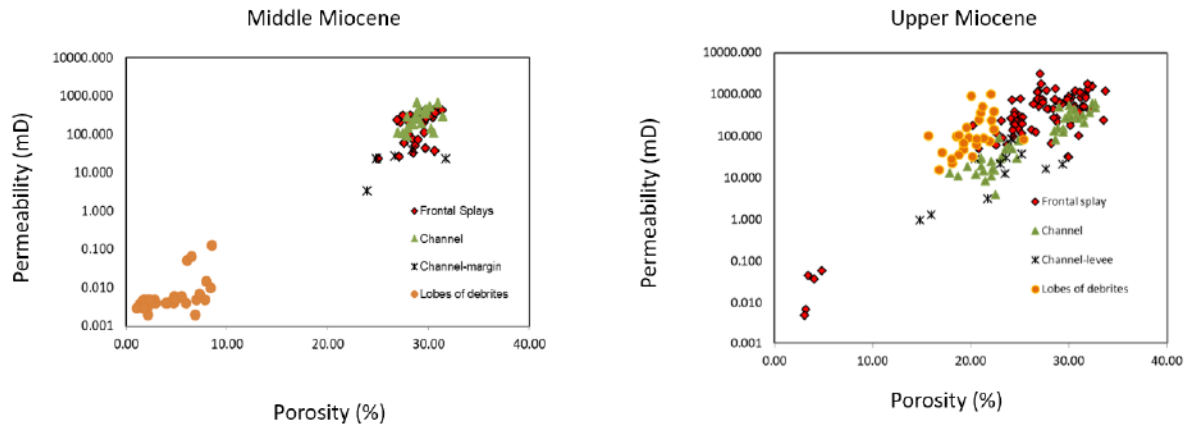


Figure 5.19 Permeability versus porosity plot for Miocene sandstones from the southern Gulf of Mexico. In terms of depositional facies, sandstones deposited in frontal splays and channel fills record the best reservoir quality. In the upper Miocene frontal splays, the low values of porosity and permeability are due to the presence of calcite cement.

Wells, depths (m) n= number of samples	Detrital components										Age
	Monocrystalline Quartz	Polycrystalline Quartz	K-Feldspar	Plagioclase	Chert	Igneous Fragments	Metamorphic Fragments	Sedimentary fragments	Micas	Others	
A depth range:2536-2544 n=8	30.00	4.67	6.1	6.22	4.44	3.89	0.50	13.33	4.66	3.11	Middle Miocene
B depth range:2503-2511 n=14	29.86	2.33	1.3	4.71	2.08	7.23	2.60	5.92	6.29	1.63	Middle Miocene
A depth range:1815-1820 n=11	47.82	5.18	0.0	6.09	5.45	1.30	0.00	16.45	5.09	2.45	Upper Miocene
E depth range:2326-2335 n=8	41.13	6.75	2.0	10.00	4.00	2.25	2.60	24.38	3.00	2.00	Upper Miocene
E depth range 2774-2776 n=8	16.50	3.38	4.5	15.25	0.00	27.63	3.00	2.63	1.125	1.00	Upper Miocene
J depth range 2934-2940 n=29	18.41	7.90	6.3	6.90	1.00	22.00	1.40	4.72	1.88	2.33	Upper Miocene
J depth range: 3720-3731 n=13	40.85	3.00	0.8	7.23	2.15	7.23	2.62	21.62	3.54	1.75	Upper Miocene
J depth range: 3882-3890 n=15	41.13	4.20	0.0	10.20	2.63	3.33	3.00	15.73	2.00	2.21	Upper Miocene

Table 5.1 Summary of the average composition of detrital components of the middle and upper Miocene sandstone.

CHAPTER 6

Final remarks, conclusions and recommendations

6.1 Final remarks

The Miocene deep-water system represents a changing sedimentary system that resulted from the interaction of three main driving forces (eustasy, tectonics and sediment supply). In general, this integrative study reveals that the relative sea-level curve matches the long-term trend of the global eustatic chart of Haq et al. (1988) with one major drop in relative sea-level (lasted for 6 million years) and three minor drops (lasted > than 2 million years) (Fig. 4.3). This reveals that local tectonism also played an important role in controlling the timing of sequences, which explains the departures from the predictions of the global cycle chart, which can be observed at smaller scales. Tectonics was one of the most important controlling factors for this deep-water system because it influences different characteristics: 1) Propitiates the slope destabilization by contraction, extension and salt tectonics; 2) Modifies the configuration of the receiving basin and, 3) controls the sediment pathways.

Also, the petrographical trend exhibited that the sandstones of the study area display an immaturity. This trend is very consistent in all the discrimination diagrams (QFL, QmFLt) of the Figs. 5.8 and 5.9 which indicated that the sediment sources evolved from a recycled orogen to a magmatic arc. So, for the middle Miocene sandstone, the sediment source was the Chiapas massif and the Chiapas fold belt, while for the late Miocene the sediment source was mainly the Chiapanecan volcanic arc. Furthermore, the mineralogical evidence collected from the petrographic analysis offer important clues. First, the sandstones are predominantly composed of

angular and poorly sorted detrital grains. Second, the sandstones contain abundant minerals and rocks that are unstable under subaerial conditions (volcanic fragments, K-feldspars, micas). These pieces of evidences suggest 1) short residence times in fluvial or alluvial settings, 2) short distances and /or rapid sediment delivery from source to sink, and 3) high relief.

Finally, the variations in the architecture of the Miocene deep-water depositional system suggest significant changes in the basin morphology and fluctuations in the amount and type of sediment. Most of the cycles in these sequences are sand-prone. In this way, high rates of sediment supply during the relative sea-level falls or tectonic activity are inferred, but the sequences also represent the relative sea-level rise. Based on the integrated analysis of the data, 5 complete cycles of sedimentation were recognized: 1) **the middle Oligocene to lower Miocene sequence A**. This deep-water system was deposited on the basin floor during a moderate tectonic activity. Seismic interpretation reveals MTC and turbidite deposits. This MTC evidenced the instability of the slope due to a combination of eustasy and tectonics. The study area was confined at this time; thus, the composition of this deposit was controlled by the sediment that fallen. The sediment pathways for the large depocenters came from the SE and NE; the structural highs located to the south impede the entry of sediments from the S and SW. 2) **The lower Miocene sequence B**. This deep-water system was deposited on the basin floor during tectonic quiescence. Seismic attribute map reveals frontal splays and low sinuosity channels with a main orientation from SE to NW, the orientation of this depositional systems was controlled by the confinement of the basin, so the main sediment entry came from the SE. 3) **The middle Miocene sequence C** was deposited in the slope during a high tectonic activity. Seismic attribute maps exhibited to the base of the sequence frontal splays (deposited in the FSST) with a SE-NE orientation, the lobate and rounded shapes evidenced the confinement of the basin which

influenced the entry of sediments from the SE. The main source of these sandstones was the Chiapas fold belt and the Chiapas Massif. To the top of the sequence there is a major influence of a volcanic source so at this time the Chiapanecan volcanic arc was the other source of sediments. Meandering channels (oriented from the SE to NW) and frontal splay complexes (oriented from the SE to NW) predominated at the top of this sequence (deposited in lowstand system tract). Massive sandstones are the main lithofacies for the depositional elements of this sequence, therefore they are excellent reservoirs. 4) **The upper Miocene sequence D** was deposited in the slope, when the area was less confined; as a result, the depositional elements (levee-channels and frontal splay complexes) have an orientation from the south to the north. The petrographic analysis suggested to different types of sources one from the Chiapas fold belt and the second one from the Chiapanecan volcanic arc. The reservoirs are placed in the FSST and are composed by massive sandstones. 5) **The upper Miocene sequence E** was deposited in the slope and is mainly mudprone. Seismic attribute maps exhibited leveed channels.

6.2 Conclusions

The main factors controlling the distribution, geometry and quality of the Miocene reservoirs rocks were retrieved through detailed stratigraphic and facies analyses combined with seismic facies and 3D seismic-derived plan-view images.

The first discovery was made while doing the interpretation of the depositional environments. Paleobathymetric analysis revealed the following results: 1) the general basinward movement of the paleotopography through the time, which reflects the overall progradation of the continental margin; 2) the fluctuations in the paleobathymetric conditions illustrated the

effects of tectonics; as a result, areas with abrupt bathymetric variations are attributable to syndepositional tectonics more than variations in the sea level.

Second, the description of the main sedimentary facies and the identification of the depositional process were critical to calibrate the depositional elements interpreted in plan-view maps obtained from seismic attributes; as well as to define the types of sediment gravity flows acting during the Miocene in the study area. The sediment gravity flows played a significant role in determining the types of depositional elements; these could be a single leveed channel or a network of shallow distributary channels dominated. The suite of depositional elements associated with each delivery mechanism was unique and predictable, thus providing insights into the stratigraphic reservoir's architecture. For example, sediment gravity flows prefer bathymetric lows, the form of sand-prone deep-water depositional elements closely follows the shape of sea-floor topography; this was the case of the ponded lobes interpreted at the base of the middle Miocene, whose shape was controlled by the confinement of the basin at that time.

Third, we established that the sequence stratigraphic framework for the study area was an important factor when predicting the lithofacies distribution and when defining five complete sedimentation cycles; each cycle included 3 recognizable events, the onset of relative sea-level fall, the end of relative sea-level fall, and the end of transgression. In general terms, each genetic sequence started with hemipelagic and pelagic sediments within condensed sections above maximum flooding surfaces. They were followed by the deposits of relative sea-level fall, which are represented by mass-transport deposits, debris flows and turbidites; all deposited in bathyal paleobathymetric conditions. This sequence stratigraphic framework helped convey that the reservoir sands, during the middle Miocene, were deposited in the lowstand systems tract and

that the best reservoir sands, during the upper Miocene were deposited during the falling-stage systems tracts.

Fourth, we discussed the influence of structural features on the depositional elements and their distribution. Establishing the correct timing of this interaction was essential in predicting the depositional response to active deformation of the slope. The interplay between sedimentation and tectonics played a key role in controlling sediment trapping and spatial distribution, as well as the sediment pathways on the slope. The halokinesis also modified the paleotopography of the slope and the basin floor, mainly creating the accommodation space for sediment deposition. In the study area the topographically complex slope was the primary factor that governed the gravity flow sedimentary processes and its distribution. Depositional systems on submarine slopes and basin floors were dominated by the deposits of sediment gravity flows especially turbidites and mass-transport deposits, which are highly sensitive to sea floor topography.

Fifth, in the study area, the sea floor topography was also affected by mass-transport deposits (MTD) during the Oligocene and lower Miocene; the presence of these MTD affected the sediment pathways on the slope and the distributions of zones of erosion, bypass and deposition from turbidity currents, the latter occurring with relative bathymetric lows. The location and geometry of depositional systems were dominated by the types of sediment gravity flows. Consequently, turbidite reservoir distribution and geometry on the slope and rise are often significantly affected by subjacent MTDs. The mass-transport deposits in this area also created accommodation space and were important for the sequestration of sediment on the slope at the top of the lower Miocene.

Sixth, the reservoir quality of the Miocene sands was controlled by a combination of depositional facies, sand composition and diagenetic factors (compaction and cementation). However, depositional facies exerted a major control on the reservoir quality compared to sand composition; similarly, compaction was more important than cementation in reducing porosity, in some cases compaction was eventually stopped. There are other diagenetic factors that have a positive impact on porosity such as dissolution and the formation of early cements (calcite and clays) that hinders burial compaction.

6.3 Recommendations

The gravity flow deposition processes interpreted from 3-D seismic data are a powerful tool to predict the distribution of gravity flow deposits and sediment quality. Therefore, this type of analysis should be done in areas with rich drilling data, and further study should be done on the genetic type, as well as the distribution of microfacies within the gravity flow depositional system.

When the information allows, it is highly recommended to map the trajectory patterns of the shelf-edge clinoforms set to predict the sandstones below the shelf edge. Such analysis yields the prediction of the presence or absence of sands that have bypassed the shelf break to produce deepwater turbidite accumulations.

This workflow can be applied in mature and frontier areas. It was helpful in the prediction of facies distribution and the internal architecture of the reservoirs. Especially if the depositional elements are identified, since they vary in a predictable and systematic manner. The depositional elements are the fundamental control on reservoir geometry and the distribution of pay and non-pay, which in turn, impacts permeability architecture and production performance.

In exploration and appraisal, an awareness of the different depositional elements and their relationship to sand thickness and net reservoir distribution will aid in the risk assessment of the hydrocarbon prospects. In studies of characterization and reservoir management detailed understanding of the organization of the reservoir facies with the depositional elements will provide the basic framework for understanding reservoir quality distribution.

The starting point for all these studies lies in the careful description, analysis and facies interpretation from core data. These interpretations can be used to calibrate wireline logs and aid in the interpretation of rock properties from seismic data.

It is also important to examine the mass-transport deposits (MTD) in detail, because hydrocarbon reservoirs, in many slope settings, are controlled by the accommodation related to MTD topography. At the exploration scale, the entire shelf margin and slope depositional systems may be contained within the scars evacuated on the upper slope by mass failure, whereas at the production scale, the rugosity on the top of MTDs creates a widespread potential for stratigraphic trapping. The location, geometry, and property distribution of such reservoirs is closely controlled by the interaction of turbidity currents with the topography, therefore, an understanding of the processes and their impact on slope stratigraphy is vital to reservoir's architecture prediction.

Reservoir quality is one of the key controls on prospectivity during petroleum exploration and one of the critical uncertainties to consider in frontier areas. For that reason, it is important to continue and complete this study with the new information from recently drilled wells to confirm the depositional model on what controls the reservoir quality of Miocene's reservoirs sands and to evaluate the economic viability of future petroleum discoveries in the study area.

REFERENCES

- Abreu, V., Sullivan, M., Pirmez, C., and Mohrig, D., 2003.** Lateral Accretion packages (LAPs): an important reservoir element in deep water sinuous channels. *Marine and Petroleum Geology* 20, 631-648.
- Altaner, S.P., and R.E. Grimm., 1990.** Mineralogy, chemistry, and diagenesis of tuffs in the Sucker Creek Formation (Miocene), Eastern Oregon: *Clays and Clay Minerals*, V.38, p. 561-572, doi:10.1346/CCMN.1990.0380601.
- Alves, T. M., Cartwright, J., and Davies, R. J., 2009.** Faulting of salt-withdrawal basins during early halokinesis: effects on the Paleogene Rio Doce Canyon system (Espírito Santo Basin, Brazil). *AAPG Bulletin*, 93, 617–652.
- Al-Ramadan, K., Morad, S., and Proust, J.N., 2005.** Distribution of diagenetic alterations within the sequence stratigraphic framework of shoreface siliciclastic deposits: evidence from Jurassic deposits of NE France, *Journal of Sedimentary Research* 75, 943-959.
- Amorosi, A., and Zuffa, G.G., 2011.** Sand composition changes across key boundaries of siliciclastic and hybrid depositional sequences. *Sedimentary Geology* 236,153-163.
- Amy, L.A., Talling, P.J., Peakall, J. Wynn R.B., and R.G. Arzola, Thynne, 2005.** Bed geometry used to test recognition criteria of turbidites and (sandy) debrites. *Sedimentary Geology* 179. 163-174.

Amy, L., Talling, P.J., Edmonds, V.O., Sumner, E.J., and Leseuer, A., 2006. An experimental investigation of sand-mud suspension settling behaviour: implications for bimodal mud contents of submarine flow deposits. *Sedimentology*, 53, 1411–1434.

Ángeles-Aquino, F., Reyes-Núñez, Quesada-Muñeton and Meneses Rocha, J.J., 1994. Tectonic Evolution, Structural Styles and Oil habitat in Campeche sound, Mexico: Gulf Coast Association of geological Societies Transactions. V 44, pp 53-62.

Anjos, S.M.C., De Ros, L.F., and Silva, C.M.A., 2003. Chlorite authigenesis and porosity preservation in the Upper Cretaceous marine sandstones of the Santos Basin, offshore eastern Brazil. *International Association of Sedimentology*. 34(2): 291-316.

Aquino-Lopez J.A., 2004. Sureste Basin, Mexico and Associated Sub-basins: An update and Future Potential. AAPG International Conference: October 24-27; Cancun México.

Armentrout, J. M., 1996. High resolution sequence biostratigraphy: examples from the Gulf of Mexico Plio-Pleistocene. Howell J.A and Aitken J.F. (Eds.), *High Resolution Sequence Stratigraphy: Innovations and Applications*, Geological Society Special Publication No.104, 65-86.

Aubry, M.P., 1984-1987, 1993, 1997 and 1999. Handbook of Cenozoic Calcareous Nannoplankton. *Micropaleontology Handbook series*. Vols. I, II, III, IV and V.

Baas, J.H., Best, J.L., and Peakall, J., 2011. Depositional processes, bedform development and hybrid flows in rapidly decelerated cohesive (mud-sand) sediment flows. *Sedimentology*, 58, 1953–1987.

Bagnold, R.A., 1954. Experiments on a gravity-free dispersion of large solid spheres in Newtonian fluid under shear. *Proceedings of the Royal Society of London, A*, 225, 49-63.

Bannerjee, I., 1977. Experimental study on the effect of deceleration on the vertical sequence of sedimentary structures in silty sediments. *Journal of Sedimentary Petrology*, 47, 771–783.

Beard, D.C., and Weyl, P.K., 1973. Influence of texture on porosity and permeability of unconsolidated sand. *American Association of Petroleum Geology Bulletin* 57 (2), 349-36.

Beaubouf, R.T., and Friedman, S.J., 2000. High resolution seismic/sequence stratigraphic framework for the evolution of Pleistocene intraslope basins, western Gulf of Mexico: depositional models and reservoir analogs. In P. Weimer, R.M., Slatt, J.L. Coleman, N. Rosen, C.H., Nelson, A.H., Bouma, M., Styzen, and D.T Lawrence, (Eds.), *Global deep-water reservoirs: Gulf Coast Section-SEPM Foundation 20th Annual Bob. F. Research Conference*, 40-60.

Berger, A., Gier, S., and Krois, P., 2009. Porosity-preserving chlorite cements in shallow marine volcanoclastic sandstones: evidence from Cretaceous sandstones of the Sawan gas field, Pakistan. *American Association of Petroleum Geology Bulletin* 93, 595-615.

Berggren, W.A., Kent, D.V., Swisher, C. C., and Aubry, M.P., 1995. A revised Cenozoic Geochronology and Chronostratigraphy. In Berggren, W.A., Kent, D.V., Aubry.

Bjorkum, P.A., and Gjelsvik, N., 1988. An isochemical model for formation of authigenic kaolinite, k-feldspar, and illite in sediments. *Journal of Sedimentary Petrology*, V. 58, p. 506–511.

Bjørlykke, K., and Aagaard, P., 1992. Clay minerals in North Sea sandstones. In: Houseknecht, D.W., Pitman, E.D. (Eds.), *Origin, Diagenesis and Petrophysics of Clay Minerals in Sandstones*. SEPM Special Publication, V. 47, pp. 65–80.

Bjørlykke, K., and Egeberg, P. K., 1993. Quartz cementation in sedimentary basins: American Association of Petroleum Geology Bulletin, V. 77, p. 1538–1548.

Bjørlykke, K., 1998. Clay mineral diagenesis in sedimentary basins - a key to prediction of rock properties. Examples from the North Sea Basin. *Clay Minerals* 33, 15-34.

Bloch, S. Lander, R.H., and Bonnell, L., 2002. Anomalously high porosity and permeability in deeply buried sandstone reservoirs: Origin and predictability. *American Association of Petroleum Geology Bulletin*. 86(2): 301-328.

Blow, W.H., 1979. *The Cenozoic Globigerinida: A Study of the Morphology, Taxonomy, Evolutionary Relationships and the Stratigraphical distribution of some Globigerinida (mainly Globigerinacea)*: Leiden, E.J.Brill (3vols), 1462 p.

Boles, J.R., and Francks, G.S., 1979. Clay diagenesis in Wilcox sandstones of Southwest Texas: Implications of smectite diagenesis on sandstone cementation. *Journal of Sedimentary Petrology*, 49, 55- 70.

Bolli, H.M., and Saunders, J.B., 1985. Oligocene to Recent low latitude planktic foraminifera. In: Bolli, H.M., Saunders J.B. and K. Perch-Nielsen (Eds.) *Plankton Stratigraphy*. Cambridge University, Press New York: 155-262.

Bouma A.H., 1962. *Sedimentology of some Flysch Deposits: A graphic Approach to Facies Interpretation* (pp.68). Amsterdam: Elsevier.

Brun, J.P., and Fort, X., 2004. Compressional salt tectonics (Angolan margin). *Tectonophysics*, 382, 129–150.

Buffler, R.T., and Sawyer D.S., 1985. Distribution of crust and early history Gulf of Mexico Basin. *Gulf Coast Association of Geological Societies Transactions*.35.333-344.

Bursik, M.I., and Woods, A.W., 2000. The effects of topography on sedimentation from particle laden turbulent density currents. *Journal of Sedimentary Research* 70, 53–63.

Carozzi, A., 1993. *Sedimentary Petrography*. PTR Prentice Hall, Englewood Cliffs, New Jersey. pp. 263.

Carvajal, C.R., Steel, R.J., and Peter, A., 2009. Sediment supply: The main driver of shelf margin growth. *Earth-Science Reviews*, 96,221–248.

Carvalho, M.V.F., De Ros, L.F., and Gomes, N.S., 1995. Carbonate cementation patterns and diagenetic reservoir facies in the Campos Basin Cretaceous turbidites, offshore eastern Brazil. *Marine and Petroleum Geology* 12, 741–758.

Catuneanu, O., 2002. Sequence stratigraphy of clastic systems: concepts, merits, and pitfalls. *Journal of African Earth Sciences* 35, 1-4.

Catuneanu, O., 2003. *Sequence Stratigraphy of Clastic Systems*, vol.16. Geological Association of Canada, Short Course Notes p248.

Catuneanu, O., 2006. *Principles of sequence stratigraphy*. Elsevier. Oxford Uk.

Catuneanu, O., 2017. *Sequence Stratigraphy; Guidelines for a Standard Methodology*. In; Montenari, M. (Ed.), *Stratigraphy and Timescales*. Elsevier.

<https://doi.org/10.1016/bs.sats.2017.07.003>

Catuneanu, O., Abreu, V., Bhattacharya, J.P., Blum, M. D., Dalrymple, R.W., Eriksson, P. G., et al., 2009. Towards the standardization of sequence stratigraphy. *Earth-Science Reviews*, 92.

Catuneanu, O., Bhattacharya, J.P., Blum, M.D., Dalrymple, R.W., Eriksson, P.G., Fielding, C.R., Fisher, W.L., Galloway, W.E., Gianolla, P., Gibling, M.R., Giles, K.A., Holbrook, J.M., Jordan, R., Kendall, C.G.St.C., Macurda, B., Martinsen, O.J., Miall, A.D., Nummedal, D., Posamentier, H.W., Pratt, B.R., Shanley, K.W., Steel, R.J., Strasser, A., and Tucker, M.E., 2010. Sequence stratigraphy: common ground after three decades of development: *First Break*, 28, 21-34.1-33.

Catuneanu O., Galloway W.E., Kendall C G.St.C., Miall A.D., Posamentier H.W., Strasser A., and Tucker M.E., 2011. Sequence Stratigraphy: Methodology and Nomenclature. *Newsletters on Stratigraphy*, 44/3, 173-245.

Catuneanu, O., Martins-Neto, M., and Eriksson, P.G., 2005. Precambrian sequence stratigraphy. *Sedimentary Geology*, v.176, Issues 1-2, p.67-95.

Catuneanu, O., and Zecchin, M., 2013. High-resolution sequence stratigraphy of clastic shelves II: controls on sequence development: *Journal of Marine and Petroleum Geology*, 39, 26-38.

Chapin, M.A., Davies, P., Gibson, J.L., and Pentigill, H.S., 1994. Reservoir Architecture of turbidite sheet sandstones in laterally extensive outcrops, Ross Formation, western Ireland. In P. Weimer, A.H. Bouma, and B.F.Perkins (Eds.). *Submarine fans and turbidite systems*. Gulf Coast Section SEPM Foundation 15th Annual Research Conference, pp.53-68.

Clark, J.D., and Pickering., 1996. Architectural elements and growth patterns of submarine channels: application to hydrocarbon exploration. American Association of Petroleum Geology Bulletin, 80, 194-221.

Corliss, B.H., and Fois E., 1990. Morphotype analysis of deep-sea benthic Foraminifera from northwestern Gulf of Mexico: Palaios v.5.589-605.

Chang, H., Mackenzie, F.T., and Schoonmark, J., 1986. Comparisons between the diagenesis of dioctahedral and trioctahedral smectite, Brazilian offshore basins. Clays and Clay Minerals, V. 34, p. 407–423.

Cruz-Mercado M.A., Reyes-Tovar E., López-Céspedes, H.G; Peterson-Rodríguez R.H., Sánchez-Rivera, R., Flores-Zamora, J.C et al., 2009. Estudio Interregional Tectónica Salina y sus implicaciones en la Exploración Petrolera Pemex. Unpublished report.

Cruz-Mercado, M.A., Flores-Zamora, J. C., Leon-Ramírez R., López-Céspedes, H. G., Peterson-Rodríguez, R. H., Reyes-Tovar E, Sánchez-Rivera, R et al., 2011. Salt Provinces in the Mexican Portion of the Gulf of Mexico Structural Characterization and Evolutionary Model: Gulf Coast Association of Geological Societies Transactions, v.61, p.93-103.

Dasgupta, P., 2003. Sediment gravity flow- the conceptual problems. Earth-Science Reviews. 62, 265-281.

Davis, R. A., 2011. Sea-Level Change in the Gulf of Mexico Texas A&M University Press.192p

De Gasperi, A., and Catuneanu, O., 2014. Sequence stratigraphy of the Eocene turbidite reservoirs in Albacora field, Campos Basin, offshore Brazil. American Association of Petroleum Geologists (AAPG) Bulletin, 98/2, 279-313.

Demmytenaere, R., Tromp, J.P., Ibrahim, A., Allman-Ward, P. and Meckel, T., 2000. Brunei Deep Water Exploration: From Sea Floor Images and Shallow Seismic Analogues to Depositional Models in a Slope Turbidite Setting., in P. Weimer, R.M. Slatt, J.L.Coleman, N. Rosen, C.H. Nelson, A. H Bouma, M. Sytzen, and Lawrence, (Eds.), Global deep-water reservoirs: GCS-SEPM Foundation 20th Annual Bob. F. Perkins Research Conference, 304-317.

De Ros, L.F., Morad, S. and Paim, P.S.G., 1994. The role of detrital composition and climate on the diagenetic evolution of continental molasses: evidence from the Cambro-Ordovician Guaritas sequence, southern Brazil. *Sedimentary Geology* 92,197-228.

De Ros L.F, Anjos, S.M and Morad, S., 1994b. Authigenesis of amphibole and its relationship to the diagenetic evolution of Lower Cretaceous sandstones of the Potiguar rift basin, northeastern Brazil. *Sedimentary Geology*. 88(3-4): 253-266.

Dickinson, W.R., 1979. Mesozoic fore-arc basin in central Oregon. *Geology*, 7, 166-170.

Dickinson, W.R., 1982. Composition of sandstones in Circum-Pacific subduction complexes and fore-arc basins, *American Association of Petroleum Geology Bulletin*. V.66, p. 121-137

Dickinson, W. R., L. S. Beard, G.R. Bankenridge, J. L. Erjavec, R. C. Ferguson, K. F. Inman, R. A. Knepp, F. A. Lindberg, Morad et al. 1301 and P. T. Ryberg., 1983. Provenance of North American Phanerozoic sandstones in relation to tectonic setting: *Geological Society of America Bulletin*, v. 94, p. 222–235, doi:10.1130/0016-7606(1983)94< 222: PONAPS>2.0.CO;2.

Doronzo D.M., and Dellino, P., 2013. Hydraulics of subaqueous ash flows as deduced from their deposits: Water entrainment, sedimentation, and deposition, with implications on

pyroclastic density current deposit emplacement. *Journal of Volcanology and Geothermal Research* 258. 176-186.

Duranti, D., and Hurst A., 2004. Fluidization and Injection in deep-water sandstones of the Eocene Alba Formation (UK North Sea). *Sedimentology* 51, 503-529.

Elliot, T., 1998. A renaissance in the analysis of turbidite systems: Implications for reservoir development and management. EAGE/AAPG Research conference, Developing and managing turbidite reservoirs: Case histories and experiences. Almeria, Spain, October 1-8.

Elmore, R.D., Engel, M.H., Crawford, L., Nick, K., Imbus, S., Sofer, Z., 1987. Evidence for a relationship between hydrocarbon migration and authigenic magnetite. *Nature*, 325, 428–430.

Ehrenberg, S. N. and Nadeau. P. H., 1989. Formation of diagenetic illite in sandstones of the Garn Formation, Haltenbanken area, mid-Norwegian continental shelf: *Clay Minerals*, V. 24, p. 233–253, doi:10.1180/claymin.1989.024.2.09.

Ehrenberg, S.N., 1990. Relationship between diagenesis and reservoir quality in sandstones of the Garn Formation, Haltenbanken, mid-Norwegian continental shelf. *American Association of Petroleum Geologists Bulletin* 74, 1538–1558.

Ehrenberg, S. N., 1993. Preservation of anomalously high porosity in deeply buried sandstones by grain-coating chlorite: Examples from the Norwegian continental shelf: *American Association of Petroleum Geologists Bulletin*, V. 77, p. 1260–1286.

Emery, D., and Myers, K.J., 1996. *Sequence Stratigraphy*. Blackwell Oxford, U.K., p.297.

Eriksson, P.G., Catuneanu, O., Sarkar, S., and Tirsgaard, H., 2005. Patterns of sedimentation in the Precambrian. *Sedimentary Geology*, v. 176, Issues 1-2, p. 17-42.

Eriksson, P.G., Mazumder, R., Catuneanu, O., Bumby, A.J., and Hondo, B. O., 2006. Precambrian continental freeboard and geological evolution: A time perspective. *Earth-Science Reviews*, vol. 79, p. 165-204.

Eriksson, P.G., Porada, H., Banerjee, S., Bouougri, E., Sarkar, S., and Bumby, A.J., 2007. Mat-destruction features. In: Schieber, J., Bose, P.K., Eriksson, P.G., Banerjee, S., Sarkar, S., Altermann, W. and Catuneanu, O. (Eds.) *Atlas of microbial mats features preserved within the siliciclastic rock record. Atlases in Geosciences, V. 2*, p. 76-105.

Eriksson, P.G., Banerjee, S., Catuneanu, O., Corcoran, P.L., Eriksson, K.A., Hiatt, E.E., Laflamme, M., Lenhardt, N., Long, D.G.F., Miall, A.D., Mints, M.V., Pufahl, P.K., Sarkar, S., Simpson, E.L., Williams, G.E., 2013. Secular changes in sedimentation systems and sequence stratigraphy. *Gondwana Research, V. 24*, p. 468-489.

Escalera- Alcocer, A., and Hernández-Romano, U., 2009. *Provincias Petroleras de México.* WEC México. Schulmberger.

Felix, M. and Peakall, J., 2006. Transformation of debris Flows into Turbidity Currents: Mechanisms Inferred from Laboratory Experiments. *Sedimentology* 53, 107-123.

Fillon, R.H., 2007. Biostratigraphy and Condensed Sections in Deepwater Settings in Weimer, P. and Slatt, R. *Introduction to the Petroleum Geology of Deepwater Settings.* American Association of Petroleum Geology Studies in Geology 57, American Association of Petroleum Geology /Datapages Discovery Series.

Folk, R.L., 1974. *Petrology of Sedimentary Rocks.* Hemphill, Austin, Texas, p. 182.

Fort, X., Brun, J.P., and Chauvel, F., 2004. Salt tectonics on the Angolan margin, synsedimentary deformation processes. *AAPG Bulletin*, 88, 1523–1544.

Fraser, H.J., 1935. Experimental study of the porosity and permeability of clastic sediments: *Journal of Geology*, V. 43, p. 910–1010.

Frazier, D.E., 1974. Depositional episodes: their relationship to the Quaternary stratigraphic framework in the northwestern portion of the Gulf Basin: The University of Texas at Austin, Bureau of Economic Geology, and Geological Circular 74-1, 28p.

Gani, M.R., 2004. From Turbid to Lucid: A Straightforward Approach to Sediment Gravity Flows and their deposits. *The sedimentary Record*, v.2, no.3, 4-8.

Galloway, W.E., 1989. Genetic stratigraphic sequences in basin analysis; I, Architecture and genesis of flooding-surface bounded depositional units: *American Association of Petroleum Geology Bulletin*, 73, no.2, 125-142.

Galloway, W.E., 2001. The many faces of submarine erosion: theory meets reality in selection of sequences boundaries. *American Association of Petroleum Geology. Hedberg Research Conference on Sequence Stratigraphic and Allostratigraphic Principles and Concepts*, Dallas, August 26-29, Program and Abstracts. V, 28-29.

Gee, M.J.R., and Gawthorpe, R.L., 2006. Submarine Channels controlled by salt tectonics: examples from 3D seismic data offshore Angola. *Marine Petroleum Geology*, 23, 443-458.

Gier, S., Worden, R.H., Johns, W.D., and Kurzweil, H., 2008. Diagenesis and reservoir quality of Miocene sandstones in the Vienna Basin, Austria. *Marine. Petroleum. Geology*. 25,681-695.

Giles, M.R., and De Boer, R.B., 1990. Origin and significance of redistributive secondary porosity. *Marine and Petroleum Geology* V.7, p.378-397, doi:10.1016/02648172 (90) 90016-A

Giles, M.R., Syevenson, S., Martin, S.V., Cannon, S.J.C., Hamilton, P.J., Marshall, J.D., and Samways, G.M., 1992. The reservoir properties and diagenesis of Brent Group: a regional perspective. In: *Geology of Brent Group*. A.C. Morton, R.S. Haszeldine, M.R. Giles and S. Brown (Eds.). Geological Society Special Publication 61, p. 289–327.

Gomez-Cabrera, P.T., and Jackson, M.P.A., 2009. Neogene stratigraphy and salt tectonics of the Santa Ana area, offshore Salina del Itsmo Basin, southeastern Mexico, in Bartolinni C. and Roman Ramos J.R, (Eds.). *Petroleum systems in the southern the Gulf of Mexico* American Association of Petroleum Geology Memoir 90 .237-255.

Gutierrez-Paredes H.C., Catuneanu O., and Hernández-Romano U., 2017a. Sequence stratigraphy of the Miocene section, Southern Gulf of Mexico. *Marine and Petroleum Geology*, 86, 711-732.

Gutierrez-Paredes H.C., Catuneanu O., and Hernández-Romano, U., 2017b. Miocene depositional environments, processes, and depositional elements in the southern Gulf of Mexico. *Geological Journal*.2017;1-30. <https://doi.org/10.1002/gj.2948>.

Guzmán, A.E. and Marquez-Dominguez, B., 2001. The Gulf of Mexico Basin South of the Border: The Petroleum Province of the Twenty-First Century, in M. W. Downey, J. C. Threet and W. A. Morgan, editors, *American Association of Petroleum Geologists*, Tulsa.

Hampton, M.A., 1975. Competence of fine grained debris flows. *Journal of Sedimentary Petrology*, 45, 833–844.

Haq, B.U., Hardenbol, J., and Vail, P.R., 1988. Mesozoic and Cenozoic chronostratigraphy and cycles of sea-level change. In *Sea Level Changes- An Integrated Approach* C.K. Wilgus, B. S Hastings, C.G.St.C. Kendall, H.W.Posamentier, C.A. Ross J.C.Van Wagoner, (Eds.), pp 125-154. SEPM Special Publication 42.

Haughton, P.D.W., Barker, S.P., and McCaffrey, W.D., 2003. Linked debrites in sand-turbidites systems—origin and significance. *Sedimentology* 50, 459–482.

Haughton, P., Davis, C., McCaffrey W., and Barker, S., 2009. Hybrid sediment gravity flow deposits- Classification, origin and significance. *Marine and Petroleum Geology*, 26, 1900-1918.

Hay, A.E., 1987. Turbidity current and submarine channel formation in Rupert Inlet, British Columbia: 2. The roles of continuous and surge-type flow. *J. Geophysical Research*, 92, 2883–2900.

Hayes, M.J., and Boles, J.R., 1992. Volumetric relations between dissolved plagioclase and kaolinite in sandstones: implications for aluminum mass transfer in San Joaquin Basin, California. In: Houseknecht, D.W., Pitman, E.D. (Eds.), *Origin, Diagenesis and Petrophysics of Clay Minerals in Sandstones*. SEPM Special Publication, V. 47, pp. 111–123.

Hawladar, H.M., 1990. Diagenesis and reservoir potential of volcanogenic sandstones-Cretaceous of the Surat Basin, Australia. *Sedimentary Geology*. 66(3-4): 181-195.

Hein, J.R., O'Neill, J.R., and Jones, M.G., 1979. Origin of authigenic carbonates in sediment from the deep Bering Sea. *Sedimentology*, 26, 681–705.

Hiscott, R.N., 1994. Traction-carpet stratification in turbidites fact or fiction. *Journal of Sedimentary Research*, 64, 204–208.

Hower, J., Eslinger, E.V., Hower M.E. and Perry, E.A., 1976. Mechanism of burial metamorphism of argillaceous sediments: 1. Mineralogical and chemical evidence. Geological Society of America Bulletin, 87, 725-737.

Hunt, D. and Tucker, M.E., 1992. Stranded parasequences and the forced regressive wedge systems tract: deposition during base-level fall. Sedimentary Geology, 81, 1-9.

Hunt, D. and Tucker, M.E., 1992. Stranded parasequences and the forced regressive wedge systems tract: deposition during base-level fall-reply. Sedimentary Geology, 95, 147-160.

Isaksen, G. H., 2004. Central North Sea hydrocarbon systems: generation, migration, entrapment, and thermal degradation of oil and gas. AAPG Bulletin, 88, 1545-1572, <http://dx.doi.org/10.1306/06300403048>.

Jeans, C.V., D.S. Wray, R.J. Merriman, and M.J. Fisher., 2000. Volcanogenetic clays in Jurassic and Cretaceous strata of England and the North Sea Basin: Clay Minerals, V.35, p.25-55, doi:10.1180/000985500546710.

Johanson, M., and Stow, D.V., 1995. A classification scheme for shale clasts in deep-water sandstones in Hartley, A.J. and Prosser, D.J., (Eds.). Characterization of Deep Marine Clastic Systems, Geological Society Special Publication, n.94, pp.221-241.

Johnson S.D., Flint, D., Hinds and Deville Wickens, H., 2001. Anatomy, geometry and sequence stratigraphy of basin floor to slope turbidite systems. Tanqua Karoo, South Africa: Sedimentology, 48,987-1023.

Joseph, P. and Lomas, S.A. 2004. Deep-water sedimentation in the Alpine Basin of SE France. Geological Society Special Publication. No.22. VIII. 448pp.

Kneller, B., and Branney, M.J., 1995. Beyond the turbidite paradigm: physical models for deposition of turbidites, and their implications for reservoir prediction. In Hartley, A.J., Prosser, C. (Eds.), *Characterization of deep Marine Clastic Systems. Special Publication, V.94.* Geological Society of London, London, UK, 31-49.

Kneller B., Dykstra, M., Fairweather L., and Milana, J. P. 2016. Mass-transport and slope accommodation: Implications for turbidite sandstone reservoirs.

Ketzer, J.M., Morad, S., and Amorosi, A., 2003. Predictive clay cementation in a sequence stratigraphy framework. In: Worden, R., Morad, S. (Eds.), *Clay Cementation in Sandstones,* International Association of Sedimentologists. Special Publication, V. 34, pp. 42–59.

Khalifa, M., and Morad, S., 2012. Impact of structural setting on diagenesis of fluvial and tidal sandstones: the Bahi Formation, Upper Cretaceous, NW Sirt Basin, North Central Libya. *Marine and Petroleum Geology.* 38, 211-231.

Kuenen, P.H., 1966. Experimental turbidite lamination in a circular flume. *Journal of Geology,* 74, 523–545.

Lander, R. H., and Bonnell, L. M., 2010. A model for fibrous illite nucleation and growth in sandstones. *American Association of Petroleum Geologists Bulletin,* 94, 1161–1187.

Lawton, T.F., Pollock, S.L., and Robinson, R.A.J., 2003. Integrating sandstone petrology and nonmarine sequence stratigraphy: application to the Late Cretaceous fluvial systems of Southwestern Utah, U.S.A. *Journal of Sedimentary. Research.* 73, 389–406.

Loutit, T. S. Hardenbol, J., and Vail, P.R., 1988. Condensed sections: the key to age determination and correlation of continental margin sequences, in Wilgus, C. K., Hastings, B. S., Kendall, C. G. St. C., Posamentier, H. W., Ross, C. A., and Van Wagoner, J. C., eds., *Sea-level Changes: An Integrated Approach: SEPM Special Publication No. 42*, pp. 183–213.

Loubere, P., Gary, A., and Lagoe, M., 1993. Sea-bed biochemistry and benthic foraminiferal bathymetric zonation of the slope of the northwestern Gulf of Mexico: *Palaios*, 8, 439-449.

Love, L.G., 1967. Early diagenetic iron sulphide in Recent sediments of the Wash, England. *Sedimentology*, 9, 327–352.

Lowe, D.R., 1982. Sediment gravity flows: depositional models with special reference to the deposits of high-density turbidity currents. *Journal of Sedimentary Petrology*, 52(1), 0279-0297.

Lowe, D.R., and Guy, M., 2000. Slurry flow deposits in the Brittania Formation (Lower Cretaceous) North Sea: a new perspective on the turbidity current and debris flow problem. *Sedimentology*, V.47, 31-70.

Lowe, D. R., Guy, M., and Palfrey, A., 2003. Facies of slurry-flow deposits, Brittania Formation (Lower Cretaceous) North Sea: Implications for flow evolution and deposit geometry. *Sedimentology*, 50, 45-80.

Lucchi, F.R., and Valmori, E., 1980. Basin-wide turbidites in a Miocene, over-supplied deep-sea plain: a geometrical analysis. *Sedimentology*, 27, 241-270.

Lugo, R. J.E, Granados, M.O.J, Segura, T.A., Castillo, D.R., Villanueva, G.L.I., Jiménez, B.D., Berlanga J.A et al., 2005. Carta de Biozonas y Bioeventos de microfósiles del Cenozoico de las Cuencas del Golfo de México. PEMEX. Informe Inédito.

Lundegard, P.D., 1992. Sandstone porosity loss- a “big picture” view of the importance of compaction: *Journal of Sedimentary Research*, v.62, p. 250-260, doi:10.1306/D42678D4-2B26-11D7-8648000102C1865D.

Luo, J.L., Hall, O., Morad, S., and Ketzer, J.M., 2009. Diagenetic and reservoir-quality evolution of fluvial and lacustrine-deltaic sandstones: evidence from Jurassic and Triassic sandstones of the Ordos Basin, northwestern China. *Journal of Petroleum. Geology*. 32, 79-102.

Makowitz, A., and Milliken, K.L., 2003. Quantification of brittle deformation in burial compaction, Frio and Mount Simon Formation sandstones. *Journal of Sedimentary Research* 73, 1007-1021.

Mahaffie, M.J., 1994. Reservoir classification for turbidite intervals at the Mars discovery, Mississippi canyon 807, Gulf of Mexico. In P. Weimer, A.H.Bouma, and B.F. Perkins (Eds.). *Submarine fans and turbidite systems* (pp.183-213). Coast section-SEPM special publication 42.

Mansurbeg, H., El-ghali, M.A.K., Morad, S., and Plink-Bjorklund, P., 2006. The impact of Meteoric water on the diagenetic alterations in deepwater, marine siliciclastic turbidites. *Journal of Geochemical Exploration* 89, 254-258.

Marchesini, L., Amorosi, A., Cibin, U., Spadafora, E., Zuffa, G.G., and Preti, D., 2000. Detrital supply versus facies architecture in the Late Quaternary deposits of the south- Eastern Po Plain (Italy). *Journal of Sedimentary Research*. 70, 829–838.

Martini, E., 1971. Standard Tertiary and Quaternary calcareous nannoplankton zonation. En A. Farinacci (i). In: *Proceedings 2nd Planktonic Conference, Roma, 1970*, vol. 2, pp739-785.

Marton, G., and Buffler, R.T., 1994. Jurassic Reconstruction of the Gulf of Mexico Basin. *International Geology Review*, 36, 545-586.

Mayall, M., and Stewart, I., 2000. The Architecture of Turbidite Slope Channels, in P. Weimer, R.M. Slatt, J.L. Coleman, N. Rosen, C.H. Bouma, M. Styzen, and D.T. Lawrence, (Eds.), *Global deep-water reservoirs: Gulf Coast section SEPM Foundation 20th Annual Bob F. Perkins Research conference*, 578-586.

Meisler, H., Leahy, P.P., and Knobel, L.L., 1984. Effect of eustatic sea-level changes on saltwater-freshwater in the northern Atlantic coastal plain. *US Geological Survey Water-Supply Paper* 2255, 28.

Mitchum, R.M., Sangree, J. B. Vail, P. R., and Wornardt, W., 1993. Recognizing sequences and systems tracts from well logs, seismic data, and biostratigraphy: examples from the Late Cenozoic of the Gulf of Mexico, in P. Weimer and H. Posamentier, (Eds.), *Siliciclastic sequence stratigraphy: recent developments and applications: American Association of Petroleum Geology Memoir* 58, 163–197.

Morán-Zenteno, D. J., Martiny, B., Tolson, G., Solís Pichardo, G., Alba Aldave, L., Hernández-Bernal, M. del S., Macías Romo, C., Martínez Serrano, R.G...Silva Romo, G., 2000. Geocronología y características geoquímicas de las rocas magmáticas terciarias de la Sierra Madre del Sur: *Boletín de la Sociedad Geológica Mexicana*, T. LIII, No. 1, p. 27-58

Morad, S ., 1986. Pyrite-chlorite and pyrite-biotite relations in sandstones. *Sedimentary Geology*, 49, 177-192.

Morad, S., Ketzer, J.M., and De Ros, F., 2000. Spatial and temporal distribution of diagenetic alterations in siliciclastic rocks: implications for mass transfer in sedimentary basins. *Sedimentology* 47, 95–120.

Morad, S., Al-Ramadan, K., Ketzer, J.M. and De Ros, L.F., 2010. The impact of diagenesis on the heterogeneity of sandstone reservoirs: a review of the role of depositional facies and sequence stratigraphy. *American Association of Petroleum Geologists Bulletin*. 94, 1267-1309.

Morán-Zenteno, D.J., Martiny,B., Tolson,G., Solis Pichardo, G., Alba Aldave, L...Romo Silva., 2000. Geocronología y características geoquímicas de las rocas magmáticas terciarias de la Sierra Madre del Sur: Boletín de la Sociedad Geológica Mexicana.

Morris, W. R., and Normark. W.R., 2000. Scaling, sedimentologic and geometric criteria for comparing modern and ancient sandy turbidite elements, in P. Weimer, R. M. Slatt, J. L. Coleman, N. Rosen, C. H. Nelson, A.H. Bouma, M. Styzen, and D. T. Lawrence, (Eds.), *Global deep-water reservoirs: Gulf Coast Section–SEPM Foundation 20th Annual Bob F. Perkins Research Conference*, p. 606–628.

Moscardelli, L., Wood, L., and P, Mann., 2006. Mass transport complexes and associated processes in the offshore area of Trinidad and Venezuela. *American Association of Petroleum Geologists Bulletin*, 90, (7), 1059-1088.

Moscardelli. L., and Wood., 2007. New classification system for mass transport complexes in offshore Trinidad. *Basin Research* 20(1), 73-98.

Mulder, T., and Alexander, J., 2001. The physical character of subaqueous sedimentary density flows and their deposits. *Sedimentology*, 48, 269-299.

Mutti, E., and Nielsen, T. H., 1981. Significance of intraformational rip-up clasts in deep sea fan deposits. International Association of Sedimentologists, 2nd European Regional Meeting Bologna, Italy.

Mutti, E., and Normark, W.R., 1987. Comparing examples of modern and ancient turbidite systems. Problems and concepts. In J.K.Legget & G.G. Zuffa (Eds.), Marine clastic sedimentology (pp.1-38).London: Graham and Trotman.

Mutti, E., and Normark, W.R., 1991. An integrated approach to the study of turbidite systems: Seismic facies and sedimentary processes of submarine fans and turbidite systems: Springer-Verlag New York Inc., 75-105.

Muto, T., and Steel, R.J., 2002. In defense of shelf-edge delta development during falling and lowstand of relative sea level. *Journal of Geology*, 110 (4), 421–436.

Nentwich, F.W., and Yole, R.W., 1997. Petrology and diagenetic history of deltaic litharenites, Oligocene Kugmallit sequence, Beaufort-Mackenzie basin, Arctic Canada. *Bulletin. Canadian. Petroleum Geologists* 45, 339-355.

Nielsen, T.H., and Kerr, R., 1978. Turbidites, Red beds, Sedimentary Structures, and Trace fossils Leg 38 Cores and Sedimentary History of the Norwegian Basin: DSDP Leg 38. doi:10.2973/dsdp.proc. 383940.119.1978.

Padilla y Sánchez, R. J., 2007. Evolución Geológica del Sureste Mexicano desde el Mesozoico al Presente en el Contexto Regional del Golfo de México. *Boletín de la Sociedad Mexicana*, tomo LIX, no1, p.19-42.

Peakall J., McCaffrey B., and Kneller B., 2000. A process model for the evolution, morphology, and architecture of sinuous submarine channels. *Journal of Sedimentary Research*, V.70.No 3 434-448.

Pearson, M.J., and Small, J.S., 1988. Illite-smectite diagenesis and palaeotemperatures in northern North Sea Quaternary to Mesozoic shale sequences. *Clay Minerals*, V. 23, p. 109–139.

PEMEX-IPM., 2000. Proyecto de Integración Bioestratigrafía. Informe Inédita.

Perch-Nielsen, K., 1985. Cenozoic Calcareous Nannofossils in Bolli, H.M. Saunders J.B & Perch-Nielsen (Eds.) *Plankton Stratigraphy*. Cambridge University, Press New York: pp 427-545.

Perry, E., and Hower, J., 1970. Burial diagenesis in Gulf Coast pelitic sediments. *Clays and Clay Minerals*, V. 18, p. 165–177.

Perry E.A., Jr., and Hower J., 1972. Late-stage dehydration in deeply buried pelitic sediments. *American Association of Petroleum Geologists Bulletin*, 56, 2013 2021.

Peterson-Rodríguez R.H., Hernández -Penaloza J., Heyn T., Jiménez-Guerrero M., Ibanez-Garduno D., Garza-Goicochea C.E.... Rojas-Rosas, R., 2013. Modelo de evolución estructural para entender el desarrollo de las trampas estructurales de HC's en la zona costa afuera de la porción occidental de la Sonda de Campeche, Mexico. Congreso Mexicano del Petróleo Riviera Maya, 5-8 de Junio 2013., Cancún Mexico.

Pickering K.T., and Corregidor J., 2005. Mass transport complexes and tectonic control on confined basin-floor submarine fans, Middle Eocene, south Spanish Pyrenees. In: Hodgson,

D.M. and Flint, S.S. (Eds.) 2005. Submarine Slope Systems: Processes and Products. Geological Society, London, Special Publications, 244. The Geological Society of London.

Pindell, J.L., 1985. Alleghenian reconstruction and subsequent evolution of the Gulf of Mexico, Bahamas and Proto-Caribbean. *Tectonics*, 4, 1-39.

Pindell, J.L., and Kennan, L., 2002. Análisis Paleogeográfico Mesozoico-Cenozoico y Dinámica de las cuencas en el Golfo de México Profundo y Márgenes. Informe Final. Tectonic Analysis Inc. and Pemex Exploration and Production. Inédito.

Pindell, J. L., and Kennan, L., 2009. Tectonic Evolution of the Gulf of Mexico, Caribbean and Northern South America in the Mantle Reference Frame: an update. In James, K.H., Lorente, M.A and Pindell, J. L. (Eds.). *The Origin and Evolution of the Caribbean Plate*, Geological Society of London, Special Publications 328.1-55.

Piper, D.J.W., and Normark, W.R., 1983. Turbidite depositional patterns and flow characteristics, Navy submarine fan, California Borderland. *Sedimentology*, V. 30, 681–694.

Pirrie, D, Ditchfield P.W and Marshall J.D., 1994. Burial diagenesis and pore-fluid evolution in a Mesozoic back-arc basin: The Marambio Group, Vega Island, Antarctica. *Journal of Sedimentary Research*. 64(3a): 541-552.

Pittman, E, D., and Larese R, E., 1991. Compaction of lithic sands: Experimental results and applications. *American Association of Petroleum Geologists Bulletin*. 75(8): 1279-1299.

Posamentier, H.W., and Allen, G.P., 1999. Siliciclastic sequence stratigraphy-concepts and application. *Concepts in Sedimentology. Soc. Econ. Paleontology. Mineralogists, Tulsa* 7, 210.

Posamentier, H.W., and Kolla V., 2003. Seismic geomorphology and stratigraphy of depositional elements in deep-water settings. *Journal of Sedimentary Research*, 73, 367-388.

Posamentier, H.W., and Walker, R.G., 2006. Deep-water turbidites and submarine fans. In Posamentier, H. W., and Walker, R.G. (Eds), *Facies Models Revisited*. Special Publication, SEPM (Society for Sedimentary Geology) no.84, 397-520.

Posamentier, H.W. 2003. Depositional elements associated with a basin floor channels-levee system: Case study from the Gulf of Mexico. *Marine and Petroleum Geology*, 20, 667-690.

Posamentier H., Davies R.J., Wood L., and Cartwright J.A., 2007. Seismic geomorphology – An Overview. In Geological Society London Special Publications. DOI: 10.1144/GSL.SP.2007.277.01.01.

Posamentier, H.W., and Vail, P.R., 1988. Eustatic controls on clastic deposition II-sequence and systems tract models. In *Sea Level Changes- An Integrated Approach* C.K. Wilgus, B.S Hastings, C.G.St.C. Kendall,H.W. Posamentier, C.A.Ross and J.C.Van Wagoner, (Eds.), pp 125-154. SEPM Special Publication 42.

Porebski, S. J., and Steel, R., 2003. Shelf-margin deltas: their stratigraphic significance and relation to deepwater sands. *Earth-Science Reviews*, 1282, 1-44.

Postma, G., Nemec, W., and Kleinspehn, K.L., 1988. Large floating clasts in turbidites: a mechanism for their emplacement. *Sedimentary Geology*, 58, 47-61. (In Johanson, M and Stow, D.V. (1995). A classification scheme for shale clasts in deep-water sandstones.in Hartley, A.J. and Prosser, D.J., (Eds.). *Characterization of Deep Marine Clastic Systems*, Geological Society Special Publication, N.94.221-241.

Poursoltani, M.R., and Gibling, M.R., 2011. Composition, porosity, and reservoir potential of the Middle Jurassic Kashafrud Formation, northeast Iran. *Marine and Petroleum Geologists*. 28, 1094-1110.

Prather B.E., 2003. Controls on reservoir distribution, architecture and stratigraphic trapping in slope settings. *Marine and Petroleum Geology*. 20(6):529-545.

Prather, B.I, Booth, J.R., Steffens, G. S., and Craig, P.A., 1998. Classification, lithologic calibration, and stratigraphic succession of seismic facies of intraslope basins, deepwater Gulf of Mexico, AAPG, Bulletin.82 (Ja) 701-728.

Primmer, T. J., C.A. Cade, J. Evans, J. G. Gluyas, M. S. Hopkins, N. H. Oxtoby, P. C. Smalley, E. A., Warren and R. H. Worden., 1997. Global patterns in sandstone diagenesis: their application to reservoir quality prediction for petroleum exploration, in J. A. Kupecz, J. G. Gluyas, and S. Bloch, eds., *Reservoir quality prediction in sandstones and carbonates: American Association of Petroleum Geologists Memoir 69*, p. 61–78.

Prost, G., and Aranda, M., 2001. Tectonics and Hydrocarbon Systems of the Veracruz Basin, Mexico, in Bartolini, C., Buffler, R. T. and Cantu- Chapa, A., (Eds.). *The Western Gulf of Mexico Basin: Tectonics, Sedimentary Basins and Petroleum Systems: American Association of Petroleum Geology Memoir 75*, p. 271-291.

Pyles, R.D., and Slatt, M.R., 2000. A High Frequency Sequence Stratigraphy Framework for Shallow Trough Deep-Water deposits of the Lewis shale and Fox Hill sandstone, Great Divide and Washakie Basins, Wyoming. GCSSEPM Foundation 20th Annual Research Conference Deep-Water Reservoirs of the World, December 3-6, 2000.

Pyles, D. R., and Jeannete, D.C., 2009. Geometry and architectural associations of cogenetic debrites-turbidite beds in basin-margin strata. Carboniferous Ross Sandstone (Ireland): applications to reservoirs located on the margins of structurally confined submarine fan. *Marine and Petroleum Geology*, 1974-1996.

Oluboyo, A.P., Gawthorpe, R.L., Bakke K., and Hadler-Jacobsen F., 2014. Salt tectonics controls on deep-water turbidite depositional systems: Miocene, southwester Lower Congo Basin, offshore Angola. *Basin Research*, 26,597-620.

Ramm, M., 2000. Reservoir quality and its relationship to facies and provenance in Middle to Upper Jurassic sequences, northeastern North Sea. *Clay Mineral.* 35, 77-94.

Reed, J.S., Eriksson, K.A., and Kowalewski, M., 2005. Climatic, depositional and burial controls on diagenesis of Appalachian Carboniferous sandstones: qualitative and quantitative methods. *Sedimentary. Geology.* 176, 225-246.

Remy R.R., 1994. Porosity reduction and major controls on diagenesis of Cretaceous-Paleocene volcanoclastic and arkosic sandstone, Middle Park Basin, Colorado. *Journal of Sedimentary Research.* 64(4): 797-806.

Richards, M., Bowman, M., and Reading, H., 1998. Submarine-fan systems I: Characterization and stratigraphic prediction. *Marine and Petroleum Geology*, 15, 687-717.

Robles-Nolasco, J., Pliego-Vidal, E., Toledo-Bante, C., Pimienta-Lugo, M., Ortega-González., Martínez-Pena, B., et al., 2004. Offshore Neogene plays, Salina del Itsmo Basin, southeast of Mexico: Tulsa, Oklahoma, E.U.A., American Association of Petroleum Geologists, International Conference, October 24-27, Cancun, Mexico, 5p.

Rogers, R., Mann, P., and Emmet, P.A., 2007. Tectonic terranes of the Chortis block base on integration of regional aeromagnetic and geologic data. In Mann, P., (Eds.), Geologic and Tectonic development of the Caribbean plate in northern Central America: Geological Society of America, Special paper 428, 65-88.

Ross, M.I., and Scotese, C.E., 1988. A hierarchical model of the Gulf of Mexico and Caribbean Region: Tectonophysics, 155, 139-168.

Rowan M.G., and Weimer P., 1998. Salt-Sediment Interaction, Northern Green Canyon and Ewing Bank (Offshore Louisiana) Northern Gulf of Mexico. AAPG Bulletin, V.82 N05B (May 1998 Part B) p1055-1082.

Rowan, M. G., Jackson, M. P. A., and Trudgill, B. D., 1999. Salt-related fault families and fault welds in the northern Gulf of Mexico. AAPG Bulletin, 83, 1454–1484.

Rowan, M. G., Lawton, T. F., Gilles, K. A., and Ratliff, R. A., 2003. Near-salt deformation in La Popa Basin, Mexico, and the northern Gulf of Mexico: a general model for passive diapirism AAPG Bulletin, 87, 733–756, <http://dx.doi.org/10.1306/01150302012>.

Ryu, I., C., and Niem, A.R., 1999. Sandstone diagenesis, reservoir potential, and sequence stratigraphy of the Eocene Tyee Basin, Oregon. Journal of Sedimentary Research. 69, 384–393.

Salem, A.M., Ketzer, J.M., Morad, S., Rizk, R.R., and Al-Aasm, I.S., 2005. Diagenesis and reservoir-quality evolution of incised-valley sandstones: evidence from the Abu Madi gas reservoirs (Upper Miocene), the Nile delta basin, Egypt. Journal of Sedimentary Research. 75, 572-584.

Salomón-Mora, L.E., Aranda-García, M., and Román- Ramos, J.R., 2009. Contractional growth faulting in the Mexican Ridges, Gulf of Mexico, in Bartolini, C. and Roman- Ramos, J.R. (Eds.). Petroleum systems in the southern Gulf of Mexico: American Association of Petroleum Geology Memoir 90, 93-115.

Salvador, A., 1987. Late Triassic- Jurassic Paleogeography and Origin of Gulf of Mexico. American Association of Petroleum Geology Bulletin, 71, 419-451.

Salvador, A., 1991. Triassic-Jurassic in Salvador, A. (Eds.). The Gulf of Mexico Basin: Geological Society of America, The Geology of North America, V.J., 131-180.

Sánchez, R. M-A., González, L. J-C., Ayala, N.M., Padilla, A. P., Del Valle, R, A., Sánchez, D. M-J., Urbano, G. D., and Martínez, N. M., 2002. Bioestratigrafía de Alta Resolución del Terciario en Pozos de la Cuenca de Veracruz y la Sonda de Campeche. Instituto Mexicano del Petróleo. Informe Inédito.

Sánchez-Hernández Hilarion., 2013. Stratigraphic characterization and evolution of Mid-Tertiary age Deep water system, Holok área, SW Gulf of Mexico. PhD Thesis, University of Aberdeen.

Sánchez-Montes de Oca, R., 1980. Geología petrolera de la Sierra de Chiapas: Boletín Asociación Mexicana Geológica Petrolera. 31, Nos. 1-2, 67-77.

Sanders, J.E., 1960. Primary sedimentary structures formed by turbidity currents and related resedimentation mechanisms. The Society of Economic Paleontologists and mineralogists (SEPM) Primary Sedimentary Structures, (SP12), 192-219.

Shanmugam, G., 1996. High-density turbidity currents: are they sandy debris flows? *Journal of Sedimentary Research*, 66, 2-10.

Shanmugam, G., 2007. The obsolescence of deep-water sequence stratigraphy in petroleum geology. *Indian Journal of Petroleum Geology*, 1-45.

Shanmugam G., 2012. *New Perspectives on Deep-water Sandstones, Volume 9: Origin, Recognition, Initiation and Reservoir Quality (Handbook of Petroleum Exploration and Production)*. Elsevier. 544p.

Shannon, P.M., Stoker, M.S., Praega, D. Van Weeringc T.C.E., De Haasc H., Nielsend, T., Dahlgrene, K.I.T., and Hjelstuenf, B.O., 2005. Sequence stratigraphic analysis in deepwater underfilled NW European Passive Margin Basins, *Marine and Petroleum Geology*, 22, 1185–1200.

Sikkema, W., and K. M. Wojcik., 2000. 3D visualization of turbidite systems, Lower Congo Basin, offshore Angola, in P. Weimer, R. M. Slatt, J. L. Coleman, N. Rosen, C. H. Nelson, A. H. Bouma, M. Styzen, and D.T. Lawrence, (Eds.). *Global deep-water reservoirs: Gulf Coast Section–SEPM Bob F. Perkins 20th Annual Research Conference*, p. 928–939.

Sinclair, H.D., and Tomasso, M., 2002. Depositional Evolution of Confined Turbidite Basins, *Journal of Sedimentary Research*, 72, No. 4, 451–456.

Slatt, R. M., Jordan D.W., and Davis R. J., 1994. Interpreting formation microscanner log images of Gulf of Mexico Pliocene turbidites by comparison with Pennsylvanian turbidite outcrops, Arkansas, in P. Weimer, A. H. Bouma and B. F. Perkins, eds., *Submarine fans and turbidite systems: Gulf Coast Section–SEPM Foundation 15th Annual Research Conference*, p. 335–348.

Slatt, R. M., Stone C. G., and Weimer. P., 2000. Characterization of slope and basin facies tracts, Lower Pennsylvanian Jackfork Group, Arkansas, with applications to deepwater (turbidite) reservoir management, in P.Weimer, R. M. Slatt, J. L. Coleman, N. Rosen, C. H. Nelson, A. H. Bouma, M. Styzen, and D. T. Lawrence, (Eds.). Global deep-water reservoirs: Gulf Coast Section–SEPM Foundation 20th Annual Bob F. Perkins Research Conference, p. 940–980.

Sohn, Y.K., 2000. Depositional processes of submarine debris flows in the Miocene fan deltas. Pohang Basin, SE Korea with special reference to flow transformation. *Journal of Sedimentary Research*, 70.491-503.

Spadafora, E., 1996. Composizione e diagenesi delle successioni epiliguri mioceniche dell'Appennino settentrionale. PhD Thesis, Bologna, p. 136.

Sumner, E.J., Amy, L., and Talling, P.J., 2008. Deposit structure and processes of sand deposition from a decelerating sediment suspension. *Journal of Sedimentary Research*, 78, 529–547.

Sumner, E.J., Talling, P.J., and Amy, L.A., 2009. The deposits of flows transitional between turbidity currents and debris flow. *Geology*, 37, 991–994.

Sumner, E.J., Talling, P.J., Amy, L.A., Wynn, R.B., Stevenson, C., and Frenz, M., 2012. Facies architecture of individual basin-plain turbidites: comparison to existing models and implications for flow processes. *Sedimentology*, doi: 10.1111/j.1365-3091.2012.01329.x.

Talling, P.J., Wynn, L.A., Peakall, J., and Robinson, M., 2004. Beds comprising debrite sandwiched within cogenetic turbidite: Origin and widespread occurrence in distal depositional environments: *Sedimentology*, 51, 163-194.

Talling, P.J., Amy, L.A., Wynn, R.B., Blackbourn, G., and Gibson, O., 2007c. Turbidity current evolution deduced from extensive thin turbidites: Marnoso-arenacea Formation (Miocene), Italian Apennines. *Journal of Sedimentary Research*. 77, 172–196.

Talling, P. J., Masson, D. G., Sumner, E. J., and Malgesini, G., 2012. Subaqueous sediment density flows: Depositional processes and deposit types. *Sedimentology*, 59(7), 1937-2003.

Twichell, D.C., Kenyon, N.H., Parson, L.M., and McGregor, B.A.M., 1991. Depositional patterns of the Mississippi Fan surface: evidence from GLORIA II and high-resolution seismic profiles, in Weimer, P., and Link, M.H., (Eds.). *Seismic facies and sedimentary processes of submarine fans and turbidite systems*: New York, Springer-Verlag, p. 349–364.

Ulmer-Scholle, D.S., Scholle, P.A., Schiber J., and Raine R.J., 2014. A color Guide to the Petrography of Sandstones, siltstones, Shales and Associated rocks. *American Association of Petroleum Geology Memoir*, 109.

Vander Merwe W.C., Flint, S., and Hodgson D.M., 2010. Sequence stratigraphy of an argillaceous, deepwater basin-plain succession: Vischkuil Formation (Permian), Karoo Basin, South Africa: *Marine and Petroleum Geology*, v. 27 p321-333.

Van Wagoner, J.C., Mitchum, R.M., Campion, K.M., and Rahmanian, V.D., 1990. Siliciclastic sequence stratigraphy in well logs, cores, and outcrops. *American Association of Petroleum Geologists. Methods Exploratory. Series*. 7, 220.

Villamil, T., Arango, C., Weimer, P., Waterman, A., Rowan, M.G., Varnai, P.,...Crews, J.R., 1998. Biostratigraphic techniques for analyzing benthic biofacies, stratigraphic condensation, and key surface identification, Pliocene and Pleistocene sediments, Northern

Green Canyon and Ewing Bank (offshore Louisiana), northern Gulf of Mexico. American Association of Petroleum Geology Bulletin, 82,961-985.

Vrolijk, P.J., and Southard, J.B., 1997. Experiments on rapid deposition of sand from high-velocity flows. Geosci. Can., 24, 45–54.

Warren, E.A., and Curtis, C.D., 1989. The chemical composition of authigenic illite within two sandstones reservoirs analysed by TEM. Clay Minerals, 24,137-156.

Weimer P., 1989. Sequence stratigraphy of the Mississippi Fan (Pliocene-Pleistocene) Gulf of Mexico. Geo-Marine Letters, 9,185-272.

Weimer, P., and Slatt, R.M., 2004. Petroleum Systems of Deepwater Settings. Distinguished Instructor Series, No.7.EAGE. Tulsa, OK. USA.

Wilkinson, M., Milliken, K.L., and Haszeldine, R.S., 2001. Systematic destruction of K-feldspar in deeply buried rift and passive margin sandstones. Journal of the Geological Society, London, 158, 675–683.

Wilson, M.J., Wilson, L., and Patey, I., 2014. The influence of individual clay minerals on formation damage of reservoir sandstones: a critical review with some new insights. Clay Minerals. 49, 147–164.

Winker, C. D., 1996. High-resolution seismic stratigraphy of a late Pleistocene submarine fan ponded by salt-withdrawal minibasins on the Gulf of Mexico continental slope: Offshore Technology Conference Program with Abstracts, p. 619–628.

Witton-Barnes, E. M., Hurley, N. F., and Slatt, R. M., 2000. Outcrop characterization and diagnostic criteria for confined vs. unconfined deep-water sandstones using outcrops and

borehole images, Lewis Shale, Wyoming, in P. Weimer, R. M. Slatt, J. L. Coleman, N. Rosen, C. H. Nelson, A. H. Bouma, M. Styzen, and D. T. Lawrence, (Eds.), 2000, Global deep-water reservoirs: Gulf Coast Section–SEPM 20th Annual Research Conference, p. 1087-1105.

Wynn, J. R., 1996. Micropaleontology in Petroleum Exploration Oxford Science Publications, 432p.

Yin, H., and Groshong, Jr. R. H., 2007. A three-dimensional kinematic model for the deformation above an active diapir. AAPG Bulletin, 91, 343–366.